

# A widespread new genus of Baetidae (Baetidae, Ephemeroptera) from Southeast Asia

Thomas Kaltenbach<sup>1,2</sup>, Nikita J. Kluge<sup>3</sup>, Jean-Luc Gattolliat<sup>1,2</sup>

**1** Museum of Zoology, Palais de Rumine, Place Riponne 6, CH-1005 Lausanne, Switzerland **2** University of Lausanne (UNIL), Department of Ecology and Evolution, CH-1015 Lausanne, Switzerland **3** Department of Entomology, Biological Faculty, Saint-Petersburg State University, Universitetskaya nab., 7/9, Saint Petersburg, 199034, Russia

Corresponding author: Thomas Kaltenbach ([thomas.kaltenbach@bluewin.ch](mailto:thomas.kaltenbach@bluewin.ch))

---

Academic editor: Eduardo Dominguez | Received 22 August 2022 | Accepted 9 November 2022 | Published 12 December 2022

---

<https://zoobank.org/0915A6D8-A8C5-4C7A-9560-1D6EF9E14B0F>

---

**Citation:** Kaltenbach T, Kluge NJ, Gattolliat J-L (2022) A widespread new genus of Baetidae (Baetidae, Ephemeroptera) from Southeast Asia. ZooKeys 1135: 1–59. <https://doi.org/10.3897/zookeys.1135.93800>

---

## Abstract

A reinvestigation of type and other material of *Baetis javanicus* Ulmer, 1913 and *Baetis sabahensis* Müller-Liebenau, 1984, together with new material from Southeast Asia revealed a new genus, *Branchiobaetis* **gen. nov.** The above species are formally assigned to the new genus *Branchiobaetis* **gen. nov.** It is characterized by the presence of accessory gills ventrally near fore coxa and at the base of maxillae, a peculiar folding of the gonostyli developing under the cuticle of last instar male larvae, together with a unique combination of other larval characters. Besides the two formerly described species, five new species are identified using a combination of morphology and molecular characters (COI, Kimura 2-parameter distances), four species from Sumatra and one from the Philippines. They are described and illustrated at the larval stage. Additionally, a complementary description of larva and adult stages of the generic type species *B. javanicus* **comb. nov.** as well as the first description of the eggs are provided. Furthermore, new reports of *B. javanicus* **comb. nov.** and *B. sabahensis* **comb. nov.** are indicated. The distribution of *Branchiobaetis* **gen. nov.** includes the Indonesian Sunda Islands, Borneo, and the Philippines. A key to the larval stage of all species is provided.

## Keywords

Accessory gills, COI, Indonesia, integrated taxonomy, Malaysia, Philippines

## Introduction

Baetidae are the family with the highest species diversity among mayflies on species and generic level. They comprise ca. 1,100 species in 114 genera (Kluge 2022), which is close to one third of all mayfly species and approximately one quarter of all mayfly genera worldwide. They have a cosmopolitan distribution except New Zealand (Gattolliat and Nieto 2009). Investigations of the molecular phylogeny of the Order Ephemeroptera revealed the relatively basal position of the family in Ephemeroptera phylogeny (Ogden et al. 2019).

The different realms were not equally studied in the past, and especially the Baetidae of the megadiverse Southeast Asia and New Guinea are still poorly known, despite substantial progress in the last decade with the establishment of several genera and many new species (e.g., Kluge and Novikova 2011, 2017; Gattolliat 2012; Kluge 2012, 2016; Kaltenbach and Gattolliat 2018, 2019, 2021; Kaltenbach et al. 2020a, b, 2021; Kluge 2020; Kluge and Suttinun 2020; Kluge et al. 2020; Suttinun et al. 2020).

Here, we describe a new genus of Baetidae with a wide distribution across Southeast Asia. It includes two known species, formerly described in the genus *Baetis* Leach, 1815, and five new species from Indonesia (Sumatra) and the Philippines. The new genus is easily distinguished from all other genera by the presence of accessory gills at the base of maxillae and between fore coxa and prosternum, a peculiar folding of the gonostyli developing under the cuticle of male last instar larvae, plus a unique combination of other larval characters.

Indonesia is an immense archipelago of more than 18,000 islands extending over a huge area from 95°E to 141°E and from 6°N to 11°S. It is one of the most biologically rich countries in the world. The high levels of species richness and endemism are mainly attributable to a complex geological history, which brought together two different biological realms (Oriental and Australasian realms), separated by a transitional region (Wallacea) (Hall 2010; Kingston 2010). The main islands are Sumatra, Java, Borneo (partly, Kalimantan Province), Sulawesi and New Guinea (partly, provinces West Papua and Papua). Borneo, Sumatra, Java, and the Malay Peninsula are forming the Sundaland Biodiversity Hotspot (Quek 2010), influenced by a dynamic and highly complex geophysical history including changing climates, fluctuating sea levels, volcanism, and orogenic activity with subsequent erosion (Quek 2010).

Similarly, the Philippines are a complex archipelago with more than 7100 islands, spanning the Asian-Australian faunal zone interface directly at the Wallace Line. The Huxley Line is dividing the country into Palawan and associated islands, the presumed former land-bridge to northern Borneo, and the truly oceanic portions of the Philippines. It possesses an extraordinary biodiversity, presumably supported by ancient land mass movements, environmental gradients along steep volcanic slopes and alterations of connectivity between neighbouring islands induced by changing sea levels (Brown and Diesmos 2010).

Taking into account the extreme diversity in Southeast Asia, the rather poor collection activities in the past, with many still unexplored regions, and the obvious richness of Baetidae in this region, we have to expect further new genera and many more species with further collections in the future.

## Materials and methods

The larvae were collected by kick-sampling and preserved in 70–96% ethanol. For some of the new species, ecological data were gathered by Morgan Gueuning (University of Lausanne, UNIL) during his own studies (Gueuning et al. 2017).

Subimagos were reared by one of us (NK) from mature larvae in cages placed in the stream. Subsequently, female imago was reared from subimago placed in a container with wet air, but without water. Imagos and subimagos were individually associated with larval and subimaginal exuviae.

The dissection of larvae was done in Cellosolve (2-Ethoxyethanol) with subsequent mounting on slides with Euparal liquid, using an Olympus SZX7 stereomicroscope. Alternatively, dissection was done in alcohol with subsequent mounting on slides with Canada balsam, using a stereomicroscope MSP 2; and examination with microscope Leica DM 1000.

The DNA of part of the specimens was extracted using non-destructive methods allowing subsequent morphological analysis (see Vuataz et al. 2011 for details). We amplified a 658 bp fragment of the mitochondrial gene cytochrome oxidase subunit 1 (COI) using the primers LCO 1490 and HCO 2198 (Folmer et al. 1994, see Kaltenbach and Gattolliat 2020 for details). Sequencing was done with Sanger's method (Sanger et al. 1977). The genetic variability between specimens was estimated using Kimura-2-parameter distances (K2P, Kimura 1980), calculated with the program MEGA 11 (Tamura et al. 2021, <http://www.megasoftware.net>). COI sequencing was done for species delimitation only. To compare COI divergence to our morphological identifications, we applied the single-locus species delimitation method ASAP (Assemble Species by Automatic Partitioning; Puillandre et al. 2020) to our COI data set. We used the ASAP webserver available at <https://bioinfo.mnhn.fr/abi/public/asap/asapweb.html>, computing the genetic distances under the Kimura 2-parameter substitution model (Kimura 1980) with all other settings set to default. The ASAP method, which is an improvement of the widely used ABGD (Automatic Barcode Gap Discovery; Puillandre et al. 2012) approach, has the advantage of providing a score that designates the most likely number of hypothetical species. Further, a phylogenetic reconstruction with Maximum Likelihood (Bootstrap, 1000 replications) was done with MEGA 11 (Suppl. material 1). HKY+G+I was the best-fit substitution model.

The GenBank accession numbers are given in Table 1; nomenclature of gene sequences follows Chakrabarty et al. (2013).

**Table 1.** Sequenced specimens of *Branchiobaetis* gen. nov.

Species	Locality	Specimen voucher catalogue #	GenBank # (COI)	GenSeq Nomenclature
<i>B. cf. javanicus</i> comb. nov.	Indonesia: Sumbawa	GBIFCH00980895	OP279184	genseq-4 COI
		GBIFCH00980896	OP279185	genseq-4 COI
	Indonesia: Bali	GBIFCH00980902	OP279186	genseq-4 COI
	Indonesia: Sumatra	GBIFCH00980893	OP279187	genseq-4 COI
		GBIFCH00980894	OP279188	genseq-4 COI
<i>B. aduncus</i> sp. nov.	Indonesia: Sumatra	GBIFCH00422219	OP279189	genseq-1 COI
<i>B. hamatus</i> sp. nov.	Indonesia: Sumatra	GBIFCH00422261	OP279192	genseq-1 COI
		GBIFCH01116020	OP279190	genseq-2 COI
		GBIFCH01115975	OP279191	genseq-2 COI
		GBIFCH00422238	OP279195	genseq-2 COI
<i>B. joachimi</i> sp. nov.	Indonesia: Sumatra	GBIFCH00422259	OP279194	genseq-2 COI
		GBIFCH00422248	OP279196	genseq-2 COI
		GBIFCH00980903	OP279193	genseq-2 COI
		GBIFCH00980898	OP279197	genseq-4 COI
		GBIFCH00422480	OP279200	genseq-2 COI
<i>B. minangkabau</i> sp. nov.	Indonesia: Sumatra	GBIFCH00406299	OP279198	genseq-2 COI
		GBIFCH00980904	OP279199	genseq-2 COI
		GBIFCH00980901	OP279201	genseq-2 COI
<i>B. jhoanae</i> sp. nov.	Philippines	GBIFCH00980901	OP279201	genseq-2 COI

Drawings were made using an Olympus BX43 microscope. To facilitate the determination of species and the comparison of important structures, we partly used a combination of dorsal and ventral aspects in one drawing. Explanations are given in Kaltenbach et al. (2020a: fig. 1).

Photographs of larvae were taken using a Canon EOS 6D camera and processed with the programs Adobe Photoshop Lightroom (<http://www.adobe.com>) and Helicon Focus v. 5.3 (<http://www.heliconsoft.com>). Images of larval parts were taken with a DMC 4500 camera on a Leica M205C stereomicroscope and an Olympus SC 50 camera on an Olympus BX51 microscope, processed with the program Olympus Stream Basic.

Photographs were subsequently enhanced with Adobe Photoshop Elements 13.

The distribution maps were generated with the program SimpleMappr (<https://simplemappr.net>, Shorthouse 2010). Google Earth (<http://www.google.com/earth/download/ge/>) was used to attribute approximate GPS coordinates to elder sample locations (Table 2).

The dichotomous key was elaborated with the support of the program DKey v.1.3.0 (<http://drawing.org/dkey>, Tofilski 2018).

The terminology follows Hubbard (1995; legs orientation) and Kluge (2004).

## Abbreviations of depositories

**AdMU** Ateneo de Manila University, Quezon City (Philippines);

**MZB** Museum Zoologicum Bogoriense (Indonesia);

**MZL** Musée de Zoologie Lausanne (Switzerland);

**PNM** Museum of Natural History of the Philippine National Museum, Manila (Philippines);

**SPbU** Saint-Petersburg State University (Russia);

**ZMH** Zoologisches Museum Hamburg (Germany).

**Table 2.** GPS coordinates of locations of *Branchiobaetis* gen. nov. (LT: locus typicus).

Species	Country	Location	Coordinates	LT		
<i>B. javanicus</i> comb. nov.	Indonesia	Java: Bogor	06°35'32"S, 106°48'00"E 06°39'29"S, 106°44'55"E 06°30'48"S, 107°00'03"E			
		Java: Dieng Plateau	07°12'54"S, 109°53'58"E			
		Java: Gunung Gede	06°47'16"S, 106°58'55"E	x		
		Java: Gunung Ungaran	07°11'01"S, 110°20'54"E			
		Java: Malang Batu	07°54'52"S, 112°35'05"E			
		Java: Ranu Bedali	07°57'03"S, 113°16'16"E			
		Java: Sarangan	07°39'50"S, 111°12'14"E			
		Java: Tjibodas (Cibodas)	06°44'29"S, 107°00'27"E			
		Java: Tjisarua (Cisarua)	06°39'30"S, 106°28'03"E			
		Lombok	08°25'32"S, 116°23'45"E			
<i>B. cf. javanicus</i> comb. nov.		Bali	08°29'59"S, 115°14'35"E 08°31'10"S, 115°15'18"E			
		Flores	08°42'55"S, 122°04'24"E			
		Sumatra	00°54'40"S, 100°28'23"E			
		Sumatra: Ranau	04°51'04"S, 103°56'15"E			
		Sumatra: Tjurup	03°27'45"S, 102°30'18"E			
		Sumba	09°38'37"S, 119°40'56"E			
		Sumbawa	08°35'52"S, 117°16'41"E			
<i>B. sabahensis</i> comb. nov.	Malaysia	Sabah (Borneo)	05°51'48"N, 116°15'37"E 05°57'13"N, 116°39'50"E 05°59'10"N, 116°34'42"E	x		
<i>B. cf. sabahensis</i> comb. nov.	Indonesia	East Kalimantan (Borneo)	02°59'22"N, 116°30'46"E 02°59'20"N, 116°33'11"E 03°00'57"N, 116°32'16"E			
<i>B. aduncus</i> sp. nov.	Indonesia	Sumatra: volcano Singgalang	00°23'03"S, 100°21'24"E	x		
		Sumatra: Aceh	03°58'36"N, 97°15'17"E			
		Sumatra: Talang	00°52'52"S, 100°37'23"E			
<i>B. hamatus</i> sp. nov.	Indonesia	Sumatra: volcano Talamau	00°02'59"N, 100°00'01"E	x		
		Sumatra: volcano Singgalang	00°19'57"S, 100°19'19"E			
<i>B. joachimi</i> sp. nov.	Indonesia	Sumatra: volcano Marapi	00°21'33"S, 100°30'42"E 00°22'33"S, 100°39'33"E 00°22'20"S, 100°41'45"E 00°20'37"S, 100°41'02"E	x		
			Sumatra: volcano Sago		00°18'01"S, 100°40'08"E 00°24'07"S, 100°16'44"E 00°23'33"S, 100°16'34"E 00°22'50"S, 100°17'39"E	
					Sumatra: above Padang	00°56'44"S, 100°32'44"E
		<i>B. minangkabau</i> sp. nov.		Indonesia	Sumatra: volcano Talamau	00°02'15"S, 99°59'24"E
			Sumatra: Sawahlunto		00°35'52"S, 100°43'02"E	
		<i>B. jhoanae</i> sp. nov.	Philippines	Luzon	12°44'N, 124°05'E	x
				Cebu	10°24'56"N, 123°49'02"E 10°20'48"N, 123°51'57"E	

## Results

### *Branchiobaetis* gen. nov.

<https://zoobank.org/13E7F863-CCA5-4EAD-87F2-423286D897B7>

Figs 1–29

**Typespecies.** *Branchiobaetis javanicus* (Ulmer, 1913), comb. nov., by present designation.

### Species included in *Branchiobaetis* gen. nov.

#### New combinations

1. *Branchiobaetis javanicus* (Ulmer, 1913), comb. nov.
2. *Branchiobaetis sabahensis* (Müller-Liebenau, 1984), comb. nov.

#### New species from Sumatra

3. *Branchiobaetis aduncus* sp. nov.
4. *Branchiobaetis hamatus* sp. nov.
5. *Branchiobaetis joachimi* sp. nov.
6. *Branchiobaetis minangkabau* sp. nov.

#### New species from the Philippines

7. *Branchiobaetis jhoanae* sp. nov.

**Diagnosis. Larva.** This new genus is distinguished by a combination of the following characters: A) body elongate and slender (Figs 24a, 25b); B) antennal scape distally with short, stout setae (Fig. 15i); flagellum with basal segments parallel sided and thereafter inclined, giving the impression of a spiral arrangement (Fig. 5a); C) labrum subrectangular, dorsally with a pair of long, simple submedian setae and a submarginal arc of long, simple setae (Fig. 14a); D) right mandible with blade-like incisor, prosthema stick-like with distolateral dentation (Fig. 6b); E) left mandible with blade-like incisor, prosthema robust, distally with denticles and comb-shape structure (Fig. 6a); F) maxillary palp 2-segmented, apex of segment II pointed; with accessory gill outside laterally between stipes and cardo (Figs 1a, 18h–j); G) labium with glossae basally broad, narrowing towards apex, shorter than paraglossae; paraglossae laterally slightly undulated, distally truncate and slightly bent inwards; labial palp with small to medium protuberance at segment II (Fig. 14j); H) femora with stout setae both on anterior and posterior side, dorsal margin with row of medium to long, spine-like setae and straight row of medium, fine setae (Figs 3a, b, 15a, d); claw robust, pointed, with one row of denticles and usually a long, subapical seta (Figs 7k, 15e); femoral patch reduced on fore and middle legs, well developed on hind legs (Fig. 7d–i); I) finger-like accessory gill ventrally between coxa and prosternum (Fig. 1b); J) hind protoptera present, well developed; K) paraproct with spines at posterior margin (Fig. 15h); L) seven pairs of tergalii (abdominal gills) on segments I–VII, anal margin with alternate short and long, fine setae (Fig. 15g); M) submarginal gonostyli developing under cuticle of last instar larvae folded in the following way: segment II sharply bent towards middle, last segment sharply bent laterally (Figs 4a–d, 10a, b).

**Imago.** Forewing with double intercalary veins longer than the distance between corresponding longitudinal vein; pterostigma with numerous cross veins (Fig. 9a, c). Hind wing with three longitudinal veins and well developed triangular costal projection (Fig. 9d, e). Imaginal gonostyli: segment I of gonostylus with projected blunt angle proximad of its middle; segment III short and triangular (Fig. 10d, e). Sternostyliger muscle present and thin (Fig. 10f).

The imago is known for a single species (*B. javanicus* comb. nov.). Therefore, it is unclear, which of its characters are species-specific and which can be considered as diagnostic for the new genus. The structure of hind wing and the presence of a thin

sterno-styliger muscle are also revealed for *B. sabahensis* comb. nov., based on details developing in last instar larvae.

**Etymology.** *Branchiobaetis* is a combination of *Branchio-*, in reference to the Latin word for gills and the accessory gills of the larvae, and *baetis*, to highlight the similarities with the genus *Baetis*. The gender is masculine.

**Description. Larva.**

**Head. Antenna.** Bases of antennae not close to each other, without carina between them. Scape at least distally (and often outside laterally) with short, stout, apically rounded setae (Fig. 15i); flagellum with basal segments parallel sided and thereafter inclined, giving the impression of a spiral arrangement (Fig. 5a).

**Labrum** (Fig. 14a). Subrectangular, wider than long. Distal margin with medial emargination and a small process. Dorsally with a pair of long, simple, submedian setae and on each side a submarginal arc of long, stout, simple setae; surface scattered with medium, simple setae. Ventrally with lateral row of medium, simple setae, anterolaterally with long, feathered setae on margin and medially with long, bifid, pectinate setae on margin, several small, stout setae near anterolateral and sometimes also lateral margin.

**Right mandible** (Figs 6b, 14b–d, 22b). Incisor and kinetodontium almost fused, incisor with denticles, outer denticle blade-like, kinetodontium with denticles; inner margin of innermost denticle of kinetodontium with row of thin setae; prostheca stick-like, distolaterally denticulate; apex of mola with tuft of feathered setae. Basal half with fine, simple setae scattered over dorsal surface.

**Left mandible** (Figs 6a, 18e, f). Incisor and kinetodontium fused, incisor with denticles, outer denticle blade-like, kinetodontium with denticles; prostheca robust, distally denticulate and with comb-shape structure; apex of mola without tuft of setae. Basal half with fine, simple setae scattered over dorsal surface.

Incisors of both mandibles are quickly worn after the larva started feeding and become much shorter than in fresh, unused mandibles. The real shape of unused mandibles can be seen during development inside the actual mandible (Figs 6a, b, 20b, d).

**Maxilla** (Figs 1a, 18h–j). Apically with three stout canines and three denti-setae; distal denti-seta tooth-like, other denti-setae slender, bifid, and pectinate; maxillary palp with two segments, apex strongly pointed. Small accessory gill located on outer side of the articulation between stipes and cardo.

**Hypopharynx** (Fig. 14h). Apex with compact tuft of long, dense setae-like processes.

**Labium** (Fig. 14j). Glossae basally broad, narrowing towards apex, shorter than paraglossae; inner margin with row of spine-like setae, increasing in length distally; apex with several short to long, robust setae; outer margin with row of spine-like setae; ventral surface with fine, simple scattered setae. Paraglossae laterally slightly undulated, distally truncated, and slightly bent inwards; apex with three rows of long, robust, distally pectinate setae; ventrally usually with several short, simple setae in distomedial area and one short, simple seta in proxolateral area; dorsally with few long, spine-like setae near inner margin. Labial palp with three segments, segment II with small to medium protuberance.

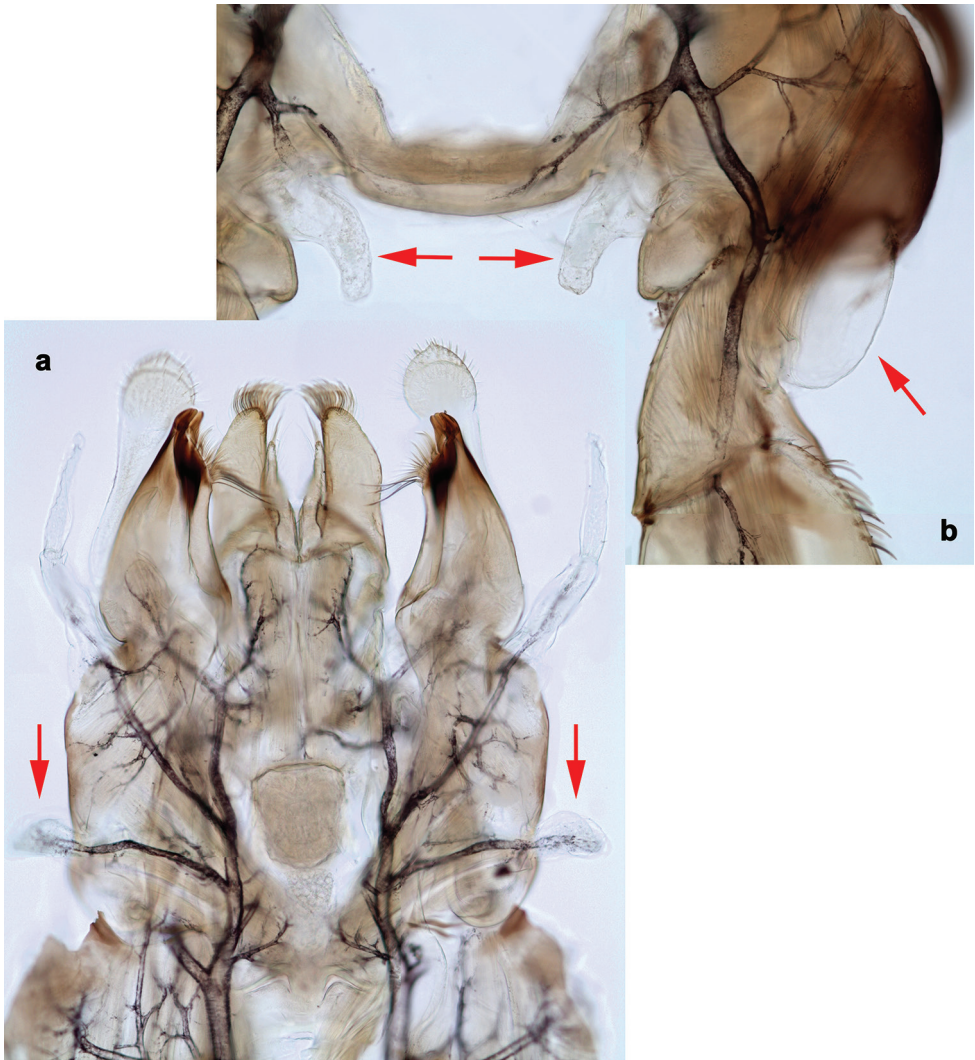


**Figure 1.** *Branchiobaetis javanicus* comb. nov., larva **a** maxillae and labium, dorsal view **b** prosternum and bases of forelegs, front view.

**Thorax.** *Hind proptera* present, well developed.

**Foreleg** (Figs 1b, 2a–c, 3a, b, 7a, d, g, k, 13a, 15a, d, e). **Femur** with row of medium to long, spine-like setae and additionally straight row of fine setae on dorsal margin; on apex short, stout setae on anterior and posterior side; femoral patch present, reduced and sometimes indistinct. Accessory gill on inner side of coxal articulation (between coxa and prosternum); bubble-like membranous swelling between coxa and trochanter and between coxa and pleurite (Figs 1b, 2a–c). **Tibia** with long patella-tibial suture in  $\frac{3}{4}$  area; dorsal margin with row of short, stout setae and row of fine setae. **Tarsus** dorsally with row of short, stout setae, ventrally with row of curved, spine-like setae

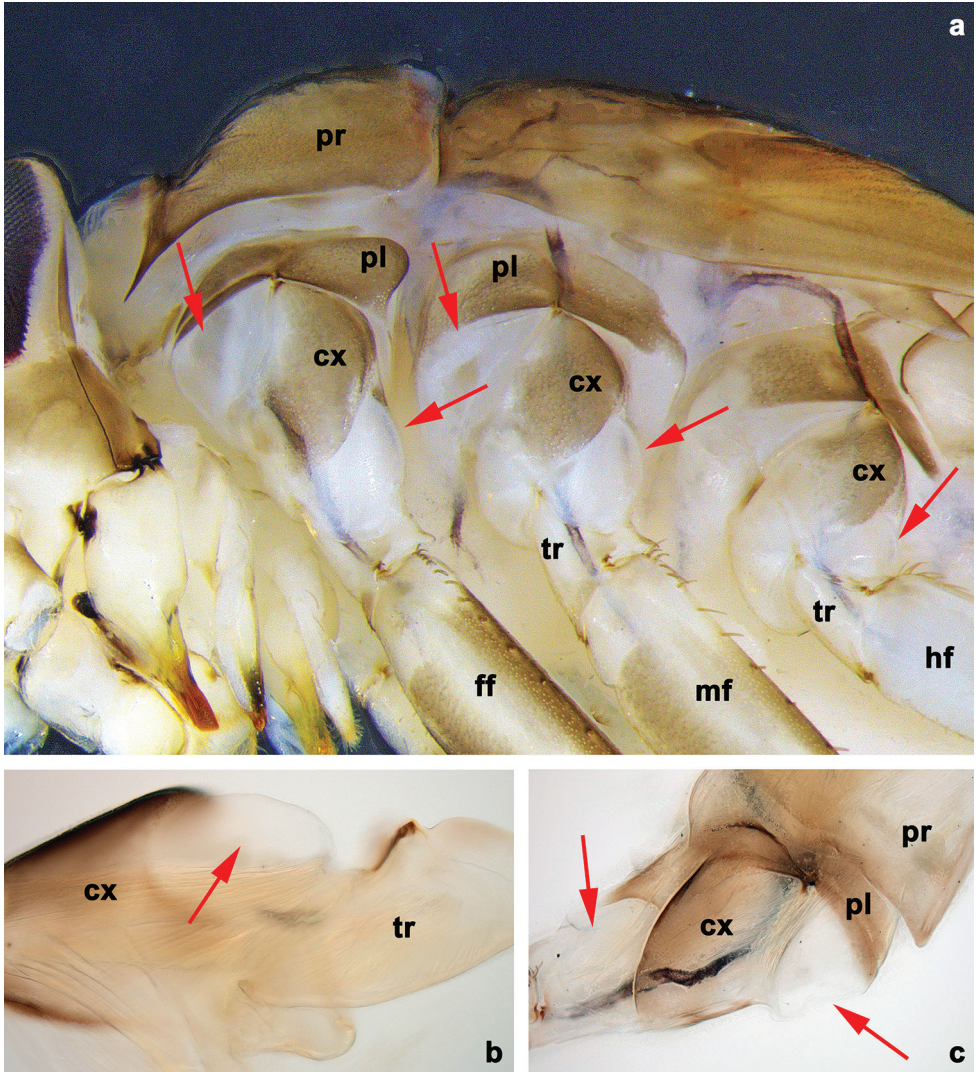


**Figure 2.** *Branchiobaetis javanicus* comb. nov., larva **a** thorax, lateral view. *Branchiobaetis joachimi* sp. nov., larva **b, c** foreleg. Abbreviations: cx, coxa; ff, forefemur; hf, hind femur; mf, middle femur; pl, pleurite; pr, pronotum; tr, trochanter.

increasing in length distally. **Claw** robust, pointed, with one row of denticles; usually with one long, subapical seta (posterior seta sensu Kluge and Novikova 2014).

**Middle and hind leg** (Figs 2a, 7b, c, e, f, h, i). As foreleg; femoral patch on middle leg also reduced, but well developed on hind leg; hind femur without apical setae on posterior side. Bubble-like membranous swelling on middle leg between coxa and trochanter and reduced between coxa and pleurite, on hind leg only between coxa and trochanter.

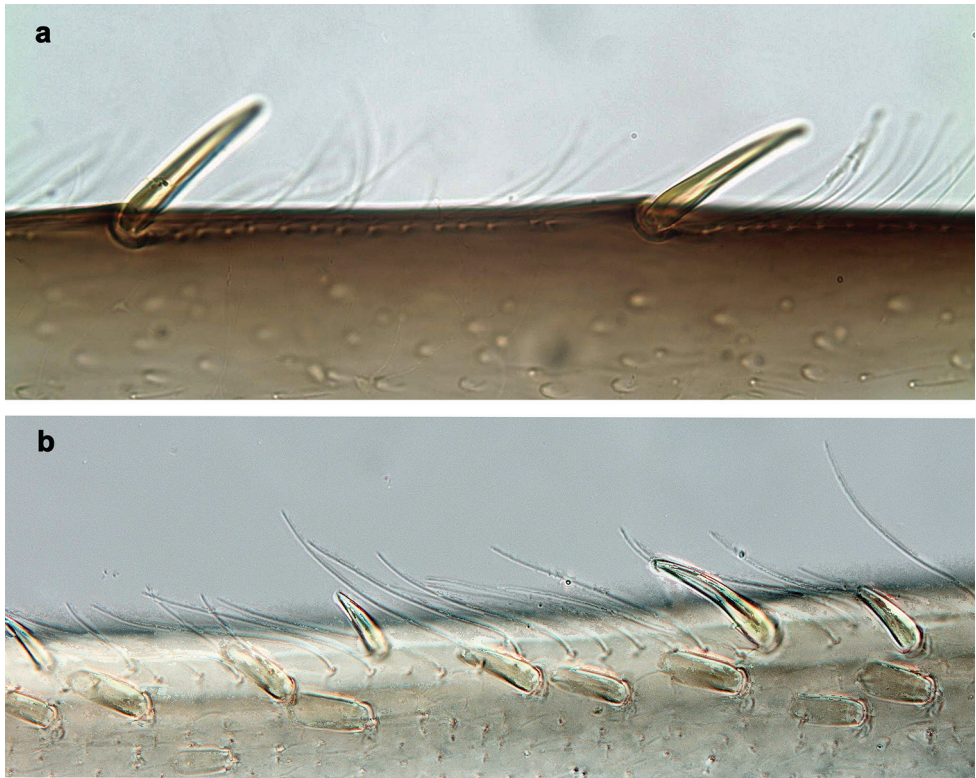


**Figure 3.** *Branchiobaetis javanicus* comb. nov., larva **a** dorsal margin of foreleg. *Branchiobaetis joachimi* sp. nov., larva **b** dorsal margin of foreleg.

**Abdomen. Tergalii** (Figs 15g, 26a–e). Present on abdominal segments I–VII, dorso-laterally oriented; costal margin with minute denticles and short, fine setae; anal margin with minute denticles and alternating both short and long, fine setae.

**Paraproct** (Fig. 15h). Posterior margin with stout spines; most species with short, stout, apically rounded setae near posterior margin. Cercotractor with numerous, small, marginal spines.

**Caudalii** (Fig. 5e). Inner lateral margin of cerci and paracercus bilaterally with primary swimming setae.

**Larval protogonostyli** (Fig. 10a) slightly projected; subimaginal gonostyli developing under cuticle of last instar larvae folded in the following way: segment II sharply bent towards middle, last segment sharply bent laterally (Figs 4a–d, 10a, b).

**Imago.** Forewing with double intercalary veins longer than distance between corresponding longitudinal vein; pterostigma with numerous cross veins (Fig. 9a, c). Hind wing with three longitudinal veins and well developed triangular costal projection (Fig. 9e). Imaginal gonostyli: segment I of gonostylus with projected blunt angle proximad of its middle; segment III short and triangular (Fig. 10d, e). Sterno-styligeral muscle clearly developed, but thin (Fig. 10f).

The imago is known from a single species (*B. javanicus* comb. nov.). Therefore, it is unclear, which of its characters are species-specific and which are generic (e.g., shape of turbinate eyes). Ulmer (1913, 1924) and Müller-Liebenau (1981) described imago and subimago and a complementary description is given below under *B. javanicus* comb. nov.

**Distribution (Figs 27–29).** Indonesia (Sunda Islands, Kalimantan), Malaysia (Sabah), Philippines.

**1. *Branchiobaetis javanicus* (Ulmer, 1913), comb. nov.**

Figs 1a, b, 3a, 5a–11d, 27b

*Baetis javanicus*: Ulmer 1913: 110 (♂ & ♀ imago); Müller-Liebenau 1981: 198 (♂ imago, larva); Sartori et al. 2016: 54 (syntypes locality).

*Baetis javanica*: Ulmer 1924: 52 (♂ & ♀ imago); Ulmer 1939: 523 (♂ imago, ♂ subimago, ♀ subimago); ibid.: 643 (larva).

**Material examined. Type locality.** INDONESIA • W. Java, Gedeh, Tjibodas; 1400 m; 24.–30.XII.1930; leg. M. A. Lieftinck; 2 ♀ larvae on slides; ZMH • Java, Cibodas; 6–11.VIII.2009; leg. N. Kluge & L. Sheyko; 4 ♂ subimagos with associated larval exuviae; [III](2)B2009, [III](7)B2009; 73 larvae; slides 7.XII.2021-1, 11.XII.2021-1, 24.XII.2021-1, 24.XII.2021-2, 24.XII.2021-3, 17.XII.2021-1; SPbU. **Other material.** INDONESIA • Java, vic. Bogor, Mt. Sulak, Chiapus; 06°39'29"S, 106°44'55"E; 624 m; 24.II.2008; leg. S. Melnitsky; 1 ♂ imago; SPbU • Lombok, Mount Rinjani National Park; 25.IX.2009; leg. N. Kluge & L. Sheyko; 1 ♀ imago with associated larval and subimaginal exuviae; [XXXIX](1)2009; 34 larvae; SPbU • Java, Bogor, Ciliwung River, downstream of botanical garden; 06°35'32"S, 106°48'00"E; 235 m; 01.V.2010; leg. J.-M. Elouard; 1 larva on slide, GBIFCH00592476, 1 larva in alcohol, GBIFCH00592468; MZL • Java, Malang Batu Jalang, cascade, forest river; 07°54'52"S, 112°35'05"E; 570 m; 09.V.2010; leg. J.-M. Elouard; 2 larvae in alcohol, GBIFCH00592466, GBIFCH00592467; MZL.

***B. cf. javanicus* comb. nov. material examined.** INDONESIA • Sumba, forest stream; 09°38'37"S, 119°40'56"E; 470 m; 27.IX.2011; leg. M. Balke; larva on slide; GBIFCH00592481; MZL; larva in alcohol; GBIFCH00592463; MZL • Sumbawa, Batu Dulang, 10 mins to Tepal, forest stream; 08°35'52"S, 117°16'41"E; 860 m; 16.IX.2011; leg. M. Balke; 2 larvae on slides; GBIFCH00592479, GBIFCH00592480; MZL; 39 larvae in alcohol; GBIFCH00592462, GBIFCH00975593, GBIFCH00975594, GBIFCH00975604, GBIFCH00975605; MZL • Bali, Ubud, Sayan, Ayung River; 08°29'59"S, 115°14'35"E; 194 m; 20.IX.2011; leg. M. Balke; larva on slide; GBIFCH00592477; MZL • Bali, Ubud, Monkey River; 08°31'10"S, 115°15'18"E; 260 m; 16.V.2010; leg. J.-M. Elouard; larva on slide; GBIFCH00592478; MZL; 2 larvae in alcohol; GBIFCH00975611; MZL • Sumatra Barat, Universitas Andalas campus, forest stream; 00°54'40"S, 100°28'23"E; 360 m; 08.XI.2011; leg. M. Balke;

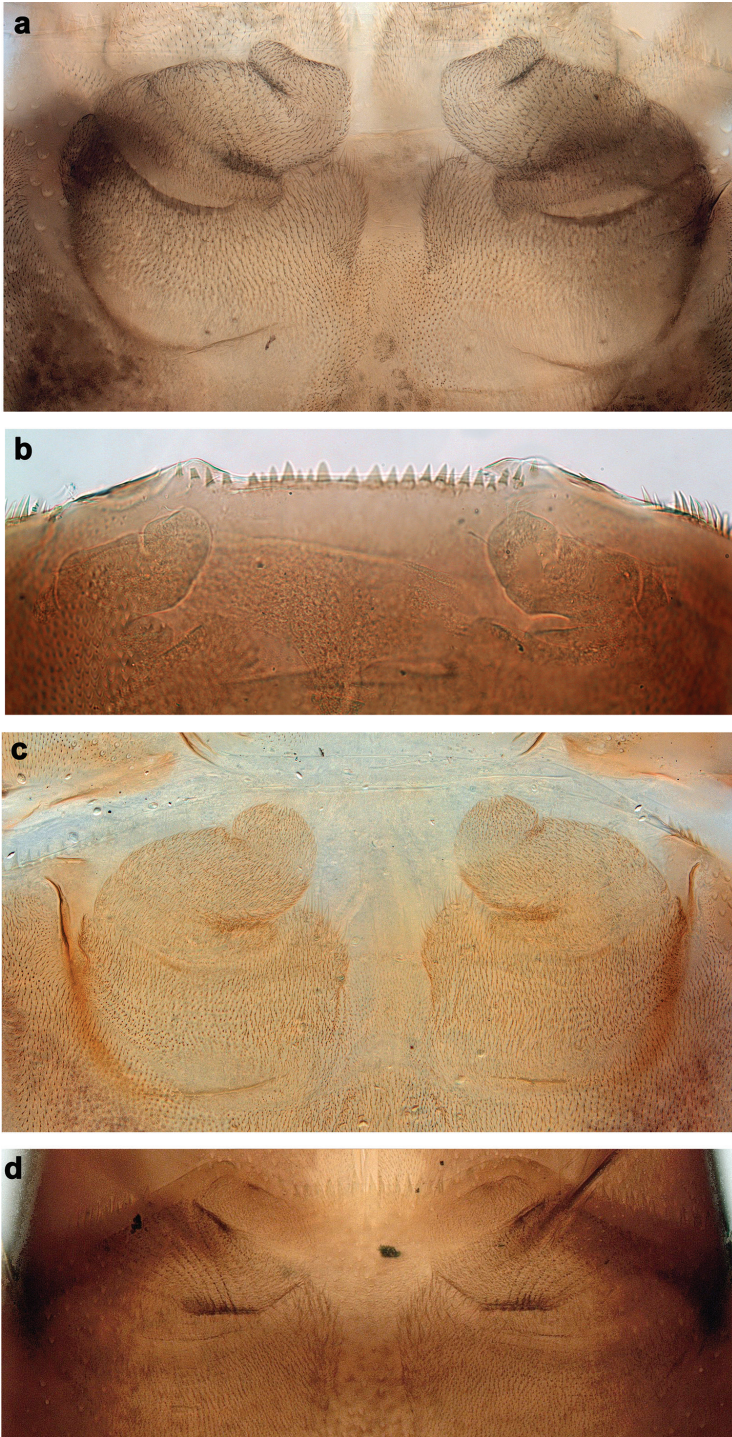


**Figure 4.** *Branchiobaetis* gen. nov., subimaginal gonostyli developing under cuticle of male last instar larva **a** *B. javanicus* comb. nov. **b** *B. sabahensis* comb. nov. (not yet fully developed) **c** *B. aduncus* sp. nov. **d** *B. joachimi* sp. nov.

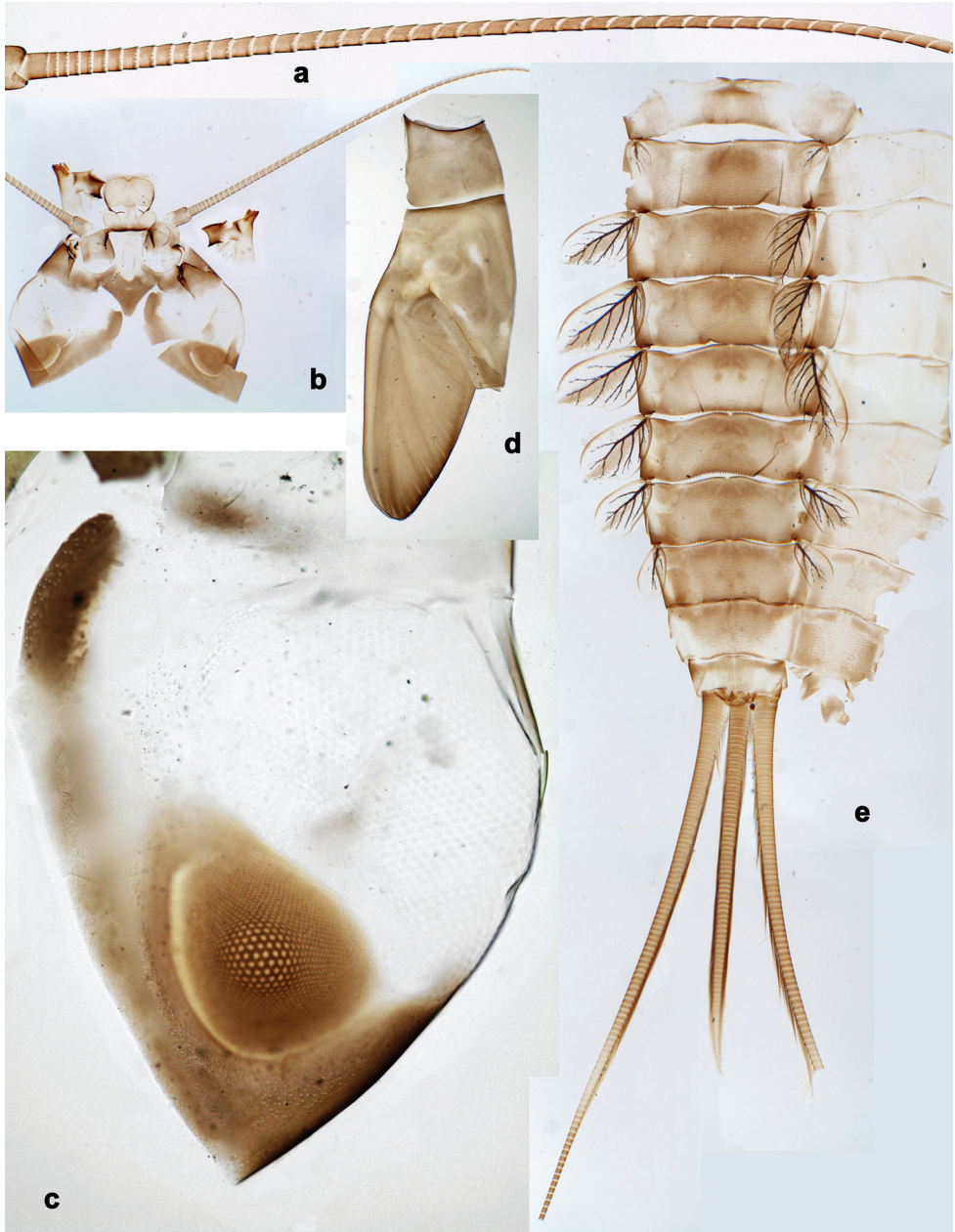


**Figure 5.** *Branchiobaetis javanicus* comb. nov., exuviae of last instar male larva **a** portion of antenna **b** head **c** enlarged right eye and precursor of turbinate eye **d** left half of pronotum and mesonotum **e** abdomen.

3 larvae on slides; GBIFCH00592474, GBIFCH00592475, GBIFCH00592502; MZL; 69 larvae in alcohol; GBIFCH00592489, GBIFCH00592501; GBIFCH00975582, GBIFCH00975583, GBIFCH00975595, GBIFCH00975596, GBIFCH00975597, GBIFCH00975603; MZL • Flores, Maumere region, river in

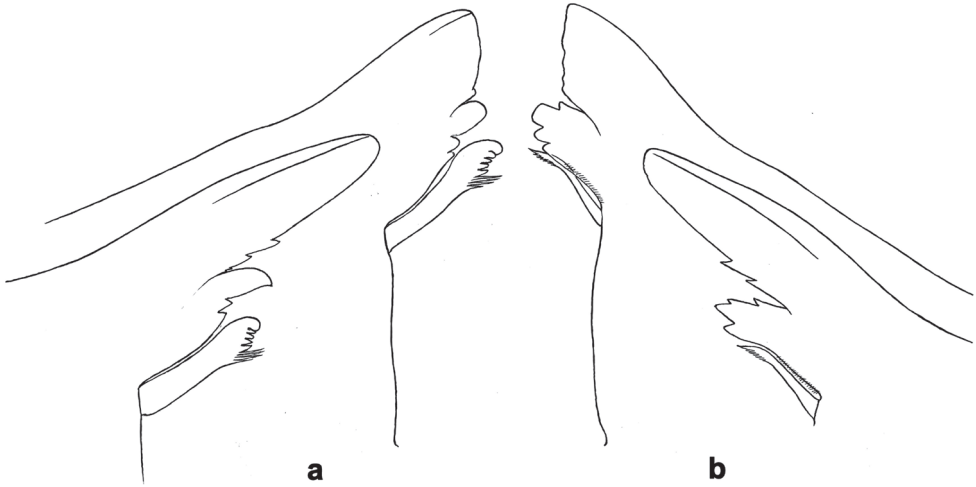


**Figure 6.** *Branchiobaetis javanicus* comb. nov., larva **a, b** apices of left and right mandibles with mandibles of next instar developing inside them.

garden land; 08°42'55"S, 124°04'24"E; 134 m; 21.IV.2012; leg. M. Balke; 2 larvae on slides; GBIFCH00592262, GBIFCH00592297; MZL; 18 larvae in alcohol; GBIFCH00592264, GBIFCH00592265, GBIFCH00975606; MZL.

**Differential diagnosis. Larva.** Following combination of characters distinguish *B. javanicus* comb. nov. from other species of *Branchiobaetis* gen. nov.: A) labial palp segment II with triangular protuberance, segment III rather long (Müller-Liebenau 1981: fig. 1b); B) dorsal margin of fore femur with row of spine-like setae, basally dense and partly arranged in double row (Fig. 7a; Müller-Liebenau 1981: fig. 1k); C) posterior margin of tergite I smooth, without spines; posterior margins of tergites II–X with triangular spines, partly longer than wide (Fig. 7j), partly as long as wide; posterior margin of sternites: I–VI smooth, without spines; VII smooth or with few small spines; VIII with few spaced, small, blunt spines; IX with triangular spines; D) paraproct not expanded, with stout setae along posterior margin.

**Morphological features and their development.** Imagos and subimagos are described by Ulmer (1913, 1924). Müller-Liebenau correctly reported that hind wing has not two, but three veins (Fig. 9e; Müller-Liebenau 1981: fig. 2b). Larva is described by Ulmer (1939); larval characters are illustrated by Müller-Liebenau (1981: fig. 1). Here we give additional figures of larvae (Figs 1a, b, 3a, 5a–7k), subimagos (Fig. 8a–h), male imago (Figs 9a, b, j, 10d–f) and female imago (Fig. 9c–g, k).

**Turbinate eyes.** Ulmer (1913, 1924) reported only colour of turbinate eyes (brown-grey), but not their shape. Turbinate eyes of male imago and subimago unusually small, cylindrical, with faceted surfaces round; faceted surface with approx. ten facets in diameter (Fig. 9b). In last instar male larva, precursors of the turbinate eyes representing a pair of reddish-brown maculae of egg-like shape; at middle of this

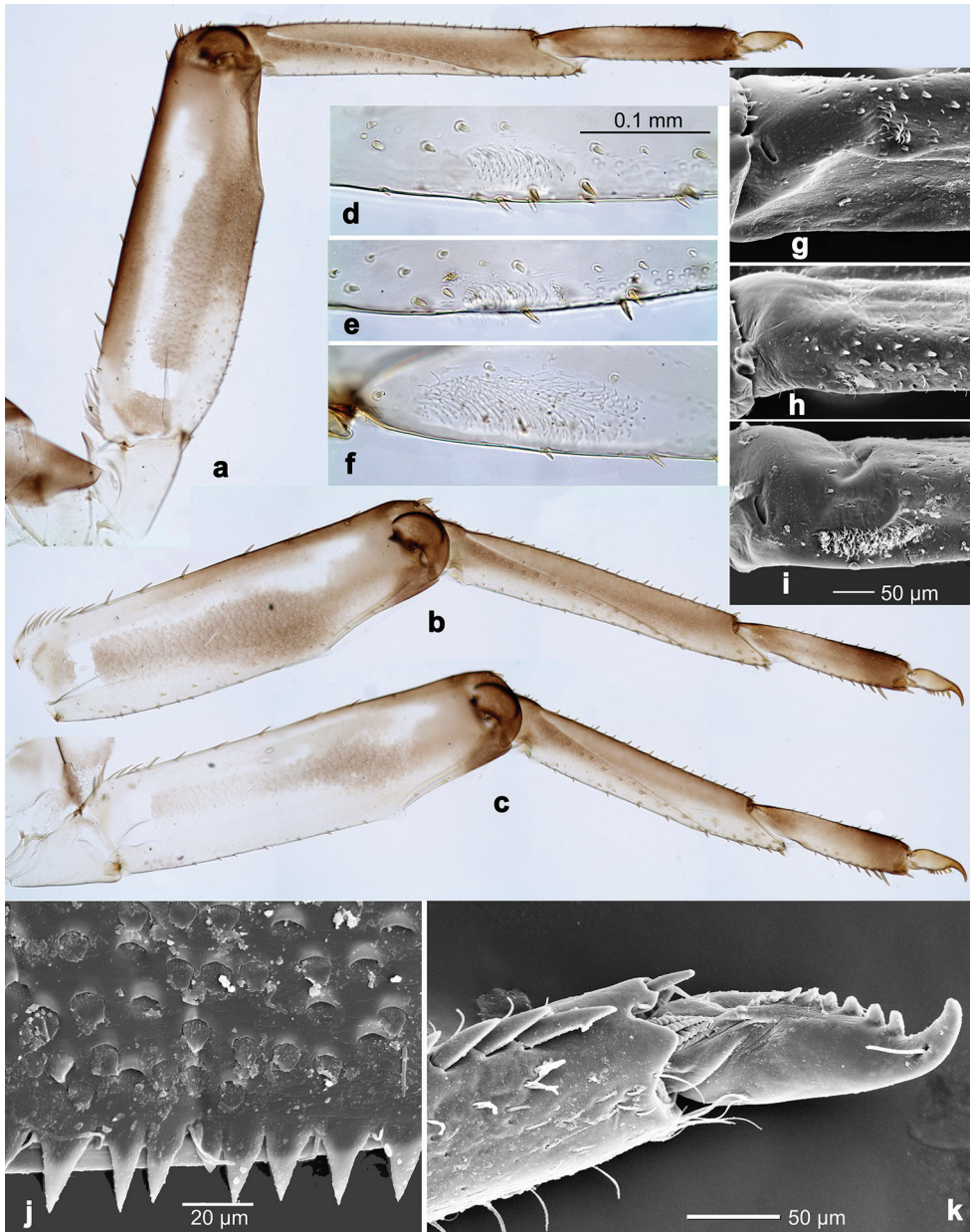


**Figure 7.** *Branchiobaetis javanicus* comb. nov., larva **a–c** fore, middle, and hind legs **d–f** femoral patch of fore, middle and hind legs **g–i** femoral patch of fore, middle and hind legs **j** abdominal tergum **k** claw.

macula, a smaller round area with well-expressed facets, approx. ten facets in diameter; peripheral area of the macula consists of very small and indistinct facets (Fig. 5c). Facetted surface of subimago and imago is developed from the round area, but not from the whole reddish brown macula.

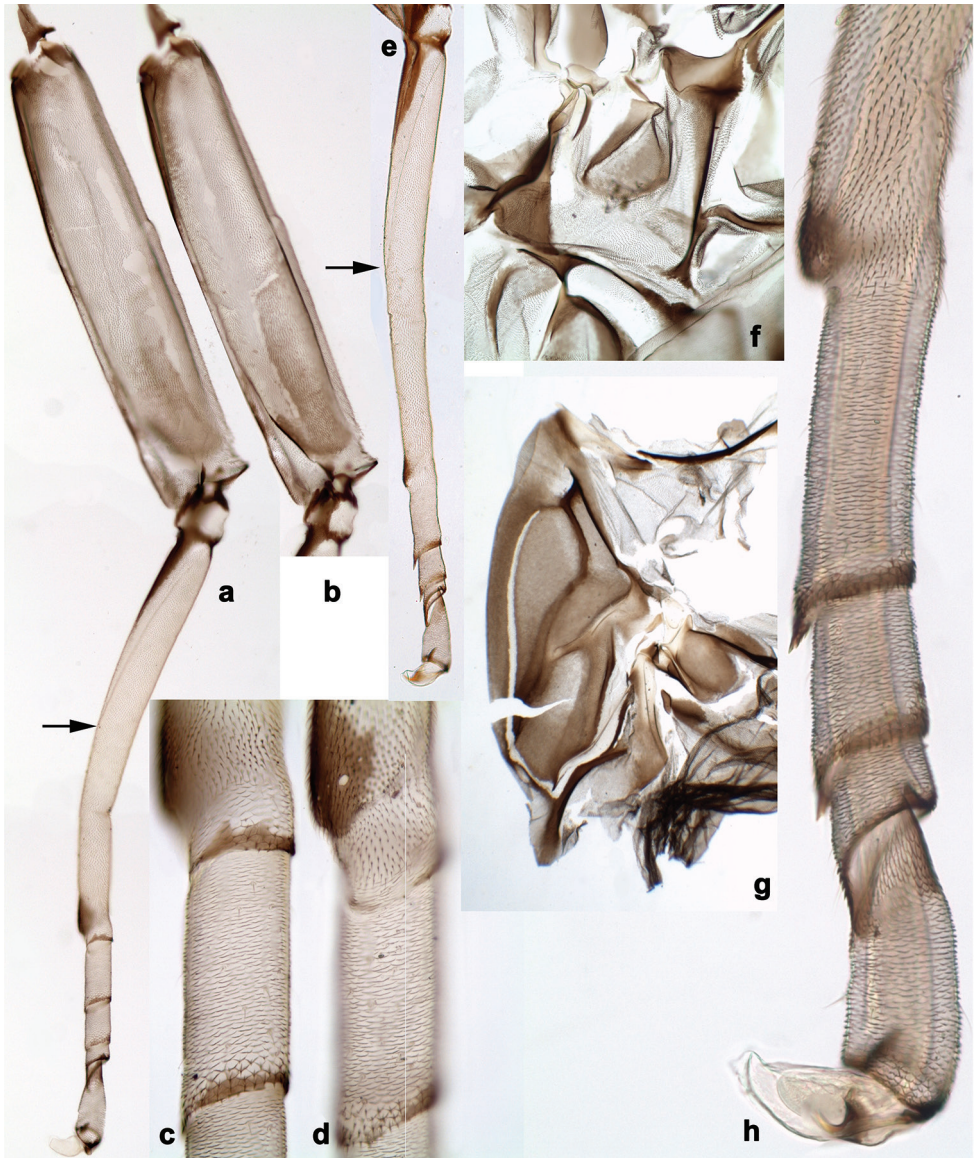


**Figure 8.** *Branchiobaetis javanicus* comb. nov., subimagines **a–g** female subimaginal exuviae **a** foreleg, anterior view **b** fore femur, posterior view **c, d** base of fore tibia, anterior and posterior view **e** middle tibia **f** left mesopleuron with prealar and postsubalar sclerites **g** right part of mesonotum **h** middle tarsus of male subimago. Arrows show apex of patella-tibial suture.

**Larval mandibles** (Fig. 6a, b). Incisors of left and right mandibles very long and parallel-sided (i.e., blade-like), with rounded apex and two small pointed denticles in proximal half.

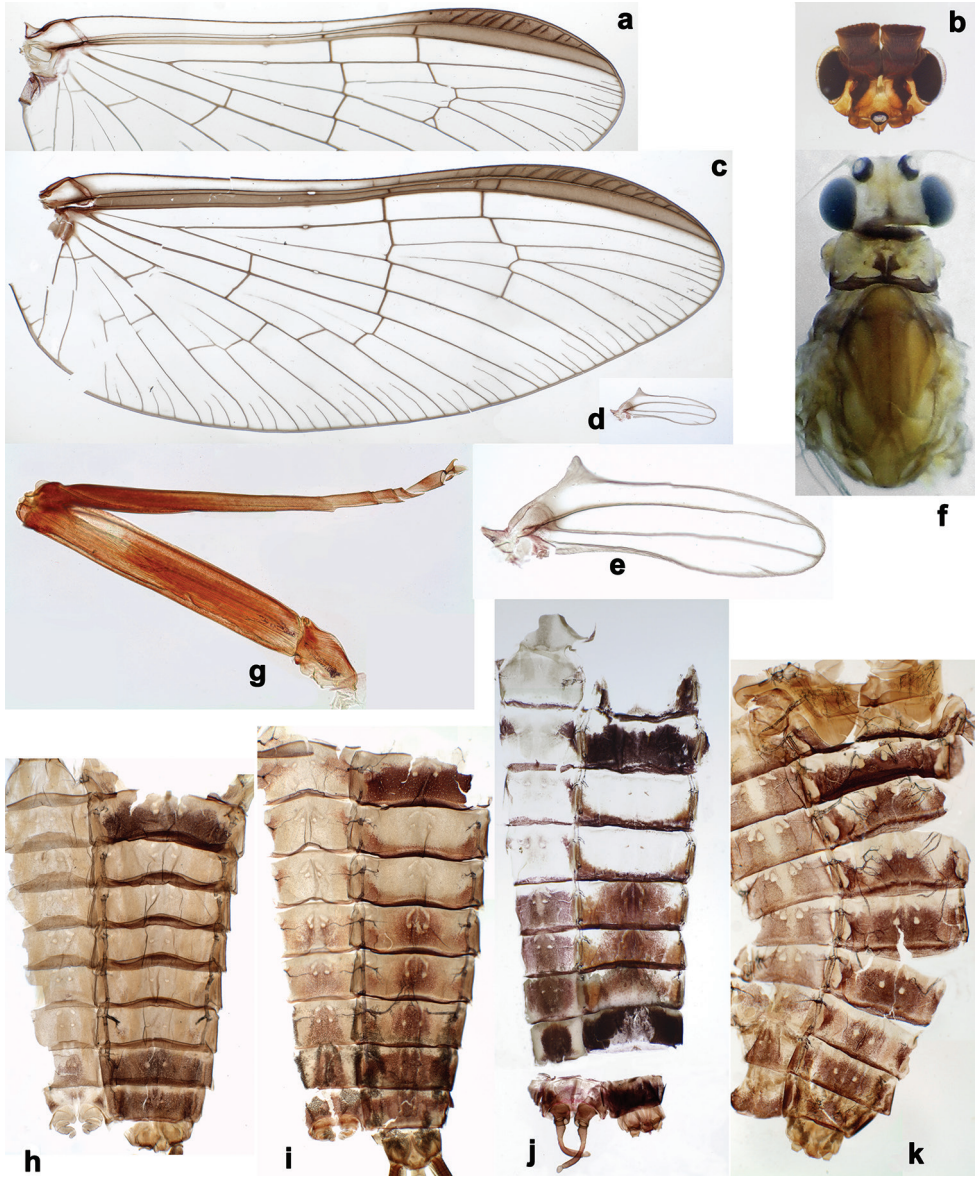


**Figure 9.** *Branchiobaetis javanicus* comb. nov. **a** fore wing of male imago **b** head of male imago **c, d** fore and hind wing of female imago **e** hind wing enlarged **f** head and thorax of female imago **g** middle leg **h, i** male subimaginal abdomen extracted from larva **j** abdomen of male imago **k** abdomen of female imago.

N.B. Such shape of mandibular incisors is only visible when they are developed inside mandibles of the previous instar (Fig. 6a, b) and possibly just after the moult, before the mandibles are hardened and the larva starts to eat. After feeding, the inci-

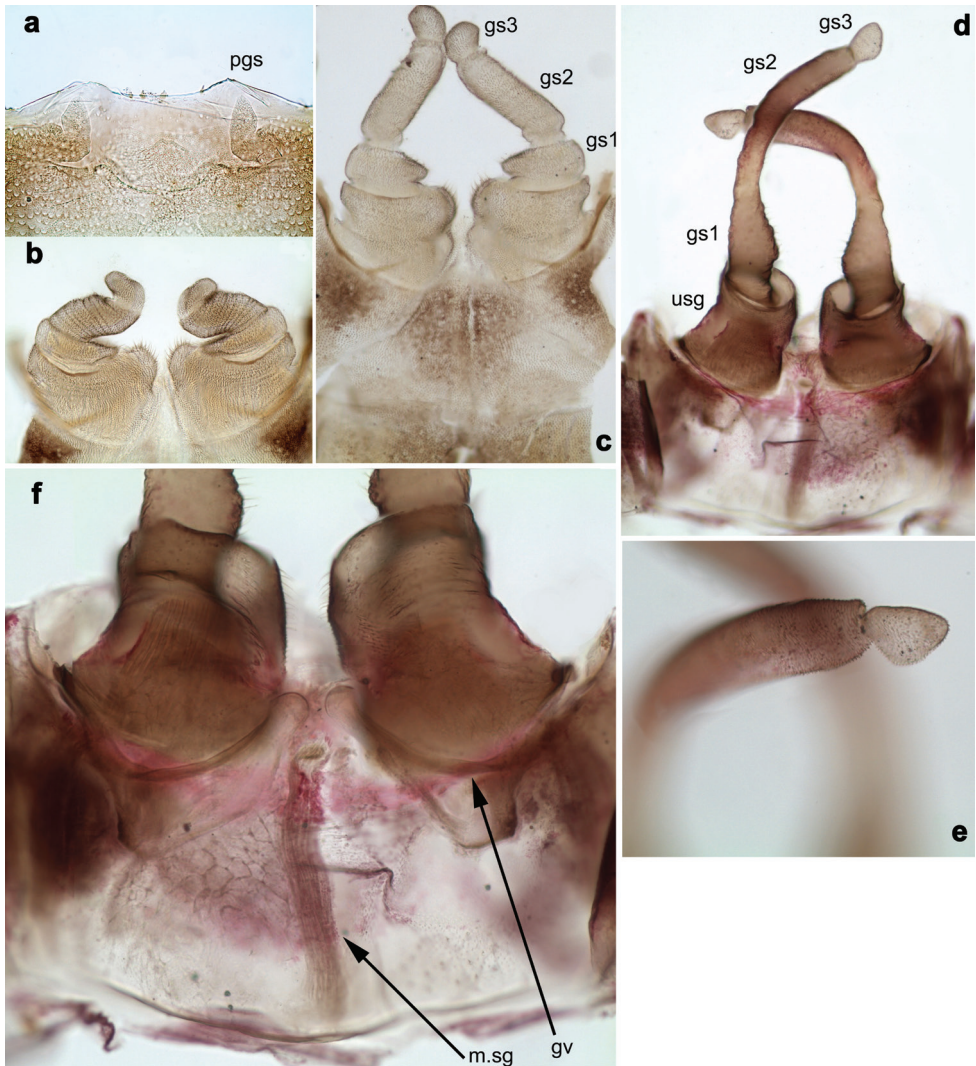


**Figure 10.** *Branchiobaetis javanicus* comb. nov., male genitalia **a** subimaginal gonostyli crumpled under larval cuticle at earlier stage of development **b** subimaginal gonostyli extracted from larva starting to molt to subimago **c** genitalia of subimago, ventral view **d** genitalia of imago, ventral view **e** the same, apex of gonostylus **f** genitalia of imago, dorsal view. Abbreviations: gs1–gs3, segments of gonostyli; gv, gonovectis; m.gs, gonostylar muscle; m.sg, styligeral muscle; pgs, larval protogonostylus; usg, unistyliger.

sors are worn and sometimes broken, so look much shorter (see outer lines of the same figures). Such worn mandibles are figured by Müller-Liebenau (1981: fig. 1e).

**Maxillary and sternal gills** (Fig. 1a, b). Presence of small ventral tracheal gills not formerly reported. Presence of a pair of maxillary gills and a pair of fore coxal gills.

Each maxillary gill located on outer side of articulation between stipes and car- do; trachea penetrating into this gill, arising from paired tracheal stem which is more

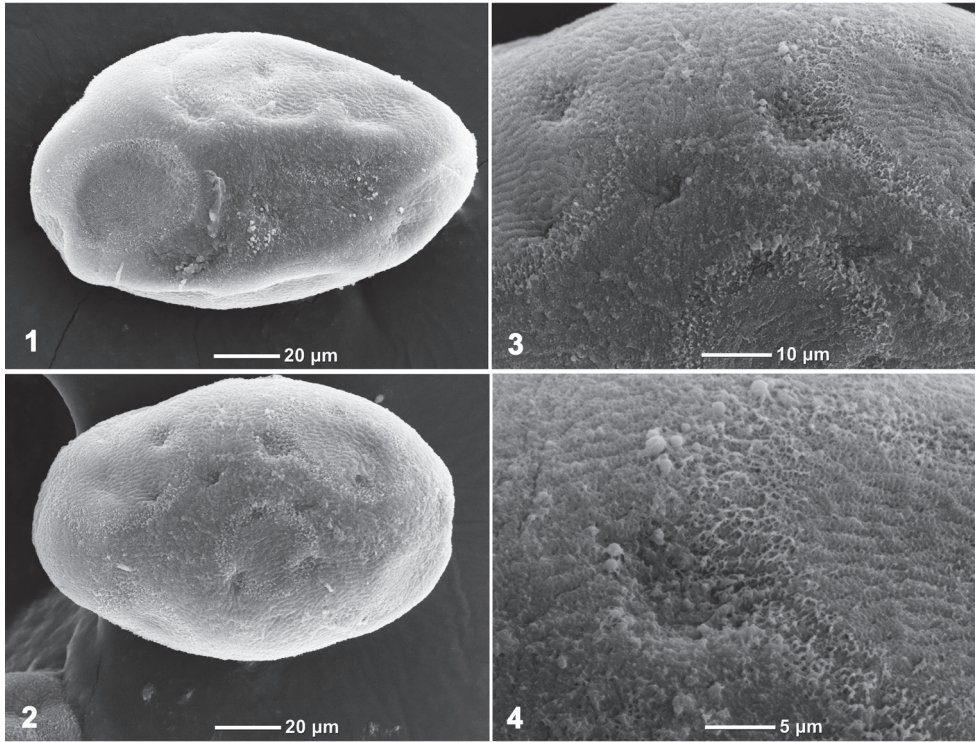


**Figure 11.** *Branchiobaetis javanicus* comb. nov., eggs.

distally divided into branch penetrating into maxilla and branch penetrating into corresponding half of labium (Fig. 1a).

Each fore coxal gill located on inner side of coxal articulation, i.e., on the membrane between coxa and prosternum; trachea penetrating into this gill, arising from trachea going into foreleg; close to its base, trachea is divided into branch passing inside prosternum and branch penetrating into gill. Inside fore coxal gill, trachea widened, thin-walled and colourless (Fig. 1b).

**Patella-tibial suture.** Patella-tibial suture present on all legs of larva, female subimago and female imago, including their fore legs (that is characteristic for Anteropatellata); greatly stretched along tibia: in larva reaching inner side of tibia in distal  $\frac{1}{4}$  (Fig. 7a, c), in subimago and imago near middle of tibia (Figs 8a, e, 9g); in all stages patella-tibial suture barely reaching inner side of tibia, not crossing it.

**Femoral patch.** Each larval leg with a femoral patch/field of minute curved setae on inner side of femur near its base (that is characteristic of Baetofemorata); femoral patch on hind leg large (Fig. 7f, i), but on fore and middle legs either much smaller (Fig. 7d, e), or indistinct (Fig. 7g, h).

**Texture of subimaginal tarsi** (Fig. 8c, d, h). In subimagos of both sexes, all tarsomeres covered with blunt microlepidies; only very basal part of first tarsomere covered with microtrichia (like tibia), and apical parts of tarsomeres with pointed microlepidies.

**Colouration of subimaginal cuticle.** Head colourless, antennae brown. Pronotum brown. Mesonotum mostly brown (Fig. 8g). Thoracic pleura with brown and colourless areas (Fig. 8f). Legs mostly light brownish with dark brown markings on femur, tibia, and tarsus (Fig. 8a–e). Abdominal terga nearly uniformly brown, slightly darker laterally; sterna lighter; cerci lighter brownish.

**Colouration of abdomen of winged males.** Abdominal colouration of male imago is adequately described by Ulmer (1913, 1924). It consists of contrasting colourless-white areas, vine-red areas and black areas, with sharply different colour patterns of the terga I–II, III–IV, V–VII, VIII–IX, and X, and sharply different colour patterns of the sterna I–IV, V–VII, VIII, and IX (Fig. 9j).

Abdominal colouration of subimago was briefly characterized by Ulmer (1924) as ‘Ähnlich der Imago, Segment III bis VII bräunlichgelb durchscheinend’. Among examined male subimagos reared from larvae or extracted from mature larvae, some individuals agree with this characteristic, i.e., their terga I–II and VIII–IX are dark brown, but terga III–VII and all sterna are uniformly light brownish (Fig. 9h); some individuals have terga and sterna III–VII differentiated somewhat approximating to that of imago (Fig. 9i).

**Gonostyli of male.** Imaginal gonostyli with characteristic species-specific shape (Fig. 10d, e; Ulmer 1924: fig. 25): unistyliger (wrongly called ‘Glied I’ in Ulmer 1924) cylindrical, somewhat narrowed at middle; segment I of gonostylus (wrongly called ‘Glied II’ in Ulmer 1924) with projected blunt angle proximad of its middle; segment III of gonostylus (wrongly called ‘Glied IV’ in Ulmer 1924) short and triangular, i.e., apically widened and truncate.

N.B. When developing subimaginal gonostyli are bent under the larval cuticle, segment II of gonostylus is bent medially (as in other Baetofemorata), and segment III is sharply bent laterally, that is a peculiar feature of *Branchiobaetis* gen. nov. (Fig. 10a, b). In subimago freed from the larval cuticle, gonostyli retain features of their previous pose under larval cuticle, with segments II sharply bent medially and segments III somewhat bent laterally (Fig. 10c); the species-specific shape of segment III is present in imaginal stage only (Fig. 10d, e). A paradoxical feature is that segment III starts to develop as unusually long (Fig. 10a), later it is bent and pressed to the 2<sup>nd</sup> segment (Fig. 10b), while subsequently it becomes shorter (Fig. 10c, d).

**Internal parts of male genitalia.** Sterno-styliger muscle developed, but slender; gonovectes S-shaped, i.e., arched, with apices curved cranially (Fig. 10f).

**Egg** (Fig. 11a–d). Eggs irregularly oval, with irregularly situated shallow cavities, and surface of chorion rugose.

**Dimension.** Size rather variable: fore wing length of male and female (and the general body length) varies from 6 mm to 10 mm; females usually larger than males.

**Larval habitat.** Tergalii unable for rhythmical respiratory movements (as in other Baetungulata), and larvae are unable to live for a long time in stagnant water. Larvae are most abundant in fast streams with cold water.

**Distribution (Fig. 27b).** Indonesia: Java, Lombok; *B. cf. javanicus* comb. nov. Indonesia: Sumatra, Bali, Sumba, Sumbawa, Flores.

**2. *Branchiobaetis sabahensis* (Müller-Liebenau, 1984), comb. nov.**

Figs 12, 13

*Baetis sabahensis*: Müller-Liebenau 1984b: 89; figs 3, 9, 14, 14a.

**Material examined.** MALAYSIA • Sabah, Ranau; 14.–16.VII.1972; leg. G. F. Edmunds; ♂ larva on slide; SPbU • Sabah, Kundasang; 04.IX.1994; leg. S. C. Kang; ♂ larva on slide; SPbU.

***B. cf. sabahensis* comb. nov. material examined.** INDONESIA • East Kalimantan, Bas. Malinau, River Seturan, loc. Seturan (2000-block 44–45), trib. Wok (Sungai Guang); 2°59'12"N, 116°33'11"E; 16.VI.2000; leg. P. Derleth & J.-L. Gattolliat; 3 larvae on slides; GBIFCH00592470, GBIFCH00592471, GBIFCH00592495; larva in alcohol; GBIFCH00270724; MZL • East Kalimantan, Bas. Malinau, River Seturan, loc. Seturan (2001-block 57), trib. Bengahau; 02°59'22"N, 116°30'46"E; 19.VIII.2000; leg. P. Derleth & R. Schlaepfer; larva on slide; GBIFCH00592494; larva in alcohol; GBIFCH00270710; MZL • East Kalimantan, Bas. Malinau, riv. Seturan, loc. Seturan (2001-block 57), trib. Benganau; 02°59'22"N, 116°30'46"E; 11.IV.2001; leg. P. Derleth & B. Feldmeyer; larva in alcohol; GBIFCH00270710; MZL.

**Differential diagnosis. Larva.** Following combination of characters distinguish *B. sabahensis* comb. nov. from other species of *Branchiobaetis* gen. nov.: A) labial palp segment II with short, thumb-like protuberance; segment III rather short and wide, ca. 0.5× length of segment II, ca. 0.8× as long as width at base, ca. 0.7× as long as maximal width (Fig. 12d; Müller-Liebenau 1984b: fig. 3b); B) incisor of right mandible with ventral denticle (Müller-Liebenau 1984b: fig. 3e; C) dorsal margin of femur with row of ca. 15 long, spine-like setae; no additional row of short setae along margin; no short, stout setae on surface of femur (Fig. 13a; Müller-Liebenau 1984b: fig. 3k); D) posterior margin of tergite I smooth, without spines; posterior margins of tergites II–III with rounded or triangular spines, posterior margins of tergites IV–X with triangular spines (Fig. 13c; Müller-Liebenau 1984b: fig. 14); posterior margins of sternites: I–V smooth, without spines; VI smooth, without spines, or with some small, triangular spines; VII–IX with triangular or blunt spines (Fig. 13d).

**Imago.** Winged stages unknown. Judging from details revealed in last instar larva, turbinate eyes not narrowed; hind wing with costal projection; sterno-styligeral muscle present and thin.

**Comments.** The original description of *Baetis sabahensis* Müller-Liebenau, 1984 was based on larvae, and certain similarities of this species with *B. javanicus* were reported. The single argument to separate *B. sabahensis* from *B. javanicus*, was the statement that "*Baetis sabahensis* sp. nov. is the only species in the genus with coxal gills on the first pair of legs" (Müller-Liebenau 1984b: 92). Larva of *B. javanicus* was described and figured by the same author earlier (Müller-Liebenau 1981), but the coxal and maxillary gills had not been reported (see above).

Larva of *Branchiobaetis sabahensis* comb. nov. can be separated from *B. javanicus* comb. nov. by the following characters: A) dense spines on abdominal sternite VIII

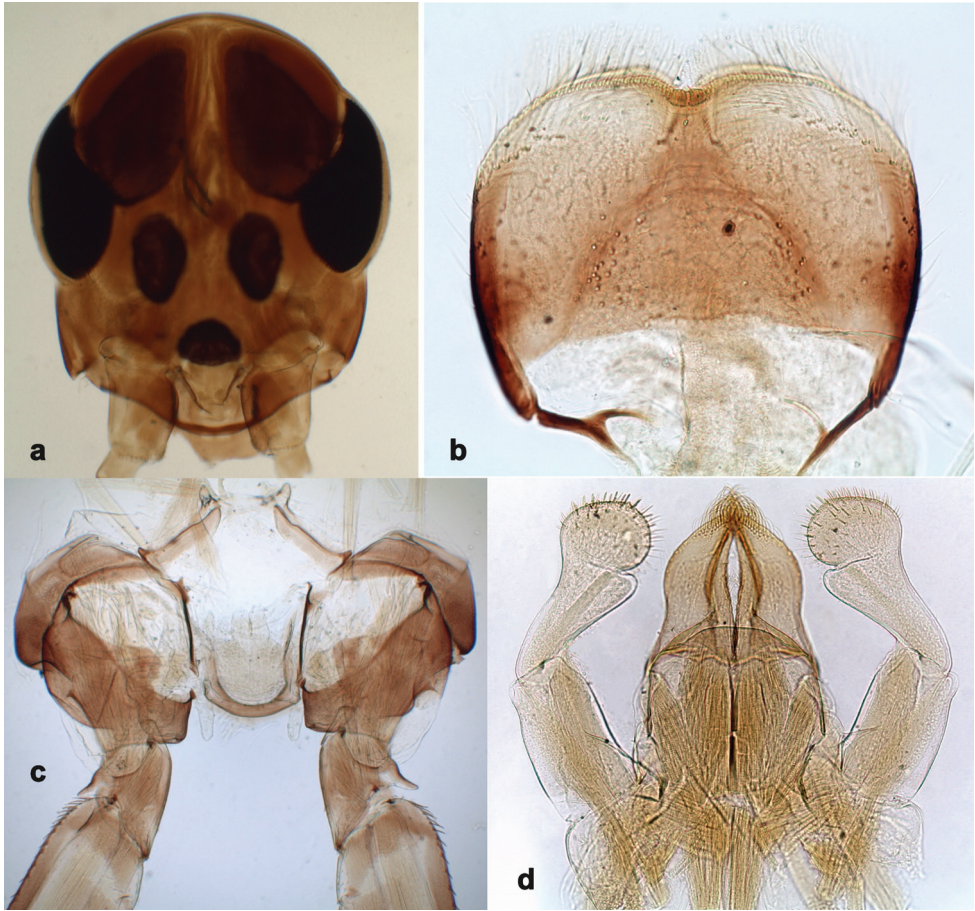


**Figure 12.** *Branchiobaetis sabahensis* comb. nov., larva **a** head of male larva **b** labrum **c** prosternum and bases of forelegs, front view **d** labium.

(Fig. 13d); B) presence of only one or two stout setae on paraproct, or complete absence (Fig. 13b); C) incisor of right mandible with ventral denticle; D) labial palp segment III short and wide (Fig. 12d; see above).

Judging by precursors of turbinate eyes developed in last instar male larva, male imago of *B. sabahensis* comb. nov. should differ from *B. javanicus* comb. nov. by usual (not narrowed) turbinate eyes (Fig. 12a).

*Branchiobaetis* cf. *sabahensis* comb. nov. Specimens from Indonesia (Kalimantan) always have a series of stout setae along posterior margin of paraproct, contrary to specimens from Malaysia (Sabah). As there are no other differentiating characters to *B. sabahensis* comb. nov. from Malaysia (Sabah), we treat this population as *B. cf. sabahensis* comb. nov., waiting for genetic investigation of fresh material in the future.

**Distribution (Fig. 27b).** Malaysia (Borneo: Sabah); *B. cf. sabahensis* comb. nov. Indonesia (Borneo: Kalimantan).

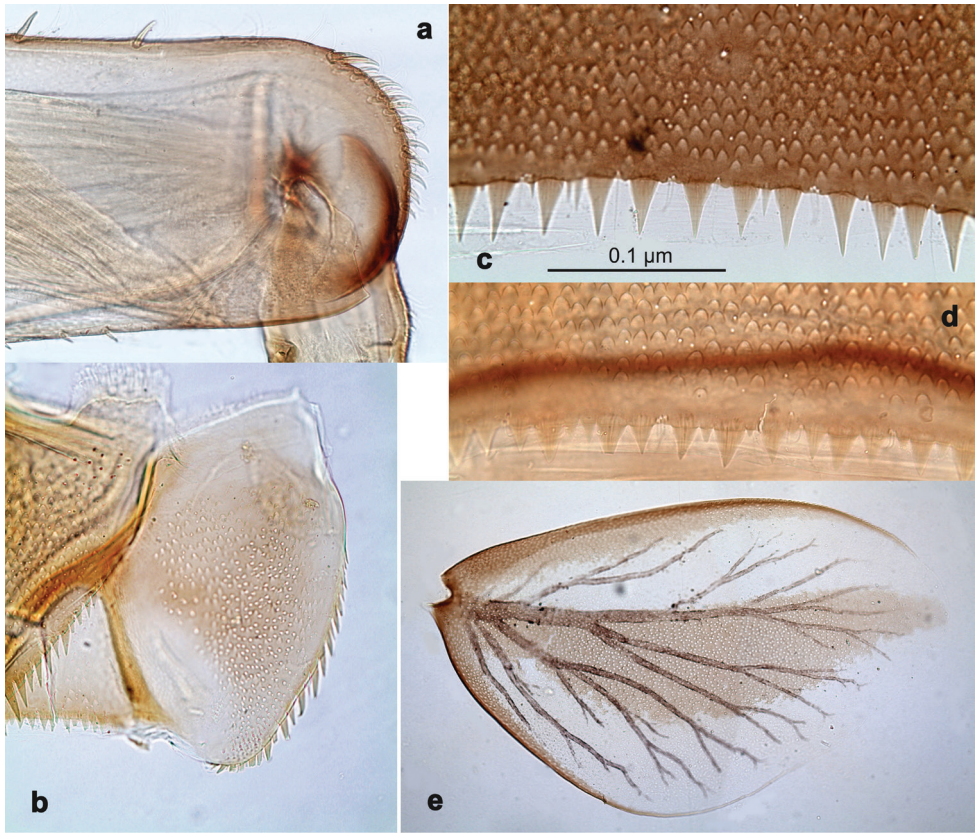


**Figure 13.** *Branchiobaetis sabahensis* comb. nov., larva **a** apex of hind femur **b** paraproct **c** abdominal tergum IX **d** abdominal sternum VIII **e** tergalius.

### 3. *Branchiobaetis aduncus* sp. nov.

<https://zoobank.org/FE94DE11-B90B-42F7-81F8-FB99DA52F090>

Figs 14, 15, 24a, 26a, 28a

**Type material. Holotype.** INDONESIA • Sumatra, volcano Singgalang, River Caruak; 00°23'03"S, 100°21'24"E; 1640 m; 23.III.2014, leg. M. Gueuning; larva on slide; GBIFCH00422219; MZL. **Paratypes.** Same data as holotype; 1 larva on slide; GBIFCH004222126; MZL; 4 larvae in alcohol; GBIFCH004222185, GBIFCH004222194, GBIFCH004222203, GBIFCH004222209; MZL. INDONESIA • Aceh, Mt. Leuser area, Kedah rainforest lodge; 03°58'36"S, 97°15'17"E; 1300 m, 3.–12.X.2013, leg. M. Balke; larva on slide; GBIFCH00515622; MZB (temporarily housed in MZL) • Sumatra Barat, Talang, 20 km south of Solok; 00°52'52"S, 100°37'23"E; 650 m; 25.V.2010; leg. J.-M. Elouard; larva on slide; GBIFCH00592486; MZL.

**Differential diagnosis. Larva.** Following combination of characters distinguish *B. aduncus* sp. nov. from other species of *Branchiobaetis* gen. nov.: A) labial

palp segment II with medium triangular protuberance, segment III apically rounded (Fig. 14j); B) incisor of right mandible with ventral denticle (Fig. 14b, d); C) dorsal margin of femur with row of medium, spine-like setae, basally longer and clavate; additional row of short, hook-like setae along margin (Fig. 15a–c); D) dorsal margin of tibia and tarsus with row of short, hook-like setae (Fig. 15a, c); E) posterior margin of tergites: I smooth, without spines; II–V rounded, wider than long; VI partly rounded, partly triangular; VII–IX triangular, narrower and longer towards last segment (Fig. 15f); posterior margins of sternites: I–VI smooth, without spines; VII–IX with small, spaced, triangular spines; F) paraproct with short, stout, apically rounded setae along posterior margin (Fig. 15h).

**Description. Larva** (Figs 14, 15, 24a, 26a). Body length 7.0–8.1 mm. Caudalii broken. Antenna: ca. 2.5× as long as head length.

**Colouration** (Fig. 24a). Head, thorax, and abdomen dorsally brown, ventrally light brown. Femur light brown, apically and dorsally along margin dark brown, with large, distomedial, dark brown spot; tibia light brown, basally along patella-tibial suture darker, tarsus dark brown. Caudalii light brown, primary swimming setae dark brown.

**Antenna** (Fig. 15i). Scape distally and outside distolaterally with short, stout, apically rounded setae.

**Labrum** (Fig. 14a). Length 0.6× maximum width. Submarginal arc of setae composed of nine or ten long, simple setae.

**Right mandible** (Fig. 14b–d). Incisor blade-like with three denticles and a ventral denticle; kinetodontium with four denticles. Margin between prostheca and mola straight.

**Left mandible** (Fig. 14e–g). Incisor blade-like with four denticles; kinetodontium with three denticles. Margin between prostheca and mola straight, with minute denticles towards subtriangular process.

Both mandibles with lateral margins slightly convex.

**Hypopharynx and superlinguae** (Fig. 14h). Lingua as long as superlinguae. Lingua longer than broad; medial tuft of stout setae well developed. Superlinguae distally rounded; lateral margins rounded; fine, long, simple setae along distal margin.

**Maxilla** (Fig. 14i). Galea-lacinia ventrally with two simple, apical setae under canines. Medially with one pectinate, spine-like seta and six or seven medium, simple setae. Maxillary palp approx. as long as galea-lacinia; palp segment II approx. as long as segment I; setae on maxillary palp fine, simple, scattered over surface of segments I and II.

**Labium** (Fig. 14j, k). Inner margin of glossa with ca. nine spine-like setae, increasing in length distally; apex with one long, one medium and one short, robust setae; outer margin with ca. nine spine-like setae; Paraglossa with three short, simple setae in anteromedial area and one in posterolateral area; dorsally with three long, spine-like setae near inner margin. Labial palp with segment I 1.1× length of segments II and III combined. Segment I ventrally with short, fine, simple setae. Segment II with medium, triangular, distomedial protuberance; distomedial protuberance 0.5× width of base of segment III; ventral surface with short, fine, simple setae; dorsally with five or six spine-like setae near outer margin. Segment III apically rounded; length 0.8× maximum width; ventrally covered with short, spine-like, simple setae and short, fine, simple setae.

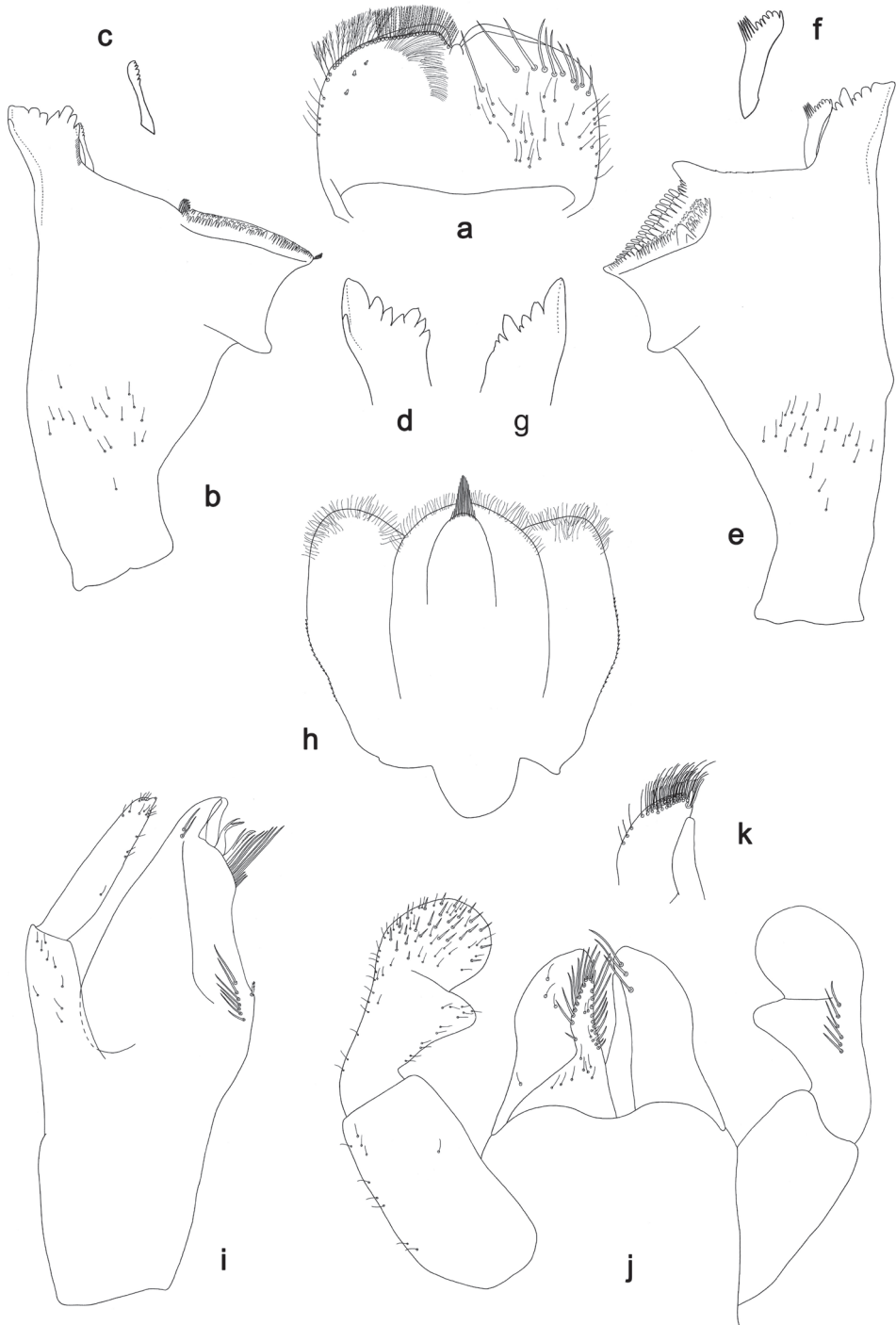


**Figure 14.** *Branchiobaetis aduncus* sp. nov., larva **a** labrum (left: ventral view, right: dorsal view) **b** right mandible **c** right prostheta **d** apex of right mandible **e** left mandible **f** left prostheta **g** apex of left mandible **h** hypopharynx and superlinguae **i** maxilla **j** labium (left: ventral view, right: dorsal view) **k** apex of paraglossa.

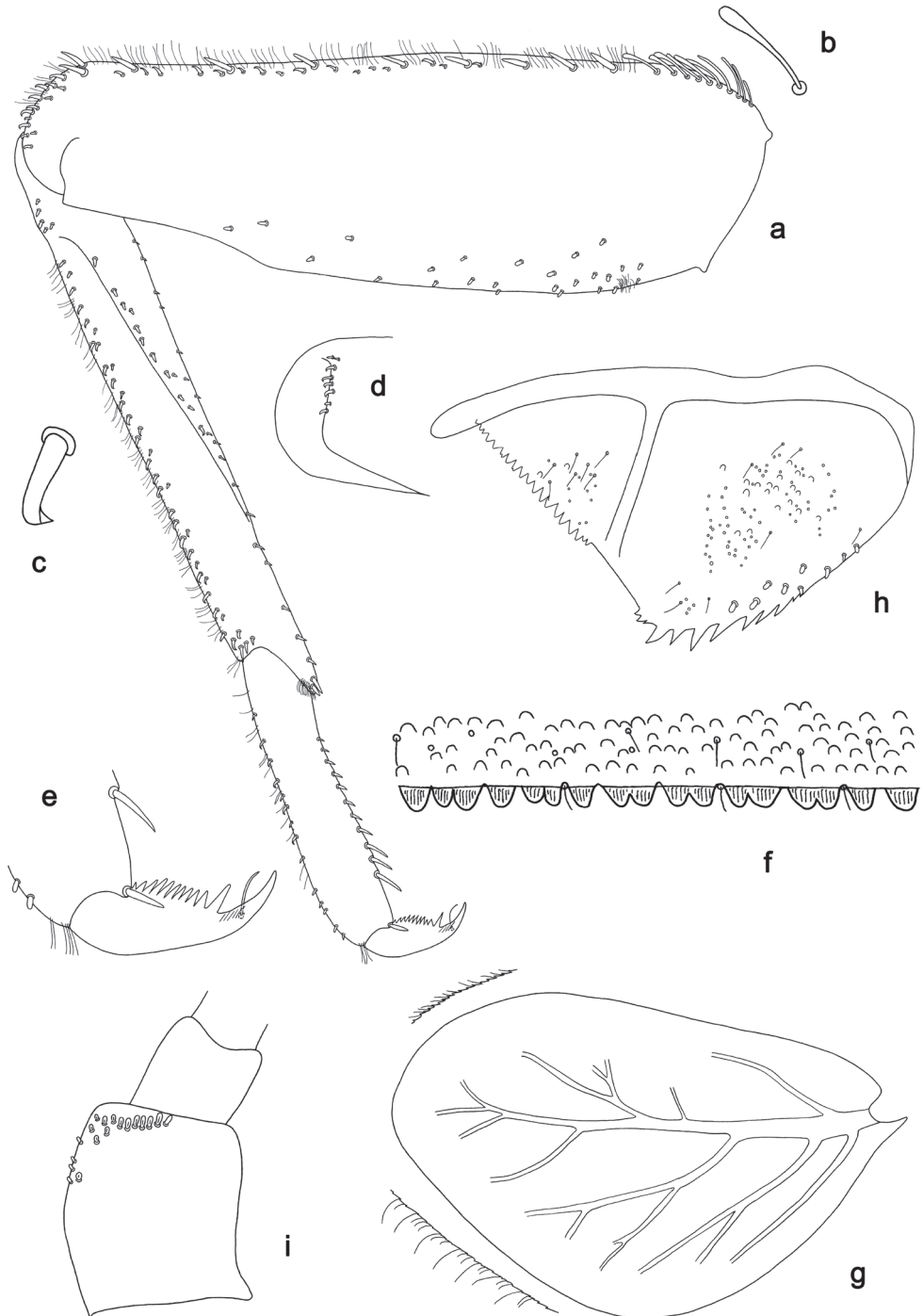


**Figure 15.** *Branchiobaetis aduncus* sp. nov., larva **a** foreleg **b** seta of femur basal dorsal margin **c** hook-like seta of leg dorsal margins **d** fore femur apex, posterior view **e** fore claw **f** tergum IV **g** tergalis IV **h** paraproct **i** base of antenna.

**Foreleg** (Fig. 15a–e). Ratio of foreleg segments 1.3:1.0:0.5:0.2. **Femur**. Length ca. 3× maximum width. Dorsal margin with row of 6–9 medium, curved, spine-like setae and basally 10–12 longer, clavate setae. Additional row of short, stout, hook-like setae along dorsal margin. Apex rounded, with pair of spine-like setae; short, stout, hook-like setae on anterior and posterior side. Short, stout, apically rounded setae scattered along ventral margin. **Tibia**. Dorsal margin with two irregular rows of short, stout, hook-like setae. Surface with short, stout, hook-like setae along patella-tibial suture. Ventral margin with row of short, curved, spine-like setae, on apex a tuft of fine, simple setae. **Tarsus**. Dorsal margin with row of short, stout, hook-like setae and row of fine, simple setae. **Claw** with one row of ten or eleven denticles, distal denticle much longer than other denticles.

**Terga** (Fig. 15f). Surface with irregular rows of U-shaped scale bases and scattered fine, simple setae. Posterior margin of tergites: I smooth, without spines; II–V rounded, wider than long; VI partly rounded, partly triangular; VII–IX triangular, narrower and longer towards last segment. Posterior margins of sternites: I–VI smooth, without spines; VII–IX with small, spaced, triangular spines.

**Tergalii** (Figs 15g, 26a). Tracheae extending from main trunk to inner and outer margins; with light brown band along main trunk of tracheae on anal side. Tergalium I 2/3 as long as segment II, tergalium IV as long as length of segments V and 1/3 VI combined, tergalium VII as long as length of segment VIII.

**Paraproct** (Fig. 15h). Posterior margin with 12–16 stout spines. Short, stout, apically rounded setae near posterior margin. Surface scattered with scale bases, micropores and fine, simple setae.

**Etymology.** Based on the Latin word *aduncus*, meaning hooked, with reference to the hook-like setae on the legs.

**Distribution.** Indonesia: Sumatra (Fig. 28a).

**Biological aspects.** The species was found at altitudes from 650 m to 1640 m, most specimens were collected in a forest stream with the following parameters: slope below 5%, width 1–3 m, depth 15–30 cm, velocity 0.2 m/s, water temperature 17 °C, pH 7, stream bed dominated by boulder, stones, and gravel.

#### 4. *Branchiobaetis hamatus* sp. nov.

<https://zoobank.org/4C505602-E896-4CA6-99BE-EFF79C82DBDF>

Figs 16, 17, 24b, 26b, 28a

**Type material. Holotype.** INDONESIA • Sumatra, volcano Talamau; River Pularian; 00°00'60"N, 100°00'01"E; 960 m; 01.IV.2014; leg. M. Gueuning; larva on slide; GBIFCH00422261; MZL. **Paratypes.** Same data as holotype; 2 larvae on slides; GBIFCH00422231, GBIFCH00422242; 20 larvae in alcohol; GBIFCH00422233, GBIFCH00422252, GBIFCH00422267, GBIFCH00422276, GBIFCH00422355, GBIFCH00422359, GBIFCH00422445, GBIFCH00422748, GBIFCH00422753, GBIFCH00422798, GBIFCH00422843, GBIFCH00423022, GBIFCH00975634,

GBIFCH00975635; MZL. INDONESIA • Sumatra, volcano Singgalang, River Sianok; 00°19'57"S, 100°19'19"E; 1150 m; 24.III.2014; leg. M. Gueuning; 2 larvae on slides; GBIFCH00422184, GBIFCH00423074; 13 larvae in alcohol; GBIFCH00422123, GBIFCH00422167, GBIFCH00422206, GBIFCH004208, GBIFCH00422215, GBIFCH00422216, GBIFCH00422224, GBIFCH00422797, GBIFCH00422889, GBIFCH00422938, GBIFCH01115975, GBIFCH01116020; MZL.

**Differential diagnosis. Larva.** Following combination of characters distinguish *B. hamatus* sp. nov. from other species of *Branchiobaetis* gen. nov.: A) labial palp segment II with medium, rounded protuberance, segment III apically slightly pointed (Fig. 16h); B) incisor of right mandible with ventral denticle (Fig. 16b); C) dorsal margin of femur with row of medium, spine-like setae, basally longer and clavate; additional row of short, hook-like setae along margin (Fig. 17a, b); D) dorsal margin of tibia and tarsus with row of short, hook-like setae (Fig. 17a, b); E) posterior margin of tergites: I smooth, without spines; II–IX triangular, narrower and longer towards last segment (Fig. 17e); posterior margin of sternites: I–VII smooth, without spines; VIII–IX with small, spaced, triangular spines; F) tergalium IV apically slightly concave (Fig. 17f); G) paraproct with short, stout, apically rounded setae along posterior margin (Fig. 17g).

**Description. Larva** (Figs 16, 17, 24b, 26b). Body length 6.8–8.5 mm. Cerci broken. Paracercus: ca. 0.4× body length. Antenna: ca. 2.5× as long as head length.

**Colouration** (Fig. 24b). Head, thorax and abdomen dorsally brown, abdominal segment X light brown; head, thorax and abdomen ventrally light brown, scape with dark brown spot at inner lateral side. Femur light brown, apically and dorsally along margin dark brown, with large, medial, dark brown spot; tibia light brown, tarsus dark brown in distal half. Caudalium light brown, cerci darker brown in area of ca. ½ of length, paracercus darker brown parallel to cerci; primary swimming setae dark brown.

**Precursors of turbinate eyes** (Fig. 25c) in male last instar larvae representing a pair of subtriangular maculae; in the middle of this macula, a smaller, round, elevated area with well-expressed facets, approx. ten facets in diameter; peripheral area of the macula with indistinct facets.

**Antenna** (Fig. 17h). Scape distally and outside distolaterally with short, stout, apically rounded setae.

**Labrum** (Fig. 16a). Length 0.6× maximum width. Submarginal arc of setae composed of 7–10 long, simple setae.

**Right mandible** (Fig. 16b, c). Incisor blade-like with three denticles and a ventral denticle; kinetodontium with four denticles. Margin between prostheca and mola straight, with minute denticles.

**Left mandible** (Fig. 16d, e). Incisor blade-like with four denticles; kinetodontium with three denticles. Margin between prostheca and mola straight, with minute denticles towards subtriangular process.

Both mandibles with lateral margins slightly convex.

**Hypopharynx and superlinguae** (Fig. 16f). Lingua as long as superlinguae. Lingua longer than broad; medial tuft of stout setae well developed. Superlinguae distally rounded; lateral margins rounded; fine, long, simple setae along distal margin.

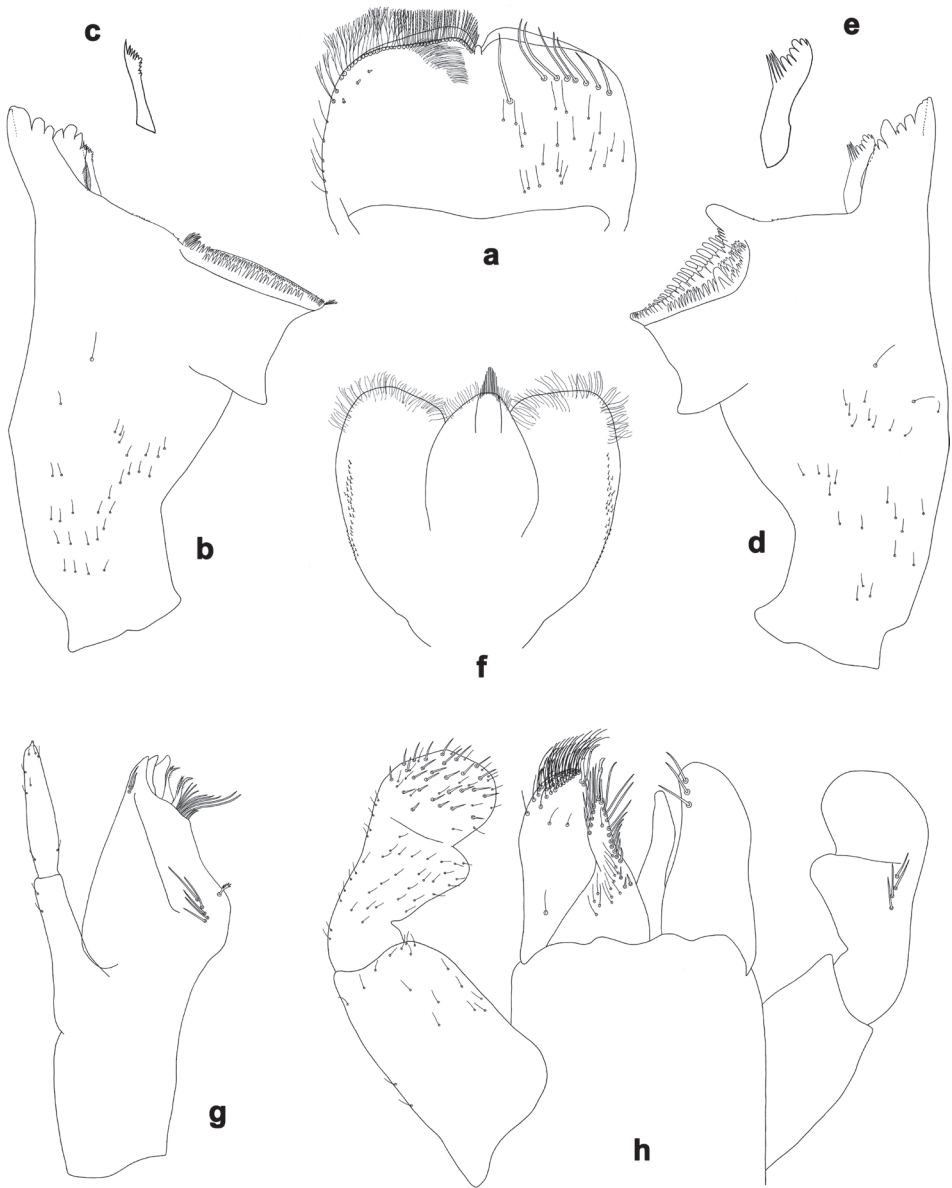


**Figure 16.** *Branchiobaetis hamatus* sp. nov., larva **a** labrum (left: ventral view, right: dorsal view) **b** right mandible **c** right prosthema **d** left mandible **e** left prosthema **f** hypopharynx and superlinguae **g** maxilla **h** labium (left: ventral view, right: dorsal view).

**Maxilla** (Fig. 16g). Galea-lacinia ventrally with two simple, apical setae under canines. Medially with one pectinate, spine-like seta and five or six medium, simple setae. Maxillary palp approx. as long as galea-lacinia; palp segment II approx. as long as segment I; setae on maxillary palp fine, simple, scattered over surface of segments I and II.

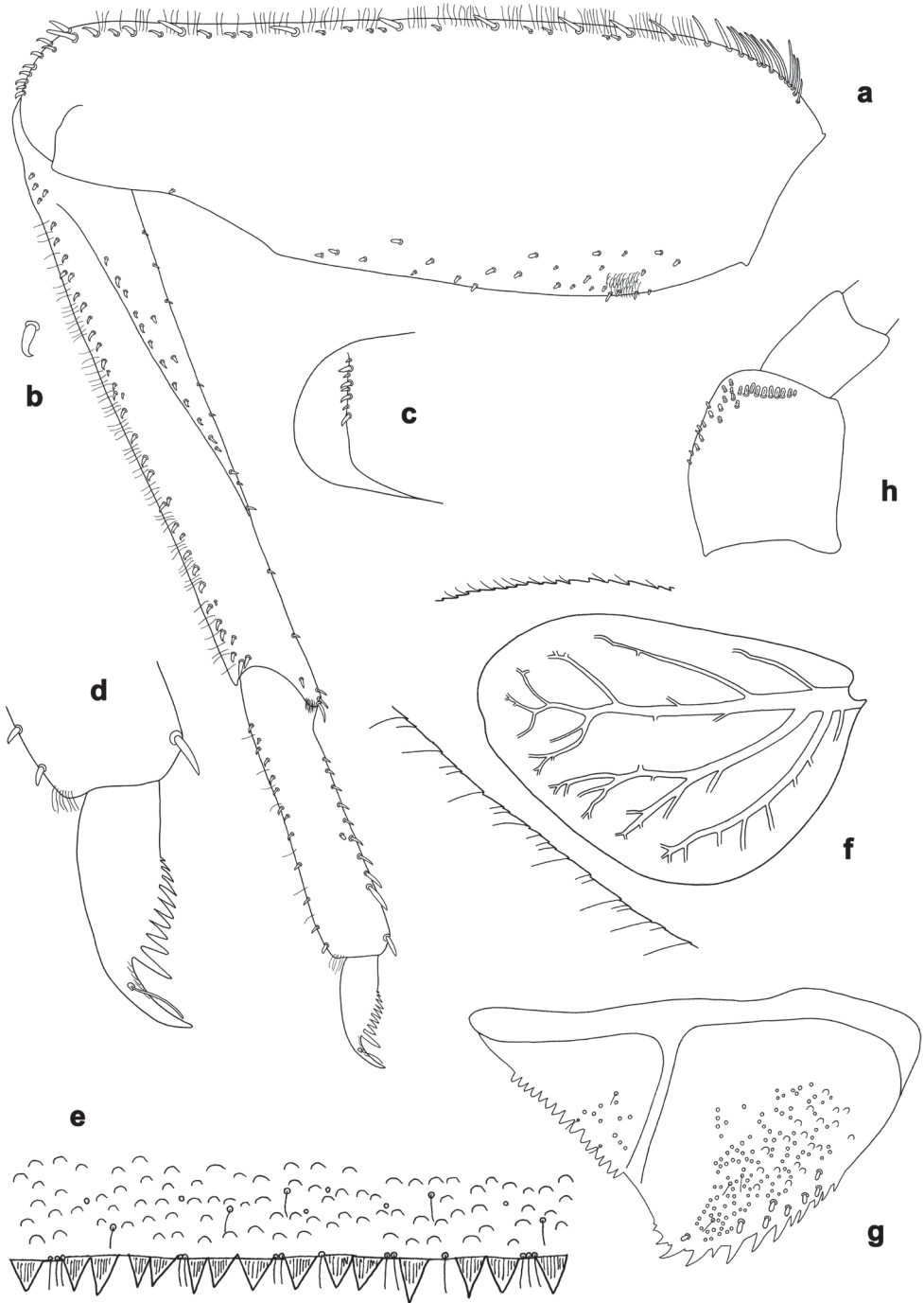


**Figure 17.** *Branchiobaetis hamatus* sp. nov., larva **a** foreleg **b** hook-like seta of leg dorsal margins **c** femur apex, posterior view **d** fore claw **e** tergum IV **f** tergalium IV **g** paraproct **h** base of antenna.

**Labium** (Fig. 16h). Inner margin of glossa with 10–12 spine-like setae, increasing in length distally; apex with two long and one medium, robust setae; outer margin with six or seven spine-like setae; Paraglossa with two short, simple setae in antero-medial area and one in posterolateral area; dorsally with three long, spine-like setae near inner margin. Labial palp with segment I approx. as long as length of segments II and III combined. Segment I ventrally with short, fine, simple setae. Segment II with medium, rounded, distomedial protuberance; distomedial protuberance 0.3× width of base of segment III; ventral surface with short, fine, simple setae; dorsally with 4–8 spine-like setae near outer margin. Segment III apically slightly pointed; length 0.8× maximum width; ventrally covered with short, spine-like, simple setae and short, fine, simple setae.

**Foreleg** (Fig. 17a–d). Ratio of foreleg segments 1.3:1.0:0.5:0.2. **Femur**. Length ca. 3× maximum width. Dorsal margin with row of 7–9 medium, curved, spine-like setae and basally 10–15 longer, clavate setae. Additional row of short, stout, hook-like setae along dorsal margin. Apex rounded, with pair of spine-like setae; short, stout, hook-like setae on anterior and posterior side. Short, stout, apically rounded setae scattered along ventral margin. **Tibia**. Dorsal margin with two irregular rows of short, stout, hook-like setae. On surface short, stout, hook-like setae along patella-tibial suture. Ventral margin with row of short, curved, spine-like setae, on apex a tuft of fine, simple setae. **Tarsus**. Dorsal margin with row of short, stout, hook-like setae and row of fine, simple setae. **Claw** with one row of ten or eleven denticles, distal denticle much longer than other denticles.

**Terga** (Fig. 17e). Surface with irregular rows of U-shaped scale bases and scattered fine, simple setae. Posterior margin of tergites: I smooth, without spines; II–IX triangular, narrower and longer towards last segment. Posterior margin of sternites: I–VII smooth, without spines; VIII–IX with small, spaced, triangular spines.

**Tergalii** (Figs 17f, 26b). Tracheae extending from main trunk to inner and outer margins; with light brown band along main trunk of tracheae on anal side. Tergalium I  $\frac{2}{3}$  as long as segment II, tergalium IV as long as length of segments V and  $\frac{1}{2}$  VI combined, tergalium VII as long as length of segment VIII.

**Paraproct** (Fig. 17g). Posterior margin with 11–16 stout spines. Short, stout, apically rounded setae near posterior margin. Surface scattered with scale bases, micropores and fine, simple setae.

**Etymology**. Based on the Latin word *hamatus*, meaning hooked, with reference to the hook-like setae on the legs.

**Distribution**. Indonesia: Sumatra (Fig. 28a).

**Biological aspects**. The specimens were collected in two sites at altitudes of 940 m and 1150 m, with following physical conditions: slope 5–10%, width of stream 3–8 m, depth 1–50 cm, velocity 0.5 m/s–0.7 m/s, pH 8, stream bed dominated by boulder, stones and gravel or stones and sand respectively. One of the sites was strongly influenced by human activities, with lot of waste and brown water.

**5. *Branchiobaetis joachimi* sp. nov.**

<https://zoobank.org/442848A3-531A-428C-827B-99A2D71D2C78>

Figs 18, 19, 24c, d, 26c, 28b

**Type material. Holotype.** INDONESIA • Sumatra, volcano Marapi, East; 00°21'33"S, 100°30'42"E; 1205 m; 03.IV.2014; leg. M. Gueuning; larva on slide; GBIF-CH00422405; MZL. **Paratypes.** Same data as holotype; 19 larvae in alcohol; GBIFCH00422228, GBIFCH00422235, GBIFCH00422238, GBIFCH00422241, GBIFCH00422254, GBIFCH00422266, GBIFCH00422402, GBIFCH00422440, GBIFCH00422489, GBIFCH00422709, GBIFCH00422844, GBIFCH00422887, GBIFCH00422932, GBIFCH00422977; MZL. INDONESIA • Sumatra, volcano Sago, River Kobun; 00°22'33"S, 100°39'33"E; 1095 m; 19.III.2014; leg. M. Gueuning; 2 larvae on slide; GBIFCH00592506, GBIFCH00592507; 22 larvae in alcohol; GBIFCH00422152, GBIFCH00422166, GBIFCH00422173, GBIFCH00422222, GBIFCH00422226, GBIFCH00422227, GBIFCH00422253, GBIFCH00422256, GBIFCH00422258, GBIFCH00422266, GBIFCH00422268, GBIFCH00422270, GBIFCH00422663, GBIFCH00422708, GBIFCH00422754, GBIFCH00422928, GBIFCH00422979, GBIFCH00423113; MZL • Sumatra, volcano Sago, River Tampo; 00°22'20"S, 100°41'45"E; 960 m; 20.III.2014; leg. M. Gueuning; 8 larvae in alcohol; GBIFCH00422232, GBIFCH00422239, GBIFCH00422249, GBIFCH00422250, GBIFCH00422255, GBIFCH00422265, GBIFCH00422619, GBIFCH00423112; MZL • Sumatra, volcano Sago, River Tampo; 00°20'37"S, 100°41'02"E; 1255 m; 21.III.2014; leg. M. Gueuning; 12 larvae in alcohol; GBIFCH00422230, GBIFCH00422236, GBIFCH00422237, GBIFCH00422243, GBIFCH00422251, GBIFCH00422264, GBIFCH00422883, GBIFCH00423026, GBIFCH00423068, GBIFCH00423116; MZL • Sumatra, volcano Sago, River Kaligain; 00°18'01"S, 100°40'08"E; 1040 m; 05.IV.2014; leg. M. Gueuning; 1 larva on slide; GBIFCH00592525; 22 larvae in alcohol; GBIFCH00422229, GBIFCH00422234, GBIFCH00422244, GBIFCH00422246, GBIFCH00422259, GBIFCH00422263, GBIFCH00422304, GBIFCH00422441, GBIFCH00422442, GBIFCH00422443, GBIFCH00422659, GBIFCH00975612, GBIFCH00975613; MZL • Sumatra, volcano Singgalang, River Airjernih; 00°24'07"S, 100°16'44"E; 840 m; 25.III.2014; leg. M. Gueuning; 1 larva on slide; GBIFCH00422159; 7 larvae in alcohol; GBIFCH00422052, GBIFCH00422142, GBIFCH00422157, GBIFCH00422160, GBIFCH00422618, GBIFCH00422752, GBIFCH00423024; MZL • Sumatra, volcano Singgalang, River Magyih; 00°23'33"S, 100°16'34"E; 845 m; 25.III.2014; leg. M. Gueuning; 1 larva on slide; GBIFCH00422211; 5 larvae in alcohol; GBIFCH00422081, GBIFCH00422154, GBIFCH00422198, GBIFCH00422201, GBIFCH00422217; MZL • Sumatra, volcano Singgalang, River Magyih; 00°22'50"S, 100°17'39"E; 1075 m; 26.III.2014; leg. M. Gueuning; 3 larvae in alcohol; GBIFCH00422098, GBIFCH00422168, GBIFCH00422221; MZL • Sumatra, volcano Singgalang, River Sianok; 00°19'57"S, 100°19'19"E; 1150 m; 24.03.2014; leg. M. Gueuning; 1 larva in alcohol; GBIFCH00422248; MZL.

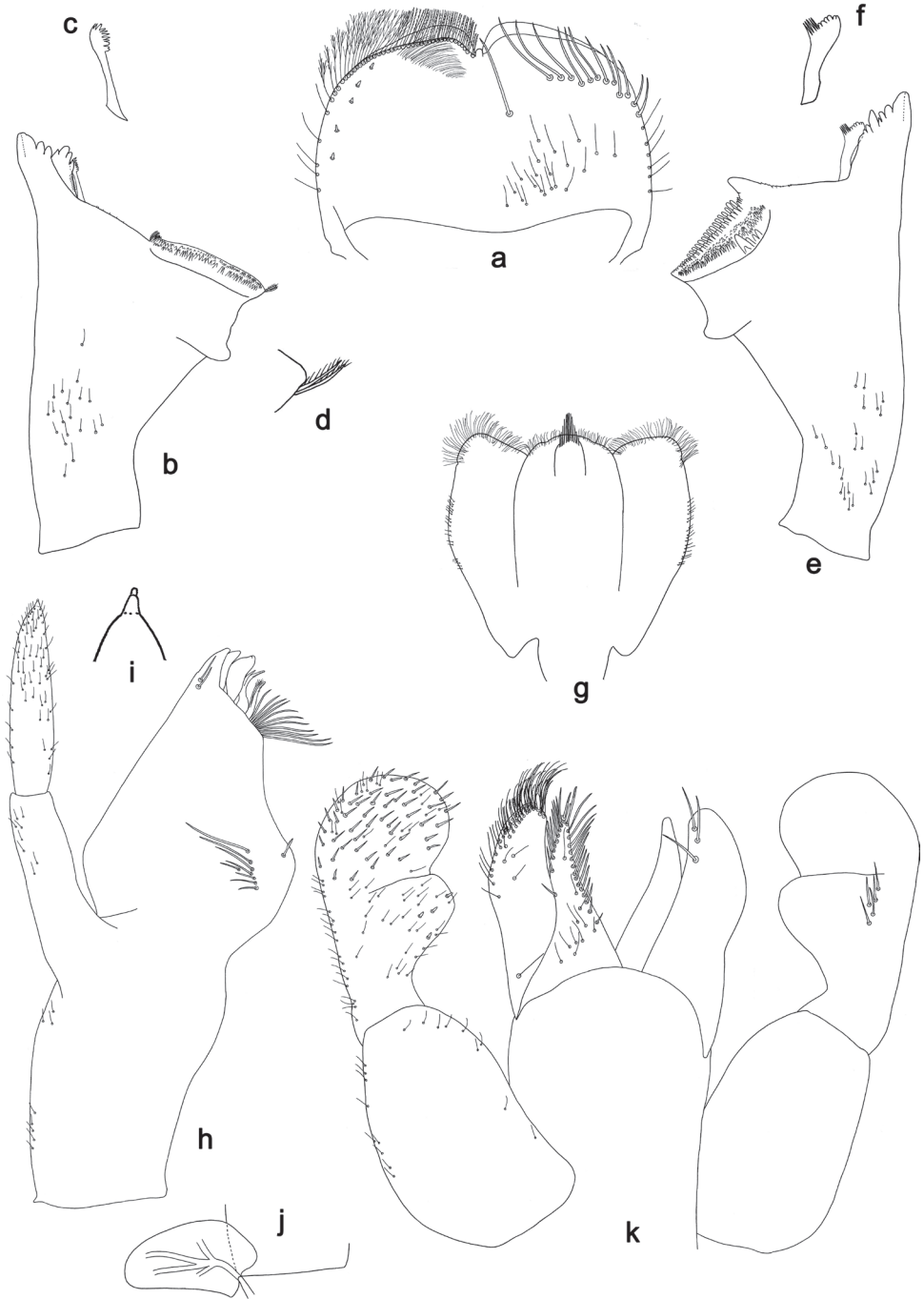


**Figure 18.** *Branchiobaetis joachimi* sp. nov., larva **a** labrum (left: ventral view, right: dorsal view) **b** right mandible **c** right prosthema **d** mola apex of right mandible **e** left mandible **f** left prosthema **g** hypopharynx and superlinguae **h** maxilla **i** apex of maxillary palp **j** accessory gill between stipes and cardo of maxilla **k** labium (left: ventral view, right: dorsal view).

**Other material.** INDONESIA • Sumatra Barat, Bukit Barisan, above Padang, creek; 00°56'44"S, 100°32'44"E; 1047 m; 08.XI.2011; leg. M. Balke (UN3); 3 larvae on slides; GBIFCH00592472, GBIFCH00592473, GBIFCH00592505; 17 larvae in alcohol; GBIFCH00975598, GBIFCH00975599, GBIFCH00975602, GBIFCH00980897, GBIFCH00980898; MZL.

**Differential diagnosis. Larva.** Following combination of characters distinguish *B. joachimi* sp. nov. from other species of *Branchiobaetis* gen. nov.: A) labial palp segment II with short, broad, rounded protuberance, with few small, stout, simple setae on protuberance; segment III apically rounded (Fig. 18k); B) dorsal margin of femur with row of medium, spine-like setae; many short, stout, apically rounded setae along dorsal margin; same type of setae scattered on surface and along ventral margin (Fig. 19a, c); C) posterior margin of tergites: I with triangular, pointed spines or short, triangular, blunt spines; II–IX with triangular, pointed spines, longer than wide (Fig. 19f); posterior margin of sternites: I–IV smooth, without spines; V with small, spaced, triangular spines; VI–IX with triangular spines; D) paraproct with short, stout, apically rounded setae along posterior margin (Fig. 19h).

**Description. Larva** (Figs 18, 19, 24c, d, 26c). Body length 7.9–9.6 mm. Cerci: ca. 0.6× body length. Paracercus: ca. 0.6× cerci length. Antenna: ca. 2.5× as long as head length.

**Colouration** (Fig. 24c, d). Head, thorax and abdomen dorsally brown or grey-brown, with pattern as in Fig. 24c or 24d; head, thorax and abdomen ventrally light brown or light grey, abdominal segment IX laterally with dark brown streaks. Femur light brown or light grey, apically and dorsally along margin dark brown, with large, distomedial, dark brown spot; tibia light brown or grey, basally dark brown along patella-tibial suture; tarsus light brown or grey, dark brown in distal half. Caudalii light grey-brown, darker brown area on ca. ½ of cerci length; primary swimming setae dark brown.

**Precursors of turbinate eyes** in male last instar larvae representing a pair of brownish, egg-shaped maculae; in the middle of this macula, a smaller, round, elevated area with well-expressed facets, ca. 14 facets in diameter; peripheral area of the macula with indistinct facets (Figs 24c, d, 25d).

**Antenna** (Fig. 19i). Scape distally and outside distolaterally with short, stout, apically rounded setae.

**Labrum** (Fig. 18a). Length 0.6× maximum width. Submarginal arc of setae composed of 10–12 long, simple setae.

**Right mandible** (Fig. 18b–d). Incisor blade-like with three denticles; kinetodontium with four denticles. Margin between prostheca and mola straight, with minute denticles.

**Left mandible** (Fig. 18e, f). Incisor blade-like with four denticles; kinetodontium with three denticles. Margin between prostheca and mola straight, with minute denticles towards subtriangular process.

Both mandibles with lateral margins almost straight.

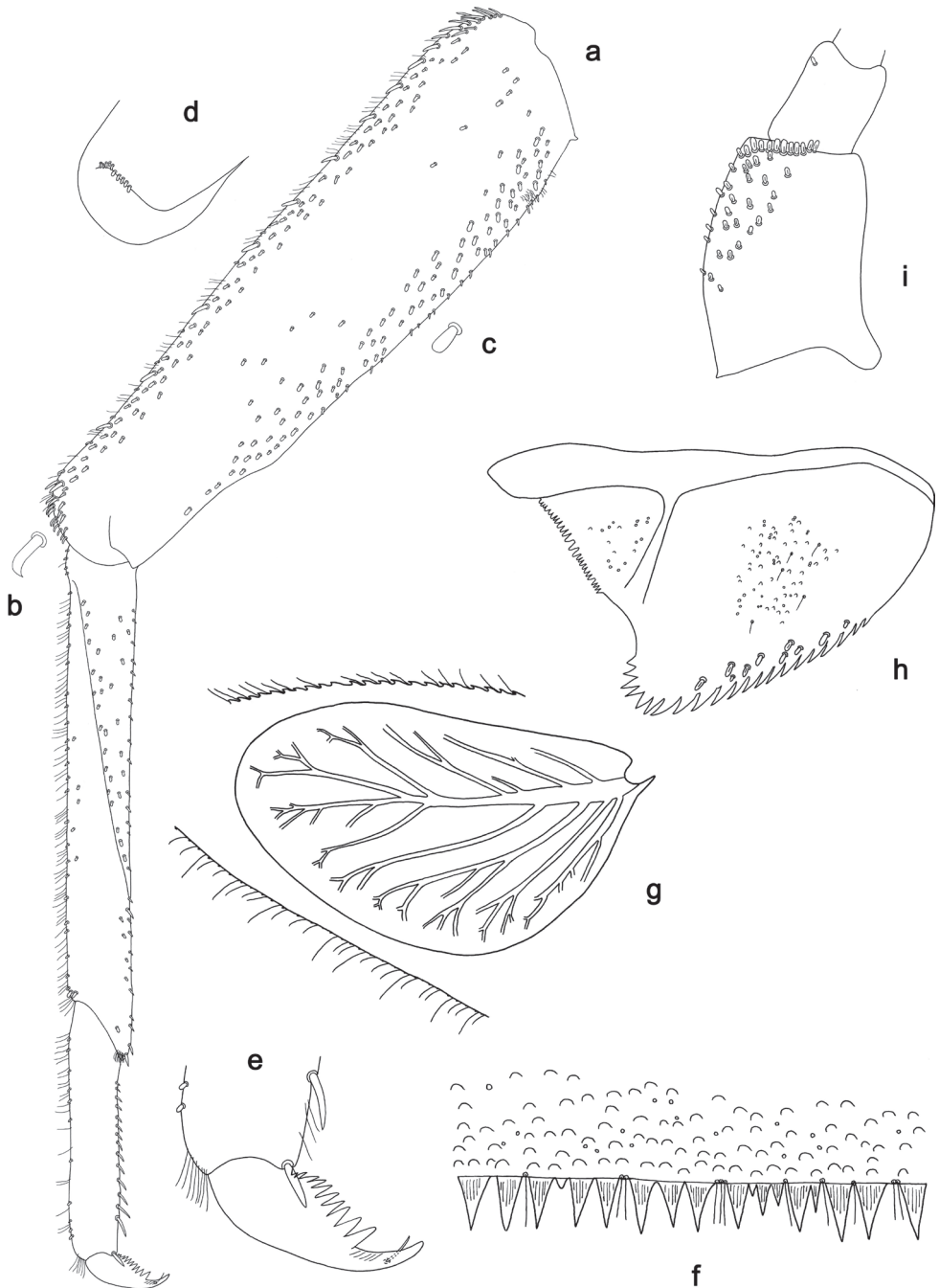


**Figure 19.** *Branchiobaetis joachimi* sp. nov., larva **a** foreleg **b** hook-like seta of femur apex **c** seta on ventral surface of femur **d** fore femur apex, posterior view **e** fore claw **f** tergum IV **g** tergalis IV **h** paraproct **i** base of antenna.

**Hypopharynx and superlinguae** (Fig. 18g). Lingua as long as superlinguae. Lingua longer than broad; medial tuft of stout setae well developed. Superlinguae distally rounded; lateral margins rounded; fine, long, simple setae along distal margin.

**Maxilla** (Fig. 18h, i). Galea-lacinia ventrally with two simple, apical setae under canines. Medially with one pectinate, spine-like seta and 8–11 short to long, simple setae, not all in a row. Maxillary palp slightly longer than galea-lacinia; palp segment II ca. 1.2× as long as segment I; setae on maxillary palp fine, simple, scattered over surface of segments I and II.

**Labium** (Fig. 18k). Inner margin of glossa with ca. 14 spine-like setae, increasing in length distally; apex with two long and one medium, robust setae; outer margin with approx. nine spine-like setae; Paraglossa with three or four short, simple setae in anteromedial area and one in posterolateral area; dorsally with three long, spine-like setae near inner margin. Labial palp with segment I approx. as long as length of segments II and III combined. Segment I ventrally with short, fine, simple setae. Segment II with short, broad, rounded, distomedial protuberance; distomedial protuberance 0.2× width of base of segment III; ventral surface with short, fine, simple setae and some short, stout, simple setae; dorsally with 4–6 spine-like setae near outer margin. Segment III about semi-circular, apically rounded; length 0.8× maximum width; ventrally covered with short, spine-like, simple setae and short, fine, simple setae.

**Foreleg** (Fig. 19a–e). Ratio of foreleg segments 1.5:1.0:0.5:0.2. **Femur**. Slender, length ca. 4× maximum width. Dorsal margin with row of 8–10 medium, curved, spine-like setae and basally 8–10 setae of same type, but standing denser and in more than one row. Further row of short, stout, hook-like setae on distal half of margin. Additionally many short, stout, apically rounded setae along dorsal margin. Same type of setae also on surface and many scattered along ventral margin. Apex rounded, with pair of medium, curved, spine-like setae and many short, hook-like setae. **Tibia**. Dorsal margin with row of short, stout, apically rounded setae. On surface same type of setae along patella-tibial suture. Ventral margin with row of short, curved, spine-like setae, on apex a tuft of fine, simple setae. **Tarsus**. Dorsal margin with row of short, stout setae and row of fine, simple setae. **Claw** with one row of ten denticles.

**Terga** (Fig. 19f). Surface with irregular rows of U-shaped scale bases and scattered micropores. Posterior margin of tergites: I with triangular, pointed spines or short, triangular, blunt spines; II–IX with triangular, pointed spines, longer than wide. Posterior margin of sternites: I–IV smooth, without spines; V with small, spaced, triangular spines; VI–IX with triangular spines.

**Tergalii** (Figs 19g, 26c). Tracheae extending from main trunk to inner and outer margins; with light brown band along main trunk of tracheae on anal side. Tergalium I  $\frac{3}{4}$  as long as segment II, tergalium IV as long as length of segments V and  $\frac{1}{2}$  VI combined, tergalium VII as long as length of segments VIII and  $\frac{1}{4}$  IX combined.

**Paraproct** (Fig. 19h). Posterior margin with 18–21 stout spines. Short, stout, apically rounded setae near posterior margin. Surface scattered with scale bases, micropores and fine, simple setae.

**Etymology.** Dedicated to Joachim Kaltenbach, the late father of the first author.

**Distribution.** Indonesia: Sumatra (Fig. 28b).

**Biological aspects.** The specimens were collected on altitudes between 845 m and 1270 m, in the following physical conditions: slope 5–10%, width of stream 0.2–8 m, depth 7–40 cm, velocity 0.3 m/s–0.8 m/s, pH 6.5–7.5, stream bed dominated by boulder, stones and gravel and only exceptionally by sand and silt. Some of the sites were influenced or polluted by human activities.

**6. *Branchiobaetis minangkabau* sp. nov.**

<https://zoobank.org/B434954C-6136-4B65-9810-804B6B5581C9>

Figs 20, 21, 25a, 26d, 28b

**Type material. Holotype.** INDONESIA • Sumatra, volcano Talamau, River Pularian; 00°02'15"S, 99°59'24"E; 960 m; 01.IV.2014; leg. M. Gueuning; larva on slide; GBIFCH00592524; MZL. **Paratypes.** Same data as holotype; larva on slide; GBIFCH00422480; MZL; 18 larvae in alcohol; GBIFCH00406299, GBIFCH00406308, GBIFCH00406398, GBIFCH00406407, GBIFCH00422240, GBIFCH00422245, GBIFCH00422247, GBIFCH00422257, GBIFCH00422262, GBIFCH00422269, GBIFCH00422481, GBIFCH00422527, GBIFCH00422534, GBIFCH00423110, GBIFCH00980904; MZL. INDONESIA • West Sumatra, Sawahlunto, Talawi Hilir, Dusun Talimato, UB Farm; 0°35'52"S, 100°43'02"E; 305 m; 25.X.2013; leg. M. Balke; larva on slide; GBIFCH00763628; MZB (temporarily housed in MZL); larva on slide; GBIFCH00592445; MZL; 2 larvae in alcohol; GBIFCH00975608, GBIFCH00980900; MZL.

**Differential diagnosis. Larva.** Following combination of characters distinguish *B. minangkabau* sp. nov. from other species of *Branchiobaetis* gen. nov.: A) labial palp segment II with small protuberance; segment III slightly pentagonal, apically slightly concave, with projecting point (Fig. 20h); B) dorsal margin of femur with row of long, spine-like setae, denser in basal area (Fig. 21a); C) posterior margin of tergites: I smooth, without spines; II–IV with rounded spines, wider than long, partly fused at base; V–IX with triangular spines, narrower and longer towards last segment (Fig. 21d); posterior margin of sternites: I–VI smooth, without spines; VII and VIII with small, spaced, triangular spines; IX with small, triangular spines; D) paraproct without short, stout, apically rounded setae along posterior margin (Fig. 21f).

**Description. Larva** (Figs 20, 21, 25a, 26d). Body length 6.5–8.5 mm. Cerci: ca. 2/3 of body length. Paracercus: ca. 1/2 cerci length. Antenna: ca. 2.5× as long as head length.

**Colouration** (Fig. 25a). Head, thorax and abdomen dorsally brown, abdominal segments I and X lighter, abdomen laterally on segments II–IX whitish; head, thorax and abdomen ventrally light brown. Legs with dark brown coxae, femur light brown, apically and dorsally along margin dark brown, with large, medial, dark brown spot; tibia light brown; tarsus basally light brown, dark brown in distal half. Caudalii light brown, primary swimming setae dark brown.

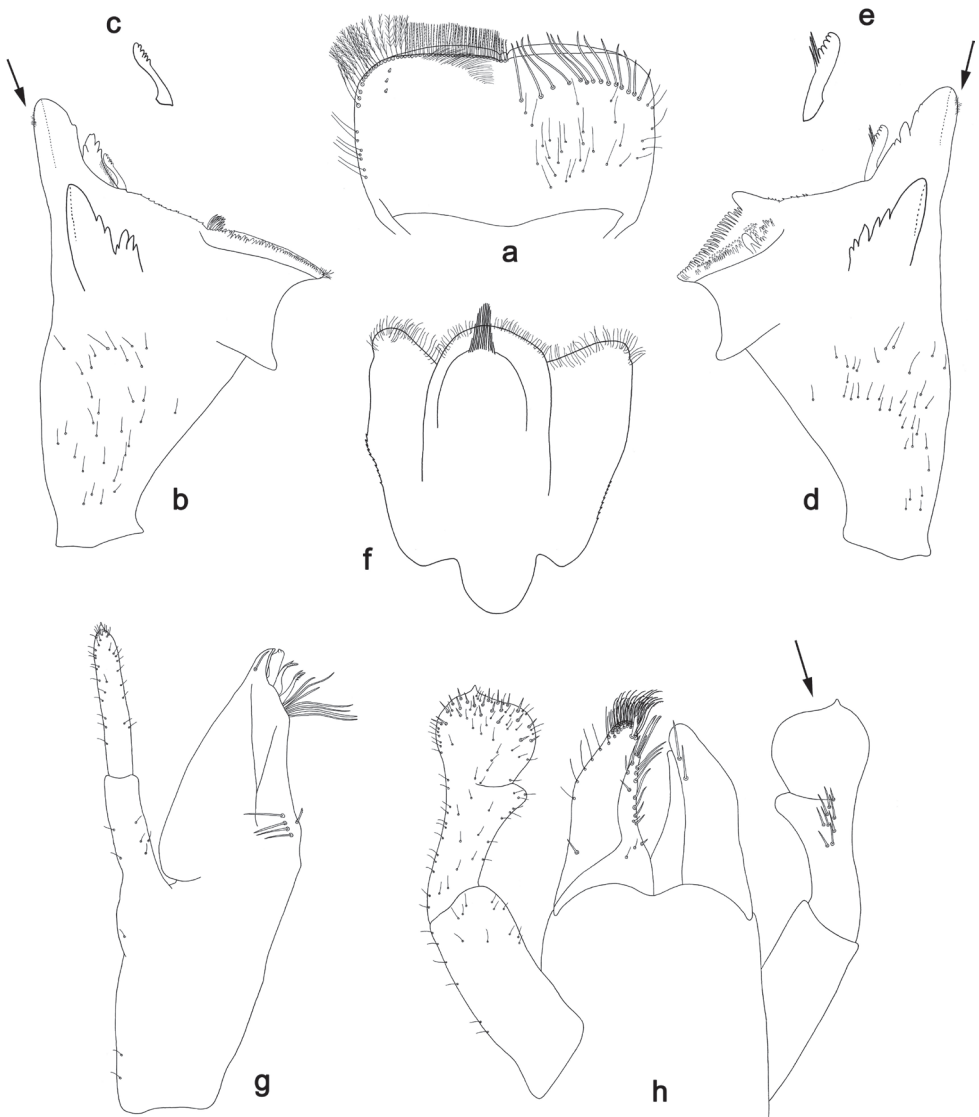


**Figure 20.** *Branchiobaetis minangkabau* sp. nov., larva **a** labrum (left: ventral view, right: dorsal view) **b** right mandible **c** right prosthema **d** left mandible **e** left prosthema **f** hypopharynx and superlinguae **g** maxilla **h** labium (left: ventral view, right: dorsal view).

*Precursors of turbinate eyes* (Fig. 25e) in male last instar larvae representing a pair of egg-shaped maculae; in the middle of this macula, a smaller, round, elevated area with well-expressed facets, ca. eight facets in diameter; peripheral area of the macula with indistinct facets.

*Antenna* (Fig. 21g). Scape distally and outside distolaterally with short, stout, apically rounded setae.

**Labrum** (Fig. 20a). Length  $0.6\times$  maximum width. Submarginal arc of setae composed of 11–13 long, simple setae.

**Right mandible** (Fig. 20b, c). Incisor and kinetodontium distally cleft. Incisor blade-like with three denticles; kinetodontium with four denticles. Minute setae outside laterally on first denticle (present on fresh mandibles only). Margin between prosthema and mola straight, with minute denticles.

**Left mandible** (Fig. 20d, e). Incisor blade-like with three denticles; kinetodontium with three denticles. Minute setae outside laterally on first denticle (present on fresh mandibles only). Margin between prosthema and mola straight, with minute denticles towards subtriangular process.

Both mandibles with lateral margins almost straight.

**Hypopharynx and superlinguae** (Fig. 20f). Lingua as long as superlinguae. Lingua longer than broad; medial tuft of stout setae well developed, long. Superlinguae distally rounded; lateral margins rounded; fine, long, simple setae along distal margin.

**Maxilla** (Fig. 20g). Galea-lacinia ventrally with one simple, apical seta under canines. Medially with one pectinate, spine-like seta and three or four medium, simple setae. Maxillary palp as long as galea-lacinia; palp segment II  $1.1\times$  as long as segment I; setae on maxillary palp fine, simple, scattered over surface of segments I and II.

**Labium** (Fig. 20h). Inner margin of glossa with approx. eight spine-like setae, increasing in length distally; apex with two long and one medium, robust setae; outer margin with two or three spine-like setae; Paraglossa with one simple seta in posterolateral area; dorsally with two long, spine-like setae near inner margin. Labial palp with segment I approx. as long as length of segments II and III combined. Segment I ventrally with short, fine, simple setae. Segment II with small, distomedial protuberance; distomedial protuberance  $0.3\times$  width of base of segment III; ventral surface with short, fine, simple setae; dorsally with 6–9 spine-like setae near outer margin, not always in a row. Segment III slightly pentagonal, apically slightly concave, with projecting point; length approx. maximum width; ventrally covered with short, spine-like, simple setae and short, fine, simple setae.

**Foreleg** (Fig. 21a–c). Ratio of foreleg segments 1.4:1.0:0.6:0.2. **Femur**. Length ca.  $3\times$  maximum width. Dorsal margin with row of 15–20 long, curved, spine-like setae, basally denser. Many short, stout, apically rounded setae scattered along ventral margin. Apex rounded, with pair of long, spine-like setae and some short, stout setae. **Tibia**. Dorsal margin with row of short, stout setae. On surface few such setae along patella-tibial suture. Ventral margin with row of short, curved, spine-like setae, on apex a tuft of fine, simple setae. **Tarsus**. Dorsal margin with row of short, stout setae. **Claw** with one row of eight or nine denticles.

**Terga** (Fig. 21d). Surface with irregular rows of U-shaped scale bases. Posterior margin of tergites: I smooth, without spines; II–IV with rounded spines, wider than long, partly fused at base; V–IX with triangular spines, narrower and longer towards last segment. Posterior margin of sternites: I–VI smooth, without spines; VII–VIII with small, spaced, triangular spines; IX with small triangular spines.

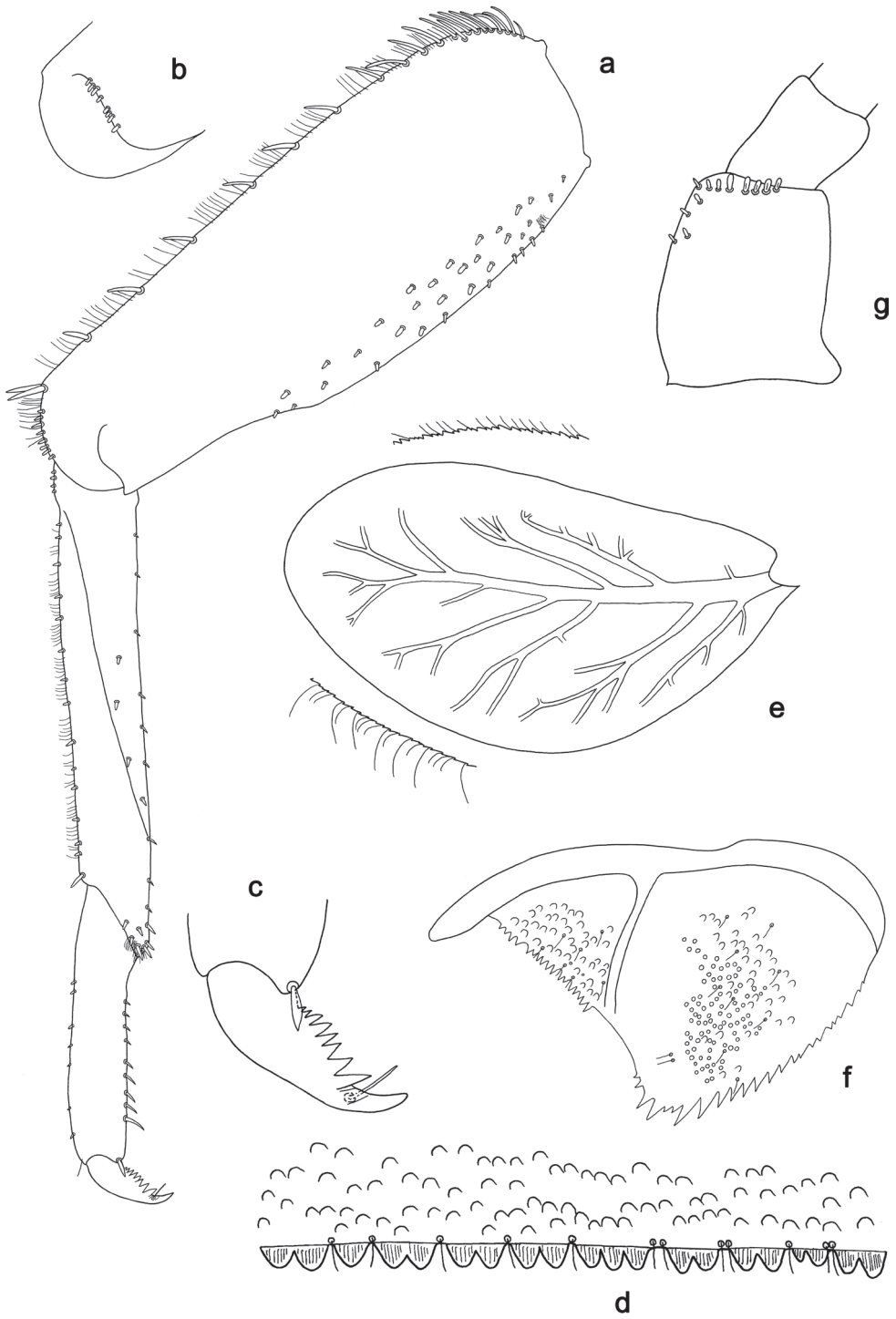


**Figure 21.** *Branchiobaetis minangkabau* sp. nov., larva **a** foreleg **b** fore femur apex, posterior view **c** fore claw **d** tergum IV **e** tergalius IV **f** paraproct **g** base of antenna.

**Tergalii** (Figs 21e, 26d). Tracheae not reaching inner and outer margins; indistinct broad, light brown band along main trunk of tracheae on anal side. Tergalius I as long as 2/3 of segment II, tergalium IV as long as length of segments V and 2/3 VI combined, tergalium VII as long as length of segments VIII and 1/3 IX combined.

**Paraproct** (Fig. 21f). Posterior margin with 14–24 stout spines. Without short, stout setae near posterior margin. Surface scattered with scale bases, micropores and fine, simple setae.

**Etymology.** Dedicated to the indigenous Minangkabau people, who live in the area of Sumatra where the specimens were collected.

**Distribution.** Indonesia: Sumatra (Fig. 28b).

**Biological aspects.** The specimens were collected on altitudes of 300 m and 960 m, most of them in a stream with the following physical conditions: slope 25%, width of stream 3–20 m, depth ca. 1.5 m, velocity slow in pool and 0.8 m/s in cascade, pH 8, stream bed dominated by bedrock and stones with patches of sand.

### 7. *Branchiobaetis jhoanae* sp. nov.

<https://zoobank.org/92CD6523-BB67-48E6-BA4E-09B10D3CA416>

Figs 22, 23, 25b, 26e, 29

**Type material. Holotype.** PHILIPPINES • S. Luzon, Sorsogon, Bulusan, San Roque; 12°44'N, 124°05'E; 290 m; 26. IX. 1996; leg. J. Mendoza; larva on slide; GBIF-CH00592344; PNM. **Paratypes.** Same data as holotype; 1 larva on slide; GBIF-CH00763660; MZL. PHILIPPINES • Cebu, Cebu City, Cantipla Uno; 10°20'48"N, 123°51'57"E; 100 m; 11. IX. 1996; leg. J. Mendoza; larva on slide; GBIF-CH00592341; AdMU; larva in alcohol; GBIFCH00515474; AdMU • Cebu, Cebu City, Bgy. Tabunan, sitio Cantipla 1; 10°24'56"N, 123°49'02"E; 753 m; 16.XII.1998; leg. Panganthion; larva on slide; GBIFCH00654920; MZL; 2 larvae in alcohol; GBIF-CH00515475, GBIFCH00980901; AdMU.

**Differential diagnosis. Larva.** Following combination of characters distinguish *B. jhoanae* sp. nov. from other species of *Branchiobaetis* gen. nov.: A) labial palp segment II with small, rounded protuberance; segment III slightly pentagonal, apically pointed, ca. 0.7× length of segment II, ca. 1.4× as long as width at base, approx. as long as maximal width (Fig. 22h); B) dorsal margin of femur with row of long, spine-like setae (Fig. 23a); C) posterior margin of tergites: I smooth, without spines; II–IX with triangular spines (Fig. 23d); posterior margin of sternites: I–VI smooth, without spines; VII–IX with small, spaced, triangular spines; D) paraproct without short, stout, apically rounded setae along posterior margin (Fig. 23f).

**Description. Larva** (Figs 22, 23, 25b, 26e). Body length 5.8–7.0 mm. Cerci: ca. ½ of body length. Paracercus: ca. 2/3 of cerci length. Antenna: ca. 2.5× as long as head length.

**Colouration** (Fig. 25b). Head, thorax, and abdomen dorsally brown; head, thorax and abdomen ventrally light brown to brown. Legs light brown to brown, large brown

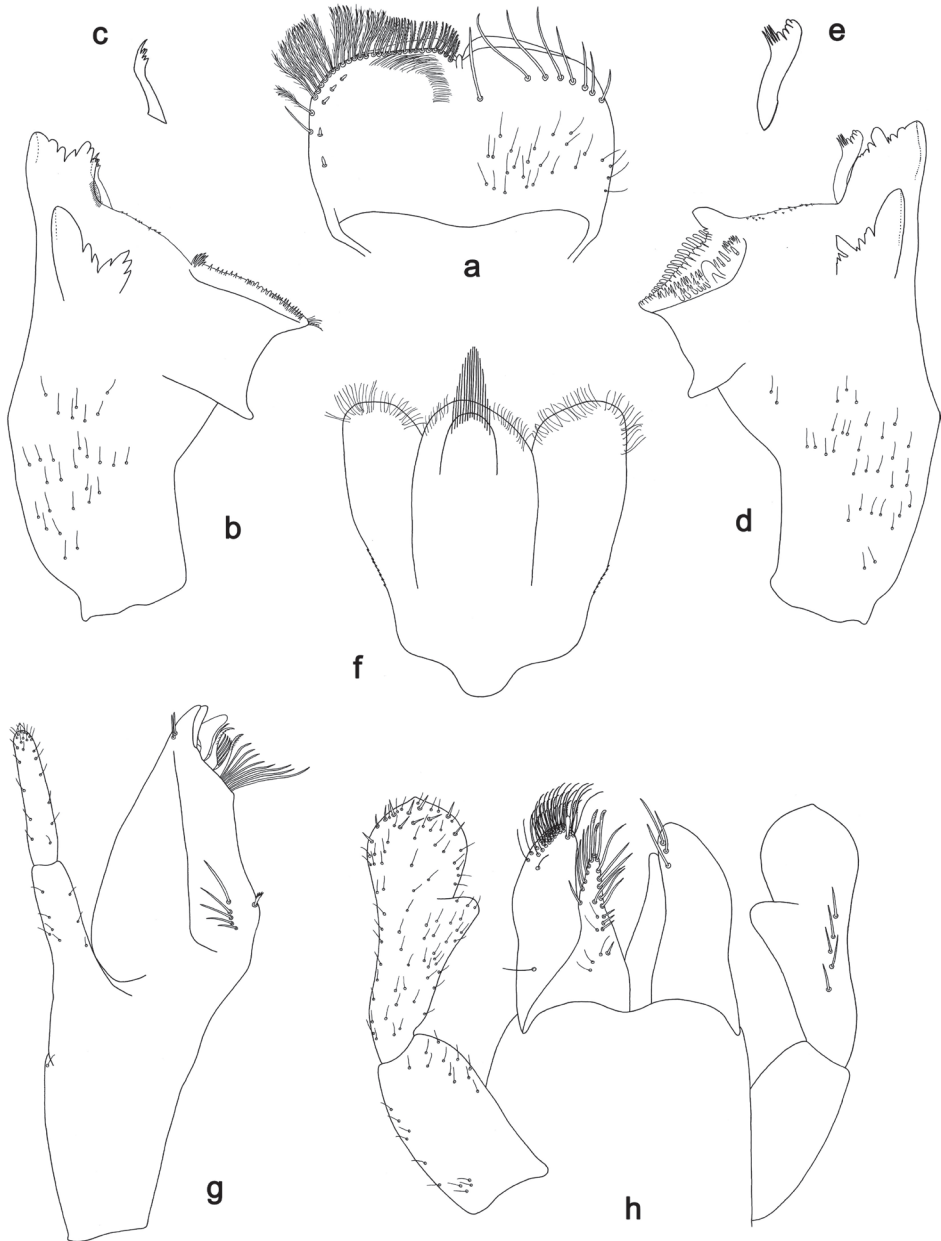


**Figure 22.** *Branchiobaetis jhoanae* sp. nov., larva **a** labrum (left: ventral view, right: dorsal view) **b** right mandible **c** right prosthema **d** left mandible **e** left prosthema **f** hypopharynx and superlinguae **g** maxilla **h** labium (left: ventral view, right: dorsal view).

areas along dorsal margin, apex and on medial surface of femur. Caudalii light brown, primary swimming setae dark brown.

**Antenna** (Fig. 23g). Scape distally with short, stout, apically rounded setae.

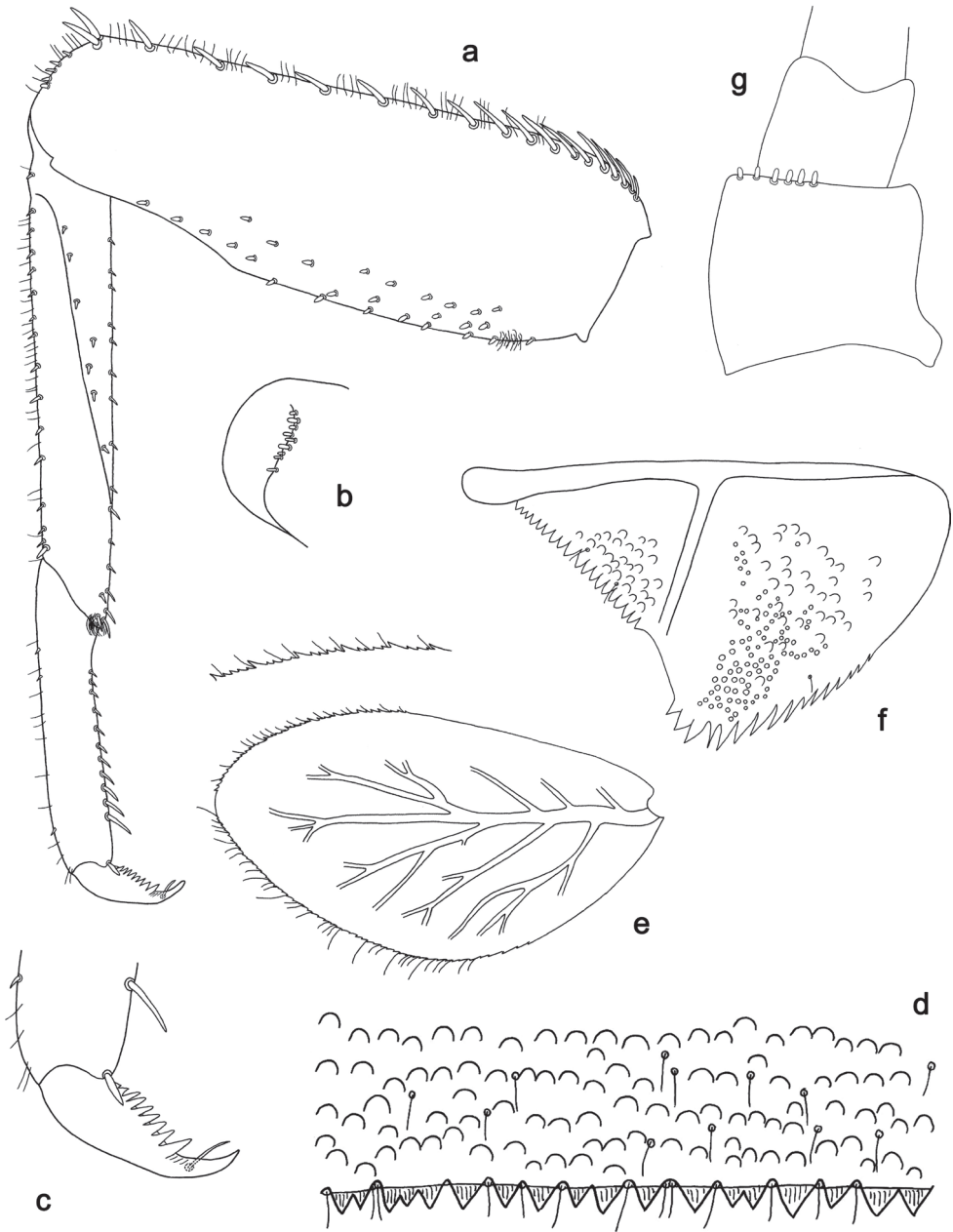


**Figure 23.** *Branchiobaetis jhoanae* sp. nov., larva **a** foreleg **b** fore femur apex, posterior view **c** fore claw **d** tergum IV **e** tergalium IV **f** paraproct **g** base of antenna.

**Labrum** (Fig. 22a). Length  $0.6\times$  maximum width. Submarginal arc of setae composed of 7–9 long, simple setae.

**Right mandible** (Fig. 22b, c). Incisor blade-like with three denticles; kinetodontium with four denticles. Margin between prostheca and mola straight, with minute denticles.

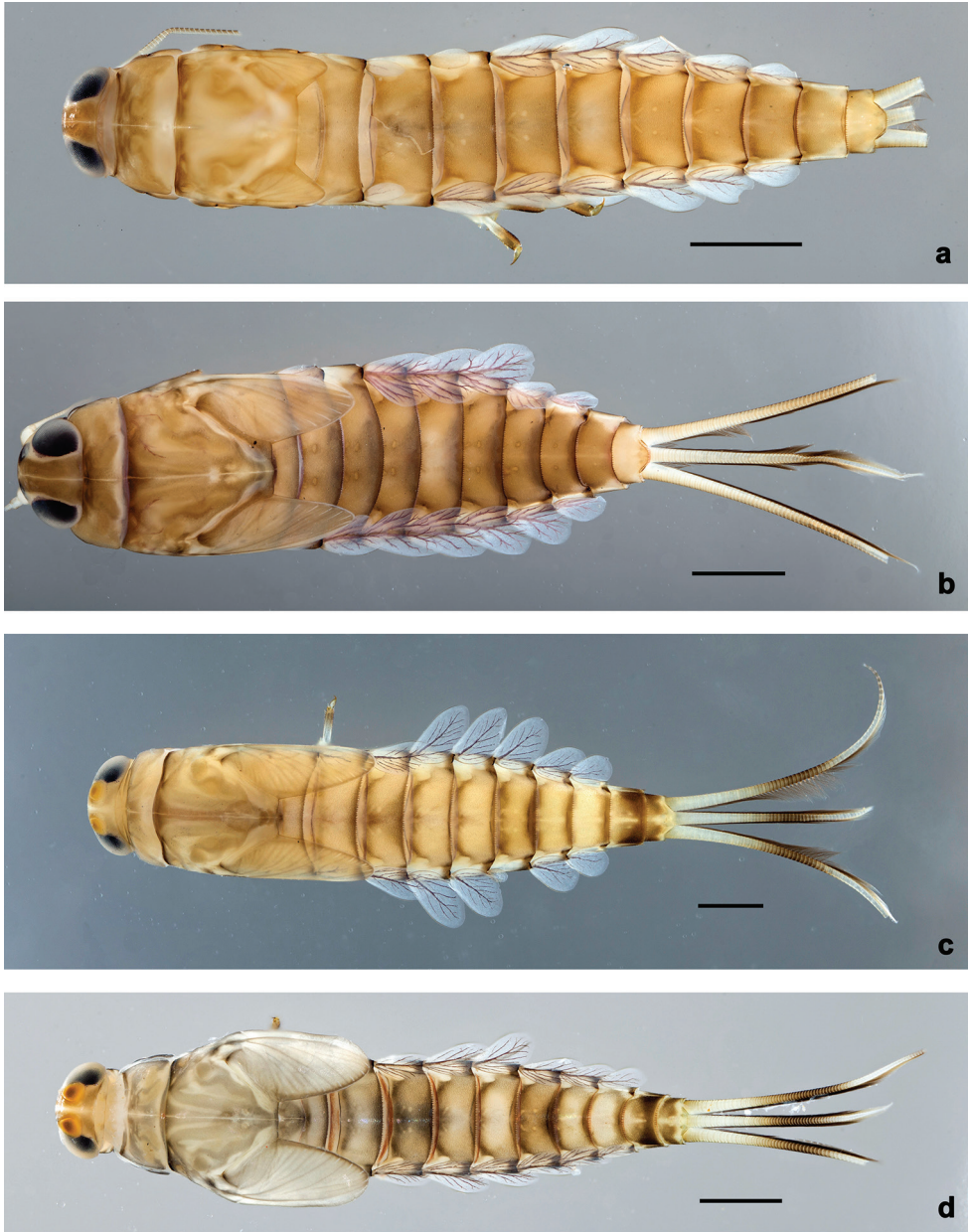


**Figure 24.** Habitus, larvae, dorsal view **a** *Branchiobaetis aduncus* sp. nov. **b** *Branchiobaetis hamatus* sp. nov. **c** *Branchiobaetis joachimi* sp. nov. (Sumatra, volcano Sago) **d** *Branchiobaetis joachimi* sp. nov. (Sumatra, Bukit Barisan, above Padang).

**Left mandible** (Fig. 22d, e). Incisor blade-like with four denticles; kinetodontium with three denticles. Margin between prostheca and mola straight, with minute denticles towards subtriangular process.

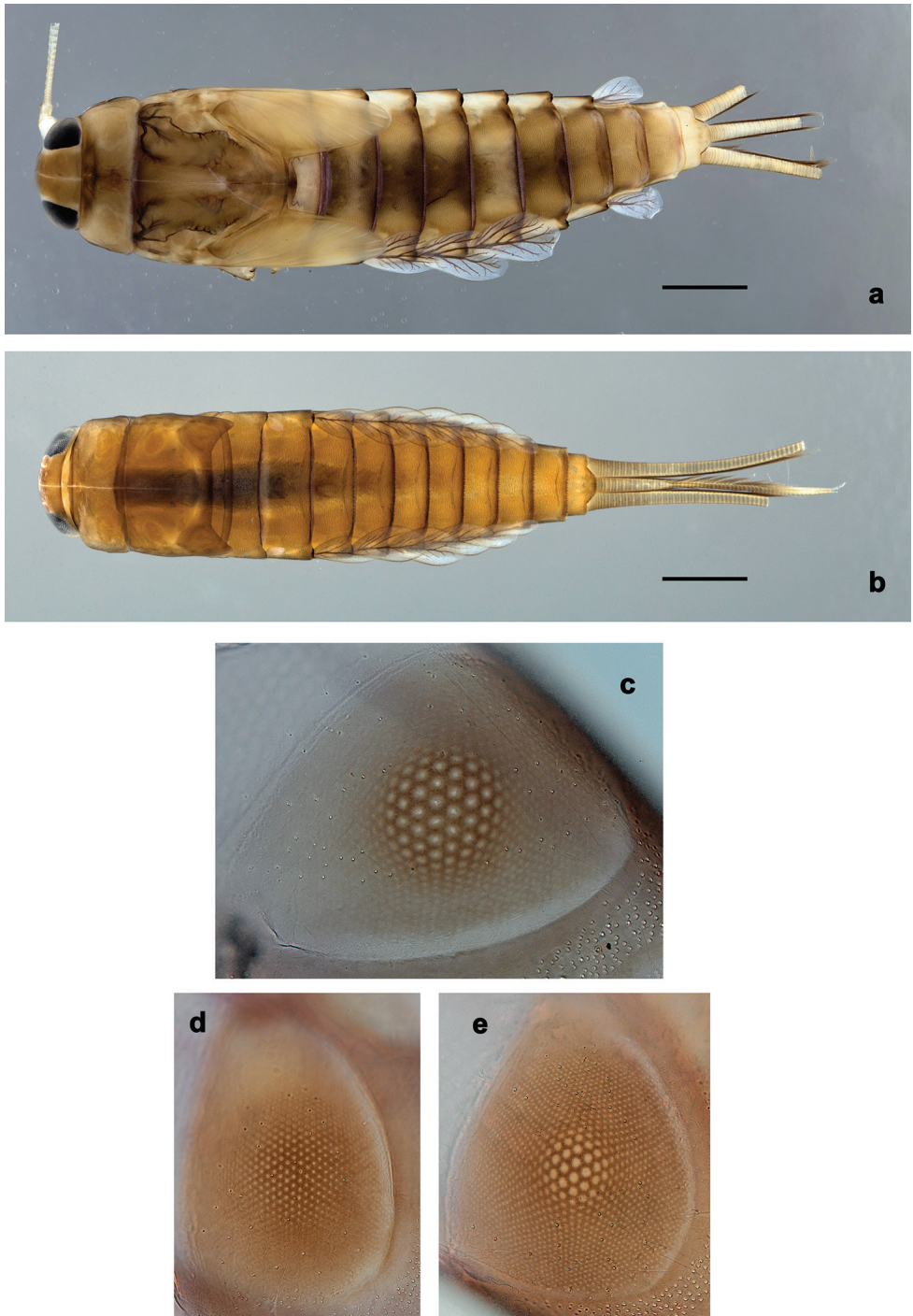


**Figure 25.** Habitus, larvae, dorsal view **a** *Branchiobaetis minangkabau* sp. nov. **b** *Branchiobaetis jboanae* sp. nov. Precursors of turbinate eyes developing in male last instar larvae **c** *Branchiobaetis hamatus* sp. nov. **d** *Branchiobaetis joachimi* sp. nov. **e** *Branchiobaetis minangkabau* sp. nov.

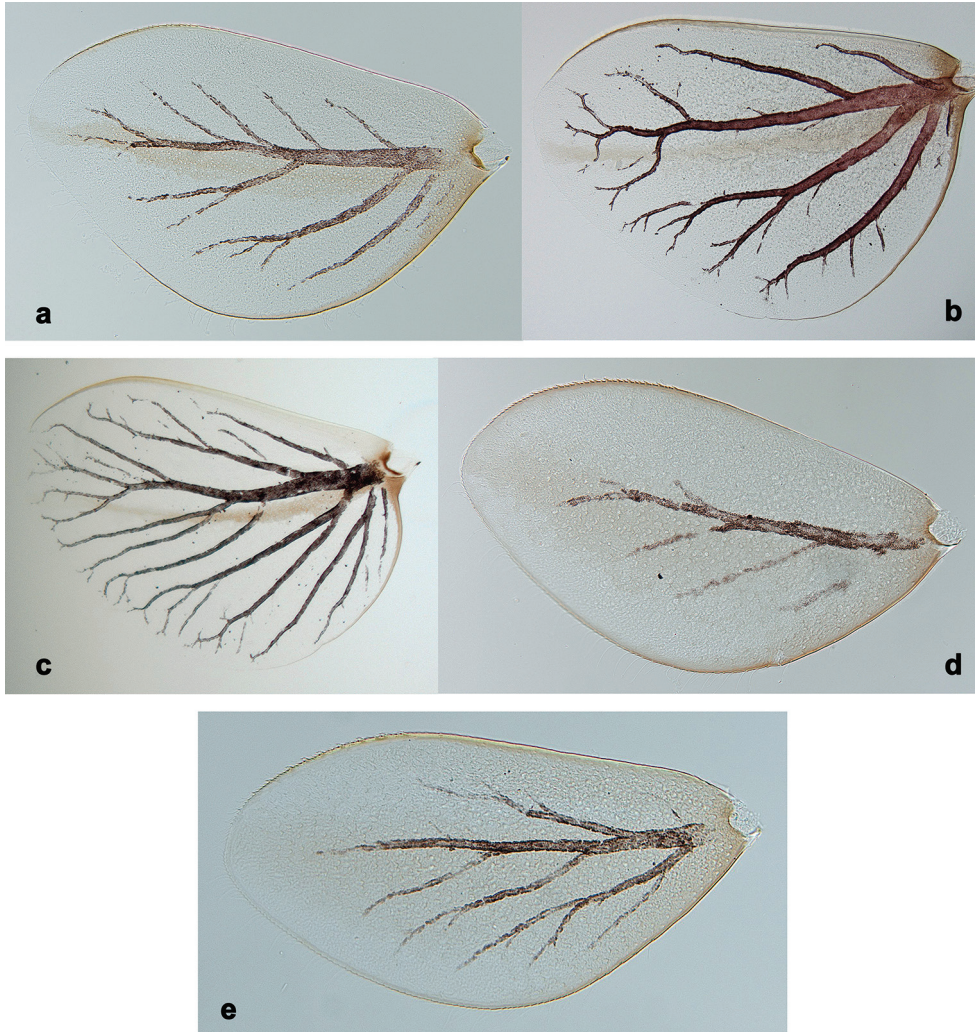


**Figure 26.** Larva, tergite IV **a** *Branchiobaetis aduncus* sp. nov. **b** *Branchiobaetis hamatus* sp. nov. **c** *Branchiobaetis joachimi* sp. nov. **d** *Branchiobaetis minangkabau* sp. nov. **e** *Branchiobaetis jhoanae* sp. nov.

Both mandibles with lateral margins slightly convex.

**Hypopharynx and superlinguae** (Fig. 22f). Lingua as long as superlinguae. Lingua longer than broad; medial tuft of stout setae well developed, long. Superlinguae distally rounded; lateral margins rounded; fine, long, simple setae along distal margin.

**Maxilla** (Fig. 22g). Galea-lacinia ventrally with two simple, apical seta under canines. Medially with one pectinate, spine-like seta and 4–6 medium, simple setae. Maxillary palp approx. as long as galea-lacinia; palp segment II approx. as long as segment I; setae on maxillary palp fine, simple, scattered over surface of segments I and II.

**Labium** (Fig. 22h). Inner margin of glossa with eight or nine spine-like setae, increasing in length distally; apex with two long and one medium, robust, pectinate

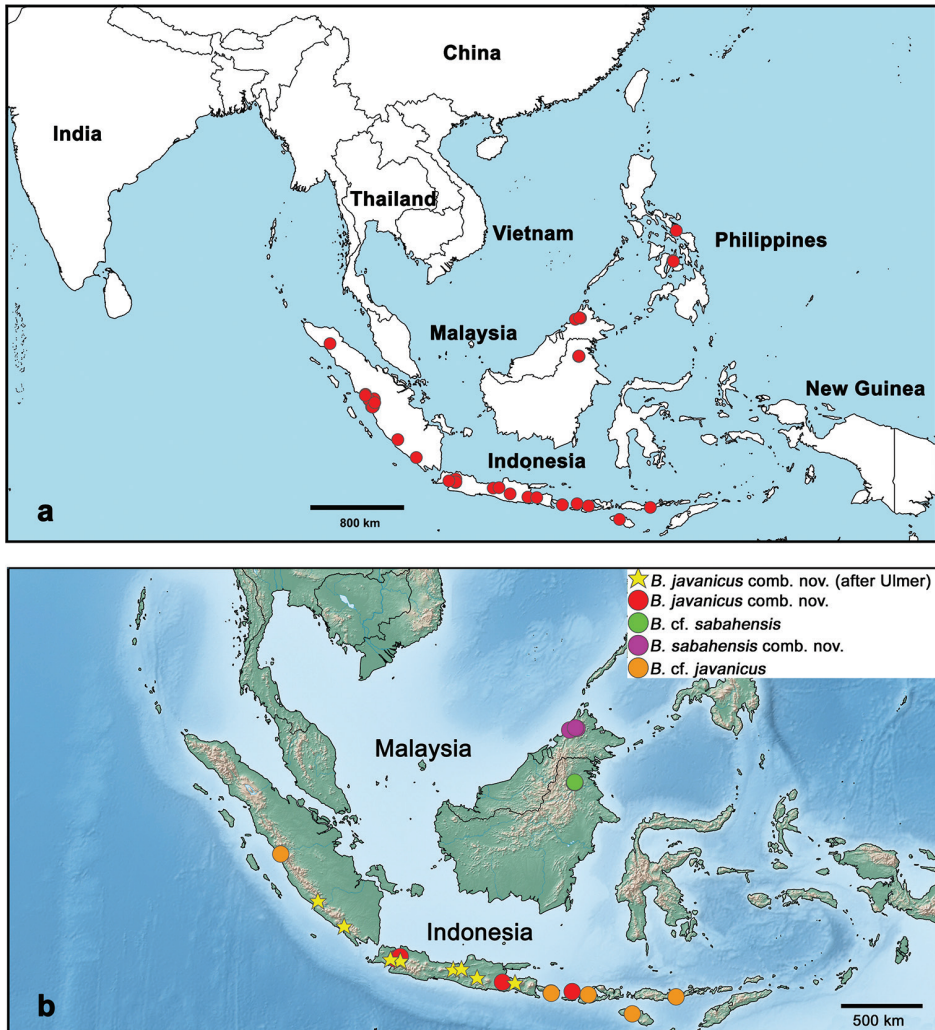


**Figure 27.** Distribution maps **a** *Branchiobaetis* gen. nov. in Southeast Asia **b** Known species of *Branchiobaetis* gen. nov.

setae; outer margin with approx. five spine-like setae; Paraglossa with one simple seta in anterolateral area and one simple seta in posterolateral area; dorsally with three long, spine-like setae near inner margin. Labial palp with segment I 0.7× as long as length of segments II and III combined. Segment I ventrally with short, fine, simple setae. Segment II with small, rounded, distomedial protuberance; distomedial protuberance 0.3× width of base of segment III; ventral surface with short, fine, simple setae; dorsally with five or six spine-like setae near outer margin. Segment III slightly pentagonal, apically pointed; length approx. maximum width; ventrally covered with short, spine-like, simple setae and short, fine, simple setae.

**Foreleg** (Fig. 23a–c). Ratio of foreleg segments 1.3:1.0:0.6:0.2. **Femur**. Length ca. 3× maximum width. Dorsal margin with row of 14–21 long, curved, spine-like setae,

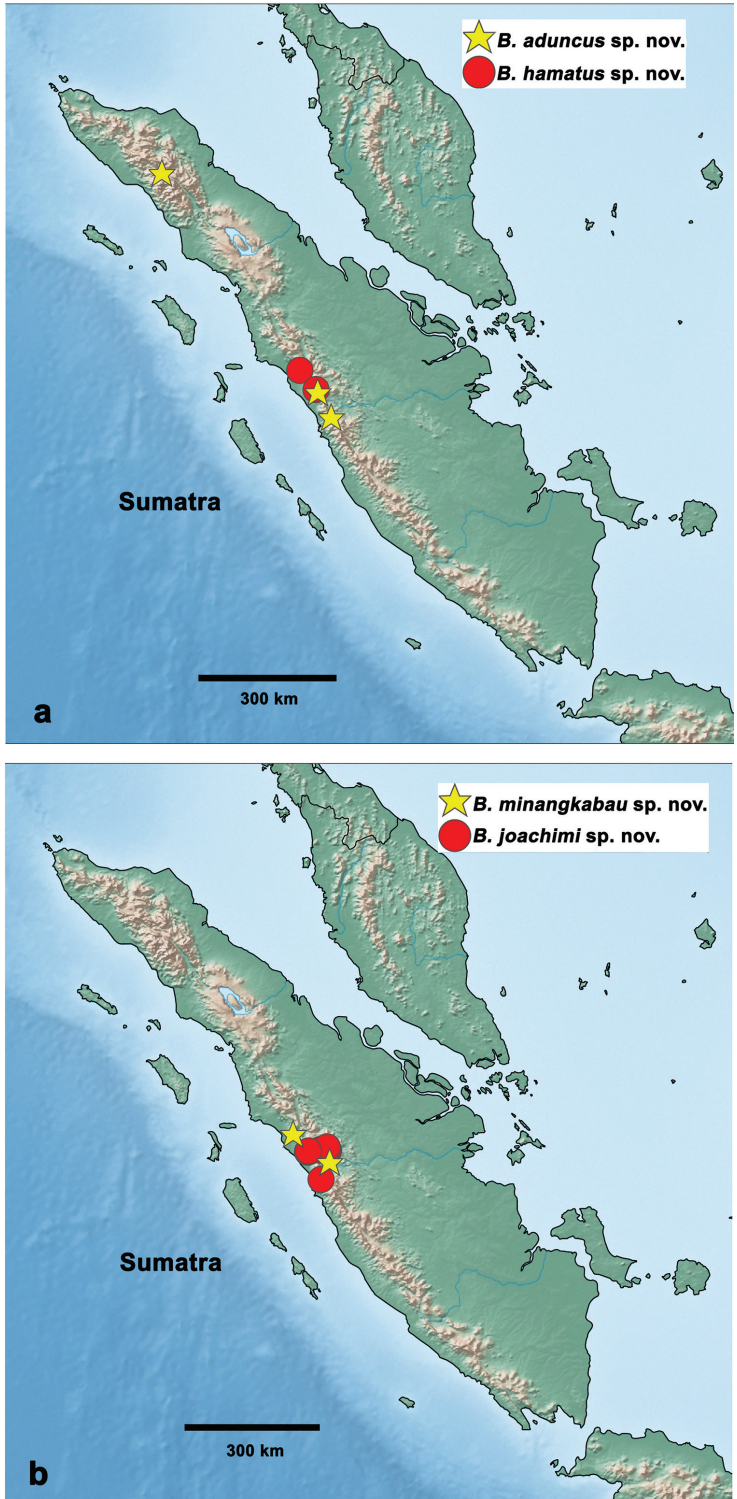


Figure 28. Distribution maps a, b new species of *Branchiobaetis* gen. nov. in Sumatra.



**Figure 29.** Distribution map. *Branchiobaetis jhoanae* sp. nov. in the Philippines.

basally denser. Many short, stout setae scattered along ventral margin. Apex rounded, with pair of long, spine-like setae and some short, stout setae. **Tibia.** Dorsal margin with row of short, stout setae. On surface few such setae along patella-tibial suture. Ventral margin with row of short, curved, spine-like setae, on apex a tuft of fine, simple setae. **Tarsus.** Dorsal margin with row of short, stout setae and fine, simple setae. **Claw** with one row of nine or ten denticles.

**Terga** (Fig. 23d). Surface with irregular rows of U-shaped scale bases and fine simple setae. Posterior margin of tergites: I smooth, without spines; II–IX with triangular spines. Posterior margin of sternites: I–VI smooth, without spines; VII–IX with small, spaced, triangular spines.

**Tergalii** (Figs 23e, 26e). Tracheae extending to inner and outer margins; indistinct, broad, light brown band along main trunk of tracheae on anal side. Tergalius I as long as 1/2 of segment II, tergalium IV as long as length of segments V and 1/4 VI combined, tergalium VII as long as length of segments VIII and 1/4 IX combined.

**Paraproct** (Fig. 23f). Posterior margin with 14–18 stout spines. Without short, stout setae near posterior margin. Surface scattered with scale bases and micropores.

**Etymology.** Dedicated to Dr. Jhoana M. Garces (Philippines) for her great contribution to the knowledge of mayflies from the Philippines.

**Distribution.** Philippines: Luzon, Cebu (Fig. 29).

**Biological aspects.** The specimens were collected on altitudes between 100 m and 750 m, on Cebu in stream runs on bottom gravel or rock surface.

### Key to the species of *Branchiobaetis* gen. nov. (larvae)

- 1 Dorsal margin of femur with row of medium, spine-like setae and many short, apically rounded setae in two or three irregular rows along margin; short, stout, apically rounded setae in middle area of anterior surface of femur (Fig. 19a).....  
..... ***B. joachimi* sp. nov.**
- Dorsal margin of femur with row of medium to long, spine-like setae, no additional row of short, apically rounded setae, or one single row of short, hooked setae along margin; no stout setae in middle area of anterior surface of femur (Figs 15a, 21a)..... **2**
- 2 Many short, stout, hook-like setae along dorsal margin of femur, tibia and tarsus (Fig. 15a, c); labial palp segment III apically rounded (Fig. 14j)..... **3**
- No short, hook-like setae along dorsal margin of femur, tibia or tarsus (Fig. 21a); labial palp segment III apically pointed (Fig. 22h) ..... **4**
- 3 Posterior margin of tergite IV with apically rounded spines (Fig. 15f); tergalium IV with convex apex (Fig. 15g) ..... ***B. aduncus* sp. nov.**
- Posterior margin of tergite IV with triangular, pointed spines (Fig. 17e); tergalium IV apically with slight concavity (Fig. 17f)..... ***B. hamatus* sp. nov.**
- 4 Labial palp segment III distally wide, with projecting point, apical margin slightly concave (Fig. 20h); posterior margin of tergite IV with rounded spines (Fig. 21d)..... ***B. minangkabau* sp. nov.**
- Labial palp segment III distally pointed, point not projecting, apical margin not concave (Fig. 22h); posterior margin of tergite IV with triangular, pointed spines..... **5**
- 5 Incisor of right mandible with ventral denticle; labial palp segment III rather short, ca. 0.5× length of segment II (Fig. 12d; Müller-Liebenau 1984b: fig. 3b, e); Borneo ..... ***B. sabahensis* comb. nov.**
- Incisor of right mandible without ventral denticle; labial palp segment III rather long, ca. 0.7× length of segment II (Figs 6b, 22b, h; Müller-Liebenau 1981: fig. 1b, e) ..... **6**
- 6 Posterior margin of tergite IV with triangular spines, wider than long; tergalium IV rather oblong; paraproct without stout setae along margin (Fig. 23d–f); Philippines ..... ***B. jboanae* sp. nov.**
- Posterior margin of tergite IV with triangular spines, longer than wide; tergalium IV with bellied shape; paraproct with stout, apically rounded setae along margin (Figs 5e, 7j; Müller-Liebenau 1981: fig. 1m, pl. 1.1); Indonesia (Sunda Islands) ..  
..... ***B. javanicus* comb. nov.**

### Genetics

The interspecific genetic distances between the species of *Branchiobaetis* gen. nov. are rather high, between 13% and 21% (Table 3).

**Table 3.** Intraspecific (bold) and interspecific genetic distances of *Branchiobaetis* gen. nov. species (COI; Kimura 2-parameter); green lines indicate species delimitation hypothesis according to the ASAP method.

	1	2	3	4	5	6	7	8	9	10	11	12	13	14	15	16	17
1 <i>B. cf. javanicus</i> (Sumbawa)																	
2 <i>B. cf. javanicus</i> (Sumbawa)	<b>0.00</b>																
3 <i>B. cf. javanicus</i> (Bali)	0.12	0.12															
4 <i>B. cf. javanicus</i> (Sumatra)	0.21	0.21	0.18														
5 <i>B. cf. javanicus</i> (Sumatra)	0.21	0.21	0.18	<b>0.00</b>													
6 <i>B. aduncus</i> sp. nov.	0.16	0.16	0.19	0.21	0.21												
7 <i>B. hamatus</i> sp. nov.	0.19	0.19	0.20	0.18	0.18	0.19											
8 <i>B. hamatus</i> sp. nov.	0.19	0.19	0.20	0.18	0.18	0.19	<b>0.00</b>										
9 <i>B. hamatus</i> sp. nov.	0.19	0.19	0.20	0.18	0.18	0.19	<b>0.00</b>	<b>0.00</b>									
10 <i>B. joachimi</i> sp. nov.	0.20	0.20	0.19	0.20	0.20	0.19	0.20	0.20	0.20								
11 <i>B. joachimi</i> sp. nov.	0.19	0.19	0.18	0.20	0.20	0.20	0.19	0.19	0.19	<b>0.01</b>							
12 <i>B. joachimi</i> sp. nov.	0.20	0.20	0.18	0.20	0.20	0.20	0.20	0.20	0.20	<b>0.01</b>	<b>0.00</b>						
13 <i>B. joachimi</i> sp. nov.	0.20	0.20	0.19	0.20	0.20	0.19	0.20	0.20	0.20	<b>0.00</b>	<b>0.01</b>	<b>0.01</b>					
14 <i>B. joachimi</i> sp. nov.	0.19	0.19	0.19	0.21	0.21	0.19	0.19	0.19	0.19	<b>0.05</b>	<b>0.05</b>	<b>0.05</b>	<b>0.05</b>				
15 <i>B. minangkabau</i> sp. nov.	0.15	0.15	0.17	0.13	0.13	0.17	0.19	0.19	0.19	0.20	0.20	0.20	0.20	0.20			
16 <i>B. minangkabau</i> sp. nov.	0.16	0.16	0.17	0.13	0.13	0.17	0.19	0.19	0.19	0.20	0.20	0.20	0.20	0.20	<b>0.00</b>		
17 <i>B. minangkabau</i> sp. nov.	0.15	0.15	0.17	0.13	0.13	0.17	0.19	0.19	0.19	0.20	0.20	0.20	0.20	0.20	<b>0.00</b>	<b>0.00</b>	
18 <i>B. jhoanae</i> sp. nov.	0.20	0.20	0.20	0.18	0.18	0.19	0.19	0.19	0.19	0.17	0.17	0.17	0.17	0.18	0.19	0.19	0.19

## Discussion

### Relationship, characters, and affinities of *Branchiobaetis* gen. nov.

The new genus *Branchiobaetis* gen. nov. obviously belongs to the family Baetidae, based on the turban eyes of the male imago (Fig. 9b), the forewing with intercalary veins (Fig. 9c), the diminished, narrowed hind wings with strongly reduced venation of male and female imago (Fig. 9e) as well as a series of larval characters, e.g. Y-shaped frontal suture ventral of lateral ocelli, labrum with distinctly expressed medial incision (Fig. 12b), kinetodontium fused with mandible and with incisor (Fig. 6a, b), left protheca stout stick-like, apically denticulate (Fig. 6a), femur with apical anterior outer projection curved toward inner side of femur (Fig. 15a) (Kluge 2004; Kluge and Novikova 2011). Based on the rank-free system of Kluge (Kluge 2004; Kluge and Novikova 2011), *Branchiobaetis* gen. nov. belongs to the Anteropatellata, because a patella-tibial suture is present on all legs of larva, female subimago and female imago, including forelegs (Figs 7a–c, 8a); to Baetovectata because of the forewings with double intercalaries (Fig. 9a, c) and the 2<sup>nd</sup> segment of the subimaginal gonostylus developing under larval cuticle bent medially (Fig. 10b); and to Baetungulata or Baetinae (sensu Kazlauskas 1972) because of the claws with one row of denticles on inner-anterior side and a maxillary palp with two segments (Figs 7k, 14i) (Kluge and Novikova 2011). Finally, the new genus is part of the Baetofemorata or the “*Baetis* complex” sensu Waltz and McCafferty (1997), because each larval leg has a femoral patch and subimagines of both sexes have all tarsomeres covered with blunt microlepidids (Fig. 8c, d, h) (Kluge and Novikova 2011).

Most interesting in the characters of *Branchiobaetis* gen. nov. is the presence of accessory gills in all species, one finger-like pair ventrally between fore coxa and prosternum and one gill on each maxilla outside between stipes and cardo (Figs 1a, b, 16j; Müller-Liebenau 1984b: fig. 3i). These gills are connected to the tracheal system and have tracheae inside, their respiratory function is therefore probable. However, their size is small in relation to the body size and the size of the tergali, which are large and with many tracheae. It remains unclear if their contribution to respiration is substantial or rather negligible. In addition, some of the species are reported to live in fast flowing and cold water, where we can expect a high oxygen content and therefore a less importance of gills. Accessory gills are rare in Baetidae and in Ephemeroptera in general, an overview and phylogenetic discussion is given by Staniczek (2010) and Zhou (2010). Mostly, these accessory gills are associated with coxae or thoracic sterna, or with maxillae, similar to *Branchiobaetis* gen. nov.; a multiple convergent development of these accessory gills is assumed (Staniczek 2010; Zhou 2010). In Baetidae, at least three different types of accessory gills were reported: coxal gills (located between coxae and sterna, or between coxae and trochanter), maxillary gills located between stipes and cardo and maxillary gills located at the maxillary palp (Müller-Liebenau 1984b; Gattolliat and Sartori 1999; Dominguez et al. 2006; Staniczek 2010; Zhou 2010; Gattolliat 2012; Shi and Tong 2015; Kluge and Bernal Vega 2018). *Moribaetis* Waltz & McCafferty, 1985 has very similar accessory coxal gills compared to *Branchiobaetis* gen. nov. (Kluge and Bernal Vega 2018: figs 85, 86). This is probably convergent, as other characters are very different and *Moribaetis* belongs to Baetungulata-non-Baetofemorata or the “non-Baetis complex” of Baetinae (sensu Waltz et al. 1994; Waltz and McCafferty 1997) (no femoral patch), whereas *Branchiobaetis* gen. nov. is part of Baetofemorata (Waltz and McCafferty 1985; Kluge and Novikova 2014; Kluge and Bernal Vega 2018).

*Rhodobaetis* Jacob, 2003, subgenus of *Baetis*, is characterized by peculiar, stout, apically rounded setae, generally called spatulae, on the antennal scape and pedicel, which usually appear as well on abdominal terga (Müller-Liebenau 1984a: figs 1f, 34; Jacob 2003; Godunko et al. 2004; Soldán et al. 2005; Soldán and Godunko 2006; Gattolliat et al. 2018; Yanai et al. 2018: figs 12A, 13C; Kluge 2022). The same type of setae is always present on antennal scapes of *Branchiobaetis* gen. nov., but only exceptionally one or two on pedicels and they never appear on abdominal terga. However, important differences between both groups are a developed, slender sterno-styliger muscle in *Branchiobaetis* gen. nov. (Fig. 10f; absent in *Rhodobaetis*), accessory coxal and maxillary gills in *Branchiobaetis* gen. nov. (Fig. 1a, b; usually absent in *Rhodobaetis*; Kluge 2022), and the folding of the gonostyli developing under cuticle of last instar male larvae (“*Branchiobaetis*-type” (see below) vs. “*Baetis*-type” in *Rhodobaetis*; Fig. 4a–d; Kluge 2004: fig. 29H). In specimens of *Baetis* (*Rhodobaetis*) *illiesi* Müller-Liebenau, 1984, from Vietnam, we discovered bubble-like membranous swellings on the legs similar to *Branchiobaetis* gen. nov. and auxiliary gills at base of forecoxae, but no maxillary gills. This is exceptional for *Rhodobaetis* and assumed to be convergent. The folding of the gonostyli developing under the cuticle of a last instar male larva of *B. illiesi* from Vietnam was in the “*Baetis*-type” (authors, unpublished observation).

There are also some similarities between *Branchiobaetis* gen. nov. and *Philibaetis* Kaltenbach & Gattolliat, 2021, from the Philippines: labrum shape and dorsal, submarginal arc of setae; blade-like incisors of both mandibles; maxillary palp with pointed apex; paraglossae laterally slightly rolling, apex truncate and slightly bent inwards (Kaltenbach et al. 2021). However, these similarities are probably due to convergence; *Branchiobaetis* gen. nov. is part of Baetofemorata (presence of femoral patch) and *Philibaetis* belongs to Baetungulata-non-Baetofemorata (absence of femoral patch; Kaltenbach et al. 2021). There are also other important differences: e.g., *Branchiobaetis* gen. nov. with accessory gills (missing in *Philibaetis*); labrum medioventrally without additional, submarginal row of lanceolate setae (present in *Philibaetis*); right prostheca distolaterally denticulate (not apically denticulate as in *Philibaetis*); labial palp segment II with protuberance (missing in *Philibaetis*); scape with stout, apically rounded setae (missing in *Philibaetis*); folding of developing gonostyli under larval cuticle in “*Branchiobaetis*-type” (see below; *Philibaetis* similar to “*Labiobaetis*-type”) (Figs 1a, b, 4a–d, 14a, j, 15i; Kaltenbach et al. 2021: figs 1b, e, f, l, 2d, 3d, 10a, b).

### Membranous swellings on the legs of *Branchiobaetis* gen. nov.

All species of *Branchiobaetis* gen. nov. have particular, membranous, bubble-like structures at the legs of the larvae. They were never described in Baetidae: a swelling of the articulatory membrane between coxa and trochanter of all legs and a swelling of the articulatory membrane between coxa and pleurite of forelegs and middle legs (less developed) (Figs 1b, 2a–c). The degree of development of these swellings seems to vary between individuals. There are no tracheae inside and no other special structure, it seems to be simply convex, enlarged membranes. The function of these structures remains unclear, we do not consider them to be accessory gills. One possible explanation is that these structures support respiration through the membranous parts of the integument by increasing the membranous surface of the body. Oxygen and CO<sub>2</sub> exchange through the membranous parts of the integument is known from many aquatic insects (Eidmann and Köhlerhorn 1970). The involvement of air compartments inside the body of aquatic insects in their hydrostatic balance was also discussed (Eidmann and Köhlerhorn 1970) and could be another possible function. However, all possible explanations of the function of the bubble-like membrane swellings at the legs of *Branchiobaetis* gen. nov. remain speculative without further investigation.

### Subimaginal gonostyli developing under larval cuticle

In *Branchiobaetis* gen. nov., the second segment of the subimaginal gonostylus developing under the cuticle of last instar male larvae is bent medially as in other Baetofemorata. However, the 3<sup>rd</sup> segment is sharply bent laterally, which is peculiar for this genus (“*Branchiobaetis*-type” of folding) and different from the “*Baetis*-type” of folding (Fig. 4a–d; Kluge 2004: fig. 29H). Other types of folding in Baetidae are illustrated in Kluge (2004: fig. 29E–J).

## Genetics

The interspecific genetic distances of *Branchiobaetis* gen. nov. are in line with values reported for other Baetidae in Southeast Asia (*Labiobaetis*: 11–24% in Indonesia, 15–27% in the Philippines; Kaltenbach and Gattolliat 2019; Kaltenbach et al. 2020a). Ball et al. (2005) reported a mean interspecific, congeneric distance of 18% for mayflies from the United States and Canada. The intraspecific distances are very low in most cases as expected, ranging from 0% to 1% (K2P). This result is certainly biased as it is based on a limited number of sequenced specimens per species, which were partly from a single population. The exception is *B. joachimi* sp. nov., where one specimen of a more distant location has a genetic distance of 5% (K2P) to all three other specimens. This larger genetic distance may be explained by a possible isolation of the location causing a higher distance. Intraspecific distances of 4–6% were also reported in some cases for *Labiobaetis* species in New Guinea, Indonesia, Borneo, and the Philippines (Kaltenbach and Gattolliat 2018, 2019, 2020; Kaltenbach et al. 2020a), as well as in aquatic beetles in the Philippines (Komarek and Freitag 2020). Ball et al. (2005) also reported a case with 6% intraspecific distance in a mayfly in North America and intraspecific K2P distances of more than 3.5% are not uncommon within Plecoptera as well (Gill et al. 2015; Gattolliat et al. 2016).

For *B. javanicus* comb. nov., we do not have a COI sequence from Java, where the type locality is. However, we have sequences from larvae with the same morphology as *B. javanicus* comb. nov. from Sumbawa, Bali and Sumatra. The specimens from these three locations present important genetic distances to each other (12–21%; K2P; Table 3). According to the most likely scenario of hypothetical species obtained with the ASAP method (Table 3), the specimens of *B. cf. javanicus* comb. nov. from Sumbawa and Bali are retained as one hypothetical species and the specimens from Sumatra as another one. However, the second likely scenario obtained with the ASAP method also separated the specimens from Bali and Sumbawa as different hypothetical species. This is also supported by the ML reconstruction (Suppl. material 1). We are treating them all as *B. cf. javanicus* comb. nov. for now. It remains unclear, if it is a question of cryptic diversity, different mitochondrial lineages of the same species or something else (see also the discussion of Molecular Operational Taxonomic Units (MOTUs) in Kaltenbach et al. 2020a: table 4). Additional material and investigations will be necessary to confirm their status. All described new species of *Branchiobaetis* gen. nov. are supported by the species delimitation with the ASAP method (Table 3) and the ML reconstruction (Suppl. material 1).

## Distribution

*Branchiobaetis* gen. nov. has a wide distribution across Southeast Asia, so far including Indonesia (Greater and Lesser Sunda Islands, Borneo), Malaysia (Borneo), and the Philippines. Taking into account the generally high diversity in Southeast Asia and the rather poor collection activities in the past, with many still unexplored regions, we have to expect more species and an even larger distribution, including most of continental Southeast Asia.

## Acknowledgements

We sincerely thank Morgan Gueuning (formerly University of Lausanne, UNIL), Michael Balke (SNSB-Zoologische Staatssammlung München, ZSM, Germany), Hendrik Freitag and his team (Biodiversity Laboratory, Ateneo de Manila University, Quezon City, Philippines), Jean-Marc Elouard (France), Pascale Derleth-Sartori (MZL), and Heath Ogden (Utah Valley University, Orem, USA) for the collection of the precious material used in this study. Additionally, Morgan Gueuning gathered ecological data from Sumatra during his own studies and made them available for our study. We are also deeply thankful to Lars Hendrich and Katja Neven (SNSB-Zoologische Staatssammlung München, ZSM, Germany) for the loan of type material, and to Luke Jacobus (Indiana University, Purdue University, Columbus, USA) for the provisioning of photos of type material important for this study. Further, we are also grateful to Michel Sartori (MZL) for his constant interest and support for our projects, and to Marion Podolak (MZL) and Céline Stoffel (MZL) for their support with lab work and preparation of the COI barcodes. Scanning electron microscopy was performed at the Center for Molecular and Cell Technologies of St. Petersburg State University. Finally, we are thankful to the reviewers for their valuable comments and corrections.

## References

- Ball SL, Hebert PDN, Burian SK, Webb JM (2005) Biological identifications of mayflies (Ephemeroptera) using DNA barcodes. *Journal of the North American Benthological Society* 24(3): 508–524. <https://doi.org/10.1899/04-142.1>
- Brown RM, Diesmos AC (2010) Philippines, Biology. In: Gillespie RG, Clague DA (Eds) *Encyclopedia of islands*. University of California Press, Berkeley, Los Angeles, London, 723–732. <https://doi.org/10.1525/9780520943728-170>
- Chakrabarty P, Warren M, Page LM, Baldwin CC (2013) GenSeq: An updated nomenclature and ranking for genetic sequences from type and non-type sources. *ZooKeys* 346: 29–41. <https://doi.org/10.3897/zookeys.346.5753>
- Dominguez E, Molineri C, Pescador ML, Hubbard MD, Nieto C (2006) Ephemeroptera of South America. In: Adis J, Arias JR, Rueda-Delgado G, Wantzen KM (Eds) *Aquatic Biodiversity in Latin America*, Vol. 2. Pensoft Publishers, Sofia-Moscow, 646 pp.
- Eidmann H, Köhler F (1970) *Lehrbuch der Entomologie*. Paul Parey, Hamburg, Berlin, 633 pp.
- Folmer O, Black M, Hoeh W, Lutz R, Vrijenhoek R (1994) DNA primers for amplification of mitochondrial cytochrome c oxidase subunit I from diverse metazoan invertebrates. *Molecular Marine Biology and Biotechnology* 3: 294–299. [http://www.mbari.org/staff/vrijen/PDFS/Folmer\\_94MMBB.pdf](http://www.mbari.org/staff/vrijen/PDFS/Folmer_94MMBB.pdf)
- Gattolliat J-L (2012) Two new genera of Baetidae (Ephemeroptera) from Borneo (East Kalimantan, Indonesia). *Annales de Limnologie – International. Journal of Limnology* 48(2): 187–199. <https://doi.org/10.1051/limn/2012012>

- Gattolliat J-L, Nieto C (2009) The family Baetidae (Insecta: Ephemeroptera): synthesis and future challenges. *Aquatic Insects* 31(sup1): 41–62. <https://doi.org/10.1080/01650420902812214>
- Gattolliat J-L, Sartori M (1999) A new species of *Afrobaetodes* (Ephemeroptera: Baetidae) and first report of this genus from Madagascar. *Annales de Limnologie* 35(3): 179–184. <https://doi.org/10.1051/limn/1999025>
- Gattolliat J-L, Vinçon G, Wyler S, Pawlowski J, Sartori M (2016) Toward a comprehensive COI DNA barcode library for Swiss Stoneflies (Insecta: Plecoptera) with special emphasis on the genus *Leuctra*. *Zoosymposia* 11: 135–155. <https://doi.org/10.11646/zoosymposia.11.1.15>
- Gattolliat J-L, Rutschmann S, Monaghan MT, Sartori M (2018) From molecular hypotheses to valid species: description of three endemic species of *Baetis* (Ephemeroptera: Baetidae) from the Canary Islands. *Arthropod Systematics & Phylogeny* 76: 509–528.
- Gill BA, Sandberg JB, Kondratieff BC (2015) Evaluation of the morphological species concepts of 16 western Nearctic *Isoperla* species (Plecoptera: Perlodidae) and their respective species groups using DNA barcoding. *Illiesia* 11: 130–146. <http://illiesia.speciesfile.org/papers/Illiesia11-11.pdf>
- Godunko RJ, Prokopov GA, Soldán T (2004) Mayflies of the Crimean Peninsula. III. The description of *Baetis milani* sp. n. with notes on taxonomy of the subgenus *Rhodobaetis* Jacob, 2003 (Ephemeroptera: Baetidae). *Acta zoologica cracoviensia* 47: 231–248. <https://doi.org/10.3409/173491504783995799>
- Gueuning M, Suchan T, Rutschmann S, Gattolliat J-L, Jamsari J, Kamil AI, Pitteloud C, Buerki S, Balke M, Sartori M, Alvarez N (2017) Elevation in tropical sky islands as the common driver in structuring genes and communities of freshwater organisms. *Scientific Reports* 7(1): 16089–16103. <https://doi.org/10.1038/s41598-017-16069-y>
- Hall R (2010) Indonesia, Geology. In: Gillespie RG, Clague DA (Eds) *Encyclopedia of islands*. University of California Press, Berkeley, Los Angeles, London, 454–460. <https://doi.org/10.1525/9780520943728-104>
- Hubbard MD (1995) Towards a standard methodology for the description of mayflies (Ephemeroptera). In: Corkum LD, Ciborowski JJH (Eds) *Current directions in research on Ephemeroptera*. Canadian Scholar's Press, Toronto, 361–369.
- Jacob U (2003) *Baetis* Leach, 1815, sensu stricto oder sensu lato. Ein Beitrag zum Gattungskonzept auf der Grundlage von Artengruppen mit Bestimmungsschlüsseln. *Lauterbornia* 47: 59–129.
- Kaltenbach T, Gattolliat J-L (2018) The incredible diversity of *Labiobaetis* Novikova & Kluge in New Guinea revealed by integrative taxonomy (Ephemeroptera, Baetidae). *ZooKeys* 804: 1–136. <https://doi.org/10.3897/zookeys.804.28988>
- Kaltenbach T, Gattolliat J-L (2019) The tremendous diversity of *Labiobaetis* Novikova & Kluge in Indonesia (Ephemeroptera, Baetidae). *ZooKeys* 895: 1–117. <https://doi.org/10.3897/zookeys.895.38576>
- Kaltenbach T, Gattolliat J-L (2020) *Labiobaetis* Novikova & Kluge in Borneo (Ephemeroptera, Baetidae). *Zookeys* 914: 43–79. <https://doi.org/10.3897/zookeys.914.47067>
- Kaltenbach T, Gattolliat J-L (2021) New species of *Labiobaetis* Novikova & Kluge from Southeast Asia and New Guinea (Ephemeroptera, Baetidae). *ZooKeys* 1067: 159–208. <https://doi.org/10.3897/zookeys.1067.72251>

- Kaltenbach T, Garces JM, Gattolliat J-L (2020a) The success story of *Labiobaetis* Novikova & Kluge in the Philippines (Ephemeroptera, Baetidae), with description of 18 new species. *ZooKeys* 1002: 1–114. <https://doi.org/10.3897/zookeys.1002.58017>
- Kaltenbach T, Garces JM, Gattolliat J-L (2020b) A new genus of Baetidae (Insecta, Ephemeroptera) from Southeast Asia. *European Journal of Taxonomy* 612(612): 1–32. <https://doi.org/10.5852/ejt.2020.612>
- Kaltenbach T, Garces JM, Gattolliat J-L (2021) *Philibaetis* gen. nov., a new genus from the Philippines (Ephemeroptera, Baetidae). *Deutsche Entomologische Zeitschrift* 68(1): 1–20. <https://doi.org/10.3897/dez.68.59462>
- Kazlauskas RS (1972) Neues über das System der Eintagsfliegen der Familie Baetidae (Ephemeroptera). *Proceedings of the XIII International Congress of Entomology in Moscow, 2–9 August 1968, Vol. 3.*, 337–338.
- Kimura M (1980) A simple method for estimating evolutionary rates of base substitutions through comparative studies of nucleotide sequences. *Journal of Molecular Evolution* 16(2): 111–120. <https://doi.org/10.1007/BF01731581>
- Kingston T (2010) Indonesia, Biology. In: Gillespie RG, Clague DA (Eds) *Encyclopedia of islands*. University of California Press, Berkeley, Los Angeles, London, 446–453. <https://doi.org/10.1525/9780520943728-103>
- Kluge NJ (2004) *The phylogenetic system of Ephemeroptera*. Academic Publishers, Dordrecht, 1–442. <https://doi.org/10.1007/978-94-007-0872-3>
- Kluge NJ (2012) Non-African representatives of the plesiomorphon *Protopatellata* (Ephemeroptera: Baetidae). *Russian Entomological Journal* 20(4): 361–376. <https://doi.org/10.15298/rusentj.20.4.02>
- Kluge NJ (2016) A new subgenus *Oculogaster* subgen. n. for viviparous representatives of *Procloeon* s. l., with discussion about status of the generic name *Austrocloeon* Barnard, 1932 and the species name *africanum* Esben-Petersen, 1913 [*Cloeon*] (Ephemeroptera, Baetidae). *Zootaxa* 4107(4): 491–516. <https://doi.org/10.11646/zootaxa.4107.4.2>
- Kluge NJ (2020) Review of *Oculogaster* Kluge, 2016 (Ephemeroptera, Baetidae, *Procloeon* Bengtsson, 1915). *Zootaxa* 4820(3): 401–437. <https://doi.org/10.11646/zootaxa.4820.3.1>
- Kluge NJ (2022) *Ephemeroptera of the world*. [www.insecta.bio.spbu.ru/z/Eph-spp/Contents](http://www.insecta.bio.spbu.ru/z/Eph-spp/Contents) [retrieved March 2022]
- Kluge NJ, Bernal Vega JA (2018) Redescription of the Central American genus *Moribaetis* Waltz & McCafferty, 1985 (Ephemeroptera, Baetidae). *Zootaxa* 4521(2): 231–257. <https://doi.org/10.11646/zootaxa.4521.2.5>
- Kluge NJ, Novikova EA (2011) Systematics of the mayfly taxon *Acentrella* (Ephemeroptera, Baetidae), with description of new Asian and African species. *Russian Entomological Journal* 20(1): 1–56. <https://doi.org/10.15298/rusentj.20.1.01>
- Kluge NJ, Novikova EA (2014) Systematics of *Indobaetis* Müller-Liebenau & Morihara, 1982, and related implications for some other Baetidae genera (Ephemeroptera). *Zootaxa* 3835(2): 209–236. <https://doi.org/10.11646/zootaxa.3835.2.3>
- Kluge NJ, Novikova EA (2017) Occurrence of *Anafroptilum* Kluge, 2012 (Ephemeroptera: Baetidae) in Oriental Region. *Zootaxa* 4282(3): 453–472. <https://doi.org/10.11646/zootaxa.4282.3.2>

- Kluge NJ, Suttinun C (2020) Review of the Oriental genus *Indocloeon* Müller-Liebenau, 1982 (Ephemeroptera: Baetidae) with descriptions of two new species. *Zootaxa* 4779(4): 451–484. <https://doi.org/10.11646/zootaxa.4779.4.1>
- Kluge NJ, Godunko RJ, Svitok M (2020) Nomenclatural changes in *Centroptella* Braasch & Soldan, 1980 (Ephemeroptera, Baetidae). *ZooKeys* 914: 81–25. <https://doi.org/10.3897/zookeys.914.46652>
- Komarek A, Freitag H (2020) Taxonomic revision of *Agraphhydrus* Régimbart, 1903. IV. Philippines. (Coleoptera: Hydrophilidae: Acidocerinae). *Koleopterologische Rundschau* 90: 201–242.
- Müller-Liebenau I (1981) Review of the original material of the baetid genera *Baetis* and *Pseudocloeon* from the Sunda Islands and the Philippines described by G. Ulmer, with some general remarks (Insecta: Ephemeroptera). *Mitteilungen aus dem Hamburgischen Zoologischen Museum und Institut* 78: 197–208.
- Müller-Liebenau I (1984a) New genera and species of the family Baetidae from West-Malaysia (River Gombak) (Insecta: Ephemeroptera). *Spixiana* 7: 253–284.
- Müller-Liebenau I (1984b) Baetidae from Sabah (East Malaysia) (Ephemeroptera). In: Landa V, Soldán T, Tonner M (Eds) *Proceedings of the Fourth International Conference on Ephemeroptera*, Czechoslovak Academy of Sciences, Budejovice, 85–89.
- Ogden TH, Breinholt JW, Bybee SM, Miller DB, Sartori M, Shiozawa D, Whiting MF (2019) Mayfly phylogenomics: Initial evaluation of anchored hybrid enrichment data for the order Ephemeroptera. *Zoosymposia* 16: 167–181. <https://doi.org/10.11646/zoosymposia.16.1.14>
- Puillandre N, Lambert A, Brouillet S, Achaz G (2012) ABGD, Automatic Barcode Gap Discovery 643 for primary species delimitation. *Molecular Ecology* 21(8): 1864–1877. <https://doi.org/10.1111/j.1365-294X.2011.05239.x>
- Puillandre N, Brouillet S, Achaz G (2020) ASAP: Assemble species by automatic partitioning. *Molecular Ecology Resources* 21(2): 609–620. <https://doi.org/10.1111/1755-0998.13281>
- Quek S-P (2010) Borneo. In: Gillespie RG, Clague DA (Eds) *Encyclopedia of islands*. University of California Press, Berkeley, Los Angeles, London, 111–116. <https://doi.org/10.1525/9780520943728-029>
- Sanger F, Nicklen S, Coulson AR (1977) DNA sequencing with chain-terminating inhibitors. *Proceedings of the National Academy of Sciences of the United States of America* 74(12): 5463–5467. <https://doi.org/10.1073/pnas.74.12.5463>
- Sartori M, Kubiak M, Rajaei H (2016) An updated list of type material of Ephemeroptera Hyatt & Arms, 1890, deposited at the Zoological Museum of Hamburg (ZMH). *ZooKeys* 607: 49–68. <https://doi.org/10.3897/zookeys.607.9391>
- Shi W, Tong X (2015) Taxonomic notes on *Baetiella* Uéno from China, with the descriptions of three new species (Ephemeroptera: Baetidae). *Zootaxa* 4012: 553–569. <https://doi.org/10.11646/zootaxa.4012.3.9>
- Shorthouse DP (2010) SimpleMapp, an online tool to produce publication-quality point maps. <https://www.simplemapp.net> [accessed March 03, 2021]
- Soldán T, Godunko RJ (2006) *Baetis atlanticus* n. sp., a new species of the subgenus *Rhodobaetis* Jacob, 2003 from Madeira, Portugal (Ephemeroptera: Baetidae). *Genus* 17: 5–17.
- Soldán T, Godunko RJ, Thomas AGB (2005) *Baetis chelif* n. sp., a new mayfly from Algeria with notes on *B. sinespinosus* Soldan & Thomas, 1983, n. stat. (Ephemeroptera: Baetidae). *Genus* 16: 155–165.

- Staniczek AH (2010) Distribution of accessory gills in mayfly larvae (Insecta: Ephemeroptera: Siphonuroidea: Eusetisura). *Stuttgarter Beiträge zur Naturkunde A, Neue Serie* 3: 85–102.
- Suttinun C, Gattolliat J-L, Boonsong B (2020) *Cymbalcloeon* gen. nov., an incredible new mayfly genus (Ephemeroptera: Baetidae) from Thailand. *PLoS ONE* 15(10): 1–17. <https://doi.org/10.1371/journal.pone.0240635>
- Tamura K, Stecher G, Kumar S (2021) MEGA 11: Molecular evolutionary genetics analysis version 11. *Molecular Biology and Evolution* 38(7): 3022–3027. <https://doi.org/10.1093/molbev/msab120>
- Tofilski A (2018) DKey software for editing and browsing dichotomous keys. *ZooKeys* 735: 131–140. <https://doi.org/10.3897/zookeys.735.21412>
- Ulmer G (1913) Ephemeriden aus Java, gesammelt von Edw. Jacobsen. *Notes from the Leiden Museum* 35: 102–120.
- Ulmer G (1924) Ephemeropteren von den Sunda-Inseln und den Philippinen. *Treubia* 6: 28–91.
- Ulmer G (1939) Eintagsfliegen (Ephemeropteren) von den Sunda-Inseln. *Archiv für Hydrobiologie (Supplement 16)*: 443–692.
- Vuataz L, Sartori M, Wagner A, Monaghan MT (2011) Toward a DNA taxonomy of Alpine *Rbithrogena* (Ephemeroptera: Heptageniidae) using a mixed Yule-Coalescent Analysis of mitochondrial and nuclear DNA. *PLoS ONE* 6(5): 1–11. <https://doi.org/10.1371/journal.pone.0019728>
- Waltz RD, McCafferty WP (1985) *Moribaetis*: A new genus of Neotropical Baetidae (Ephemeroptera). *Proceedings of the Entomological Society of Washington* 87: 239–251.
- Waltz RD, McCafferty WP (1997) New generic synonymies in Baetidae (Ephemeroptera). *Entomological News* 108: 134–140.
- Waltz RD, McCafferty WP, Thomas A (1994) Systematics of *Alainites* n. gen., *Dipheter*, *Indobaetis*, *Nigrobaetis* n. stat., and *Takobia* n. stat. (Ephemeroptera, Baetidae). *Bulletin de la Société d'Histoire Naturelle de Toulouse* 130: 33–36.
- Yanai Z, Gattolliat J-L, Dorchin N (2018) Taxonomy of *Baetis* Leach in Israel (Ephemeroptera, Baetidae). *ZooKeys* 794: 45–84. <https://doi.org/10.3897/zookeys.794.28214>
- Zhou C-F (2010) Accessory gills in mayflies (Ephemeroptera). *Stuttgarter Beiträge zur Naturkunde A, Neue Serie* 3: 79–84.

## Supplementary material I

### ML reconstruction *Branchiobaetis* gen. nov.

Authors: Thomas Kaltenbach, Nikita J. Kluge, Jean-Luc Gattolliat

Data type: image

Copyright notice: This dataset is made available under the Open Database License (<http://opendatacommons.org/licenses/odbl/1.0/>). The Open Database License (ODbL) is a license agreement intended to allow users to freely share, modify, and use this Dataset while maintaining this same freedom for others, provided that the original source and author(s) are credited.

Link: <https://doi.org/10.3897/zookeys.1135.93800.suppl1>



# Key to the Chinese species of the subgenus *Sphodromimus* Casale, 1984 (Carabidae, Chlaeniini, *Chlaenius*) with descriptions of two new species

Yuyao Qin<sup>1,2</sup>, Christoph Germann<sup>3</sup>, Hongbin Liang<sup>2</sup>

**1** College of Life Sciences, Hebei University, Baoding 071002, China **2** Key Laboratory of Zoological Systematics and Evolution, Institute of Zoology, Chinese Academy of Sciences, Beijing 100101, China **3** Naturhistorisches Museum Basel, Augustinergasse 2, CH-4051 Basel, Switzerland

Corresponding author: Hongbin Liang ([lianghb@ioz.ac.cn](mailto:lianghb@ioz.ac.cn))

Academic editor: B. Guéorguiev | Received 23 August 2022 | Accepted 18 November 2022 | Published 12 December 2022

<https://zoobank.org/7E562C71-BD10-446E-9E10-2AA52A9888FB>

**Citation:** Qin Y, Germann C, Liang H (2022) Key to the Chinese species of the subgenus *Sphodromimus* Casale, 1984 (Carabidae, Chlaeniini, *Chlaenius*) with descriptions of two new species. ZooKeys 1135: 61–91. <https://doi.org/10.3897/zookeys.1135.93843>

## Abstract

The subgenus *Sphodromimus* Casale, 1984 in China has been studied, revealing two new species: *Chlaenius* (*Sphodromimus*) *caperatus* **sp. nov.** from Hunan Province and *Chlaenius* (*Sphodromimus*) *yinggelingensis* **sp. nov.** from Hainan Province. A new replacement name is proposed for *C. (Sphodromimus) wrasei* (Kirschenhofer, 2003) [nec *Chlaenius (Lithochlaenius) wrasei* Kirschenhofer, 1997]: *Chlaenius (Sphodromimus) davidi* **nom. nov.**. The status of *Chlaenius (Sphodromimus) enleensis* Mandl, 1992 is upgraded from subspecies to full species, and *Chlaenius (Sphodromimus) tamdaoensis* Kirschenhofer, 2003 is proposed as its new synonym. *Chlaenius (Sphodromimus) pilosus* (Casale, 1984) is reported as a new record from China. A key to all known species of the subgenus *Sphodromimus* from China is provided.

## Keywords

Coleoptera, distribution, genitalia, ground beetles, taxonomy

## Introduction

*Vachinius* Casale, 1984 was erected as a genus for *Pristonychus subglaber* Andrewes, 1937, and *Sphodromimus* Casale, 1984 was erected as a subgenus of *Vachinius* at the same time (Casale, 1984). Recently, both *Vachinius* and *Sphodromimus* were considered sub-

genera of the genus *Chlaenius* Bonelli, 1810 (Azadbakhsh and Kirschenhofer 2019). *Chlaenius peterseni* (Louwerens, 1967), *C. flavofemoratus* Laporte, 1834, and *C. tamdaoensis* Kirschenhofer, 2003 were transferred from the subgenus *Haplochlaenius* to the subgenus *Sphodromimus* by Azadbakhsh and Kirschenhofer (2019). To date, in total 14 species are recognized in the subgenus *Sphodromimus*, distributed in the Oriental Region, e.g., China, Indonesia, Laos, Myanmar, Nepal, Philippines, Thailand, Vietnam (Morvan 1991, 1997; Lassalle 2001; Kirschenhofer 2003, 2012; Brunk 2015; Zettel 2020).

The subgenus differs from other subgenera of genus *Chlaenius* mainly by its large size (length 19.0–26.0 mm), elytral intervals densely punctate and pubescent, slightly convex, not costulate, and the apical lamella of the aedeagus is denticulate on the dorsal side (Casale 1984). Before the present study, four species of this subgenus had been recorded from China: *Chlaenius (Sphodromimus) deuvei* (Morvan, 1997), *Chlaenius (Sphodromimus) flavofemoratus* Laporte, 1834, *Chlaenius (Sphodromimus) hunanus* (Morvan, 1997), and *Chlaenius (Sphodromimus) wrasei* (Kirschenhofer, 2003). When examining specimens from south China, we found two new species and a new country record based on comparison with types and/or original descriptions. In this paper, we describe the new species and report the newly found one, upgrade one subspecies to full species, propose a new replacement name, and provide a revised key to all known species of subgenus *Sphodromimus* in China.

## Materials and methods

Specimens examined during our study are deposited in the following collections:

- CAS** California Academy of Science, San Francisco, USA;  
**DWC** working collection David W. Wrase, Gusow-Platkow, Germany (part of Zoologische Staatssammlung, München);  
**IZAS** Institute of Zoology, Chinese Academy of Sciences, Beijing, China;  
**MNHN** Muséum National d’Histoire Naturelle, Paris, France;  
**NHMB** Naturhistorisches Museum Basel, Switzerland;  
**SCAU** South China Agriculture University, Guangzhou, China.

Abbreviations for measurements used in the paper are as follows:

- BL** length of body, measured from the apical margin of the labrum to the elytral apex;  
**BW** width of body, measured across the elytral greatest width;  
**EL** length of elytra, measured from the base of the scutellum to the elytra apex;  
**ML** length of metepisternum, measured along its outer side;  
**MW** width of metepisternum, measured along its anterior side;  
**PAW** width of apical pronotum, measured between the apices of the anterior angle;

- PBW** width of basal pronotum, measured along its basal margin;  
**PL** length of pronotum, measured along its median line;  
**PW** width of pronotum, measured across its greatest width.

The methods of dissection, illustrations, and measurements mainly follow our previous work (Shi et al. 2013a, b). Terminology of female genitalia follows Deuve (1993) and Liebherr and Will (1998).

## Taxonomic account

### Subgenus *Sphodromimus* Casale, 1984

*Sphodromimus* Casale, 1984: 372; Morvan 1991: 60 (described new species); Morvan 1997: 16 (described new species); Lorenz 1998: 320 (catalogue); Lassalle 2001: 240 (described new species); Kirschenhofer 2003: 32 (described new species); Lorenz 2005: 341 (catalogue); Kirschenhofer 2012: 84 (described new species); Kirschenhofer 2013: 9 (new combination from *Haplochlaenius*); Brunk 2015: 5 (described new species); Kirschenhofer 2017: 497 (catalogue); Azadbakhsh and Kirschenhofer 2019: 1 (*Sphodromimus* considered subgenus of *Chlaenius*); Zettel 2020: 29 (described new species).

**Type species.** *Vachinius holzschuhi* (Casale, 1984) (type locality: East Nepal, Tashigaon 2100 m; holotype in NHMB), by original designation.

**Diagnosis.** *Sphodromimus* can be distinguished from other subgenera in *Chlaenius* by the following character combinations: body large, BL 19–26 mm; body black or metallic colored, luster matt or strongly shiny, antennae, mandibles usually dark brown, elytra black, ventral side black; head finely punctate; penultimate labial palpomere with 5–7 setae, apex truncate; antennae long, antennomere 3 longer than 4; mentum tooth stout, bifid; pronotum long, with sides usually sinuate before posterior angles, posterior lateral seta situated before posterior angles, anterior lateral seta absent; proepisterna sparsely punctate and pubescent; elytral intervals flat or convex, not ribbed, densely punctate and pubescent, basal margin reaching the scutellum; hind wings reduced in all species except *Chlaenius flavofemoratus* Laporte, 1834 and *Chlaenius peterseni* (Louwerens, 1967); prosternal process unbordered at apex; metepisterna wider than long in all species except *C. flavofemoratus* and *C. peterseni*, coarsely punctate, pubescent; legs sparsely pubescent, tarsi nearly smooth dorsally, claws simple, protibiae sulcate on dorsal side; abdominal sternites finely punctate laterally; apical lamella of aedeagus denticulate on dorsal side; apical gonocoxite without ensiform setae; receptaculum very short to absent.

**Comparisons.** This subgenus is most similar to subgenera *Haplochlaenius* Lutshnik and *Vachinius* Casale, but differs in having elytra with intervals flat or slightly convex, densely punctate and pubescent, and with basal margin complete, connected with

scutellum (intervals strongly ribbed in *Haplochlaenius*, basal margin obsolete near scutellum; intervals smooth in *Vachinius*; cfr. Azadbakhsh and Kirschenhofer 2019).

**Species and distribution.** Subgenus is composed of 16 species distributed in the Oriental Region (China, Indonesia, Laos, Myanmar, Nepal, Philippines, Thailand, Vietnam), including the two new species described below.

### Key to species of subgenus *Sphodromimus* Casale, 1984 from China

- 1 Pronotum copper-green to violet, shining, with metallic luster ..... **2**
- Pronotum black and matt ..... **4**
- 2 Pronotum cordate, widest at apical third, anterior angles projected forward, strongly sinuate before posterior angles (Figs 21, 23); hind wings reduced; metepisterna short, MW/ML = 1.03–1.17 (Figs 12, 15) ..... **3**
- Pronotum subquadrate, widest at middle, anterior angles not projected forward, lateral margins rounded or straight before posterior angles (Fig. 22); hind wings developed; metepisterna long, MW/ML = 0.75–0.92 (Fig. 14) ..... ***C. flavofemoratus* Laporte, 1834**
- 3 Legs entirely black (Fig. 9A, B). Guangdong, Xinyi; Guangxi, Daming Shan ..  
..... ***C. davidi* nom. nov.**
- Distal half of femora red-brown (Fig. 4A–D). Hainan, Yinggeling.....  
..... ***C. yinggelingensis* sp. nov.**
- 4 Posterior angles of pronotum slightly projected backward (Fig. 19); apex of apical lamella of aedeagus concaved in the middle, both sides thickened, each with a denticulation (Fig. 27A); receptaculum tiny, seminal canal short (Fig. 36A). Guangxi, Mao'er Shan; Guangxi, Huaping ..... ***C. dewei* (Morvan, 1997)**
- Posterior angles of pronotum not projected (Figs 17, 18, 20); apex of apical lamella of aedeagus truncated or rounded ..... **5**
- 5 Pronotum subquadrate, nearly as long as wide (PW/PL = 1.02–1.07), lateral margins straight before posterior angles (Fig. 20); apex of apical lamella of aedeagus truncated; right side of median lobe with a large denticulation, left side with a small denticulation (Fig. 28A). Yunnan, Dawei Shan; Vietnam, the Black River ..... ***C. pilosus* (Casale, 1984)**
- Pronotum cordate, much wider than long (PW/PL = 1.18–1.26), lateral margins faintly sinuate before posterior angles (Fig. 17, 18); apex of apical lamella of aedeagus untruncated ..... **6**
- 6 Pronotum with apical width equal to or slightly shorter than basal width (PAW/PBW = 0.99–1.00) (Fig. 17); apex of apical lamella of aedeagus rounded (Fig. 25A); receptaculum long, seminal canal short (Fig. 34A). Hunan, Guidong ..... ***C. caperatus* sp. nov.**
- Pronotum apical width clearly shorter than basal width of pronotum (PAW/PBW = 0.87–0.97) (Fig. 18); apical lamella of aedeagus triangular (Fig. 26A); receptaculum short, seminal canal long (Fig. 35A). Hunan Jiuyi Shan; Guangdong, Nanling ..... ***C. hunanus* (Morvan, 1997)**

***Chlaenius (Sphodromimus) caperatus* sp. nov.**

<https://zoobank.org/DC3445D1-970D-43DE-B622-8EA561F22632>

Figs 1A–D, 11, 17, 25A–E, 34A–C, 40

**Type locality.** China, Hunan, Guidong: Qiyun Shan (25.9010°N, 114.0068°E), altitude 1299.12 m.

**Type material. Holotype.** Male (IZAS) [genitalia dissected and glued on plastic film pinned under specimen], Hunan, Guidong, Qiyun Shan, 25.9010°N, 114.0068°E, 1299.12 m, 2017.XI.12–14, S.P. Yu, Y.Z. Liu leg., Institute of Zoology, IZAS/Holotype *Chlaenius (Sphodromimus) caperatus* sp. nov. des. by Y.Y. Qin, 2022 [red label].

**Paratypes.** Total 8 specimens: 2 ♂♂ and 3 ♀♀ (IZAS), same data as holotype; 1 ♀ (IZAS), Hunan, Guidong, Qiyun Shan, 25.9007°N, 114.01318°E, 1487.17 m, 2017.XI.12–14, S.P. Yu, Y.Z. Liu leg., Institute of Zoology, IZAS; 1 ♂ and 1 ♀ (SCAU) “Hunan, Guidong, Dongluo, Chishuixian, 1350–1450 m, 2011.XII.1, M.Y. Tian, Q. Gao, F.F. Sun leg., SCAU. All paratypes also bear the following label: Paratype. *Chlaenius (Sphodromimus) caperatus* sp. nov. des. by Y.Y. Qin, 2022 [red label].

**Diagnosis.** Dorsum black. PW/PL = 1.18–1.21; PAW/PBW = 0.99–1.00 (Fig. 17); pronotum with anterior angles rounded, moderately projected forward; disc sparsely punctate and pubescent with deep transverse rugosities, but with a glabrous area in the middle. Elytral intervals flat, densely punctate and pubescent. Hind wings reduced. Metepisterna short, MW/ML = 1.1–1.3 (Fig. 11). Apex of apical lamella rounded (Fig. 25A–E).

**Comparisons.** This new species is most similar to *Chlaenius (Sphodromimus) hunanus* (Morvan, 1997) (Fig. 2A, B), sharing the large size, shape of pronotum, black elytra, and reduced hind wings, but can be distinguished from the latter by: (1) PAW/PBW = 0.99–1.00 (Fig. 17), (0.87–0.97 in *C. hunanus*, Fig. 18); (2) apex of lamella of median lobe rounded (apex of lamella triangular in *C. hunanus*, Fig. 26A–E); (3) in female genitalia, receptaculum longer (shorter in *C. hunanus*, Fig. 35A–C), and seminal canal shorter (longer in *C. hunanus*, Fig. 35A–C).

**Description.** BL = 20.3–22.0 mm, BW = 7.6–8.9 mm [BL = 21.0 mm, BW = 7.0 mm in holotype], PAW = 3.6–3.9 mm, PBW = 3.6–3.9 mm, PW = 5.0–5.5 mm, PL = 4.3–4.5 mm, MW = 1.9–2.0 mm, ML = 1.5–1.8 mm. Head, pronotum, elytra, legs, and venter black; antennae, labial and maxillary palpi, apex of mouthparts, and tarsomeres dark brown.

**Head.** Vertex punctate and pubescent with a glabrous and rugose area in the middle; antennae long, reaching middle of elytra; antennomere 3 ~ 1.5× longer than antennomere 4.

**Pronotum** cordiform, PW/PL = 1.18–1.21 (Fig. 17), widest at apical third; anterior margin slightly concave, its width equal to its basal width, PAW/PBW = 0.99–1.00; lateral margins rounded before middle, then distinctly narrowed to base, faintly sinuate before posterior angles; anterior angles rounded, moderately projected forward; posterior angles obtuse, slightly sharp at tips; disc gently convex, sparsely punctate and pubescent, with deep transverse rugosities, with a small glabrous area in the middle; median line distinct, not reaching anterior margin and base; basal foveae deep and long, punctate, pubescent.

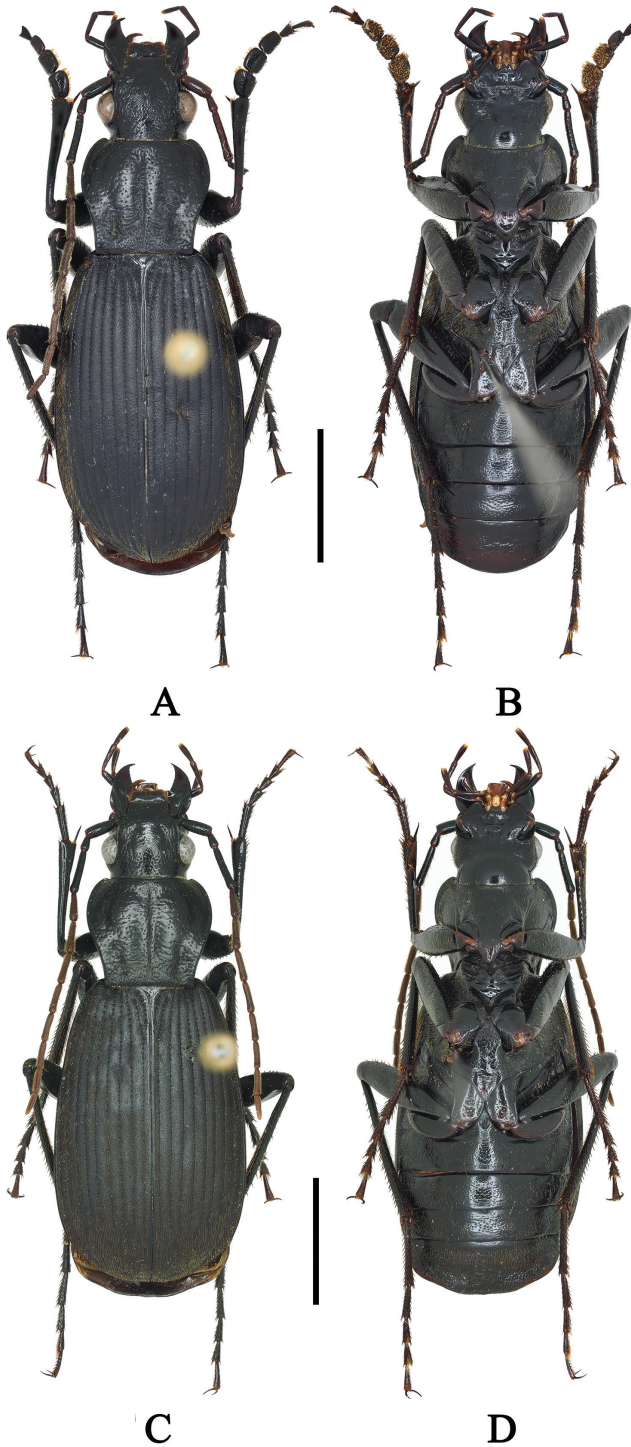
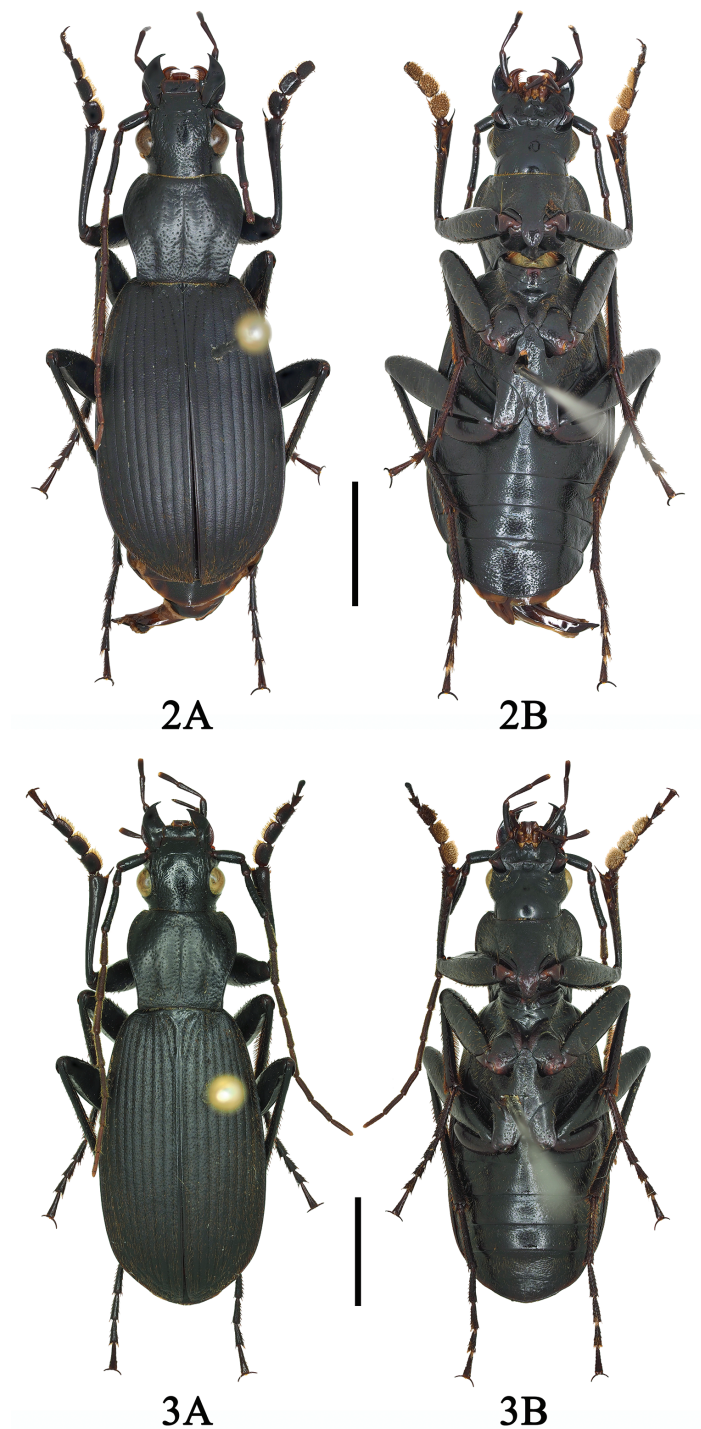


**Figure 1.** A, B *Chlaenius (Sphodromimus) caperatus* sp. nov. (holotype, Hunan, Guidong)  
C, D *C. (Sphodromimus) caperatus* sp. nov. (female paratype, Hunan, Guidong). Scale bars: 5.0 mm.



**Figures 2, 3.** 2A, B *Chlaenius (Sphodromimus) hunanus* (Morvan, 1997) (male, Guangdong, Nanling)  
3A, B *(Sphodromimus) deuwei* (Morvan, 1997) (male, Guangxi, Huaping). Scale bars: 5.0 mm.

**Elytra** elongate, EL/BW = 1.45–1.61; gently convex, widest near posterior third, rounded at apex in males, subtruncate in females; striae with fine punctures; parascutellar striae well developed; parascutellar pores present; intervals flat, densely punctate and pubescent; sutural angles sharp; hind wings reduced.

**Venter** densely punctate, pubescent, metepisterna (Fig. 11) short, MW/ML = 1.25–1.33; abdominal sternites III–VI with one setiferous puncture each side, sternite VII with one pair of setiferous punctures in males, two pairs in females; all abdominal sternites with distinct impressions laterally.

**Legs** long and slender; tarsi nearly smooth dorsally.

**Male genitalia.** Median lobe (Fig. 25B–E) long, strongly bent to ventral side; apical orifice opened dorsally, long and wide, not reaching basal bulb, slightly turned to left side; in dorsal view, apical lamella (Fig. 25A) slightly bent to left side, length nearly equal to its basal width, apex rounded; in left lateral view, apical portion distinctly bent into a hook ventrally (Fig. 25B, E), basal orifice  $\sim 90^\circ$  relative to preapical shaft; left paramere large and round; right paramere helical carved; endophallus with coiled flagellum; basal part of flagellum strongly bent with an oval sclerite facing the right; apical part of flagellum distinctly bent with a triangular bursa.

**Female genitalia.** Spermatheca (Fig. 34A–C) with seminal canal  $\sim 15\times$  as long as receptaculum; receptaculum short linear; seminal canal inserted at base of common oviduct; spermathecal gland rounded and inserted near apex of seminal canal; villous canal long, tortuously contorted, adhered to common oviduct.

**Distribution.** (Fig. 40) This species is known only from Guidong, Hunan. Its distribution seems isolated by a mountain barrier from *C. hunanus*.

**Etymology.** The new species *caperatus* is named for its rugosity on the vertex, pronotal disc, and abdominal sternites.

**Remarks.** We have not examined the types of *C. (S.) hunanus*, but Dr. Deuve (MNHN) kindly helped us to compare types and sent us illustrations of the apical lamella of holotype. More than 60 specimens collected from Nanling, Guangdong fit Morvan's descriptions and illustration (1997: 17, fig. 13), and we determined them as *C. (S.) hunanus*. Nanling is located  $\sim 100$  km north of the type locality of *C. (S.) hunanus* Jiuyi Shan, Hunan (Fig. 40).

***Chlaenius (Sphodromimus) yinggelingsis* sp. nov.**

<https://zoobank.org/95948EBD-4279-457D-BB06-0A501D8198D9>

Figs 4A–D, 12, 21, 29A–E, 37A–C, 40

**Type locality.** China, Hainan, Yinggeling.

**Type material. Holotype.** Male (IZAS) [genitalia dissected and glued on plastic film pinned under specimen], Hainan, Yinggeling, 2009.V.11, Xinlei Huang leg., Institute of Zoology, IZAS/Holotype *Chlaenius (Sphodromimus) yinggelingsis* sp. nov. des. by Y.Y. Qin, 2022 [red label].

**Paratypes.** Total 4 specimens: 1 ♂ (IZAS), same data as holotype; 2 ♀♀ (IZAS), Hainan, Jianfengling, Mingfenggu, 947 m, 2015.I.23, Deyao Zhou leg., Institute of

Zoology, IZAS; 1♀ (IZAS), Hainan, Wuzhishan, 18°54'N, 109°41'E, 1000–1600 m, 2012.IV.18, PAN & LI leg. All paratypes also bear the following label: Paratype. *Chlaenius (Sphodromimus) yinggelingensis* sp. nov. des. by Y.Y. Qin, 2022 [red label].

**Diagnosis.** Pronotum metallic coppery to green.  $PW/PL = 1.12-1.21$ ;  $PAW/PBW = 0.84-0.91$  (Fig. 21); pronotum cordate with posterior angles right angled, rounded at tips; disc sparsely punctate and pubescent with shallow, transverse rugosities. Elytral intervals distinctly convex, with a row of setae laterally and sparse setae centrally. Hind wings reduced. Metepisterna short or width nearly equal to length;  $MW/ML = 1.03-1.17$  (Fig. 12). Distal half of femora red-brown, the rest of legs black.

**Comparisons.** This new species is similar to *Chlaenius (Sphodromimus) flavofemoratus* (Figs 7A–C), in having a large size, coloration of the pronotum and femora, and the absence of a spermatheca, but can be distinguished from the latter by: (1) pronotum cordate (subquadrate in *C. flavofemoratus*); (2) metepisterna wider than or nearly equal to long (longer than wide in *C. flavofemoratus* as in Fig. 14); (3) hind wings reduced (developed in *C. flavofemoratus*); (4) interval convex throughout (convex basally, flat apically in *C. flavofemoratus*).

It is also similar to *Chlaenius (Sphodromimus) peterseni* (Louwerens, 1967) from the Philippines in having pronotum with green metallic luster and elytral intervals slightly convex, but differs in having meso- and metafemora with yellow coloration in the middle, pronotum with lateral margins sinuate before posterior angles, hind wings reduced (femoral black, pronotum with lateral margins straight, and hind wings developed in *C. peterseni*, Fig. 5A, B)

**Description.** BL = 20.9–21.6 mm, BW = 7.5–7.9 mm [BL = 21.3 mm, BW = 7.7 mm in holotype], PAW = 3.4–3.6 mm, PBW = 3.7–4.0 mm, PW = 4.8–5.3 mm, PL = 4.1–4.5 mm, MW = 1.7–1.8 mm, ML = 1.5–1.6 mm. Head, elytra, and venter black; pronotum metallic green to metallic coppery; antennae, labial and maxillary palpi, apex of mouthparts, and tarsomeres dark brown; distal half of femora red-brown, the rest of legs black.

**Head.** Vertex sparsely, finely punctate and pubescent; antennae long, reaching middle of elytra; antennomere 3 ~ 1.5× longer than antennomere 4.

**Pronotum** cordiform,  $PW/PL = 1.12-1.21$  (Fig. 21), widest at apical third; anterior margin slightly concave,  $PAW/PBW = 0.84-0.91$ ; lateral margins rounded before middle, then distinctly narrowed to base, straight before posterior angles; anterior angles rounded, moderately projected forward; posterior angles almost right angled, slightly sharp at tips; disc sparsely punctate and pubescent, with shallow transverse rugosities, without glabrous area in the middle; median line distinct, not reaching anterior margin and base; basal foveae deep and long, punctate, pubescent.

**Elytra** elongate,  $EL/BW = 1.67-1.73$ , gently convex, widest near posterior third, rounded at apex in males, subtruncate in females; basal margin sinuate, reaching the scutellum (but slightly obsolete on one side in a female); striae with deep punctures; parascutellar striae well developed; parascutellar pores present; intervals distinctly convex, with a row of setae laterally and sparse setae centrally; sutural angles obtuse; hind wings reduced.

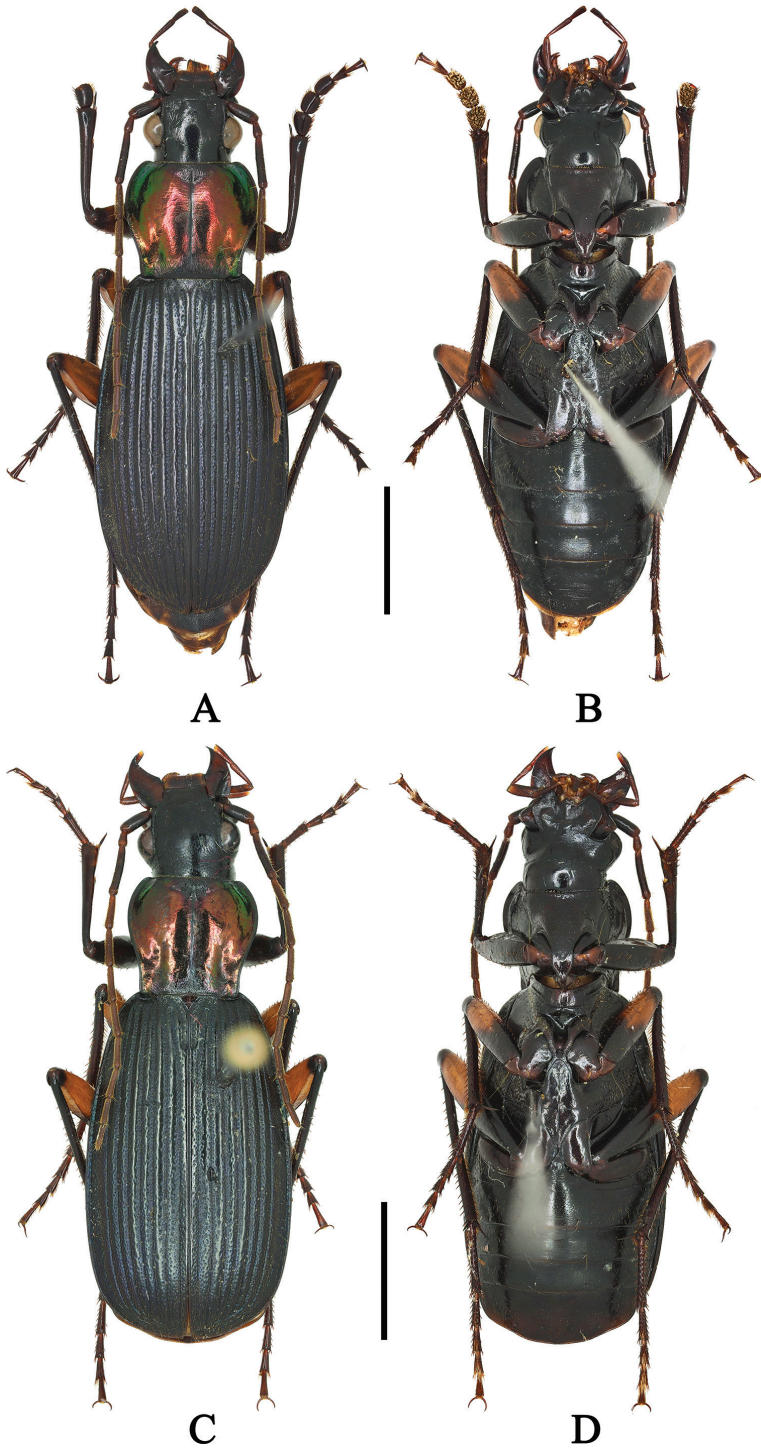
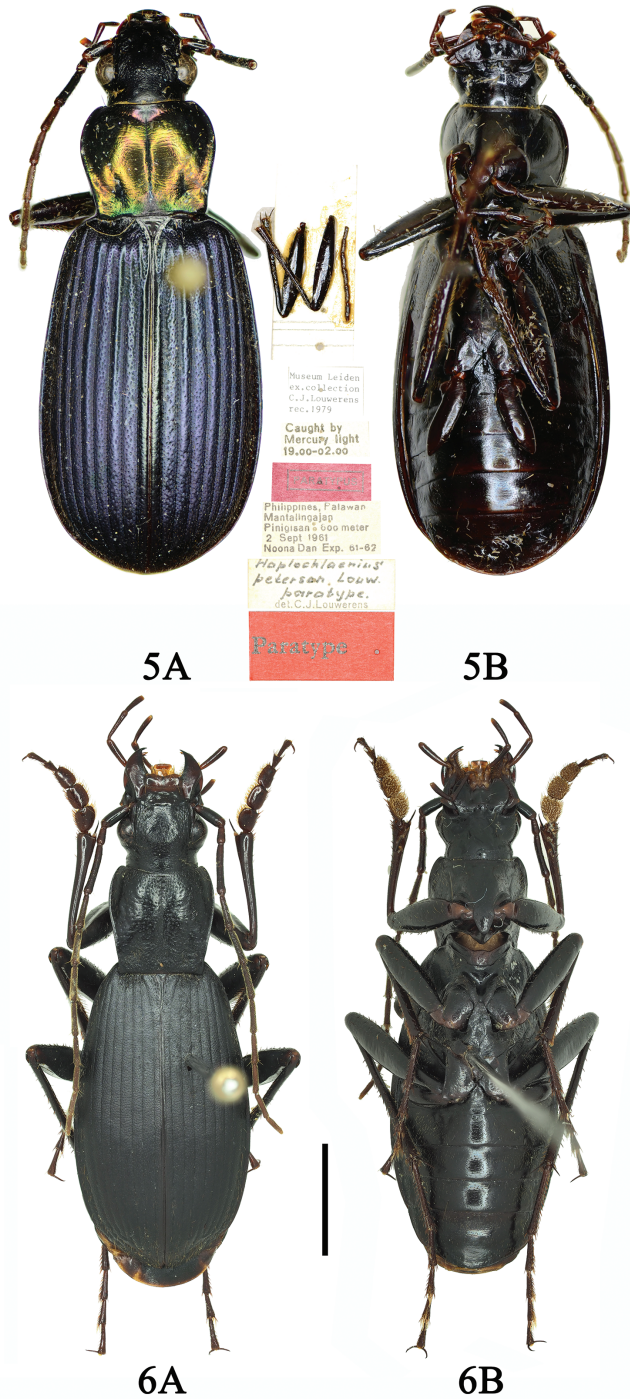


**Figure 4.** **A, B** *Chlaenius (Sphodromimus) yinggelingensis* sp. nov. (holotype, Hainan, Yinggeling) **C, D** *C. (S.) yinggelingensis* sp. nov. (female paratype, Hainan, Jianfengling). Scale bars: 5.0 mm.



**Figures 5, 6. 5A, B** *Chlaenius* (*Sphodromimus*) *peterseni* (Louwerens, 1967) (female paratype, Philippine, photos by Shi Hongliang) **6A, B** *C. (Sphodromimus) pilosus* (Casale, 1984) (male, Yunnan, Pingbian). Scale bar: 5.0 mm.

**Venter** sparsely pubescent, punctate; metepisterna (Fig. 12) short or width nearly equal to length, MW/ML = 1.03–1.17; abdominal sternites III–VI with one setiferous puncture each side, sternite VII with one pair of setiferous punctures in males, two pairs in females; all abdominal sternites with a few impressions laterally.

**Legs** long and slender; tarsi nearly smooth dorsally.

**Male genitalia.** Median lobe (Fig. 29B–E) long, strongly bent to ventral side; apical orifice opened dorsally, long and wide, not reaching basal bulb; in dorsal view, apical lamella (Fig. 29A) wide and short, wider than long, apex subtruncate, each side distinctly widened and thickened; in left lateral view, apex with a denticulation bent to back; in right lateral view, each side convex into a denticulation, right side smaller than left side, basal orifice  $\sim 90^\circ$  relative to preapical shaft; left paramere large and oval; right paramere helically curved; endophallus with flagellum thick and straight; basal part of flagellum with a disciform sclerite facing the left.

**Female genitalia.** Bursa copulatrix (Fig. 37A–C) asymmetric, base with a bifid irregular protrusion; villous canal long, tortuously contorted, adhered to common oviduct; spermatheca and spermathecal gland absent.

**Distribution.** (Fig. 40) China (Hainan).

**Etymology.** The new species *yinggelingensis* is named for the type locality Yinggeling, Hainan.

**Remarks.** We dissected two females in *C. yinggelingensis*, four in *C. davidi* and nine in *C. flavofemoratus*. As a result, we could not find either spermatheca or spermathecal gland. The absence of spermatheca is uncommon in Carabidae and only occasionally found in Trechini (Deuve 1993: fig. 250). They are also absent at least in other two species of the subgenus, *C. (Sphodromimus) davidi* and *C. (Sphodromimus) flavofemoratus* (see female genitalia descriptions below).

### ***Chlaenius (Sphodromimus) pilosus* (Casale, 1984), new record from China**

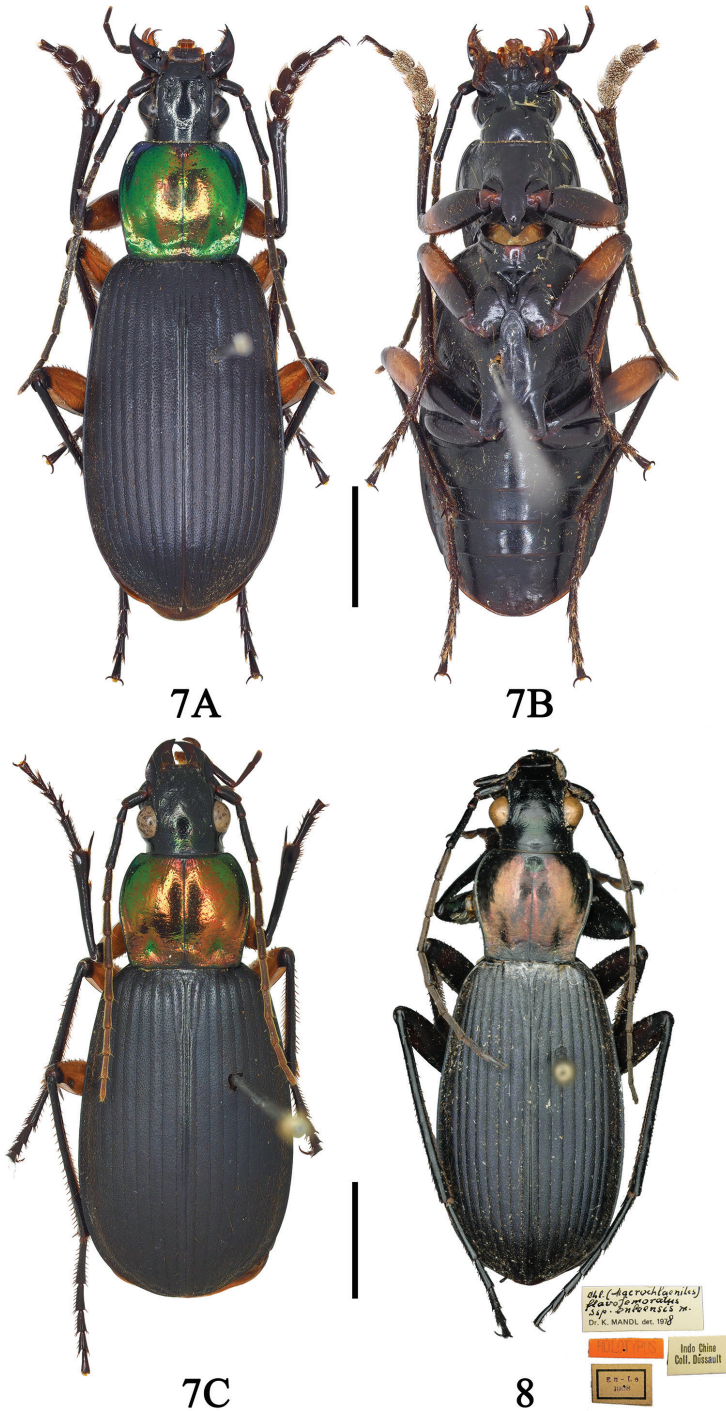
Figs 6A, B, 13, 20, 28A–E, 40

*Vachinius (Sphodromimus) pilosus* Casale, 1984: 379; Lorenz 1998: 320 (catalogue); Lorenz 2005: 341 (catalogue); Brunk and Kirschenhofer 2016: 54 (record); Azadbakhsh and Kirschenhofer 2019: 1 (transferred from genus *Vachinius*).

**Type locality.** Vietnam, Chapa, Tonkin, Coll. J. Clermont.

**Material examined.** CHINA – Yunnan Prov.: 4 ♂♂ (IZAS), Pingbian, Dawei Shan, 2100 m, 2010.V.23, X.D. Yang, X.Y. Zhu leg.

**Diagnosis.** Dorsum black. PW/PL = 1.02–1.07; PAW/PBW = 0.98–1.00 (Fig. 20); pronotum subquadrate with anterior angles rounded, slightly projected forward; disc densely and completely rugose, punctate. Elytral intervals flat and densely punctate and pubescent. Hind wings reduced. Metepisterna short, MW/ML = 1.3–1.4 (Fig. 13). Apical lamella of median lobe truncated, right side with a large denticulation, left side with a small denticulation (Fig. 28A–E), sometimes, such denticulation absent.



**Figures 7, 8. 7A, B** *Chlaenius (Sphodromimus) flavofemoratus* Laporte, 1834 (male, Yunnan, Menglun) **C** *C. (Sphodromimus) flavofemoratus* Laporte, 1834 (female, Yunnan, Menglun) **8** *C. (Sphodromimus) enleensis* Mandl, 1992 (holotype, Indo China) Scale bars: 5.0 mm.

**Description.** BL = 19.6–21.9 mm, BW = 7.3–7.6 mm, PAW = 3.33–3.55 mm, PBW = 3.40–3.55 mm, PW = 4.35–4.55 mm, PL = 4.05–4.45 mm, MW = 1.65–1.80 mm, ML = 1.20–1.35 mm. Head, pronotum, elytra, legs, and venter black; antennae, labial and maxillary palpi, apex of mouthparts and tarsomeres dark brown.

**Head.** Vertex punctate and pubescent with a rugose area; antennae long, reaching middle of elytra; antennomere 3 ~ 1.5× longer than antennomere 4.

**Pronotum** subquadrate, PW/PL = 1.02–1.07 (Fig. 20), widest at apical third; anterior margin slightly concave, its width equal to width of basal margin, PAW/PBW = 0.98–1.00; lateral margins slightly bent before middle, then gently narrowed to base, straight before posterior angles; anterior angles rounded, slightly projected forward; posterior angles right angled, slightly rounded at tips; disc gently convex, sparsely punctate, pubescent, with a few transverse rugosities, without glabrous area in the middle; median line distinct, deep, reaching anterior margin and base; basal foveae deep, short, broad, punctate, and pubescent.

**Elytra** elongate, EL/BW = 1.64–1.77; gently convex near anterior third, widest near posterior third, rounded at apex in males; striae with deep punctures; parascutellar striae well developed; parascutellar pores present; intervals flat, densely punctate and pubescent; sutural angles sharp; hind wings reduced.

**Venter** densely punctate, pubescent, metepisterna (Fig. 13) short, MW/ML = 1.30–1.38; abdominal sternites III–VI with one setiferous puncture each side, sternite VII with one pair of setiferous punctures in males, two pairs in females; all abdominal sternites with distinct impressions laterally.

**Legs** long and slender; tarsi nearly smooth dorsally.

**Male genitalia.** Median lobe (Fig. 28B–E) stout, strongly bent to ventral side; apical orifice opening dorsally, long and wide, not reaching basal bulb; in dorsal view, apical lamella (Fig. 28A) wide and short, wider than long, apex truncated; in left lateral view, apical right side with a large denticulation towards the base and outside, basal left side only thickened and convex or convex into a small denticulation, basal orifice ~ 90 ° relative to preapical shaft; left paramere large and round; right paramere helically curved; endophallus with flagellum coiled; basal part of flagellum with a disciform sclerite facing the right; apical part of flagellum with strip of sclerite.

**Female genitalia** unknown.

**Distribution.** China (Yunnan), Vietnam.

**Remarks.** The type locality is situated in the mountains of the Black River, northern Vietnam, not far from the Chinese frontier. Our identification is based on the original description and illustration of the male genitalia of the holotype by Casale (1984: 379, figs 11, 13).

***Chlaenius (Sphodromimus) davidi* nom. nov.**

Figs 9A, B, 15, 23, 31A–E, 39A–C, 40

*Vachinius (Sphodromimus) wrasei* Kirschenhofer, 2003: 37 (type locality: China, Guangdong); Lorenz 2005: 342 (catalogue); Brunk and Kirschenhofer 2016:

54 (record); Azadbakhsh and Kirschenhofer 2019: 1 (genus *Chlaenius*, subgenus *Sphodromimus*) [nec *C. (Lithochlaenius) wrasei* (Kirschenhofer, 1997)]

**Type locality.** Guangdong, Xinyi, Datianding.

**Material examined.** Total 10 specimens. CHINA – **Guangdong:** Holotype female (DWC, photo), China, Guangdong, 1500 m, Xinyi: Datianding (22.16/111.15) -VIII-1997 – leg. Li/Holotypus, *Chlaenius (Sphodromimus) wrasei* sp. nov. det. Kirschenhofer, 2001 [red label]/COLL WRASE, BERLIN; 1 ♂ and 4 ♀♀ (IZAS), Guangdong, Xinyi, Yunkai Shan, 1508.21m/22.291317°N, 111.209888°E, 2017.V.30, Y.Z. Liu, S.P. Yu leg., Inst. of Zoology; 2 ♀♀ (IZAS), Guangdong, Xinyi, Yunkai Shan, 1250.55 m/22.292692°N, 111.203833°E, 2017.V.31, Y.Z. Liu, S.P. Yu leg., Inst. of Zoology; **Guangxi:** 2 ♂♂ (IZAS), Guangxi Prov, Daming Shan, Tianping Protect Station, N 23.49811, E 108.43715/1230 m, 2011.V.27 N, Xinlei Huang Coll., Inst. of Zoology.

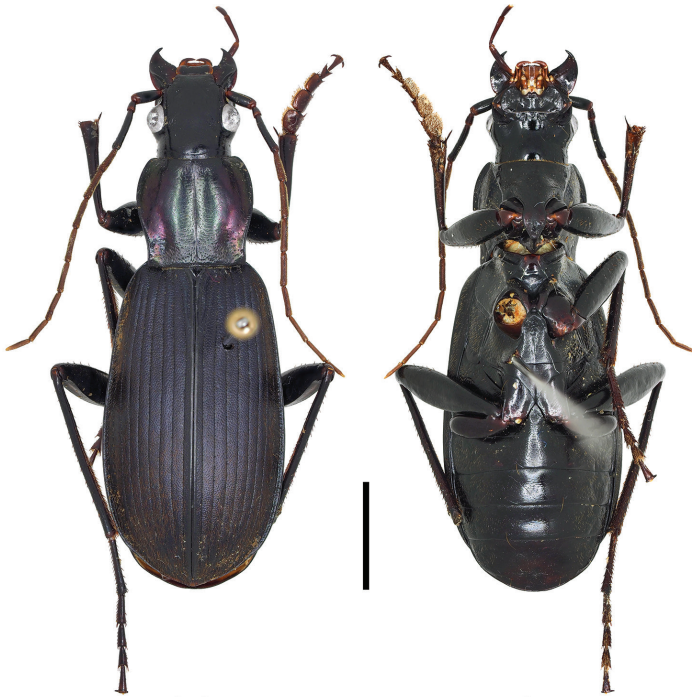
**Diagnosis.** Pronotum fully metallic purple, or greenish purple. PW/PL = 1.09–1.11; PAW/PBW = 0.83–0.93 (Fig. 23); pronotum cordate with posterior angles nearly right angled, rounded at tips; disc sparsely punctate and pubescent, with dense, shallow, transverse rugosities, without glabrous area in the middle. Elytral intervals convex basally, flat apically, densely punctate and pubescent. Hind wings reduced. Metepisterna short, MW/ML = 1.11–1.15 (Fig. 15). Legs totally black.

**Comparisons.** This species is most similar to *Chlaenius (Sphodromimus) enleensis* Mandl, 1992 (Figs 8, 10A, B), sharing the large size, general shape of apical lamella, metepisterna short (Figs 15, 16), and reduced hind wings, but can be distinguished from the latter by: (1) pronotum purple or greenish purple (Fig. 23) (green to coppery, but not purple in *C. enleensis*, Fig. 24); (2) femora black (middle of mesofemora and metafemora brown in *C. enleensis*); (3) elytral intervals convex basally, flat apically (interval convex throughout in *C. enleensis*); (4) apical lamella wider at base (narrower in *C. enleensis*, Figs 32A, C, D, 33A, C, D)

**Description.** BL = 21.3–24.4 mm, BW = 8.0–8.7 mm. PL = 4.5–5.0 mm, PW = 5.0–5.5 mm, MW = 2.0–2.1 mm, ML = 1.7–1.9 mm. Head, elytra, venter, and legs dark and black; pronotum fully purple or greenish purple; antennae, labial and maxillary palpi, apex of mouthparts and tarsomeres dark brown.

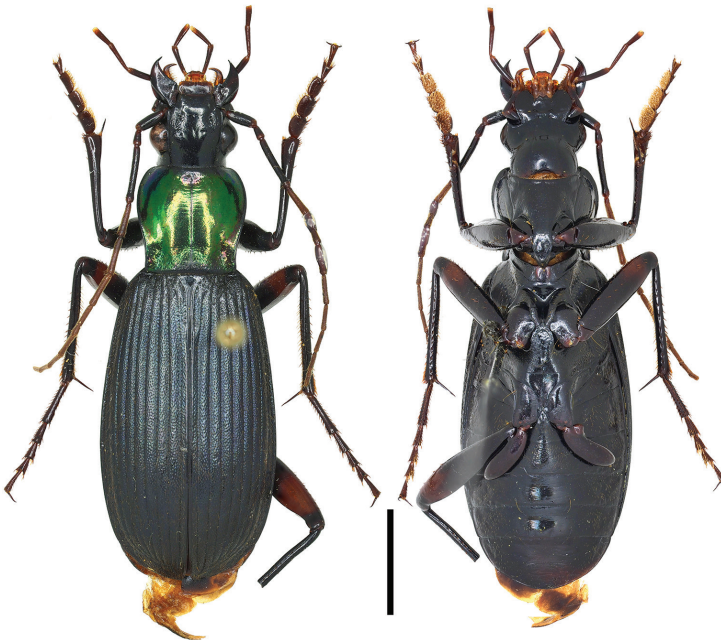
**Head.** Vertex finely punctate, pubescent, without a distinct glabrous area; antennae long, reaching middle of elytra; antennomere 3 ~ 1.5× longer than antennomere 4.

**Pronotum** cordiform, PW/PL = 1.09–1.11 (Fig. 23), widest at apical third; anterior margin slightly concave, PAW/PBW = 0.83–0.93; lateral margins distinctly narrowed from middle to base, distinctly sinuate before posterior angles; anterior angles rounded, slightly projected forward; posterior angles nearly right angled, rounded at tips; disc gently convex, sparsely punctate and pubescent, with dense shallow transverse rugosities, without glabrous area in the middle; median line distinct, fine, not reaching anterior margin and base; basal foveae deeply arcuate, punctate and pubescent.



9A

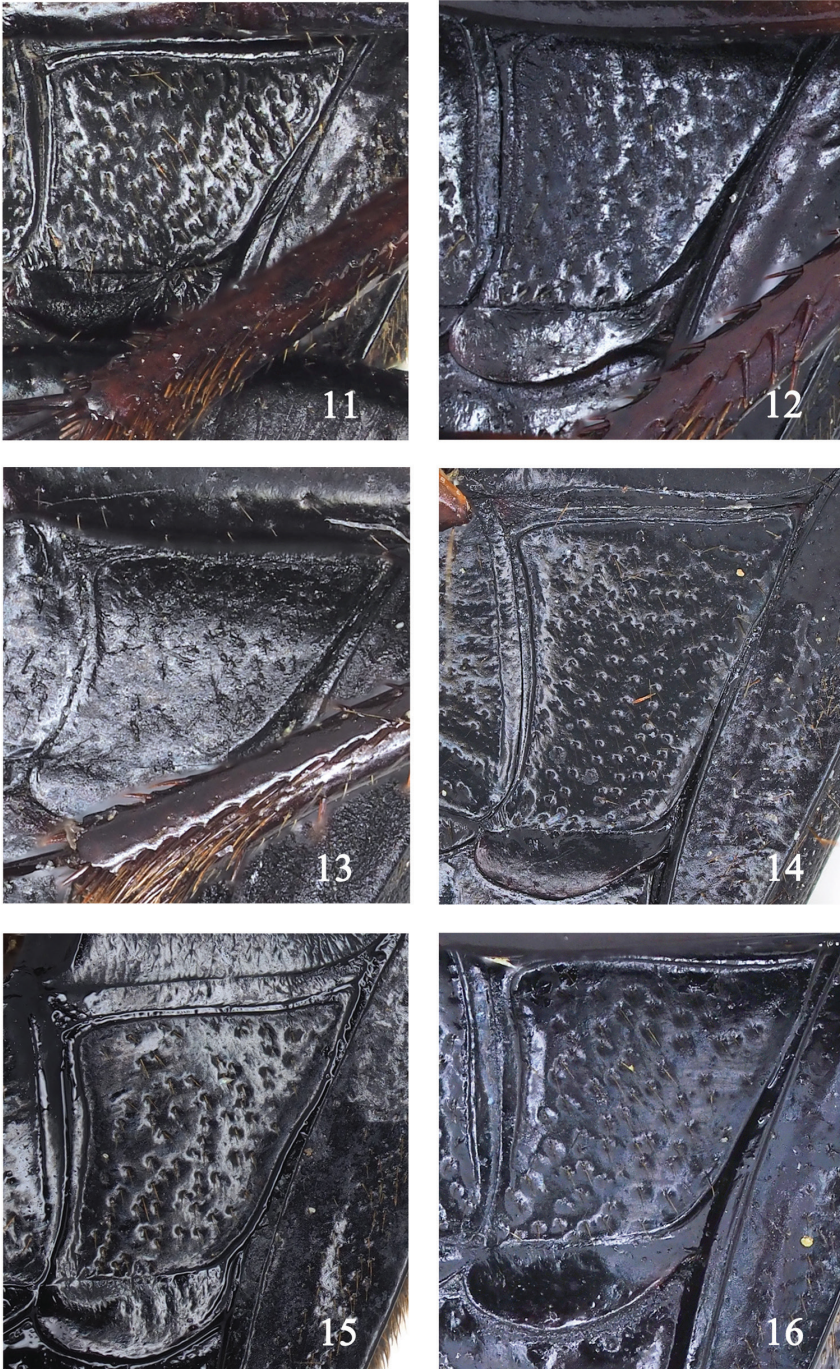
9B



10A

10B

**Figures 9, 10. 9A, B** *Chlaenius* (*Sphodromimus*) *davidi* nom. nov. (male, Guangdong, Xinyi)  
**10A, B** *C. (Sphodromimus) enleensis* (male, Vietnam, Tam Dao). Scale bars: 5.0 mm.



**Figures 11–16.** Metepisternum features of *Sphodromimus* spp. **11** *Chlaenius* (*Sphodromimus*) *caperatus* sp. nov., holotype **12** *C. (S.) yinggelingensis* sp. nov., holotype **13** *C. (S.) pilosus* (Casale, 1984), male **14** *C. (S.) flavofemoratus* Laporte, 1834, male **15** *C. (S.) davidi* nom. nov.; male **16** *C. (S.) enleensis* Mandl, 1992, male.

**Elytra** elongate, EL/BW = 1.61–1.75, gently convex near anterior third, widest near posterior third, rounded at apex in males, subtruncate in females; striae with deep punctures; parascutellar striae well developed; parascutellar pores present; intervals convex at base, flat from middle to apex, densely punctate and pubescent; sutural angles obtuse and right; hind wings reduced.

**Venter** densely punctate, pubescent, metepisterna (Fig. 15) short, MW/ML = 1.11–1.15; abdominal sternites III–VI with one setiferous puncture each side, sternite VII with one pair of setiferous punctures in males, two pairs in females; all abdominal sternites with distinct impressions laterally.

**Legs** long and slender; tarsi nearly smooth dorsally.

**Male genitalia.** Median lobe (Fig. 31B–E) long, strongly bent to ventral side; apical orifice opened dorsally, long and wide, not reaching basal bulb; in dorsal view, apical lamella triangular (Fig. 31A), distinctly bent to right side, longer than basal width, each side of middle apical lamella with a denticulation or absent on right side; in left lateral view, apical portion slightly bent dorsally at apex, basal orifice ~ 90° relative to preapical shaft; left paramere larger than right paramere, both helically curved; endophallus with flagellum thick and straight; basal part of flagellum with irregular bursa; apical part of flagellum with drop-shaped sclerite.

**Female genitalia.** Bursa copulatrix (Fig. 39A–C) round, base with a distinct long digitiform protrusion; villous canal long, tortuously contorted, adhered to common oviduct; spermatheca and spermathecal gland absent.

**Distribution.** (Fig. 40) China (Guangdong; Guangxi).

**Remarks.** *Chlaenius* (*Sphodromimus*) *wrasei* was originally described as a member of the genus *Vachinius*. Azadbakhsh and Kirschenhofer (2019) moved it to the genus *Chlaenius*. However, in a result of this treatment, it became a junior homonym of *Chlaenius* (*Lithochlaenius*) *wrasei* (Kirschenhofer, 1997). Herein, we propose a new replacement name for the former – *Chlaenius* (*Sphodromimus*) *dauidi* nom. nov., based on the first name of the well-known specialist on the ground beetles, David W. Wrase.

This species was described based on a single female from Datianding, Xinyi, Guangdong, China. Recently, one male and six females were collected from the type locality, and those specimens fit well with the original description and illustration of *C. dauidi* nom. nov. Two more males were collected in Guangxi, which are identical to the holotype.

### ***Chlaenius* (*Sphodromimus*) *flavofemoratus* Laporte, 1834**

Figs 7A–C, 14, 22, 30A–E, 38A–C, 40

*Chlaenius flavofemoratus* Laporte, 1834: 81; Chaudoir 1856: 244 (synonymized with *Chlaenius femoratus* Dejean, 1826); Chaudoir 1876: 93 (mention); Andrewes 1941: 308 (key to species; distinguished from *Chlaenius femoratus* Dejean, 1826); Andrewes 1947: 6 (Burma, Indo–China, The Malay Island, Hong Kong); Mandl 1992: 99 (*Macrochlaenites*; Java, Burma); Lorenz 1998: 318 (catalogue); Lorenz 2005: 338 (catalogue); Kirschenhofer 2017: 491 (catalogue); Azadbakhsh and Kir-

schenhofer 2019: 1 (transferred to subgenus *Sphodromimus* from subgenus *Haplochlaenius*)

*nigricoxis* Motschulsky, 1865: 339 (type locality: Hong Kong); Chaudoir 1876: 94 (redescription); Bates 1892: 312 (Bhamò, Palon, Karin Chebà, Laos, Java); Mandl 1992: 99 (synonymized with *C. flavofemoratus* Laporte, 1834); Lorenz 1998: 318 (catalogue); Lorenz 2005: 338 (catalogue). Synonymy.

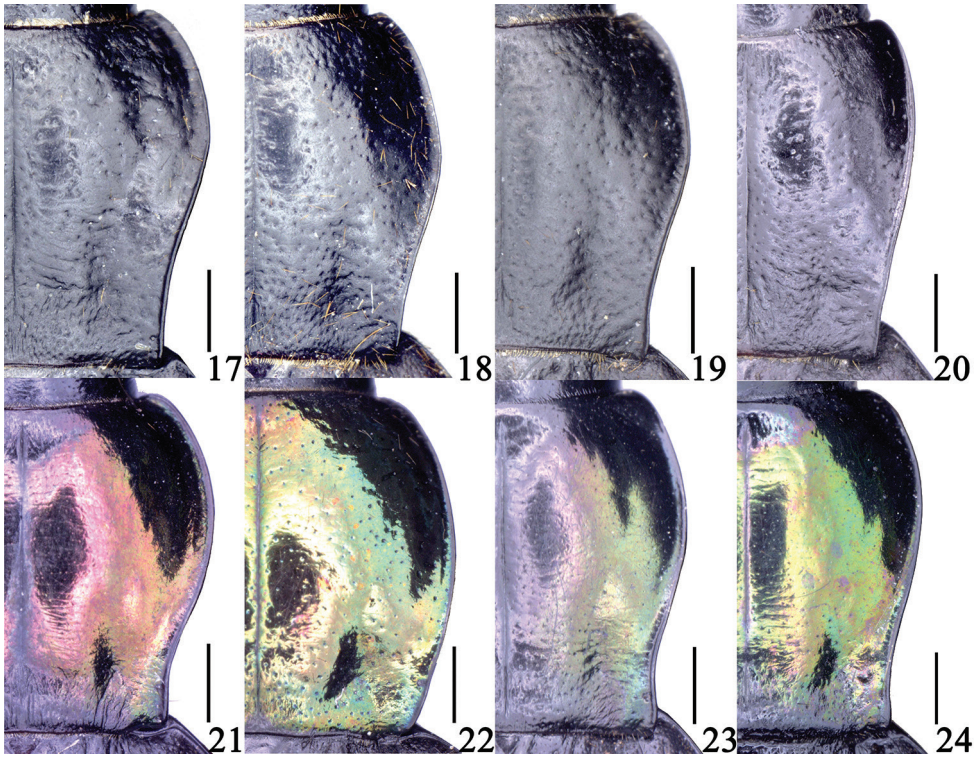
**Type locality.** Indonesia, Java.

**Material examined.** Total 83 specimens. CHINA – **Fujian:** 1 ♀ (IZAS), Fujian, Nanping, 1985.VI.7; 1 ♀ (IZAS), Fujian, Nanjing, 1991.V.15; **Guangdong:** 3 ♂♂ (IZAS), Guangdong, Haifeng, Jimingsi, 23.037605°N, 115.25343°E, 178.09m/2017.V.22, Y.Z. Liu, S.P. Yu leg., Inst. of Zoology; **Guangxi:** 1 ♂ (IZAS), Guangxi, Longsheng, Liliu, 1985. IV Jun Li leg.; 1 ♂ (IZAS), Guangxi, Guilin, Longsheng, 2003.VII.7 Jianxin Cui leg.; 1 ♀ (IZAS), Guangxi, Nanning, 1980.IV.21, Rongquan Cai leg.; 1 ♂ (IZAS), Guangxi, Jingxi, 840 m, 1998.IV.1 Chunsheng Wu leg.; **Guizhou:** 1 ♂ and 1 ♀ (IZAS), Guizhou, Luodian, 420 m, 1979.IV.16, Qingqiang Li leg.; 1 ♀ (IZAS), Guizhou, Luodian, 1979.V.1; **Hainan:** 1 ♂ (IZAS), Hainan, Baisha, Yinggeling, 2011.V.1, 600 m, light trap, Wenxin Lin leg., Inst. of Zoology; **Yunnan:** 4 ♂♂ and 1 ♀ (IZAS), Yunnan, Jinghong, Virgin Forest Park, Peacock Villa, 22.0304°N, 100.8763°E, 682 m/2021.VIII.6 N, along road Pingzhou Zhu leg., Inst. of Zoology; 1 ♂ (IZAS), Yunnan, Xishuangbanna, Botanical Garden, Chao Wu leg.; 1 ♀ (IZAS), Yunnan, Hekou, Qiaotou, Bajiaotian village/ 22.85348°N, 104.14211°E, 886 m, 2021.IV.21 N, Y. Xu, Z.Q. Yan coll., Inst. of Zoology; 1 ♂ (CAS), China, Yunnan Province, Tengchong, Shangying, Longwenqiao, field, beach, 25°01'19.9"N, 98°40'40.4"E/1290 m, 2003.X.20 D., H.B. Liang, X.C. Shi Coll., Institute of Zool., CAS & California Acad. Sciences; 1 ♂ and 3 ♀♀ (IZAS), Yunnan, Xishuangbanna, Menglun, Botanical Garden, 549 m, 21°56.035'N, 101°15.154'E /2005.V.25, Guo Zheng leg, Inst. of Zoology, CAS; 4 ♂♂ and 6 ♀♀ (CAS), Yunnan, Xishuangbanna, Menglun, Botanical Garden, 558 m, 21°55.035'N, 101°16.500'E /2007.V.20, Guo Zheng leg, Inst. of Zoology, CAS; 3 ♂♂ and 8 ♀♀ (IZAS), Yunnan, Xishuangbanna, Menglun, Botanical Garden, 558 m, 21°55.035'N, 101°16.500'E /2007.VII.10, Guo Zheng leg, Inst. of Zoology, CAS; 1 ♂ and 4 ♀♀ (CAS), Yunnan, Xishuangbanna, Menglun, Botanical Garden, 572 m, 21°54.646'N, 101°16.257'E /2007.I.10, Guo Zheng leg, Inst. of Zoology, CAS; 2 ♀♀ (IZAS), Yunnan, Xishuangbanna, Menglun, Botanical Garden, 2009.XII.1, Guo Tang leg, Inst. of Zoology; 2 ♀♀ (IZAS), China, Yunnan Prov., Nabanhe N.R. Guomenshan, alt.1150 m, 2009.V.6, Jiayao Hu, Ziwei Yin leg.; 1 ♂ (IZAS), Yunnan, Jinghong, Menghai, Nabanhe N.R. Guomenshan, Forest, 2009.VI.26, 1114 m/22.24644°N, 100.60610°E, pitfall, L.Z. Meng leg., Inst. of Zoology; 1 ♂ (IZAS), China, Yunnan, Hekou, Longpu, 240 m, 2011.IV.13D, 22.65404°N, 103.98193°E/Xinlei Huang leg., Inst. of Zoology, CAS; 1 ♂ (IZAS), Yunnan, Xishuangbanna, Menglun, Botanical Garden, 540 m, 21.92987°N, 101.24820°E, 2011.IV.21N/Hongbin Liang, Kaiqing Li leg., Institute of Zool., CAS; 1 ♂ (CAS), Yunnan, Xishuangbanna, Menglun, Botanical Garden, 540 m, 21.92987°N, 101.24820°E, 2011.IV.22/Yan Li leg., Institute of Zool.,

CAS; 1 ♂ (IZAS), Yunnan Prov. Menglun, Botanical Garden, vegetation, 21.91175°N, 101.28163°E / 650 m, 2009.XI.15, Guo Tang Coll., Inst. of Zoology; 1 ♀ (IZAS), Yunnan, Xishuangbanna, Menglun, Botanical Garden, 2011.V.04, 560 m / 21°55'39.66"N, 101°15'18.09"E, Jingxin Liu leg., Inst. of Zoology; 1 ♀ (IZAS), Yunnan, Xishuangbanna, 29 km NW, Jinghong, vic. Da Nuo You / 22°12.41'N, 100°38.29'E, 790 m, 2009.V.16 leg. L. Meng, rice follow; 1 ♀ (IZAS), Yunnan, Xishuangbanna, 20km NW, Jinghong, vic. Man Dian (NNNR) / 22°07.80'N, 100°40.05'E, 740 m, 2008.V.13 leg. A. Weigei rubb. plant; 1 ♂ and 1 ♀ (CAS), Yunnan, Lushui, Pianma, Gangfang, Xuetang 26.12218°N, 98.57546°E / 1625 m, 2005.V.16N, D. Kavanaugh, D.Z. Dong leg., Inst. of Zoology, CAS; 1 ♂ (CAS), China, Yunnan, Mengla, Biodiversity Corridor, 660 m, 2011.IV.25D, 21.40482°N, 101.63035°E / Xinlei Huang leg., G213 1999 km, Inst. of Zoology, CAS; 1 ♂ (IZAS), Yunnan, Yangbi, Pingpo, 1422 m, 25°35'33"N, 100°2'56"E / 2002.VI.27, Min Wu leg.; 1 ♀ (CAS), China, Yunnan Province, Tengchong, Qushi Town, Xiaojiangqiao, riverside, 25°14'22.2"N, 98°37'38.0"E / 1445 m, 2003.X.21, night, H.B. Liang, X.C. Shi Coll., Institute of Zool., CAS & California Acad. Science; 1 ♀ (CAS), Yunnan, Gaoligongshan, Nujiang Prefecture, 1500 m, 26°07.3'N, 98°34.5'E, 1998.X.14, D.H. Kavanaugh leg.; 2 ♂♂ (IZAS), Yunnan, Xishuangbanna, Menglun Town NO.55, 2009.V.04, Hu Li leg.; 4 ♀♀ (IZAS), Yunnan, Xishuangbanna, Menglun, Botanical Garden, 2012.V.16, L.Z. Meng leg., Inst. of Zoology; 1 ♂ (IZAS), Yunnan, Xishuangbanna, Menglun, 1982.IV.26, Linyao Wang leg.; 1 ♂ (IZAS), Yunnan, 1980.VI.5, Fen Liu leg.; 1 ♀ (IZAS), Yunnan, Gaoligong, Cikai Town, Pulahe joint of Nujiang, 27.74843°N, 98.66498°E / 1530 m 2004.X.23, night, D. Kavanaugh, D.Z. Dong leg. Inst. of Zoology, CAS; 1 ♂ (IZAS), Yunnan, Lancang, Mafang By pitfall traps, 22.57925°N, 99.99849°E / 1723 m, 2004.VI.16, W.B. Gu coll, Inst. of Zoology, CAS; 1 ♀ (CAS), Yunnan, Lushui, Liuku, Gaoligong Shan, 25°51'20"N, 98°50'58"E / 800 m, 2002.IX.19, H.B. Liang, night, Sino-American Exped., Inst. of Zoology, CAS; 1 ♂ (CAS), China, Yunnan, Gaoligongshan, Nujiang Prefecture, Gangfang, Sancha Lukou / 26 07.3'N, 98 34.5'E, 1500 m, 1998.X.12, D.H. Kavanaugh collector.; **MYANMAR:** 1 ♂ (NHML), Carin Cheba, 900–1100 m, L. Fea / Fry Coll., 1905.100. / *Chlaenius flavofemoratus* Cast. = *nigricoxis* Mots., comp with type, H.E. Andrewes det.; **VIETNAM:** 1 ♀ (IZAS), Tonkin, Hoa Binh, leg: A. de Cooman.

**Diagnosis.** Pronotum metallic green to metallic coppery. PW/PL = 1.14–1.26; PAW/PBW = 0.76–0.92 (Fig. 22); pronotum subquadrate with anterior angles rounded, not projected forward; disc gently convex, sparsely punctate. Elytral intervals convex basally, flat apically, densely punctate and pubescent. Hind wings developed. Metepisterna long, MW/ML = 0.75–0.92 (Fig. 14). Distal half of femora red-brown, the rest of legs black. This species is similar to *Chlaenius (Haplochlaenius) costiger* Chaudoir, 1856, but intervals interval convex basally and flat apically, not costulate.

**Description.** BL = 22.3–25.3 mm, BW = 8.5–10.4 mm, PAW = 3.5–4.0 mm, PBW = 4.3–4.6 mm, PW = 5.5–5.8 mm, PL = 4.5–4.9 mm, MW = 1.9–2.5 mm, ML = 2.4–3.0 mm. Head, elytra, and venter black; pronotum metallic green to metallic coppery; antennae, labial and maxillary palpi, apex of mouthparts and tarsomeres dark brown; distal half of femora red-brown, the rest of legs black.



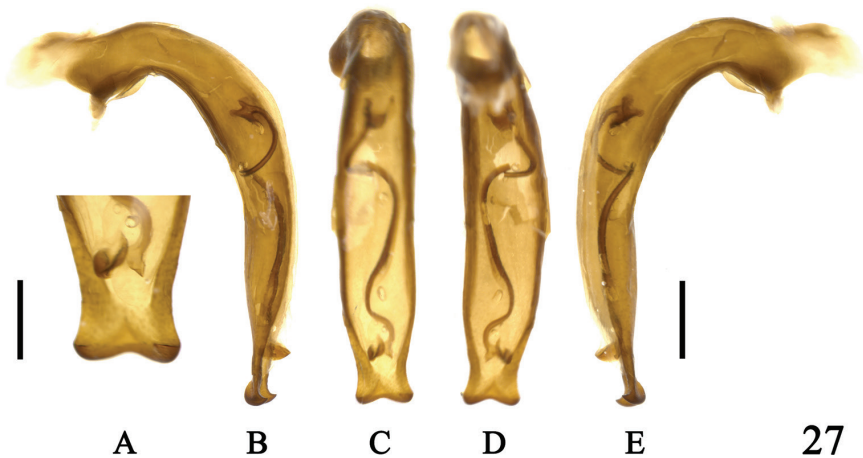
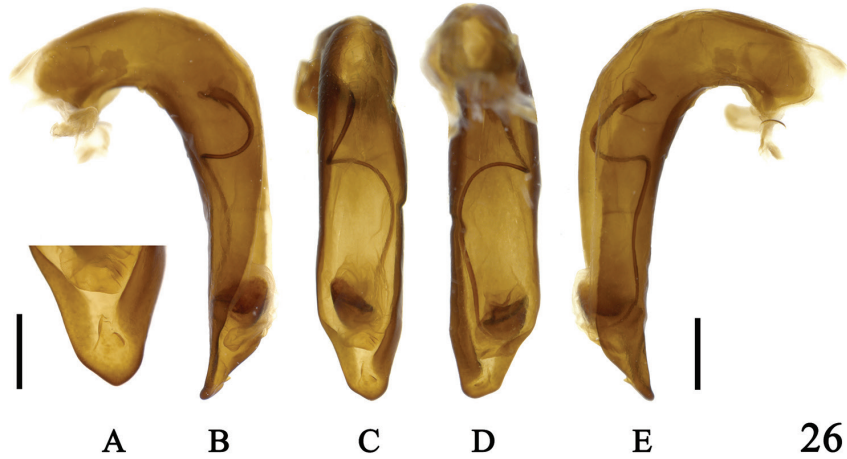
**Figures 17–24.** Pronotum features of *Sphodromimus* spp. **17** *Chlaenius (Sphodromimus) caperatus* sp. nov.; holotype **18** *C. (S.) hunanus* (Morvan, 1997) male **19** *C. (S.) deuwei* (Morvan, 1997); male **20** *C. (S.) pilosus* (Casale, 1984), male **21** *C. (S.) yinggelingsensis* sp. nov.; holotype **22** *C. (S.) flavofemoratus* Laporte, 1834, male **23** *C. (S.) davidi* nom. nov., male **24** *C. (S.) enleensis* Mandl, 1992, male. Scale bars: 1.0 mm.

**Head.** Vertex finely punctate and pubescent, with a glabrous area in the middle; antennae long, reaching middle of elytra; antennomere 3 ~ 1.7× longer than antennomere 4.

**Pronotum** subquadrate,  $PW/PL = 1.14–1.26$  (Fig. 22), widest at apical four-ninth; anterior margin slightly concave,  $PAW/PBW = 0.76–0.92$ ; lateral margins rounded or straight before posterior angles; anterior angles rounded, not projected forward; posterior angles obtuse; disc gently convex, sparsely punctate, without glabrous area in the middle; median line distinct, fine, reaching anterior margin and base; basal foveae deep, punctate and pubescent.

**Elytra** elongate,  $EL/BW = 1.47–1.83$ ; slightly convex, widest near posterior third, rounded at apex in males, subtruncate in females; parascutellar striae well developed; parascutellar pores present; striae with deep punctures; interval convex basally, flat apically, densely punctate and pubescent; sutural angles obtuse; hind wings developed.

**Venter** densely punctate, pubescent; metepisterna (Fig. 14) long,  $MW/ML = 0.75–0.92$ ; abdominal sternites III–VI with one setiferous puncture each side, sternite VII with one pair of setiferous punctures in males, two pairs in females.



**Figures 25–27.** Aedeagus of *Sphodromimus* spp. **25** *Chlaenius* (*Sphodromimus*) *caperatus* sp. nov., holotype **26** *C. (Sphodromimus) hunanus* (Morvan, 1997) (Guangdong, Nanling) **27** *C. (Sphodromimus) deuvei* (Morvan, 1997) (Guangxi, Huaping) **A** apical lamella **B** left lateral view **C** dorsal view **D** ventral view **E** right lateral view. Left scale bars: 0.5 mm (**A**); right scale bars: 1.0 mm (**B–E**).

**Legs** long and slender; tarsi nearly smooth dorsally.

**Male genitalia.** Median lobe (Fig. 30B–E) large, long, strongly bent to ventral side; apical orifice opened dorsally, long and wide, not reaching basal bulb; in dorsal view, apical lamella (Fig. 30A) slightly bent to left side, width slightly longer than length, apex rounded; in left lateral view, apical portion slightly bent ventrally at apex, left side near apical lamella with a large denticulation; internal sac with flagellum slender, apex with a helical sclerite, not reaching to apical orifice; left paramere larger than right paramere, both rounded; endophallus with flagellum fine and slightly bent; basal part of flagellum without a sclerite; apical part of flagellum with a drop-shaped bursa.

**Female genitalia.** Bursa copulatrix (Fig. 38A–C) very long, base with trapeziform protrusion; villous canal long, tortuously contorted, adhered to common oviduct; spermatheca and spermathecal gland absent.

**Distribution.** (Fig. 40) China (Fujian; Guangdong; Guangxi; Guizhou; Hainan; Hong Kong; Yunnan), Indonesia, Laos, Myanmar, Vietnam.

**Remarks.** Due to the fully developed hind wings and the shape of pronotum, this species is very special among species of *Sphodromimus*. It also has a wider distribution than other species. But the morphological characteristic of the apical lamella of the aedeagus, denticulate on the dorsal side, and the mentum with a bifid tooth show that the species belongs to *Sphodromimus*. The subspecies *C. (Sphodromimus) flavofemoratus enleensis* Mandl, 1992 was upgraded as a valid species (see below).

***Chlaenius (Sphodromimus) enleensis* Mandl, 1992, stat. nov.**

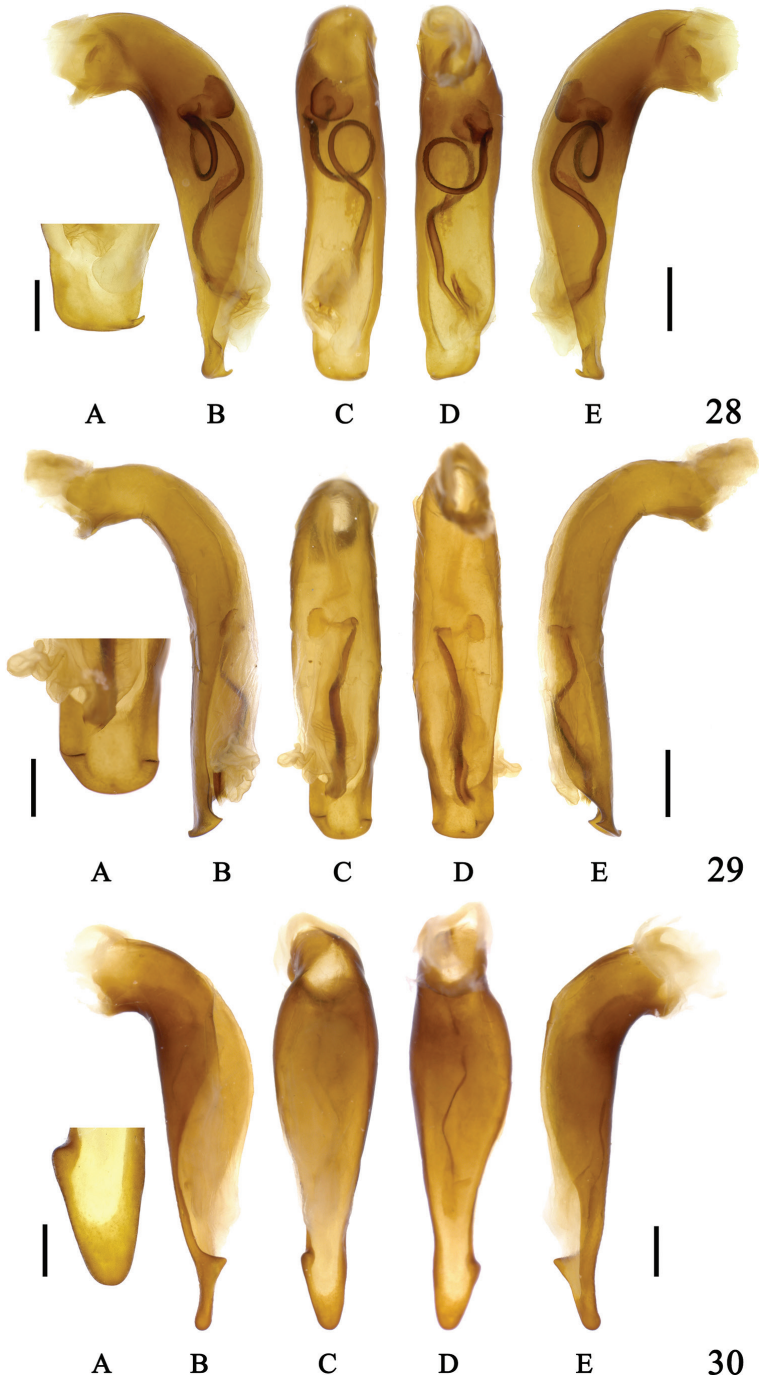
Figs 8, 10A, B, 16, 24, 32A–F, 33A–E, 40

*Chlaenius flavofemoratus enleensis* Mandl, 1992: 100; Lorenz 1998: 318 (synonymized with *C. flavofemoratus* Laporte, 1834, catalogue); Lorenz 2005: 338 (catalogue); Kirschenhofer 2017: 491 (as a subspecies of *C. flavofemoratus*; catalogue); Azadbakhsh and Kirschenhofer 2019: 1 (transferred to subgenus *Sphodromimus* from subgenus *Haplochlaenius*).

*tamdaoensis* Kirschenhofer, 2003: 32 (type locality: Vietnam, Tam Dao; genus *Chlaenius*, subgenus *Haplochlaenius*); Lorenz 2005: 342 (catalogue); Azadbakhsh and Kirschenhofer 2019: 1 (genus *Chlaenius*, subgenus *Sphodromimus*) syn. nov.

**Type locality.** Indo China.

**Material examined.** Total 5 specimens. VIETNAM: **Holotype**, Male (NHMB), Indo Chine coll. Dussault/ En-Le 1908/*Chl (Macrochlaeniles) flavofemoratus* ssp. *enleensis* Dr. K. MANDL det. 1978/Holotype [red label]. **Paratype** (DWC, photo), 1 ♂ (IZAS), VIETNAM, Tam Dao, 20–28.VI.1990, Dr. Blazicek lgt./Paratypus, *Chlaenius (Haplochlaenius) tamdaoensis* mihi det. Kirschenhofer 2001 [red label]/COLL WRASE, BERLIN; 1 ♂ (IZAS), Vietnam, Tam Dao, 60 km NW Hanoi, 900 m, 1997 May–June, S. Ryabov [internal sac fully everted]; 1 ♂ (IZAS), Vietnam, Cao Bang, Nguen Binh, 800 m, 2003.V.13, S. Ryabov [internal sac partially everted]; 1 ♂ (IZAS), Tonkin, Hoa-Binh, leg. A. de Cooman [genitalia damaged by dermestid beetle].



**Figures 28–30.** Aedeagus of *Sphodromimus* spp. **28** *Chlaenius (Sphodromimus) pilosus* (Casale, 1984) (Yunnan, Pingbian) **29** *C. (Sphodromimus) yinggelingensis* sp. nov, holotype **30** *C. (Sphodromimus) flavofemoratus* Laporte, 1834 (Yunnan, Menglun) **A** apical lamella **B** left lateral view **C** dorsal view **D** ventral view **E** right lateral view. Left scale bars: 0.5 mm (**A**); right scale bars: 1.0 mm (**B–E**).



**Figures 31–33.** Aedeagus of *Sphodromimus* spp. **31** *Chlaenius (Sphodromimus) davidi* nom. nov. (Guangdong, Xinyi) **32** *C. (Sphodromimus) enleensis* Mandl, 1992 (Vietnam, Tam Dao) **33** *C. (Sphodromimus) enleensis* Mandl, 1992 (holotype, “Indo Chine”) **A** apical lamella **B** left lateral view **C** dorsal view **D** ventral view **E** right lateral view **F** endophallus. Left scale bars: 0.5 mm (**A**); right scale bars: 1.0 mm (**B–F**).

**Diagnosis.** Pronotum green to coppery.  $PW/PL = 1.06–1.12$ ;  $PAW/PBW = 0.82–0.95$  (Fig. 24); pronotum cordate with anterior angles rounded, not projected forward; disc sparsely punctate and pubescent, with shallow transverse rugosities. Elytral intervals gently convex throughout; densely punctate and pubescent. Hind wings reduced. Metepisterna short;  $MW/ML = 1.11–1.17$  (Fig. 16). Apex of femora dark brown or yellow-brown, the rest of legs black.

**Description.**  $BL = 21.7–24.1$  mm,  $BW = 8.2–8.7$  mm.  $PL = 4.5–4.9$  mm,  $PW = 5.0–5.3$  mm,  $MW = 2.0–2.1$  mm,  $ML = 1.7–1.8$  mm. Head, elytra, venter dark and black; pronotum green to coppery; antennae, labial and maxillary palpi, apex of mouthparts and tarsomeres dark brown; apex of femora dark brown or yellow-brown, the rest of legs black.

**Head.** Vertex finely punctate, pubescent, without a distinct glabrous area; antennae long, reaching middle of elytra; antennomere 3  $\sim 1.5\times$  longer than antennomere 4.

**Pronotum** cordiform,  $PW/PL = 1.06–1.12$  (Fig. 24), widest at apical third; anterior margin slightly concave,  $PAW/PBW = 0.82–0.95$ ; lateral margins distinctly narrowed from middle to base, slightly sinuate before posterior angles; anterior angles rounded, not projected forward; posterior angles nearly right angled, rounded at tips; disc gently convex, sparsely punctate and pubescent, with shallow, transverse rugosities, without glabrous area; median line distinct, fine, not reaching anterior margin and base; basal foveae deeply arcuate, punctate and pubescent.

**Elytra** elongate,  $EL/BW = 1.58–2.22$ , gently convex near anterior third, widest near posterior third, rounded at apex in males; striae with deep punctures; parascutellar striae well developed; parascutellar pores present; intervals gently convex throughout, densely punctate and pubescent; sutural angles sharp at tips; hind wings reduced.

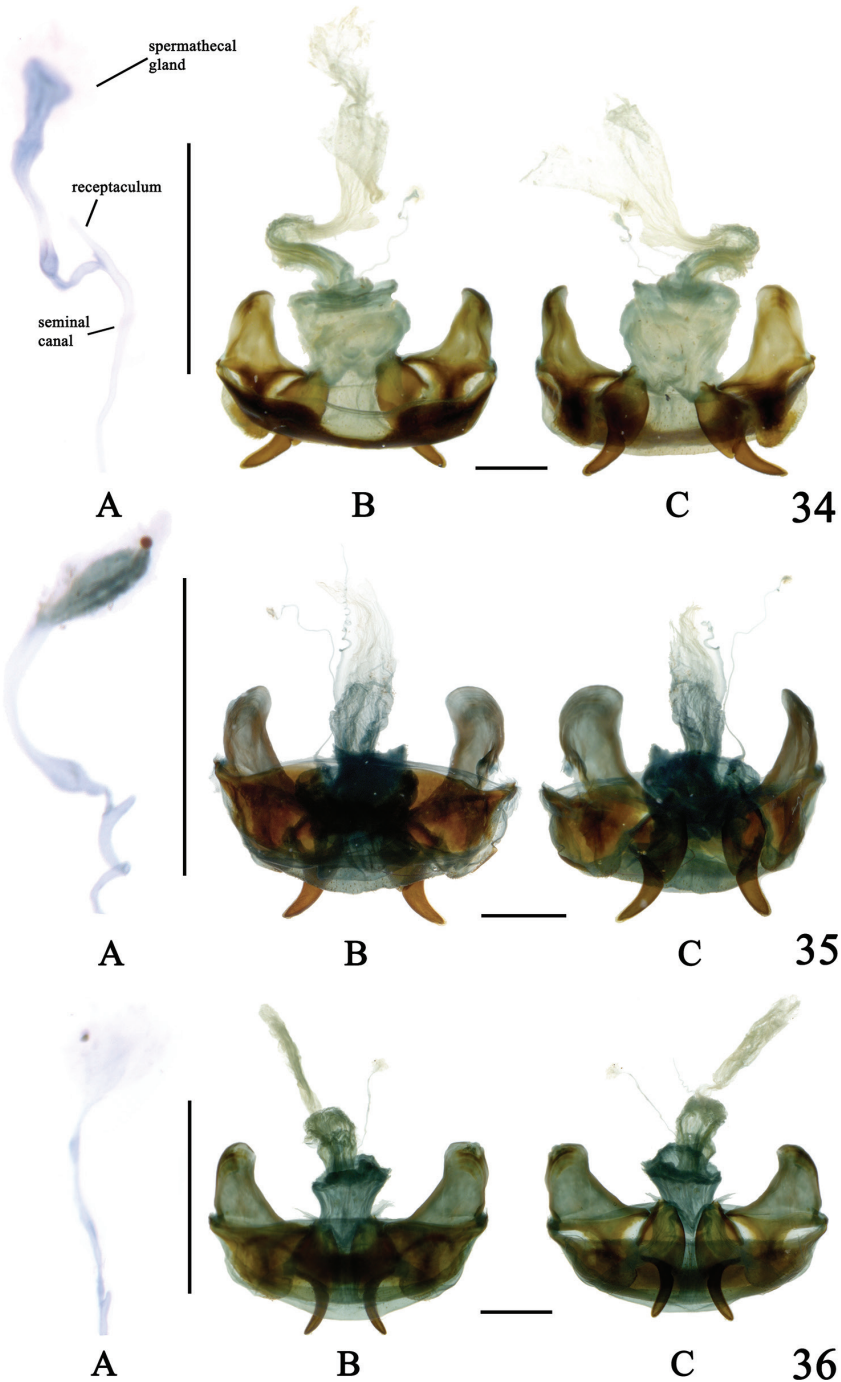
**Venter** densely punctate, pubescent, metepisterna (Fig. 16) short,  $MW/ML = 1.11–1.17$ ; abdominal sternites III–VI with one setiferous puncture each side, sternite VII with one pair of setiferous punctures in males; all abdominal sternites with distinct impressions laterally.

**Legs** long and slender; tarsi nearly smooth dorsally.

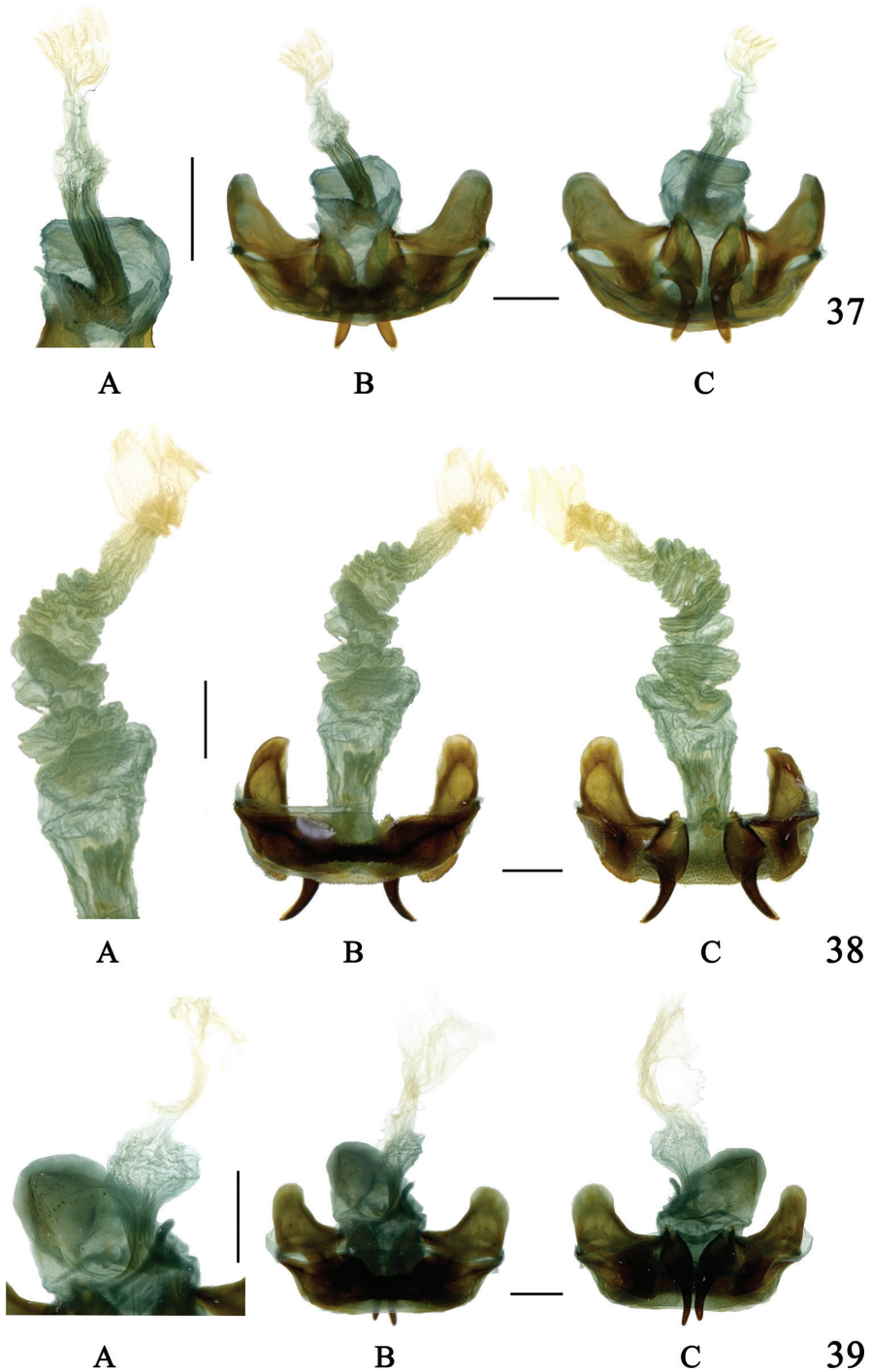
**Male genitalia.** Median lobe (Figs 32B–E, 33B–E) long, strongly bent to ventral side; apical orifice opened dorsally, long and wide, not reaching basal bulb; in dorsal view, apical lamella linear, longer than basal width (Figs 32A, 33A), distinctly bent to right side, with a denticulation laterally in the middle, left denticulation distinctly larger than the right one; in left lateral view, apical portion slightly bent dorsally at apex, basal orifice  $\sim 90^\circ$  relative to preapical shaft; left paramere larger than right paramere, both helically curved; endophallus (Fig. 32F) with flagellum helically thick and straight; basal part of flagellum with irregular bursa; apical part of flagellum with triangular sclerite.

**Female genitalia** unknown.

**Distribution.** (Fig. 40) Vietnam (Indo Chine). We mark En-le, Yunnan on the map with a question mark ‘?’.



**Figures 34–36.** Internal reproductive system of females **34A–C** *Chlaenius (Sphodromimus) caperatus* sp. nov., paratype **35A–C** *C. (Sphodromimus) hunanus* (Morvan, 1997) **36A–C** *C. (Sphodromimus) deuvei* (Morvan, 1997) **A** spermatheca **B** dorsal view **C** ventral view. Vertical scale bars: 0.5 mm (**A**); horizontal scale bars: 1.0 mm (**B, C**)



**Figures 37–39.** Internal reproductive system of females **37** *Chlaenius (Sphodromimus) yinggelingensis* sp. nov., paratype **38** *C. (Sphodromimus) flavofemoratus* Laporte, 1834 **39** *C. (Sphodromimus) davidi* nom. nov. **A** bursa copulatrix **B** dorsal view **C** ventral view. Scale bars: 1.0 mm.



**Figure 40.** Distribution of *Chlaenius* (*Sphodromimus*) species in China and adjacent areas (a possible distribution of *C. enleensis*, En-le, Yunnan, represented by a question mark).

**Remarks.** Lorenz (1998) and Lorenz (2005) proposed *C. flavofemoratus enleensis* Mandl, 1992 as a synonym of *C. flavofemoratus*, but Kirschenhofer (2017) treated it as a distinct subspecies. Based on its original description, its pronotum longer than *C. flavofemoratus*, and black femora indicated it probably represented a different species. After the examination of the holotype and its dissected genitalia, we find that it has the same apical lamella as *C. tamdaoensis*. As a consequence of this surprising discovery, the locality should also be critically revised. The labels of the holotype contain two localities (“En-le” and “Indo Chine”), the latter including today’s Vietnam. Based on the type locality of *C. tamdaoensis*, it is very unlikely that *C. flavofemoratus enleensis* also occurs in Yunnan’s En-le. Hence, we think that the label of En-le is likely to be the wrong one and may have been erroneously added, as it rarely happened in the historical collections of the NHMB (e.g., Caldara et al. 2022). We upgrade *C. enleensis* as a valid species and consequently treat *C. tamdaoensis* as synonym of *C. enleensis*.

## Acknowledgements

We thank Dr. Beulah Garner for hosting the second author (LHB) at NHML, David W. Wrase (Berlin, Germany), for providing images of type specimens, Dr Mingyi Tian (SCAU), Dr. Lizhen Li (Shanghai Normal University) for loan of specimens,

Dr. Herbert Zettel (Wien, Austria) for providing literature, and Dr. Thierry Deuve (MNHN) for checking types of *C. hunanus* and for discussions on female genitalia structure. This work was supported by National Natural Science Foundation of China (Grant No. 31970400), and National Science & Technology Fundamental Resources Investigation Program of China (Grant No. 2019FY101800).

## References

- Andrewes HE (1941) XVIII. Papers on Oriental Carabidae. XXXVII. Annals & Magazine of Natural History 7(39): 307–317. <https://doi.org/10.1080/03745481.1941.9727934>
- Andrewes HE (1947) Entomological results from the Swedish expedition 1934 to Burma and British India. Arkiv för Zoologi 38A: 1–55.
- Azadbakhsh S, Kirschenhofer E (2019) A new species and subspecies of genus *Chlaenius* Bonelli, 1810 with remark on the taxonomic position of *Haplochlaenius* Lutshnik, 1933 and *Vachinius* Casale, 1984 and a new synonym of subgenus *Macrochlaenites* Kuntzen, 1919 (Coleoptera: Carabidae: Chlaeniini). Oriental Insects 53(4): 566–587. <https://doi.org/10.1080/00305316.2018.1561539>
- Bates HW (1892) Viaggio di Leonardo Fea in Birmania e regioni vicine. XLIV. List of the Carabidae. Annali del Museo Civico di Storia Naturale di Genova 32: 267–428.
- Brunk I (2015) A new species of the genus *Vachinius* Casale, 1984 from the Philippines (Coleoptera, Carabidae, Chlaeniini). Entomologische Blätter für Biologie und Systematik der Käfer 111: 5–10.
- Brunk I, Kirschenhofer E (2016) *Vachinius (Vachinius) arakanensis* sp.n. (Coleoptera: Carabidae: Chlaeniini) from Myanmar. Zeitschrift der Arbeitsgemeinschaft Oesterreichischer Entomologen 68: 51–55.
- Caldara R, Toševski I, Mendel H, Germann C (2022) In search of some type-specimens of *Rhampbus* [Clairville], 1798 (Coleoptera: Curculionidae). Zootaxa 5169(4): 371–380. <https://doi.org/10.11646/zootaxa.5169.4.6>
- Casale A (1984) The new Asiatic genus *Vachinius* (Carabidae: Callistinae), with three new species. Bollettino del Museo Regionale di Scienze Naturali, Torino 2: 371–382.
- Chaudoir M (1856) Mémoire sur la famille des carabiques. 6–e partie. Bulletin de la Société Impériale des Naturalistes de Moscou 29(3): 187–291.
- Chaudoir M (1876) Monographie des chlénien. Annali del Museo Civico di Storia Naturale di Genova 8: 3–315.
- Deuve T (1993) L'abdomen et les genitala des femelles de Coléoptères Adephaga. Mémoires du Muséum National d'Histoire Naturelle 15: 1–184.
- Kirschenhofer E (2003) Über neue und wenig bekannte Carabidae aus der äthiopischen und orientalischen Region (Coleoptera: Carabidae, Chlaeniinae, Pterostichinae). Entomofauna 24: 29–60.
- Kirschenhofer E (2012) Neue Arten der Gattung *Vachinius* Casale, 1984 von Laos. Mitteilungen des Internationalen Entomologischen Vereins Frankfurt a.M. 1–2: 83–90.

- Kirschenhofer E (2013) Ein Beitrag zur Kenntnis der Tribus Chlaeniini (= Callistini sensu auct.) der palaarktischen, afrotropischen und orientalischen Region (Coleoptera: Carabidae). Zeitschrift der Arbeitsgemeinschaft Österreichischer Entomologen 65: 23–36.
- Kirschenhofer E (2017) Tribe Chlaeniini Brullé, 1834. In: Löbl I, Löbl D (Eds) Catalogue of Palaearctic Coleoptera (Vol. 1. 2<sup>nd</sup> Edn.). Brill, Leiden, Boston, 491–497.
- Laporte FLN (1834) Études entomologiques, ou description d'insectes nouveaux: et observations sur leur synonymie. Méquignon–Marvis Paris, vol. 13, 159 pp.
- Lassalle B (2001) Chasses en Birmanie. Entomologiste 57: 239–243.
- Liebherr JK, Will KW (1998) Inferring phylogenetic relationships within Carabidae (Insecta, Coleoptera) from characters of the female reproductive tract. In: Ball GE, Casale A, Vigna Taglianti A (Eds) Phylogeny and classification of Caraboidea (Coleoptera: Adephaga), Proceedings of a Symposium (28 August 1996, Florence, Italy), 20 International Congress of Entomology. Torino, Museo Regionale di Scienze Naturali. Atti Museo Regionale di Scienze Naturali 5: 107–170.
- Lorenz W (1998) Systematic List of Extant Ground Beetles of the World. Wolfgang Lorenz, Tutzing, 502 pp.
- Lorenz W (2005) Systematic List of Extant Ground Beetles of the World (Insecta Coleoptera Geadephaga: Trachypachidae and Carabidae incl. Paussinae, Cicindelinae, Rhysodinae), second edition. Wolfgang Lorenz, Tutzing, 530 pp.
- Mandl K (1992) Ein Beitrag zur Kenntnis einiger Chlaeniinae–(Callistinae–) Formen aus der paläarktischen und der orientalischen Region. (Zugleich zweite Auswertung der vom Naturhistorischen Museum in Wien erworbenen Chlaeniinae–Spezialsammlung Ernst Grundmanns) (Carabidae: Coleoptera) 2. Teil. Annalen der Naturhistorischen Museums in Wien 93 B: 59–103.
- Morvan DM (1991) Contribution à la Connaissance des Coleopteres Carabidae de Thailand. Elytron 5: 55–62.
- Morvan DM (1997) Étude faunistique des coléoptères du Népal avec extension aux provinces chinoises du Yunnan et du Sichuan. Genre *Andrewesius* Jedlicka et *Vacinius* Casale. Loened Aziad Amprevedned Feureskalleged C'wiledig 2: 1–23.
- Shi H, Sciaky R, Liang H, Zhou H (2013a) A new subgenus *Wraseillus* of the genus *Pterostichus* Bonelli (Coleoptera, Carabidae, Pterostichini) and new species descriptions. Zootaxa 3664(2): 101–135. <https://doi.org/10.11646/zootaxa.3664.2.1>
- Shi H, Zhou H, Liang H (2013b) Taxonomic synopsis of the subtribe Physoderina (Coleoptera, Carabidae, Lebiini), with species revisions of eight genera. ZooKeys 284: 1–129. <https://doi.org/10.3897/zookeys.309.5499>
- Zettel H (2020) A new species of *Chlaenius* subgen. *Sphodromimus* Casale, 1984 (Coleoptera: Carabidae) from the Philippines. Zeitschrift der Arbeitsgemeinschaft Oesterreichischer Entomologen 72: 29–35.



# To be or not to be... Integrative taxonomy and species delimitation in the daddy long-legs spiders of the genus *Physocyclus* (Araneae, Pholcidae) using DNA barcoding and morphology

Samuel Nolasco<sup>1,2</sup>, Alejandro Valdez-Mondragón<sup>2,3</sup>

**1** Posgrado en Ciencias Biológicas (Doctorado), Centro Tlaxcala de Biología de la Conducta (CTBC), Universidad Autónoma de Tlaxcala (UATx), Carretera Federal Tlaxcala-Puebla, Km. 1.5, C. P. 90062, Tlaxcala, Mexico **2** Laboratory of Arachnology (LATLAX), Laboratorio Regional de Biodiversidad y Cultivo de Tejidos Vegetales (LBCTV), Instituto de Biología, Universidad Nacional Autónoma de México (UNAM), sede Tlaxcala, Ex-Fábrica San Manuel, San Miguel Contla, 90640 Santa Cruz Tlaxcala, Tlaxcala, Mexico **3** CONACYT (Investigador por México), Laboratory of Arachnology (LATLAX), Laboratorio Regional de Biodiversidad y Cultivo de Tejidos Vegetales (LBCTV), Instituto de Biología, Universidad Nacional Autónoma de México (UNAM), sede Tlaxcala, Ex-Fábrica San Manuel, San Miguel Contla, 90640 Santa Cruz Tlaxcala, Tlaxcala, Mexico

Corresponding author: Alejandro Valdez-Mondragón ([lat\\_mactans@yahoo.com.mx](mailto:lat_mactans@yahoo.com.mx))

Academic editor: Cristina Rheims | Received 8 September 2022 | Accepted 17 November 2022 | Published 12 December 2022

<https://zoobank.org/757FC1E4-7DD2-4CAE-A735-8E07E71F0F42>

**Citation:** Nolasco S, Valdez-Mondragón A (2022) To be or not to be... Integrative taxonomy and species delimitation in the daddy long-legs spiders of the genus *Physocyclus* (Araneae, Pholcidae) using DNA barcoding and morphology. ZooKeys 1135: 93–118. <https://doi.org/10.3897/zookeys.1135.94628>

## Abstract

Integrative taxonomy is crucial for discovery, recognition, and species delimitation, especially in underestimated species complex or cryptic species, by incorporating different sources of evidence to construct rigorous species hypotheses. The spider genus *Physocyclus* Simon, 1893 (Pholcidae, Arteminae) is composed of 37 species, mainly from North America. In this study, traditional morphology was compared with three DNA barcoding markers regarding their utility in species delimitation within the genus: 1) Cytochrome c Oxidase subunit 1 (CO1), 2) Internal Transcribed Spacer 2 (ITS2), and 3) Ribosomal large subunit (28S). The molecular species delimitation analyses were carried out using four methods under the corrected *p*-distances Neighbor-Joining (NJ) criteria: 1) Automatic Barcode Gap Discovery (ABGD), 2) Assemble Species by Automatic Partitioning (ASAP), 3) General Mixed Yule Coalescent model (GMYC), and 4) Bayesian Poisson Tree Processes (bPTP). The analyses incorporated 75 terminals from 22 putative species of *Physocyclus*. The average intraspecific genetic distance (*p*-distance) was found to be < 2%, whereas the average interspecific genetic distance was 20.6%. The ABGD, ASAP, and GMYC methods were the most congruent, delimiting 26 or 27 species, while the bPTP method delimited 33 species. The use of

traditional morphology for species delimitation was congruent with most molecular methods, with the male palp, male chelicerae, and female genitalia shown to be robust characters that support species-level identification. The barcoding with CO1 and 28S had better resolution for species delimitation in comparison with ITS2. The concatenated matrix and traditional morphology were found to be more robust and informative for species delimitation within *Physocyclus*.

### Keywords

Arteminae, cellar spiders, molecular markers, molecular methods, North America

## Introduction

Species delimitation is the act of identifying species-level biological diversity (Carstens et al. 2013). It arises from the need to classify, identify, and establish the limits between species (DeSalle et al. 2005; Carstens et al. 2013; Rannala and Yang 2020). The assignment of individual organisms into pre-existing species or higher-level categories (e.g., genus, family, order, etc.) and the designation of new species with proper diagnoses to distinguish them were, for a long-time, roles performed by taxonomist using only traditional morphology and/or somatic characters (Jörger and Schrödl 2013; Rannala and Yang 2020). However, the presence of plastic characters (i.e., characters with high morphological variation), relatively few distinctive morphological traits among species, and morphological stasis due to environmental selection in some groups of organisms (Bickford et al. 2007; Carstens et al. 2013), often makes species delimitation using only morphological evidence extremely difficult or impossible (DeSalle et al. 2005; Rannala and Yang 2020). Spiders are no exception, and due to the complications of using only morphology to identify and delimit species in some groups of araneomorphs and mygalomorphs spiders, different molecular methods have been applied to delimit spider species (Huber et al. 2005; Galtier et al. 2009; Hamilton et al. 2011; Ortiz and Francke 2016; Candia-Ramírez and Francke 2020; Navarro-Rodríguez and Valdez-Mondragón 2020; Valdez-Mondragón 2020; Hazzi and Hormiga 2021). Studies using DNA and RNA have been successful in classifying difficult groups and uncovering underestimated biodiversity (Fox et al. 1977; Wayne et al. 1987; Wilson 1995; Bond 2004).

The spiders of the family Pholcidae C. L. Koch, commonly known as cellar spiders or daddy long-legs spiders, is currently composed of 1,896 species in 97 genera (WSC 2022). Pholcidae is the ninth largest spider family in the World and the most diverse within the Synspermiata clade. The family is composed of five subfamilies: Arteminae Simon, 1893, Modisiminae Simon, 1893, Ninetinae Simon, 1890, Pholcinae C. L. Koch, 1850, and Smeringopinae Simon, 1893 (Huber 2011; Dimitrov et al. 2013; Eberle et al. 2018; Huber and Carvalho 2019). Arteminae includes 107 species distributed in nine genera: *Artema* Walckenaer, 1837, *Aucana* Huber, 2000, *Chisosa* Huber, 2000, *Holocnemius* Berland, 1942, *Nita* Huber & El-Hennawy, 2007, *Pholcitrichocyclus* Ceccolini & Cianferoni, 2022, *Physocyclus* Simon, 1893, *Tibetia* Zhang, Zhu & Song, 2006, and *Wugigarra* Huber, 2001 (WSC 2022).

*Physocyclus* comprises 37 described species, classified into two species groups proposed by Valdez-Mondragón (2013, 2014). To date, the *globosus*-group includes 15 species, while 22 species are recognized in the *dugesi*-group (Valdez-Mondragón 2013, 2014; Jiménez and Palacios-Cardiel 2013; Nolasco and Valdez-Mondragón 2020, 2022). Recently, five species from Mexico were described by Nolasco and Valdez-Mondragón (2020, 2022) based only on traditional morphology, four from the *globosus*-group and one of the *dugesi*-group. The genus is distributed mainly in arid and semiarid ecosystems, as well as tropical dry forests, mostly in North America, with some species in Central America (Valdez-Mondragón 2010, 2013, 2014; Jiménez and Palacios-Cardiel 2013; Nolasco and Valdez-Mondragón 2020, 2022). Most species in the genus are found under 1900 m a.s.l., with the exception of *Physocyclus dugesi* Simon 1893 and *Physocyclus globosus* (Taczanowski, 1874), whose distributions are influenced by synanthropic activities that have allowed them to occupy higher elevations in association with human dwellings (Valdez-Mondragón 2010). *Physocyclus globosus* is considered a cosmopolitan species, with records from North and Central America, the Caribbean Islands, the Pacific Islands, South America, Asia, Africa, and Oceania (Valdez-Mondragón 2010; WSC 2022).

The most recent taxonomic revisions and morphological phylogenetic analyses (Valdez-Mondragón 2010, 2013, 2014), as well as new species descriptions using traditional morphology (Jiménez and Palacios-Cardiel, 2013; Nolasco and Valdez-Mondragón 2020, 2022) have revealed 20 new species from Mexico, which represents 54% of the known species diversity in *Physocyclus*.

The general morphology among the different genera of pholcid spiders is conservative, with slight differences in somatic structures. However, primary sexual structures such as male palps and female genitalia, as well as secondary sexual structures such as male chelicerae, are important features used for identification and species diagnosis due to the fact that genitalia evolve more rapidly than non-genital morphological features (Huber 2003; Huber et al. 2018; Valdez-Mondragón 2020). Speciation in arthropods is associated with marked changes in genital morphology, which explains the usefulness of genitalia in distinguishing closely related species (Huber et al. 2005). Sexual structures have different intraspecific and interspecific variation rates in spiders (Eberhard 1985; Eberhard et al. 1998). However, some groups show an overlapping of characters due to minimal morphological variation, making the identification and delimitation of species difficult (Hamilton et al. 2011; Zhang and Li 2014; Ortiz and Francke 2016; Tyagi et al. 2019; Valdez-Mondragón et al. 2019; Candia-Ramírez and Francke 2020; Navarro-Rodríguez and Valdez-Mondragón 2020; Hazzi and Hormiga 2021). Additionally, speciation without changes in genital shape has been recorded in some pholcid spiders, as demonstrated by Huber et al. (2005) with two species of "*Psilochorus*" from South America that showed the same genitalia shape but extreme differences in size and coloration pattern.

Spiders with generally simple genitalia, such as mygalomorphs and some araneomorphs (Synspermiata), are complicated cases for species delimitation and identification using morphology (Huber et al. 2005; Hamilton et al. 2011; Huber and Dimitrov

2014; Valdez-Mondragón 2013, 2014, 2020; Nolasco and Valdez-Mondragón 2022). Additionally, intrasexual polymorphism has been described among females in some pholcids species. Huber & Pérez-González (2001a, b) described two different epigyne morphotypes in females of *Ciboneya antraia*. In the same way, Valdez-Mondragón (2010) described discontinued interspecific variation in the epigyne shape in females of *Physocyclus enaulus* Crosby, 1926, with three distinct morphotypes.

Due to the poor morphological variation and simple genitalia in some taxonomic groups, approximations based on DNA barcoding using mitochondrial data are often used to establish limits between species, detect species complexes, and/or discover new species in different spider groups (Barrett and Hebert 2005; DeSalle et al. 2005; Bickford et al. 2007; Galtier et al. 2009; Carstens et al. 2013; Navarro-Rodríguez and Valdez-Mondragón 2020; Rannala and Yang 2020; Valdez-Mondragón 2020). Barcoding based on cytochrome c oxidase subunit 1 (CO1) is the common standard in animal Barcoding (including spiders), and its effectivity and resolution has been tested in many studies (Astrin et al. 2006; Planas and Ribera 2015; Ortiz and Francke 2016; Valdez-Mondragón et al. 2019; Navarro-Rodríguez and Valdez-Mondragón 2020; Valdez-Mondragón 2020). While the mitochondrial marker CO1 seems to be suitable for DNA barcoding, it is susceptible to over- and underestimating the diversity in some cases (Astrin et al. 2006; Ortiz and Francke 2016). As such, it is preferable to complement the use of the CO1 marker with other informative mitochondrial (16S) or nuclear (ITS1 or ITS2) markers, as well as morphological evidence, to obtain better resolution (Astrin et al. 2006; Agnarsson 2010; Planas and Ribera 2015; Ortiz and Francke 2016; Valdez-Mondragón et al. 2019; Navarro-Rodríguez and Valdez-Mondragón 2020). The nuclear molecular marker 28S has been used mainly in phylogenetic analyses, providing high resolution for basal clades (Bruvo-Madarić et al. 2005; Álvarez-Padilla et al. 2009; Arnedo et al. 2009; Dimitrov and Hormiga 2011; Dimitrov et al. 2013). Due to its low substitution rate, 28S is useful for estimating phylogenetic hypotheses of taxa with very old divergence times (Hillis and Dixon 1991). However, this marker has never been tested in species delimitation analyses within the family Pholcidae.

In modern systematics, integrative taxonomy studies that combine different sources of evidence, such as molecular markers and morphological data, are commonly implemented to help delimit and diagnose new species or even identify cryptic species complexes (Astrin and Stueben 2008; Álvarez-Padilla et al. 2009; Correa-Ramírez et al. 2010; Hamilton et al. 2011; Montes de Oca et al. 2015; Planas and Ribera 2015; Valdez-Mondragón and Francke 2015; Cao et al. 2016; Valdez-Mondragón et al. 2019; Newton et al. 2020; Valdez-Mondragón and Cortez-Roldán 2021). Recent publications on spider taxonomy have additionally used other sources of information, such as Ecological Niche Modeling (ENM), lineal morphology, and even geometric morphology to characterize species (Valdez-Mondragón et al. 2019; Navarro-Rodríguez and Valdez-Mondragón 2020; Solís-Catalán 2020).

From the first proposal for a DNA barcoding initiative using a single locus (the CO1 mitochondrial gene for animals) as a diagnostic for assigning species (Hebert et al. 2003), the field of species delimitation has been refined and improved, incorporating different theories (e.g., coalescence) and methods (DeSalle et al. 2005; Hickerson et

al. 2006; Pons et al. 2006; Puillandre et al. 2012, 2021; Carstens et al. 2013; Rannala and Yang 2020). Species delimitation analyses using DNA Barcoding, initially with only a single locus (CO1), is limited as a diagnostic for assigning species based on the fact that intraspecific and interspecific sequence distances may be similar in large populations (Hebert et al. 2003; Rannala and Yang 2020). Therefore, many studies have opted for a multi-locus approach, combining CO1 with other molecular markers to give additional robust evidence for species delimitation (Astrin et al. 2006; Agnarsson 2010; Planas and Ribera 2015; Ortiz and Francke 2016; Ballesteros and Hormiga 2018; Navarro-Rodríguez and Valdez-Mondragón 2020; Hazzi and Hormiga 2021).

The aim of this study is to carry out different species delimitation methods within the spider genus *Physocyclus* under an integrative taxonomic approach. To carry out this, we use a combination of molecular markers (CO1, ITS2, and 28S) and traditional morphology of diagnostic features (e.g., male palps, male chelicerae, and female epigynes) to test the validation of the currently recognized species within the genus.

## Materials and methods

### Biological material

Specimens were provided by the Laboratory of Arachnology (**LATLAX**) **IB-UNAM**, Tlaxcala, Mexico; the Colección Nacional de Arácnidos (**CNAN**), Institute of Biology, Universidad Nacional Autónoma de México (**IB-UNAM**), Mexico City; Centro de Investigaciones Biológicas de Noreste (**CIBNOR**), La Paz, Baja California Sur, Mexico; and Colección Aracnológica de la Facultad de Biología de la Universidad Michoacana de San Nicolás de Hidalgo (**CAFBUM**), Michoacan, Mexico. Specimens were preserved in 80% ethanol for morphological studies and 96% ethanol for molecular studies. Female sexual structures (epigyne) were dissected in 80% ethanol and cleaned with potassium hydroxide (10% KOH). This to remove all soft tissue and observe with clarity the taxonomically important internal structures, such as the pore plates. The left male palps were dissected and observed in 80% ethanol. Structures were photographed submerged in commercial gel alcohol to hold them in the appropriate position, while the preparation was done with structures completely covered with 80% ethanol. Specimen observations and identifications were carried out using a Zeiss Discovery V8 stereo microscope. A Zeiss Axiocam 506 color camera attached to a Zeiss AXIO Zoom V16 stereo microscope was used to photograph focal structures (male palps, female epigynes, and male chelicerae). Digital images of morphological structures were edited in Adobe Photoshop CS6.

### Taxon sampling

The molecular analyses were based on a total of 194 sequences of 23 putative species. Species used in the molecular analyses are listed in Table 1. The ingroup includes 188 sequences of 22 species of *Physocyclus* previously described by Valdez-Mondragón (2010, 2013, 2014) and Nolasco and Valdez-Mondragón (2020, 2022). The CO1 se-

**Table 1.** Specimens sequenced for each species of *Physocylus*, DNA voucher numbers, localities, and GenBank accession numbers for CO1, ITS2, and 28S. Mexican state abbreviations: BC, Baja California; BCS, Baja California Sur; COL, Colima; GRO, Guerrero; HGO, Hidalgo; JAL, Jalisco; MICH, Michoacán, OAX, Oaxaca; PUE, Puebla. \*\*Non-Mexican localities.

Species	DNA Code LATLAX	Locality (Mexico)	CO1	ITS2	28S
<i>P. bicornis</i>	Ara0394	GRO: Copala	OP293157	OP296540	OP295410
<i>P. bicornis</i>	Ara0396	GRO: Quechultenango	OP293158	OP296538	OP295411
<i>P. bicornis</i>	Ara0398	GRO: Coyuca	OP293159	OP296539	
<i>P. bicornis</i>	Ara0445	GRO: Quechultenango	OP293160	OP296541	OP295412
<i>P. brevicornus</i>	Ara0515	JAL: Cocula	OP293161	OP296542	OP295413
<i>P. brevicornus</i>	Ara0516	MICH: Morelia	OP293162		
<i>P. brevicornus</i>	Ara0518	MICH: Morelia	OP293163	OP296543	OP295414
<i>P. cornutus</i>	Ara0405	BCS: Los Cabos	OP293164		OP295415
<i>P. cornutus</i>	Ara0406	BCS: Los Cabos	OP293165		OP295416
<i>P. dugesi</i>	Ara0597	HGO: Tula	OP293166	OP296544	OP295417
<i>P. dugesi</i>		Costa Rica**	AY560787		AY560750
<i>P. enaulus</i>	Ara0391	COA: Saltillo	OP293167	OP296545	OP295418
<i>P. enaulus</i>	Ara0392	COA: Saltillo	OP293168	OP296546	OP295419
<i>P. enaulus</i>	Ara0393	COA: Saltillo	OP293169	OP296547	OP295420
<i>P. enaulus</i>		U.S.A.**	MG268722		
<i>P. franckei</i>	Ara0378	HGO: Tolantongo	OP293170	OP296548	
<i>P. franckei</i>	Ara0379	HGO: Cárdenas	OP293171	OP296549	OP295421
<i>P. franckei</i>	Ara0381	HGO: Cardonal	OP293172	OP296550	
<i>P. franckei</i>	Ara0382	HGO: Cardonal	OP293173	OP296551	
<i>P. gertschi</i>	Ara0575	GRO: José Azueta	OP293174	OP296552	OP295422
<i>P. gertschi</i>	Ara0576	GRO: José Azueta	OP293175	OP296553	OP295423
<i>P. gertschi</i>	Ara0577	GRO: José Azueta	OP293176	OP296554	OP295424
<i>P. globosus</i>	Ara0473	COL: Coquimatlán	OP293177	OP296555	OP295425
<i>P. globosus</i>	Ara0533	BCS: Comundú	OP293178		
<i>P. globosus</i>	Ara0535	GRO: Técpan	OP293179	OP296556	OP295426
<i>P. globosus</i>		Quintana Roo	MT888253		
<i>P. globosus</i>		Cuba**	AY560788		AY560751
<i>P. lautus</i>	Ara0459	MICH: Cárdenas	OP293180	OP296557	OP295427
<i>P. lautus</i>	Ara0579	MICH: Coahuayana	OP293181	OP296558	OP295428
<i>P. lautus</i>	Ara0583	JAL: La Huerta	OP293182		OP295429
<i>P. lyncis</i>	Ara0437	JAL: Zapopan	OP293183	OP296559	OP295430
<i>P. lyncis</i>	Ara0754	JAL: Zapopan	OP293184	OP296560	OP295431
<i>P. mariachi</i>	Ara0745	JAL: Hostotipaquillo	OP293185	OP296561	OP295432
<i>P. mariachi</i>	Ara0746	JAL: Hostotipaquillo	OP293186	OP296562	OP295433
<i>P. mariachi</i>	Ara0748	JAL: Plan de Barrancas	OP293187	OP296564	OP295434
<i>P. merus</i>	Ara0898	SLP: Villa de Reyes	OP293188	OP296565	OP295435
<i>P. merus</i>	Ara0915	SLP: Villa de Reyes	OP293189		OP295436
<i>P. merus</i>	Ara0916	SLP: Villa de Reyes	OP293190	OP296566	OP295437
<i>P. merus</i>	Ara0917	SLP: Villa de Reyes	OP293191	OP296567	OP295438
<i>P. merus</i>	Ara0918	SLP: Villa de Reyes	OP293192		OP295438
<i>P. michoacanus</i>	Ara0585	MICH: Tzitzio	OP293193	OP296568	OP295440
<i>P. michoacanus</i>	Ara0586	MICH: Tzitzio	OP293194	OP296569	OP295441
<i>P. michoacanus</i>	Ara0598	JAL: Jilotlán	OP293195		OP295442
<i>P. modestus</i>	Ara0467	PUE: Miahuatlán	OP293196	OP296570	OP295443
<i>P. modestus</i>	Ara0469	GRO: Tepecoacuilco	OP293197	OP296571	OP295444
<i>P. modestus</i>	Ara0480	GRO: Escudero	OP293198		OP295445
<i>P. modestus</i>	Ara0482	GRO: Quechultenango	OP293199		
<i>P. mysticus</i>	Ara0450	BC: Ensenada	OP293200	OP296572	
<i>P. mysticus</i>	Ara0451	BC: Ensenada	OP293201	OP296573	
<i>P. mysticus</i>	Ara0452	BCS: Mulegé	OP293202		OP295446

Species	DNA Code LATLAX	Locality (Mexico)	CO1	ITS2	28S
<i>P. mysticus</i>	Ara0453	BCS: Mulegé	OP293203		OP295447
<i>P. mysticus</i>	Ara0524	BC: Ensenada	OP293204		
<i>P. paredesi</i>	Ara0483	OAX: Tadelá	OP293205	OP296574	OP295448
<i>P. paredesi</i>	Ara0484	OAX: Tadelá	OP293206	OP296575	OP295449
<i>P. paredesi</i>	Ara0485	OAX: Totolapa	OP293207	OP296576	OP295450
<i>P. paredesi</i>	Ara0486	OAX: Totolapa	OP293208		OP295451
<i>P. pocamadre</i>	Ara0371	BCS: Mulegé	OP293209		
<i>P. reddelli</i>	Ara0487	HGO: Araya	OP293210	OP296577	OP295452
<i>P. reddelli</i>	Ara0488	HGO: Araya	OP293211	OP296578	
<i>P. rothi</i>	Ara0383	BCS: Comundú	OP293212	OP296579	OP295453
<i>P. rothi</i>	Ara0384	BCS: Comundú	OP293213	OP296580	OP295456
<i>P. rothi</i>	Ara0386	BCS: La Paz	OP293214		OP295454
<i>P. rothi</i>	Ara0387	BCS: La Paz	OP293215		OP295455
<i>P. sikuapu</i>	Ara0749	MICH: Costa Aquila	OP293216	OP296581	OP295457
<i>P. sikuapu</i>	Ara0750	MICH: Costa Aquila	OP293217	OP296582	OP295458
<i>P. sikuapu</i>	Ara0751	MICH: Costa Aquila	OP293218	OP296583	OP295459
<i>P. sikuapu</i>	Ara0752	MICH: Costa Aquila	OP293219	OP296584	OP295460
<i>P. validus</i>	Ara0502	COL: Coquimatlán	OP293220	OP296585	
<i>P. validus</i>	Ara0503	GRO: Eduardo Neri	OP293221	OP296586	OP295461
<i>P. xerophilus</i>	Ara0372	BCS: Mulegé	OP293222	OP296587	OP295464
<i>P. xerophilus</i>	Ara0373	BCS: Mulegé	OP293223	OP296588	OP295462
<i>P. xerophilus</i>	Ara0374	BCS: Mulegé	OP293224	OP296589	OP295465
<i>P. xerophilus</i>	Ara0375	BCS: Mulegé	OP293225	OP296590	
<i>P. xerophilus</i>	Ara0376	BCS: Mulegé	OP293226	OP296591	OP295463
<i>P. xerophilus</i>	Ara0377	BCS: Mulegé	OP293227	OP296592	
<i>Chisosa</i> sp.	Ara0454	PUE: Miahuatlán	OP293228	OP296593	OP295466
<i>Chisosa</i> sp.	Ara0455	PUE: Miahuatlán	OP293229	OP296594	OP295467

quence matrix is composed of 75 sequences (22 species), ITS2 with 55 sequences (20 species), and 28S with 58 sequences (21 species). Four different partitions were used in the analyses: 1) CO1: 642 bp, 2) ITS2: 505 bp, 3) 28S: 891 bp, and 4) the concatenated matrix CO1+ITS2+28S: 2038 bp. Since this study is focused solely on species delimitation within *Physocyclus* and not on the molecular dating and phylogenetic relationships within Arteminae, only *Chisosa* sp. (Arteminae) was used as an outgroup, to root the trees in the various analyses.

## DNA extraction, amplification, and sequencing

For DNA extraction, we used the Qiagen DNeasy extraction kit, following the modifications suggested by Valdez-Mondragón and Francke (2015) and Valdez-Mondragón (2020). Three legs from each specimen were used for DNA extraction, using males, females, and juveniles, depending on the available specimens per species. The criterion for selecting tissues was based on tissue antiquity, considering only specimens collected in the last five years in order to extract high DNA quality. Amplification of the CO1 locus was carried out using two different primer sets: LCO1490/HCO2198 and LCO-JJ/HCO-JJ; for ITS2, the primer set 5.8S and CAS28SB1d was used; and for 28S, 28S-B1 and 28S-B2 (Table 2). Polymerase chain reactions (PCR) were carried out in a Verity-Applied Biosystems 96 Well Thermal Cycler. The final volume of

**Table 2.** Primer sets used in this study for PCR amplification.

Molecular marker	Primer	Sequence (5'-3')	Author
COI	HCO2198	TAAACTTCAGGGTGACCAAAAAATC	Folmer et al. (1994)
	LCO1490	GGTCAACAAATCATAAAGATATTGG	
	HCO-JJ	AWACTTCVGGRTGCVCAARAATCA	Astrin and Stueben (2008)
LCO-JJ	CHACWAAYCATAAAGATATYGG		
ITS2	5.8S	CGCCTGTTTATCAAAAACAT	Ji et al. (2003); Planas and Ribera (2014)
	CAS28sB1d	TTC TTT TCC TCC SCT TAY TRA TAT GCT TAA	
28S	28S-B1	GACCGATAGCAAACAAGTACCG	Bruvo-Madarić et al. (2005)
	28S-B2	CACGGGTCGATGAAGAACGC	

each PCR tube was 20 µl: 2.3 µl injectable H<sub>2</sub>O, 2.0 µl Q-solution, 10 µl Multiplex-Mix PCR, 1.6 µl of each primer (forward and reverse), and 2.5 µl of extracted DNA sample. The cycles and optimal temperatures for COI and ITS2 amplification were as follows: Initial heating phase of 15 min at 95 °C, 35 amplification cycles of 35 s at 94 °C (denaturing), 1 min 30 s at 40 °C (alignment), and 1 min 30 s at 72 °C (elongation), with a final elongation of 10 min at 72 °C. Two different protocols were used to amplify the 28S region. The first followed Eberle et al. (2018): initial heating phase of 15 min at 95 °C, 35 amplification cycles of 35 s at 95 °C (denaturing), 1 min at 51 °C (alignment), and 1 min at 72 °C (elongation), with a final elongation of 10 min at 72 °C. The second protocol is a modification of Eberle et al. (2018): initial heating phase of 15 min at 95 °C, 35 amplification cycles of 35s at 94 °C (denaturing), 1 min 30 s at 59 °C (alignment), and 1 min 30 s at 72 °C (elongation), with a final elongation of 10 min at 72 °C. Gel electrophoresis was carried out with 0.5% agarose using the molecular weight marker Perfect DNA 100 bp Ladder Novage to calculate fragment size of amplifications. Gels were visualized in a photodoc BioDoc-It2 Imager 315 Imaging System LMS-20 Transilluminator. PCR products were purified using a QIAquick Qiagen purification kit. Tissue selection, DNA extraction, amplification, and purification were performed at the Laboratory of Molecular Biology at Laboratorio Regional de Biodiversidad y Cultivo de Tejidos Vegetales (**LBCTV**), IB-UNAM, Tlaxcala City. Sanger sequencing was done at the Laboratory of Molecular Biology and Health, IB-UNAM, Mexico City.

### DNA sequence alignment and editing

Both forward and reverse DNA strands were sequenced. DNA sequences were edited in Geneious v. 8.1.9 (Rozen and Skaletsky 2000). Multiple alignment of sequences was implemented using MAFFT v. 7 (Katoh and Toh 2008) through online platform (<https://mafft.cbrc.jp/alignment/server/>), with the following commands: Auto (FFT-NS-2, FFTNS-I or L-INS-I, depending on data size). In some cases, alignment was done manually and edited with BioEdit v. 7.0.5.3 (Hall 1999). The concatenated matrix (COI+ITS2+28S) was built in Geneious v. 8.1.9. The aligned matrices were subsequently used in the molecular analyses.

## Molecular analysis and species delimitation

Four different molecular delimitation methods were used under the corrected  $p$ -distances Neighbor-Joining (NJ) criteria: 1) ABGD (Automatic Barcode Gap discovery) (Puillandre et al. 2012), 2) ASAP (Assemble Species by Automatic Partitioning) (Puillandre et al. 2021), 3) GMYC (General Mixed Yule Coalescent) (Pons et al. 2006), and 4) bPTP (Bayesian Poisson Tree Process) (Zhang et al. 2013; Kapli et al. 2017).

### $p$ -distances under Neighbor-Joining (NJ)

The genetic distance tree was reconstructed with MEGA v. 10.1.7 (Kumar et al. 2016) under the following parameters: Number of replicates = 1000, Bootstrap support values = 1000 (significant values  $\geq 50\%$ ), Substitution type = nucleotide, Model =  $p$ -distance, Substitution to include = d: Transitions + Transversions, Rates among sites = Gamma distributed with invariant sites (G+I), Missing data treatment = Pairwise deletion.

### Automatic Barcode Gap Discovery (ABGD)

This method aims to find gaps in genetic divergence, considering that intraspecific genetic variation is theoretically smaller than interspecific divergences. It first generates a prior partition of the data into putative species (initial partitions, IP). Then, these initial partitions are recursively partitioned until there is no further partitioning of the data (recursive partitions, RP). ABGD analyses were carried out on the online platform (<https://bioinfo.mnhn.fr/abi/public/abgd/>) using the following options: K2P distances non-corrected,  $P_{\min} = 0.001$ ,  $P_{\max} = 0.1$ , Steps = 10, Relative gap width (X) = 1, Nb bins = 20.

### Assemble Species by Automatic Partitioning (ASAP)

This is an ascending hierarchical clustering method. Sequences are merged into groups that are successively merged further until all sequences form a single group. Partitions are equivalent to each sequence merge step. The software analyzes all partitions and scores the most probable groups into a tree (Puillandre et al. 2021). ASAP analyses were run on the online platform (<https://bioinfo.mnhn.fr/abi/public/asap/>) using Kimura (K80) distance matrices and configured under following parameters: Substitution model =  $p$ -distances, Probability = 0.01, Best scores = 10, Fixed seed value = -.

### General Mixed Yule Coalescent (GMYC)

This approach applies single (Pons et al. 2006) or multiple (Monaghan et al. 2009) time thresholds to delimit species in a Maximum Likelihood context, using ultrametric trees as input (Ortiz and Francke 2016). Ultrametric trees were generated with phylogenetic analyses in the BEAUti and BEAST v. 1.10.4 software (Drum-

mond et al. 2002–2018) using a coalescent (constant population) tree prior. An independent log normal uncorrelated clock was applied to each partition with their respective evolution model and substitution rates (CO1: GTR + I + G; ITS2: K2P; 28S: GTR + I + G). Five independent analyses were run, each with 40 million iterations. Tracer 1.6 (Rambaut and Drummond 2003–2013) was used to evaluate convergence values, with the ESS (Effective Sample Size) > 200. Tree Annotator 2.6.0 (a BEAST package) was used to construct maximum credibility of clades trees, after discarding the first 25% of each independent run as burn-in. Finally, the GMYC method was implemented in the web platform (<https://species.h-its.org/gmyc/>), which uses the original R implementation of the GMYC model (Fujisawa and Barraclough 2013).

### Bayesian Poisson Tree Processes (bPTP)

This method is similar to GMYC, but does not require an ultrametric tree as input because the models of speciation rate are implemented directly using the number of substitutions calculated from branch lengths. The Bayesian and Maximum Likelihood variants were carried out on the online platform (<https://species.h-its.org/ptp/>), with the following options: Rooted tree, MCMC = 1000000, Thinning = 100, Burn-in = 0.1, Seed = 123. The resulting trees were edited with the iTOL online version (<https://itol.embl.de/>) (Letunic and Bork 2021) and Photoshop CS6. To delimit different species, we used the congruence integration criteria. It is based on the correspondence among the different molecular methods to generate a highly supported species hypothesis (DeSalle et al. 2005; Hamilton et al. 2011; Navarro-Rodríguez and Valdez-Mondragón 2020; Valdez-Mondragón 2020).

## Results

### Molecular analyses of genetic distances

The corrected *p*-distances under NJ using the CO1 matrix recovered 22 species of *Physocyclus*. This is concordant with the morphology analysis of features commonly used to identify and diagnose at the species level (Valdez-Mondragón 2013, 2020; Valdez-Mondragón and Francke 2015) (Fig. 1). Both the morphology and all genetic distance analyses using CO1 recovered groups that correspond with a described species. The NJ analyses using the ITS2 marker recovered 20 species (Fig. 2), whereas analyses with 28S recovered 21 species (Fig. 3). The average genetic *p*-distances among *Physocyclus* species were 16.4% (min: 14.89%, max: 17.96%) for CO1, 29.4% (min: 25.37%, max: 38.59%) for ITS2, and 14.4% (min: 14.15%, max: 17.87%) for 28S (Figs 1–3, Table 3). The average intraspecific distances using CO1 were below 2% for most species (18/22). However, four species (*P. enaulus* Crosby, 1926, *P. modestus* Gertsch, 1971, *P. mysticus* Chamberlin, 1924, and

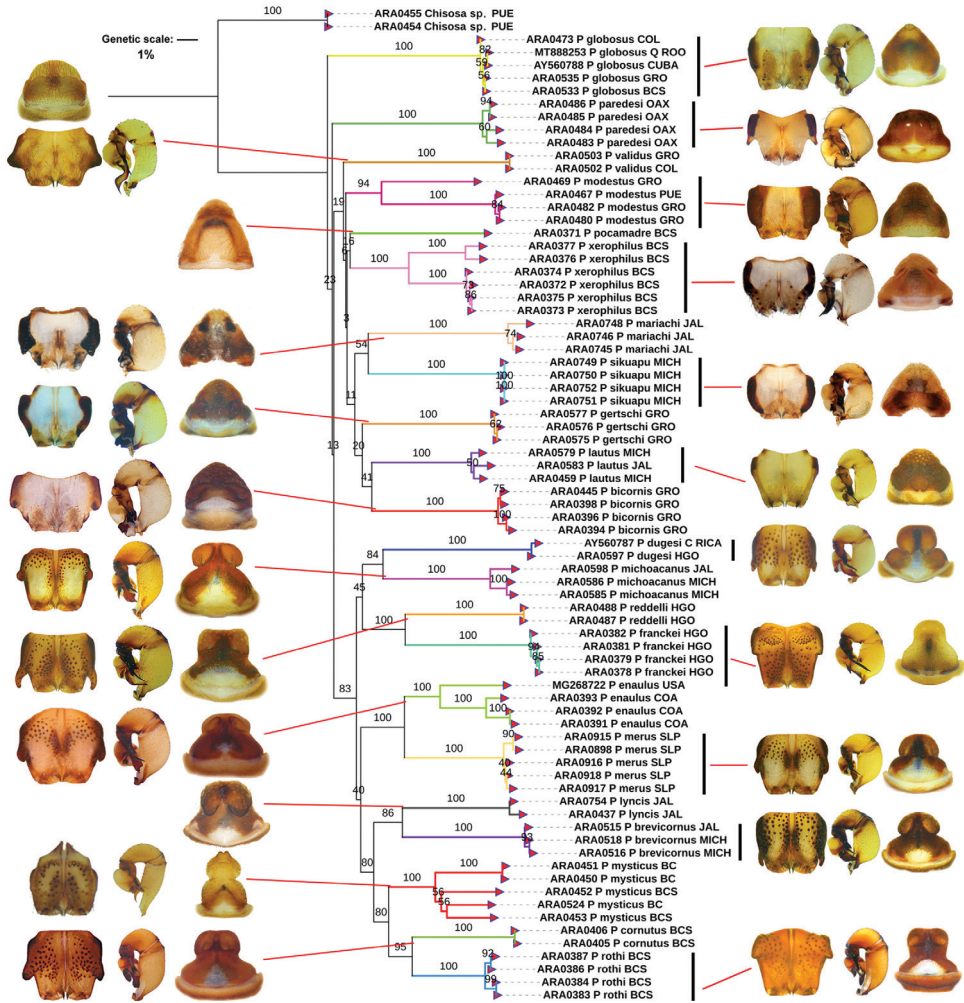


**Figure 1.** Neighbor-Joining (NJ) with corrected  $p$ -distances tree constructed with CO1 barcode sequences from different species of *Physocyclus*. Branch colors indicate putative species. Male chelicerae, male palps, and female epigynes are shown for each species. Numbers above branches represent significant Bootstrap support values (> 50%).

*P. xerophilus* Nolasco & Valdez-Mondragón, 2020) showed average intraspecific genetic distances between 4–6% (Table 3), with high Bootstrap support in each case (> 94%) (Fig 1). The Bootstrap support values for all species were high (100%) (Fig. 1). The *globosus* and *dugesi* species groups were not recovered in the CO1 topology. In the ITS2 tree, six species (*P. bicornis* Gertsch, 1971, *P. lautus* Gertsch, 1971, *P. lyncis* Nolasco & Valdez-Mondragón, 2022, *P. modestus*, *P. mysticus*, and *P. validus* Gertsch, 1971) had average intraspecific genetic distances below 2%, while the rest showed average intraspecific genetic distances over 2% (Fig. 2). Bootstrap

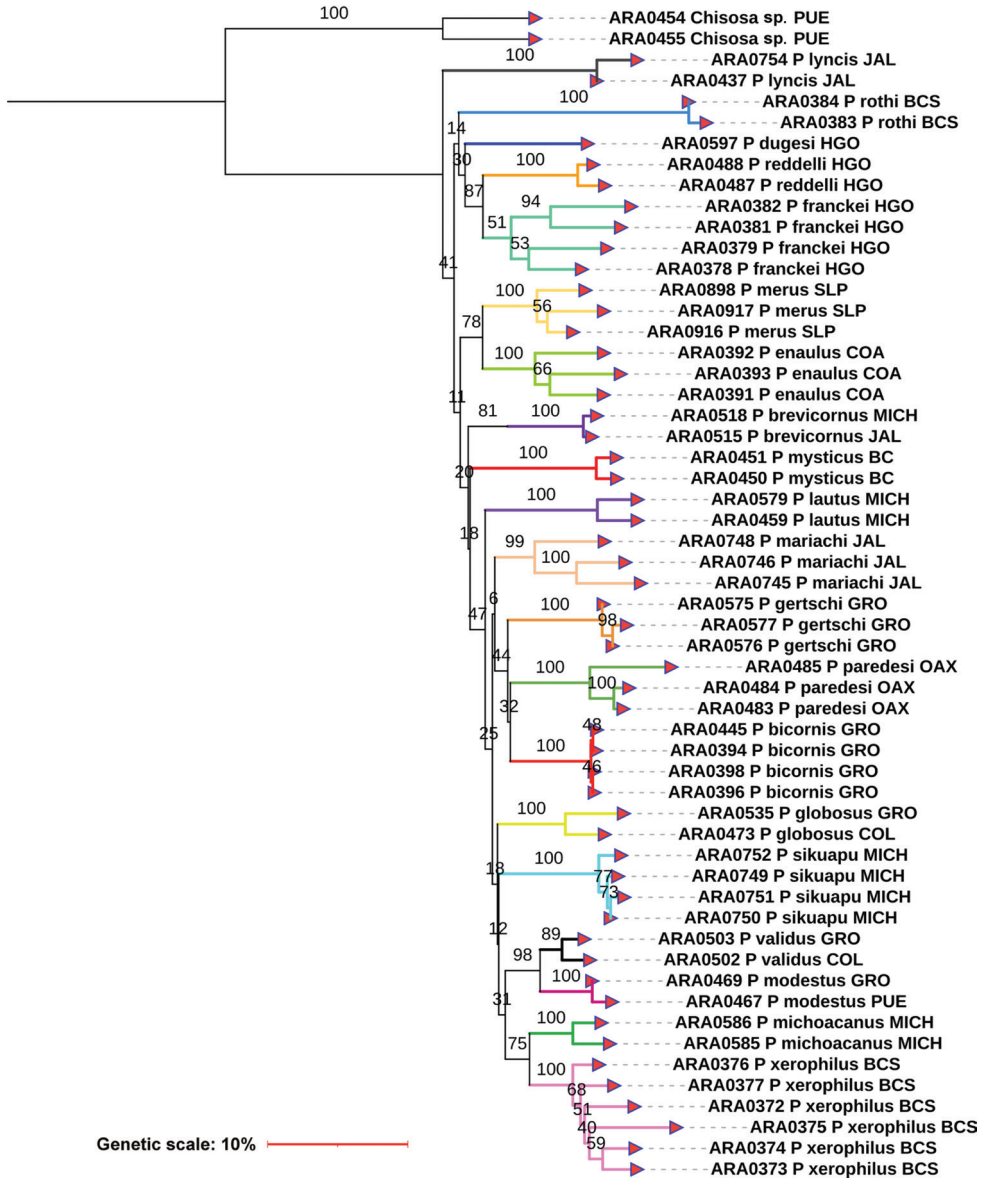


**Figure 2.** Neighbor-Joining (NJ) with corrected  $p$ -distances tree constructed with ITS2 barcode sequences from different specimens and species of *Physocyclus*. Branch colors indicate putative species. Numbers above branches represent significant Bootstrap support values (> 50%).

support values for species in the ITS2 topology were significant (over 89%), except for *P. franckei* (51%). Using the 28S marker, average intraspecific genetic distances for all species were below 2% (Fig. 3) with high Bootstrap support values (> 95%).

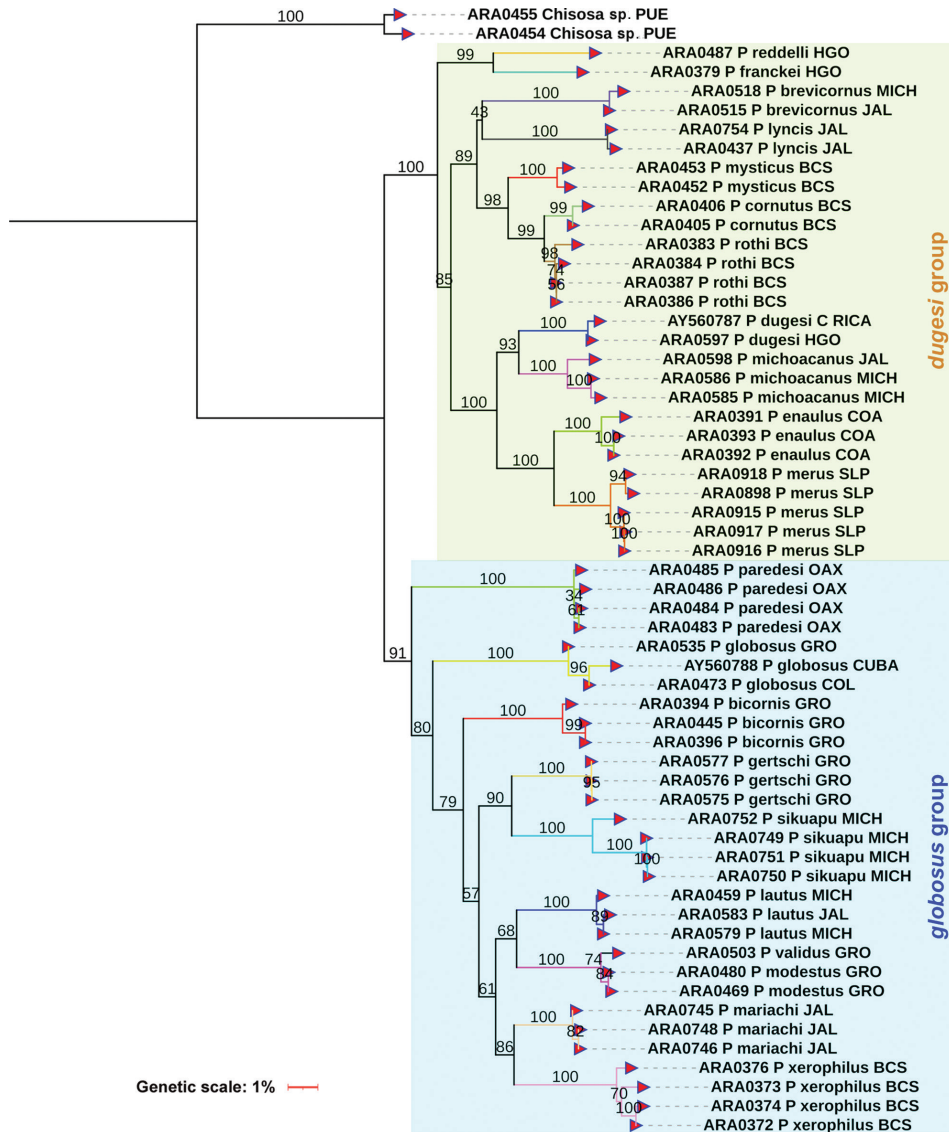


**Figure 3.** Neighbor-Joining (NJ) with corrected  $p$ -distances tree constructed with 28S barcode sequences from different specimens and species of *Physocyclus*. Branch colors indicate putative species. Numbers above branches represent significant Bootstrap support values (> 50%).

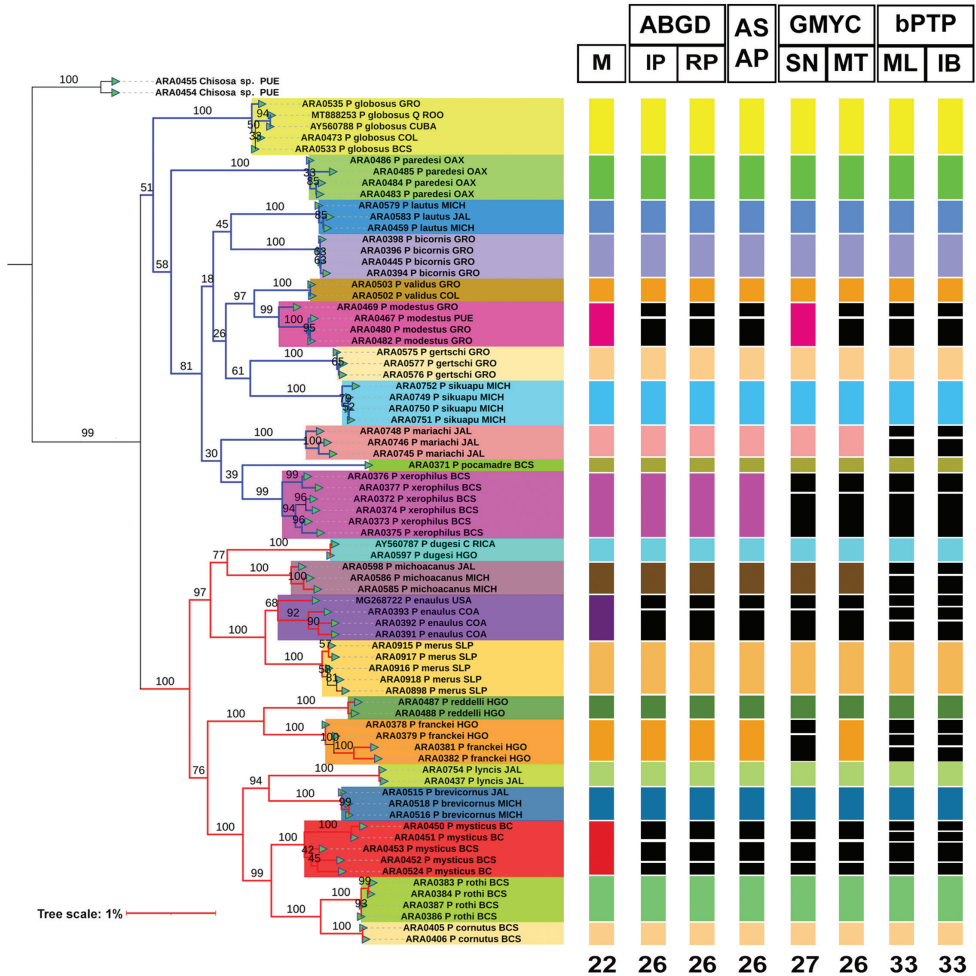
The 28S tree was the only one to recover both the *globosus* and *dugesi* species groups with high Bootstrap support values (100% for the *dugesi* group and 91% for the *globosus* group) (Fig. 3).

Table 3. Average CO1 genetic distances ( $p$ -distances) among *Physocylus* species.

Species	1	2	3	4	5	6	7	8	9	10	11	12	13	14	15	16	17	18	19	20	21	22	
1. <i>P. bicornis</i>	0.7																						
2. <i>P. brevicornus</i>	18.4	0.3																					
3. <i>P. cornutus</i>	16.4	14.1	0.2																				
4. <i>P. dagesi</i>	20.3	17.1	18.5	0.5																			
5. <i>P. enaulus</i>	17.6	17.3	15.3	17.6	4.5																		
6. <i>P. franckei</i>	20.3	17.7	17.9	18.2	17.4	0.3																	
7. <i>P. gertschi</i>	13.8	18.3	17.1	20.1	19.7	19.4	0.2																
8. <i>P. globosus</i>	18.3	19.5	18.4	18.4	16.5	18.9	16.8	0.4															
9. <i>P. lautus</i>	12.9	17.4	15.9	17.8	16.9	18.4	14.3	17.1	1.4														
10. <i>P. lynx</i>	18.0	12.7	15.8	17.3	16.2	19.1	18.3	18.3	17.3	1.1													
11. <i>P. mariachi</i>	16.4	20.1	20.1	18.4	20.0	19.2	16.5	19.6	15.6	18.3	1.5												
12. <i>P. merus</i>	17.6	17.2	15.8	17.9	11.0	19.7	19.1	17.9	16.9	15.5	19.4	0.9											
13. <i>P. michoacanus</i>	18.3	17.0	17.2	14.7	15.0	16.6	17.4	16.7	15.3	16.3	20.3	17.0	1.9										
14. <i>P. modestus</i>	15.6	19.1	17.6	18.8	16.4	18.5	16.1	15.8	14.1	18.9	17.9	17.9	17.1	5.8									
15. <i>P. mysticus</i>	18.2	14.3	12.8	16.0	15.0	16.9	17.4	16.9	16.2	15.3	17.8	14.6	15.8	16.9	5.7								
16. <i>P. paredesi</i>	18.0	19.5	19.2	18.5	17.0	19.4	17.0	17.5	16.3	18.0	18.9	18.2	19.8	17.8	17.6	1.3							
17. <i>P. pocamadre</i>	15.8	18.7	16.5	19.6	16.6	19.8	16.3	16.9	13.8	16.1	15.8	16.4	17.9	15.1	15.4	16.4	0.0						
18. <i>P. reddelli</i>	19.2	17.5	18.5	17.1	16.6	13.0	19.2	19.4	17.5	16.8	18.6	17.0	17.1	18.4	15.8	17.7	16.9	0.0					
19. <i>P. rothi</i>	16.0	13.0	9.7	16.4	14.3	14.6	14.2	17.0	15.6	14.6	17.3	15.5	14.9	16.6	11.0	17.8	16.5	17.5	0.8				
20. <i>P. sikenapu</i>	16.6	17.9	18.5	18.3	18.2	19.1	14.5	18.3	15.7	17.1	15.1	18.1	19.0	16.0	16.8	16.8	15.6	16.6	16.6	0.0			
21. <i>P. validus</i>	16.7	20.0	19.5	20.4	18.9	19.5	16.1	17.4	16.9	18.8	19.0	18.3	17.8	16.8	18.9	17.6	16.2	18.9	19.5	16.8	0.0		
22. <i>P. xerophilus</i>	15.9	18.6	17.7	19.3	17.1	17.9	14.3	15.8	13.9	18.2	15.7	16.4	18.1	14.8	16.9	15.8	13.7	16.7	17.4	15.3	15.2	4.0	

## Molecular methods for species delimitation

The Maximum Likelihood (ML) tree of the concatenated matrix (CO1+ITS2+28S) (Fig. 4) found congruence among the four different molecular species delimitation methods and using traditional morphology. This was found for 15 species: *Physocyclus bicornis*, *P. brevicornus*, *P. cornutus*, *P. dugesi*, *P. gertschi*, *P. globosus*, *P. lautus*, *P. lyncis*,



**Figure 4.** Maximum Likelihood (ML) tree of *Physocyclus* (log likelihood: -3749.87) constructed with the concatenated matrix (CO1+ITS2+28S). Bar colors represent putative species in the tree and in the columns, which represent the different species delimitation methods analyzed. Branch colors represent species groups: *globosus* (blue) and *dugesi* (red). Numbers below the columns represent the species recovered in each species delimitation method (not considering *Chisosa* sp.). Numbers above branches represent Bootstrap support values for ML (> 50% significant). Column abbreviations: Morphology (M); ABGD with initial (IP) and recursive (RP) partitions; ASAP; GMYC with single (SN) and multi (MT) thresholds; bPTP with Maximum Likelihood (ML) and Bayesian Inference (IB) variants.

*P. merus*, *P. paredesi*, *P. pocamadre*, *P. reddelli*, *P. rothi*, *P. sikuapu*, and *P. validus* (Fig. 4). *Physocyclus mariachi* and *P. michoacanus* are recovered as distinct species by most methods except for bPTP, whereas *P. franckei* is not recovered under the bPTP and GMYC methods in the single threshold (SN) (Fig. 4). *Physocyclus enaulus*, *P. modestus*, *P. mysticus*, and *P. xerophilus* were found to contain more than two species (2–4) by most of the species delimitation methods (Fig. 4).

The most congruent methods with morphology were the barcoding method ABGD, ASAP, and GMYC, which delimited 26 (ABGD IP and RP, ASAP, and GMYC MT) and 27 (GMYC SN) putative species, respectively. The most incongruent result of the analyses was bPTP, which delimited 33 putative species under ML and IB variants (Fig. 4).

Both species groups (*globosus* and *dugesii*) were recovered in the ML analysis using the concatenated matrix (CO1+ITS2+28S) (Fig. 4). The *dugesii* group was recovered with significant Bootstrap support (100%), whereas the *globosus* group had Bootstrap support value of 51%.

## Discussion

Two different approaches (DNA taxonomy and DNA barcoding) were proposed by DeSalle et al. (2005) to overcome several weaknesses of traditional morphology-based taxonomic systematics, and to resolve the crucial need for accurate and rapid species identification tools (Hebert et al. 2003; Tautz et al. 2003). DNA barcoding is useful for recognizing cryptic species (two or more distinct species that are erroneously classified as the same species due to similar morphology) (Bickford et al. 2007). Even only with CO1, DNA barcoding is helpful in species diagnosis due to the fact that sequence divergences are ordinarily much lower among individuals of the same species than between closely related species (Hebert et al. 2004). For some groups of arachnids, traditional morphology fails to recognize and delineate species boundaries. Also, identify sister or cryptic species requires other types or evidence such as molecular data, ecological niche modeling, morphometric morphology, haplotype networks, and biogeographical approximations (Hebert et al. 2003, 2004; Hamilton et al. 2011, 2014; Montes de Oca et al. 2015; Ortiz and Francke 2016; Cruz-López et al. 2019; Valdez-Mondragón et al. 2019; Newton et al. 2020; Valdez-Mondragón and Cortez-Roldán 2021). However, as demonstrated herein, spiders of the genus *Physocyclus* have robust morphology for diagnosis and identification at the species level, mainly of primary and secondary sexual characters, such as chelicerae and palps (males) or epigynes (females).

In the genetic distance analyses performed with independent matrices of CO1, ITS2, and 28S, all the species terminals were recovered. The genetic intraspecific distances for ITS2 were found to be relatively high in the majority of species (over 2%). However, the average intraspecific genetic distances using the CO1 and 28S markers were lower in the majority of species (< 2%). Agnarsson (2010), Valdez-Mondragón et al. (2019), and Navarro-Rodríguez and Valdez-Mondragón (2020) mention that ITS2 is inadequate for resolving relationships between closely related species of spiders. Our

data corroborate this, showing the unreliability of this gene for genetic distance (and species delimitation) analyzes when used on its own. However, the use of a concatenated matrix of nuclear (28S and ITS2) and mitochondrial (CO1) markers provides better results with more robust evidence for delimiting species based on molecular data (Astrin et al. 2006; Agnarsson 2010; Planas and Ribera 2015; Ortiz and Francke 2016; Navarro-Rodríguez and Valdez-Mondragón 2020).

When looking at CO1, Pholcid spiders generally show high genetic divergences among species (Astrin et al. 2006). In contrast to reports for spiders in general that show values of 14.4% (Hebert et al. 2003) and 16.4% (Barrett and Hebert 2005), Pholcids' average interspecific genetic distance for CO1 is 19.8% (Astrin et al. 2006). Our results found a value of average interspecific distance at the CO1 marker observed in *Physocyclus* of 16.4% (Fig. 1, Table 3). This value fits within the average limits of other spiders; however, this tendency in the Pholcidae family is not always the case. The average interspecific genetic distance for CO1 in other genera such as *Ixchela* Huber, 2000 (Modisiminae) were found to be lower, 12% (Valdez-Mondragón 2020). Although most species were included in the analyses (22 of 37), missing species might have an effect and overestimate the average interspecific distances, because perhaps the sister species of each species is not found in the data set. However, the results and topologies were consistent along the analyzes.

With regards to molecular delimitation methods, ABGD used to be sensitive to sampling effect and tended to moderately over-split, as demonstrated in the mygalomorph genera *Aphonopelma* Pocock, 1901 by Hamilton et al. (2014) and *Bonnetina* Vol, 2000 by Ortiz and Francke (2016) and Candia-Ramírez and Francke (2020). Similar results were observed in *Loxosceles* Heineken & Lowe, 1832 (Valdez-Mondragón et al. 2019; Navarro-Rodríguez and Valdez-Mondragón 2020), where the ABGD method generated an inflated number of delimited species. However, within the pholcid genus *Ixchela*, it was observed by Valdez-Mondragón (2020) that the most incongruent method was bPTP (both ML and IB variants), as was also found in the molecular analyses herein with the genus *Physocyclus*.

The most congruent methods that delimited a similar number of species in this study were ABGD, ASAP, and GMYC, which was corroborated by traditional morphology (Fig. 4). The bPTP method delimited a higher number of species in comparison with morphology. These results contrast with those found by Ortiz and Francke (2016), Valdez-Mondragón et al. (2019), and Navarro-Rodríguez and Valdez-Mondragón (2020), in which the bPTP and GMYC analyses were the most congruent methods with the morphology in spiders. This may be due to the inclusion of the 28S marker, which might be causing tree-based analyzes (bPTP) to generate an overestimation in the number of putative species recovered. According to Luo et al. (2018), GMYC and bPTP are negatively influenced by gene flow and are sensitive to the ratio of population size to divergence time, reflecting the important impact of incomplete lineage sorting on species delimitation.

In such cases of incongruency between the molecular methods and morphology, as in *Physocyclus enaulus*, *P. modestus*, *P. mysticus*, and *P. xerophilus*, no significant morphological

differences were found within individuals of each species. However, *P. enaulus* was the exception, where Valdez-Mondragón (2010) recorded three different morphotypes of epigyne shape. Unfortunately, we could not get sequences of all the morphotypes. As Valdez-Mondragón (2010, 2014) mentions, the morphology of somatic and sexual characters in the genus *Physocyclus* is usually highly conserved. Similarly, morphological changes might not be correlated with species boundaries, or may not be useful for delimiting species if interspecific recognition occurs in non-visual signs (chemical or mating calls), or even biogeographical traits (microhabitats). Furthermore, it is possible that the species may be under stabilizing selection that promotes morphological stasis (Bickford et al. 2007).

According with Hamilton et al. (2011), species delimitation based only on molecular data can rarely be achieved, and additional types of evidence such as biogeographical information is needed. In the case of the multiple species inferred within *P. mysticus*, no significant morphological or habitat differences are apparent. All specimens are from xerophytic scrub and present similar microhabitats of living under big boulders on the ground. Sympatric speciation may be possibly, as other species of the genus *Physocyclus* have been collected in the same locality (Valdez-Mondragón 2010, 2013). *Physocyclus modestus* presents a similar case, being one widespread species from Guerrero, Morelos, Oaxaca, and Puebla. However, habitat differences exist among the different populations of this species. Some specimens are from xerophytic scrub, while others are found in lowland forest. Microhabitat likely has a direct influence on the diversification of pholcids spiders, as was demonstrated by Eberle et al. (2018). Therefore, the morphological and molecular evidence suggest that *P. modestus* might be a species complex, as observed in *P. mysticus*. However, more male and female specimens from different populations are needed to confirm this assumption.

As Carstens et al. (2013) suggested, probing different methods or lines of evidence is necessary for properly implementing species delimitation. When the information and results are incongruent, it is better to be conservative about assumptions of species delimitation. In the case of some species in this study (e.g., *P. enaulus* and *P. xerophilus*), more detailed analyses of the morphological structures are necessary. Maybe including ultra-morphology, lineal morphology, or geometric morphometry in somatic features such as length legs, carapace shape, or even in sexual structures (Valdez-Mondragón et al. 2019). Lineal and geometric morphology has provided strong evidence for splitting species in cases where traditional morphology fails to delimit species. This has been demonstrated in araneomorph spiders (Planas and Ribera 2015; Valdez-Mondragón et al. 2019) and in brown recluse spiders of the genus *Loxosceles* (Solís-Catalán 2020). In this works, significant differences were found in carapace length, male palp shape, and length leg I among different species from the Canary Islands and central Mexico. *Physocyclus enaulus* is a widespread species from northern Mexico and southern United States. Valdez-Mondragón (2010) reported three different types of ventral apophyses in the female epigyne, which suggests that it might comprise a species complex rather than wide intraspecific morphological variation.

Although the number of described species in the genus *Physocyclus* has doubled in the last decade (Valdez-Mondragón 2010, 2013, 2014; Jiménez and Palacios-Cardiel 2013; Nolasco and Valdez-Mondragón 2020, 2022), the diversity of this genus in Mexico is still poorly known. Provinces such as the Sonoran and Chihuahuan Deserts have been poorly sampled, despite their arid and semiarid ecosystems being common habitats for the genus *Physocyclus*. Furthermore, cave habitats have been virtually unexplored in this genus, and will likely produce new troglomorphic species (Valdez-Mondragón 2010, 2020; Huber et al. 2018).

In regard to the molecular methods used herein, each one presents its advantages and disadvantages. Barcoding methods (ABGD) can distinguish within-population differences caused by species divergences, analyzing the gaps of a data set and using it as a barcode to recognize different species (Puillandre et al. 2012; Rannala 2015; Rannala and Yang 2020). However, this method does not consider the rates of intra- and interspecific variation as an initial parameter, causing barcode values to vary among species groups and, in some cases, generating over splitting (Hickerson et al. 2006; Rannala 2015; Rannala and Yang 2020). The hierarchical integration of the ASAP method allows for many possible clusterings of terminals to be tested (Puillandre et al. 2021). However, it can offer different delimitation species hypothesis with similar asap-scores. In the case of *Physocyclus* spiders here, both methods offered a high congruence between themselves and the morphological evidence.

The coalescence method (GMYC) is robust because it uses an a priori ultrametric species tree, taking into account the groups formed in the topology. However, this method assumes that the lineages in each population coalesce before any speciation event occurs, implying the absence of incomplete lineage sorting and ignoring the coalescent process within populations of ancestral species (Rannala and Yang 2020). The bPTP method accommodates the use of large data sets with thousands of species and considers the rates of intra- and interspecific genetic variation. However, it does not take into account the stochastic fluctuations in the coalescent process among the different loci in large multi-locus analyses (Rannala and Yang 2020). The coalescent analyses for species delimitation (GMYC, bPTP) do not require reciprocal monophyly to delimit species (Knowles and Carstens 2007) and can incorporate statistical uncertainty in gene trees. They are based on Maximum Likelihood and Bayesian Inferences and not only on corrected genetic distances.

In conclusion, CO1 and 28S provide robust evidence for species-level delimitation in the genus *Physocyclus*, with high congruence among all methods. The genetic variability of ITS2 makes it an unreliable molecular marker for species delimitation on its own, however, it provides good information when used in combination with others mitochondrial and nuclear markers. Sexual morphological characters (male palps, male chelicerae, and female epigyne) are robust features for identifying and diagnosing *Physocyclus* species. However, in some cases, morphology alone is not enough to detect sister species, cryptic species, or even species complexes.

## Acknowledgements

The first author thanks the Doctorate Program of the Centro Tlaxcala de Biología de la Conducta (CTBC), Universidad Autónoma de Tlaxcala, Tlaxcala City. The first author also thanks to the American Arachnological Society (AAS) and the Student Research Grants (2022) for financial support for field work. The second author thanks the program “Jóvenes investigadores por México (Cátedras CONACyT)” and the Consejo Nacional de Ciencia y Tecnología (CONACyT) for scientific support for the project No. 59: “Laboratorio Regional de Biodiversidad y Cultivo de Tejidos Vegetales (LBCTV), Instituto de Biología, Universidad Nacional Autónoma de México (UNAM), sede Tlaxcala”. The second author also thanks SEP-CONACyT for financial support of the project of Basic Science (Ciencia Básica) 2016, No. 282834. We thank Dr. Edmundo González Santillán and Dr. Oscar F. Francke (ex-curator) of the Colección Nacional de Arácnidos (CNAN), Instituto de Biología, UNAM, for providing specimen loans, MSc. Laura Márquez Valdelamar for the molecular sequencing of the samples, Brett O. Butler for the English language review of the manuscript, and the reviewers for their comments and suggestions that improved the manuscript. We also thank the students of the Laboratory of Arachnology (LATLAX), IBUNAM, Tlaxcala, for their help in the field and processing of the material in the laboratory. Specimens were collected under Scientific Collector Permit FAUT-0309 from the Secretaría de Medio Ambiente y Recursos Naturales (SEMARNAT) provided to Dr. Alejandro Valdez-Mondragón.

## References

- Agnarsson I (2010) The utility of ITS2 in spider phylogenetics: Notes on prior work and an example from *Anelosimus*. *The Journal of Arachnology* 38(2): 377–382. <https://doi.org/10.1636/B10-01.1>
- Álvarez-Padilla F, Dimitrov D, Giribet G, Hormiga G (2009) Phylogenetic relationships of the spider family Tetragnathidae (Araneae, Araneoidea) based on morphological and DNA sequence data. *Cladistics* 25(2): 109–106. <https://doi.org/10.1111/j.1096-0031.2008.00242.x>
- Arnedo MA, Hormiga G, Scharff N (2009) Higher-level phylogenetics of linyphiid spiders (Araneae, Linyphiidae) based on morphological and molecular evidence. *Cladistics* 25(3): 231–262. <https://doi.org/10.1111/j.1096-0031.2009.00249.x>
- Astrin JJ, Stueben PE (2008) Phylogeny in cryptic weevils: molecules, morphology and new genera of western Palearctic *Cryptorhynchinae* (Coleoptera: Curculionidae). *Invertebrate Systematics* 22(5): 503–522. <https://doi.org/10.1071/IS07057>
- Astrin JJ, Huber BA, Misof B, Klütsch CFC (2006) Molecular taxonomy in pholcid spiders (Pholcidae: Araneae): evaluation of species identification methods using CO1 and 16S and rRNA. *Zoologica Scripta* 35(5): 441–457. <https://doi.org/10.1111/j.1463-6409.2006.00239.x>

- Ballesteros JA, Hormiga G (2018) Species delimitation of the North American orchard-spider *Leucauge venusta* (Walckenaer, 1841) (Araneae, Tetragnathidae). *Molecular Phylogenetics and Evolution* 121: 183–197. <https://doi.org/10.1016/j.ympev.2018.01.002>
- Barrett RDH, Hebert PDN (2005) Identifying spiders through DNA barcodes. *Canadian Journal of Zoology* 83(3): 481–491. <https://doi.org/10.1139/z05-024>
- Bickford D, Lohman DJ, Sodhi NS, Ng PKL, Meier R, Winker L, Ingram KK, Das I (2007) Cryptic species as a window on diversity and conservation. *Trends in Ecology & Evolution* 22(3): 148–155. <https://doi.org/10.1016/j.tree.2006.11.004>
- Bond JE (2004) Systematics of the Californian euctenizine spider genus *Apomastus* (Araneae: Mygalomorphae: Cyrtaucheniidae): the relationship between molecular and morphological taxonomy. *Invertebrate Systematics* 18(4): 361–376. <https://doi.org/10.1071/IS04008>
- Bruvo-Madarić B, Huber BA, Steinacher A, Pass G (2005) Phylogeny of pholcid spiders (Araneae: Pholcidae): combined analysis using morphology and molecules. *Molecular Phylogenetics and Evolution* 37(3): 661–673. <https://doi.org/10.1016/j.ympev.2005.08.016>
- Candia-Ramírez D, Francke O (2020) Another stripe on the tiger makes no difference? Unexpected diversity in the widespread tiger tarantula *Davus pentaloris* (Araneae: Theraphosidae: Theraphosinae). *Zoological Journal of the Linnean Society* 192(1): 75–104. <https://doi.org/10.1093/zoolinnean/zlaa107>
- Cao X, Liu J, Chen J, Zheng G, Kuntner M, Agnarsson I (2016) Rapid dissemination of taxonomic discoveries based on DNA barcoding and morphology. *Scientific Reports* 6(1): e37066. <https://doi.org/10.1038/srep37066>
- Carstens BC, Pelletier TA, Reid NM, Satler J (2013) How to fail at species delimitation. *Molecular Ecology* 22(17): 4369–4383. <https://doi.org/10.1111/mec.12413>
- Correa-Ramírez MM, Jiménez ML, García-De León FJ (2010) Testing species boundaries in *Pardosa sierra* (Araneae: Lycosidae). *The Journal of Arachnology* 38(3): 538–554. <https://doi.org/10.1636/Sh09-15.1>
- Cruz-López JA, Monjaraz-Ruedas R, Francke OF (2019) Turning to the dark side: Evolutionary history and molecular species delimitation of a troglomorphic lineage of armoured harvestman (Opiliones: Stygnopsidae). *Arthropod Systematics & Phylogeny* 77(2): 285–302. <https://doi.org/10.26049/ASP77-2-2019-0>
- DeSalle R, Egan MG, Siddall M (2005) The unholy trinity: Taxonomy, species delimitation and DNA barcoding. *Philosophical Transactions of the Royal Society, London, Series B* 360(1462): 1905–1916. <https://doi.org/10.1098/rstb.2005.1722>
- Dimitrov D, Hormiga G (2011) An extraordinary new genus of spiders from Western Australia with an expanded hypothesis on the phylogeny of Tetragnathidae (Araneae). *Zoological Journal of the Linnean Society* 161(4): 735–768. <https://doi.org/10.1111/j.1096-3642.2010.00662.x>
- Dimitrov D, Astrin JJ, Huber BA (2013) Pholcid spider molecular systematics revisited, with new insights into the biogeography and evolution of the group. *Cladistics* 29(2): 132–146. <https://doi.org/10.1111/j.1096-0031.2012.00419.x>
- Drummond AJ, Suchard MA, Xie D, Rambaut A (2012, August) (2002–2018) Bayesian phylogenetics with BEAUti and the BEAST 1.7. *Molecular Biology and Evolution* 29(8): 1969–1973. <https://doi.org/10.1093/molbev/mss075>

- Eberhard WG (1985) *Sexual Selection and Animal Genitalia*. Harvard University Press, Cambridge, Massachusetts, 244 pp. <https://doi.org/10.4159/harvard.9780674330702>
- Eberhard WG, Huber BA, Rodríguez RL, Briceno RD, Salas I, Rodríguez V (1998) One size fits all? Relationships between the size and degree of variation in genitalia and other body parts in twenty species of insects and spiders. *Evolution* 52(2): 415–431. <https://doi.org/10.1111/j.1558-5646.1998.tb01642.x>
- Eberle J, Dimitrov D, Valdez-Mondragón A, Huber BA (2018) Microhabitat change drives diversification in pholcid spiders. *BMC Evolutionary Biology* 18(1): 141. <https://doi.org/10.1186/s12862-018-1244-8>
- Folmer M, Black W, Lutz R, Vrijenhoek R (1994) DNA primers for amplification of mitochondrial cytochrome c oxidase subunit I from diverse metazoan invertebrates. *Molecular Marine Biology and Biotechnology* 3: 294–299. [https://doi.org/10.1603/00222585\(2005\)042\[0756:MOBLIA\]2.0.CO;2](https://doi.org/10.1603/00222585(2005)042[0756:MOBLIA]2.0.CO;2)
- Fox GE, Pechman KR, Woese CR (1977) Comparative cataloging of 16S ribosomal ribonucleic acid: Molecular approach to procaryotic systematics. *International Journal of Systematic and Evolutionary Microbiology* 27(1): 44–57. <https://doi.org/10.1099/00207713-27-1-44>
- Fujisawa T, Barraclough TG (2013) Delimiting species using single-locus data and the Generalized Mixed Yule Coalescent approach: A revised method and evaluation on simulated data sets. *Systematic Biology* 62(5): 707–724. <https://doi.org/10.1093/sysbio/syt033>
- Galtier N, Nabholz B, Glemin S, Hurst GDD (2009) Mitochondrial DNA as a marker of molecular diversity: A reappraisal. *Molecular Ecology* 18(22): 4541–4550. <https://doi.org/10.1111/j.1365-294X.2009.04380.x>
- Hall TA (1999) BioEdit: A user-friendly biological sequence alignment editor and analysis program for Windows 95/98/NT. *Nucleic Acids Symposium Series* 41: 95–98.
- Hamilton CA, Formanowicz DR, Bond JE (2011) Species delimitation and phylogeography of *Aphonopelma hentzi* (Araneae, Mygalomorphae, Theraphosidae): Cryptic diversity in North American tarantulas. *PLoS ONE* 6(10): e26207. <https://doi.org/10.1371/journal.pone.0026207>
- Hamilton CA, Hendrixson BE, Brewer MS, Bond JE (2014) An evaluation of sampling effects on multiple DNA barcoding methods leads to an integrative approach for delimiting species: A case study of the North American tarantula genus *Aphonopelma* (Araneae, Mygalomorphae, Theraphosidae). *Molecular Phylogenetics and Evolution* 71: 79–93. <https://doi.org/10.1016/j.ympev.2013.11.007>
- Hazzi N, Hormiga G (2021) Morphological and molecular evidence support the taxonomic separation of the medically important Neotropical spiders *Phoneutria depilata* (Strand, 1909) and *P. boliviensis* (F.O. Pickard-Cambridge, 1897) (Araneae, Ctenidae). *ZooKeys* 1022(31): 13–50. <https://doi.org/10.3897/zookeys.1022.60571>
- Hebert PDN, Cywinska A, Ball SL, deWaard JR (2003) Biological identifications through DNA barcodes. *Proceedings of the Royal Society of London, Series B: Biological Sciences* 270(1512): 313–321. <https://doi.org/10.1098/rspb.2002.2218>
- Hebert PDN, Penton EH, Burns JM, Janzen DH, Hallwachs W (2004) Ten species in one: DNA barcoding reveals cryptic species in the Neotropical skipper butterfly *Astraptes fulgerator*. *Proceedings of the National Academy of Sciences of the United States of America* 101(41): 14812–14817. <https://doi.org/10.1073/pnas.0406166101>

- Hickerson MJ, Meyer CP, Moritz C (2006) DNA barcoding will often fail to discover new animal species over broad parameter space. *Systematic Biology* 55(5): 729–739. <https://doi.org/10.1080/10635150600969898>
- Hillis DM, Dixon MT (1991) Ribosomal DNA: molecular evolution and phylogenetic inference. *Quarterly Review of Biology* 66(4): 411–453. <https://doi.org/10.1086/417338>
- Huber BA (2003) Rapid evolution and species-specificity of arthropod genitalia: Fact or artifact? *Organisms, Diversity & Evolution* 3(1): 63–71. <https://doi.org/10.1078/1439-6092-00059>
- Huber BA (2011) Phylogeny and classification of Pholcidae (Araneae): An update. *The Journal of Arachnology* 39(2): 211–222. <https://doi.org/10.1636/CA10-57.1>
- Huber BA, Carvalho LS (2019) Filling the gaps: descriptions of unnamed species included in the latest molecular phylogeny of Pholcidae (Araneae). *Zootaxa* 4546 (1): 001–096. <https://doi.org/10.11646/zootaxa.4546.1.1>
- Huber BA, Dimitrov D (2014) Slow genital and genetic but rapid non-genital and ecological differentiation in a pair of spider species (Araneae, Pholcidae). *Zoologischer Anzeiger* 253(5): 394–403. <https://doi.org/10.1016/j.jcz.2014.04.001>
- Huber BA, Pérez-González A (2001a) A new genus of pholcid spiders (Araneae: Pholcidae) endemic to Western Cuba, with a case of female genitalic dimorphism. *American Museum Novitates* 3329: 1–23. [https://doi.org/10.1206/0003-0082\(2001\)329<0001:ANGOPS>2.0.CO;2](https://doi.org/10.1206/0003-0082(2001)329<0001:ANGOPS>2.0.CO;2)
- Huber BA, Pérez-González A (2001b) Female genital dimorphism in a spider (Araneae: Pholcidae). *The Zoological Society of London* 255(3): 301–304. <https://doi.org/10.1017/S095283690100139X>
- Huber BA, Rheims CA, Brescovit AD (2005) Speciation without changes in genital shape: a case study on Brazilian pholcid spiders (Araneae: Pholcidae). *Zoologischer Anzeiger* 243(4): 273–279. <https://doi.org/10.1016/j.jcz.2004.12.001>
- Huber BA, Eberle J, Dimitrov D (2018) The phylogeny of pholcid spiders: A critical evaluation of relationships suggested by molecular data (Araneae, Pholcidae). *ZooKeys* 789: 51–101. <https://doi.org/10.3897/zookeys.789.22781>
- Ji Y, Zhang D, He L (2003) Evolutionary conservation and versatility of a new set of primers for amplifying the ribosomal internal transcribed spacer regions in insects and other invertebrates. *Molecular Ecology Notes* 3(4): 581–585. <https://doi.org/10.1046/j.1471-8286.2003.00519.x>
- Jiménez ML, Palacios-Cardiel CC (2013) A new species of *Physocyclus* (Araneae: Pholcidae) from Mexico. *Zootaxa* 3717(1): 96–99. <https://doi.org/10.11646/zootaxa.3717.1.8>
- Jörger KM, Schrödl M (2013) How to describe a cryptic species? practical challenges of molecular taxonomy. *Frontiers in Zoology* 10(1): 59. <https://doi.org/10.1186/1742-9994-10-59>
- Kapli P, Lutteropp S, Zhang J, Kobert K, Pavlidis P, Stamatakis A, Flouri T (2017) Multi-rate Poisson tree processes for single-locus species delimitation under maximum likelihood and Markov chain Monte Carlo. *Bioinformatics* 33: 1630–1638. <https://doi.org/10.1093/bioinformatics/btx025>
- Katoh K, Toh H (2008) Recent developments in the MAFFT multiple sequence alignment program. *MAFFT version 7. Briefings in Bioinformatics* 4(4): 286–298. <https://doi.org/10.1093/bib/bbn013> [accessed 13 April 2022]
- Knowles LL, Carstens BC (2007) Delimiting species without monophyletic gene trees. *Systematic Biology* 56(6): 887–895. <https://doi.org/10.1080/10635150701701091>

- Kumar S, Stecher G, Tamura K (2016) MEGA7: Molecular evolutionary genetics analysis v.7.0 for bigger datasets. *Molecular Biology and Evolution* 33(7): 1870–1874. <https://doi.org/10.1093/molbev/msw054>
- Leticia I, Bork P (2021) Interactive Tree Of Life (iTOL) v5: An online tool for phylogenetic tree display and annotation. *Nucleic Acids Research* 49(1): 293–296. <https://doi.org/10.1093/nar/gkab301>
- Luo A, Ling C, Ho YM, Zhu CD (2018) Comparison of Methods for Molecular Species Delimitation Across a Range of Speciation Scenarios. *Systematic Biology* 67(5): 830–846. <https://doi.org/10.1093/sysbio/syy011>
- Monaghan MT, Wild R, Elliot M, Fujisawa T, Balke M, Inward DJ, Vogler AP (2009) Accelerated species inventory on Madagascar using coalescent-based models of species delimitation. *Systematic Biology* 58(3): 298–311. <https://doi.org/10.1093/sysbio/syp027>
- Montes de Oca L, D'Elía G, Pérez-Miles F (2015) An integrative approach for species delimitation in the spider genus *Grammostola* (Theraphosidae, Mygalomorphae). *Zoologica Scripta* 45(3): 322–333. <https://doi.org/10.1111/zsc.12152>
- Navarro-Rodríguez I, Valdez-Mondragón A (2020) Description of a new species of *Loxosceles* Heineken & Lowe (Araneae, Sicariidae) recluse spiders from Hidalgo, Mexico, under integrative taxonomy: Morphological and DNA barcoding data (CO1+ITS2). *European Journal of Taxonomy* 704(704): 1–30. <https://doi.org/10.5852/ejt.2020.704>
- Newton LG, Starrett J, Hendrixson BE, Derkarabetian S, Bond JE (2020) Integrative species delimitation reveals cryptic diversity in the southern Appalachian *Antrodiaetus unicolor* (Araneae: Antrodiaetidae) species complex. *Molecular Ecology* 29(12): 2269–2287. <https://doi.org/10.1111/mec.15483>
- Nolasco S, Valdez-Mondragón A (2020) On the daddy long-legs spiders of the genus *Physocyclus* (Araneae: Pholcidae) from Mexico: description of a new species from the Baja California Peninsula. *Revista Mexicana de Biodiversidad* 91(1): 913316. <https://doi.org/10.22201/ib.20078706e.2020.91.3316>
- Nolasco S, Valdez-Mondragón A (2022) Four new species of the spider genus *Physocyclus* Simon, 1893 (Araneae: Pholcidae) from Mexico, with updated taxonomic identification keys. *European Journal of Taxonomy* 813: 173–206. <https://doi.org/10.5852/ejt.2022.813.1739>
- Ortiz D, Francke O (2016) Two DNA barcodes and morphology for multi-method species delimitation in *Bonnetina* tarantulas (Araneae: Theraphosidae). *Molecular Phylogenetics and Evolution* 101: 176–193. <https://doi.org/10.1016/j.ympev.2016.05.003>
- Planas E, Ribera C (2014) Uncovering overlooked island diversity: colonization and diversification of the medically important spider genus *Loxosceles* (Arachnida: Sicariidae) on the Canary Islands. *Journal of Biogeography* 41(7): 1255–1266. <https://doi.org/10.1111/jbi.12321>
- Planas E, Ribera C (2015) Description of six new species of *Loxosceles* (Araneae: Sicariidae) endemic to the Canary Islands and the utility of DNA barcoding for their fast and accurate identification. *Zoological Journal of the Linnean Society* 174(1): 47–73. <https://doi.org/10.1111/zoj.12226>
- Pons J, Barraclough TG, Gomez-Zurita J, Cardoso A, Duran DP, Hazell S, Kamoun S, Sumlin WD, Vogler AP (2006) Sequence based species delimitation for the DNA

- taxonomy of undescribed insects. *Systematic Biology* 55(4): 595–609. <https://doi.org/10.1080/10635150600852011>
- Puillandre N, Lambert A, Brouillet S, Achaz G (2012) ABGD, Automatic Barcode Gap Discovery for primary species delimitation. *Molecular Ecology* 21(8): 1864–1877. <https://doi.org/10.1111/j.1365-294X.2011.05239.x>
- Puillandre N, Brouillet S, Achaz G (2021) ASAP: Assemble species by automatic partitioning. *Molecular Ecology Resources* 21(2): 609–620. <https://doi.org/10.1111/1755-0998.13281>
- Rambaut A, Drummond AJ (2003–2013). TRACER, MCMC trace analysis tool. Version 1.6. Institute of Evolutionary Biology, University of Edinburgh, Edinburgh, Department of Computer Science, University of Auckland, Auckland.
- Rannala B (2015) The art and science of species delimitation. *Current Zoology* 61(5): 846–853. <https://doi.org/10.1093/czoolo/61.5.846>
- Rannala B, Yang Z (2020) Species Delimitation. *Phylogenetics in the Genomic Era*, No commercial publisher, Authors open access book, 5.5:1–5.5:18. <https://hal.archives-ouvertes.fr/hal-02536468>
- Rozen S, Skaletsky JH (2000) Primer3 on the www for general users and for biologist programmers. In: Krawertz S, Misener S (Eds) *Bioinformatics Methods and Protocols: Methods in Molecular Biology*. Humana Press, Totowa, N, J. 365–386. <https://doi.org/10.1385/1-59259-192-2:365>
- Solís-Catalán KP (2020) Análisis morfológico de estructuras sexuales y somáticas de las especies mexicanas de arañas del género *Loxosceles* Heineken y Lowe (Araneae, Sicariidae) del Centro-Occidente de México. Tesis de Maestría en Ciencias. Universidad Autónoma de Tlaxcala.
- Tautz D, Arctander P, Minelli A, Thomas RH, Vogler AP (2003) A plea for DNA taxonomy. *Trends in Ecology & Evolution* 18(2): 70–74. [https://doi.org/10.1016/S0169-5347\(02\)00041-1](https://doi.org/10.1016/S0169-5347(02)00041-1)
- Tyagi K, Kumar V, Kundu S, Pakrashi A, Prasad P, Caleb JTD, Chandra K (2019) Identification of Indian spiders through DNA barcoding: Cryptic species and species complex. *Scientific Reports* 9(1): 14033. <https://doi.org/10.1038/s41598-019-50510-8>
- Valdez-Mondragón A (2010) Revisión taxonómica de *Physocyclus* Simon, 1983 (Araneae: Pholcidae) con la descripción de especies nuevas de México. *Revista Iberica de Aracnología* 18: 3–80.
- Valdez-Mondragón A (2013) Morphological phylogenetic analysis of the spider genus *Physocyclus* (Araneae: Pholcidae). *The Journal of Arachnology* 41(2): 184–196. <https://doi.org/10.1636/K12-33.1>
- Valdez-Mondragón A (2014) A reanalysis of the morphological phylogeny of the spider genus *Physocyclus* Simon, 1983 (Araneae: Pholcidae) with the description of a new species and description of the female of *Physocyclus paredesi* Valdez-Mondragón from México. *Zootaxa* 3866: 202–220. <https://doi.org/10.11646/zootaxa.3866.2.2>
- Valdez-Mondragón A (2020) COI mtDNA barcoding and morphology for species delimitation in the spider genus *Ixchela* Huber (Araneae: Pholcidae), with the description of two new species from Mexico. *Zootaxa* 4747 (1): 054–076. <https://doi.org/10.11646/zootaxa.4747.1.2>

- Valdez-Mondragón A, Cortez-Roldán M (2021) COI mtDNA barcoding and morphology for the description of a new species of ricinuleid of the genus *Pseudocellus* (Arachnida: Ricinulei: Ricinoididae) from El Triunfo Biosphere Reserve, Chiapas, Mexico. *European Journal of Taxonomy* 778: 1–25. <https://doi.org/10.5852/ejt.2021.778.1563>
- Valdez-Mondragón A, Francke OF (2015) Phylogeny of the spider genus *Ixchela* Huber, 2000 (Araneae: Pholcidae) based on morphological and molecular evidence (CO1 and 16S), with a hypothesized diversification in the Pleistocene. *Zoological Journal of the Linnean Society* 175(1): 20–58. <https://doi.org/10.1111/zoj.12265>
- Valdez-Mondragón A, Navarro-Rodríguez CI, Solís-Catalán KP, Cortez-Roldán MR, Juárez-Sánchez AR (2019) Under an integrative taxonomic approach: The description of a new species of the genus *Loxosceles* (Araneae, Sicariidae) from Mexico City. *ZooKeys* 892: 93–133. <https://doi.org/10.3897/zookeys.892.39558>
- Wayne L, Brenner D, Colwell R, Grimont P, Kandler O, Krichevsky M, Moore L, Moore W, Murray R, Stackebrandt E, Starr MP, Truper HG (1987) Report of the ad hoc committee on reconciliation of approaches to bacterial systematics. *International Journal of Systematic and Evolutionary Microbiology* 37(4): 463–464. <https://doi.org/10.1099/00207713-37-4-463>
- Wilson KH (1995) Molecular biology as a tool for taxonomy. *Clinical Infectious Diseases* 20(Supplement\_2): 117–121. [https://doi.org/10.1093/clinids/20.Supplement\\_2.S117](https://doi.org/10.1093/clinids/20.Supplement_2.S117)
- WSC [World Spider Catalog] (2022) World Spider Catalog. Version 22.0. Natural History Museum Bern. <https://doi.org/10.24436/2> [accessed on august 16, 2022]
- Zhang Y, Li S (2014) A spider species complex revealed high cryptic diversity in South China caves. *Molecular Phylogenetics and Evolution* 79: 353–358. <https://doi.org/10.1016/j.ympev.2014.05.017>
- Zhang J, Kapli P, Pavlidis P, Stamatakis A (2013) A general species delimitation method with applications to phylogenetic placements. *Bioinformatics* 29(22): 2869–2876. <https://doi.org/10.1093/bioinformatics/btt499>

# A new species of *Nidirana* (Anura, Ranidae) from northern Guangxi, China

Wei-Cai Chen<sup>1,2</sup>, Jian-Ping Ye<sup>3</sup>, Wan-Xiao Peng<sup>1</sup>, Peng Li<sup>1</sup>,  
Tong-Ping Su<sup>2</sup>, Gui-Dong Yu<sup>4</sup>, Zhi-Ying Cheng<sup>4</sup>

**1** Key Laboratory of Environment Change and Resources Use in Beibu Gulf Ministry of Education, Nanning Normal University, Nanning 530001, China **2** Guangxi Key Laboratory of Earth Surface Processes and Intelligent Simulation, Nanning Normal University, Nanning 530001, China **3** Maoershan National Nature Reserve, Guilin 541000, China **4** Guangxi Forest Inventory and Planning Institute, Nanning 530001, China

Corresponding author: Wei-Cai Chen ([chenweicai2003@126.com](mailto:chenweicai2003@126.com))

Academic editor: Annemarie Ohler | Received 2 September 2022 | Accepted 16 November 2022 | Published 12 December 2022

<https://zoobank.org/3C8C2AAD-B83C-4FB6-9A72-34ADE05DA610>

**Citation:** Chen W-C, Ye J-P, Peng W-X, Li P, Su T-P, Yu G-D, Cheng Z-Y (2022) A new species of *Nidirana* (Anura, Ranidae) from northern Guangxi, China. ZooKeys 1135: 119–137. <https://doi.org/10.3897/zookeys.1135.94371>

## Abstract

A new species of music frog, *Nidirana guibeiensis* **sp. nov.**, is described from northern Guangxi, China. Based on two mtDNA fragments analyzed, phylogenetic trees reveal that *N. guibeiensis* **sp. nov.** is most closely related to *N. leishanensis*. However, the new species can be identified by conspicuous diagnostic morphological characteristics as well as bioacoustics. In contrast to the known *Nidirana* species, the advertisement calls of the new species can be divided into three types, calls with one, two, and three notes. In addition, the new species has nest construction behavior, which is inconsistent with *N. leishanensis*. *Nidirana guibeiensis* **sp. nov.** occurs in paddy fields or still pools at 300–1300 m a.s.l.

## Keywords

Bioacoustics, morphology, nest construction, phylogeny

## Introduction

The genus *Nidirana* Dubois, 1992 is widespread in eastern and southeastern Asia (Frost 2021; AmphibiaChina 2022). Recently, the known diversity of *Nidirana* has increased dramatically, due to combined morphological, molecular, and bioacoustical analyses (Li et al. 2019; Lyu et al. 2020a, 2020b, 2021). To date, there are 17 recog-

nized *Nidirana* species. Most have been reported in the past five years (AmphibiaChina 2022). Five *Nidirana* species have been confirmed to occur in Guangxi: *N. guangxiensis* Mo, Lyu, Huang, Liao & Wang, 2021, *N. leishanensis* Li, Wei, Xu, Cui, Fei, Jiang, Liu & Wang, 2019, *N. shiwandashanensis* Chen, Peng, Li & Liu, 2022, *N. xiangica* Lyu & Wang, 2020a, and *N. yaoica* Lyu, Mo, Wan, Li, Pang & Wang, 2019. *Nidirana adenopleura* (Boulenger, 1909) has always been considered to occur throughout Guangxi (Fei et al. 2009; Mo et al. 2014). However, recent research has indicated the misidentifications of specimens allocated to *N. adenopleura*, and no evidence supports the occurrence of *N. adenopleura* in Guangxi (Lyu et al. 2021; Chen et al. 2022).

In 2022, we conducted surveys in northern Guangxi and collected 15 *Nidirana* specimens. These specimens differ from the known *Nidirana* species in morphology, phylogeny, and bioacoustics. Herein, we describe these specimens as a new species of *Nidirana*.

## Materials and methods

### Sampling and morphological examination

Fourteen adults and one subadult were collected at the Maoershan National Nature Reserve ( $n = 3$ ), Zhongfeng Town, Ziyuan County ( $n = 11$ ), and Lingtan Town, Xing'an County ( $n = 1$ ) in northern Guangxi, China (Fig. 1). After euthanasia with isoflurane, all specimens were fixed in 10% formalin, then transferred to 75% ethanol, and finally deposited at Nanning Normal University (NNU). Before being fixed, muscle samples were taken and stored in 100% ethanol for molecular analysis. The definition of morphological characteristics and measurements followed Chen et al. (2022). The following measurements were taken with digital calipers to the nearest 0.1 mm:

<b>SVL</b>	snout-vent length (from the tip of snout to posterior margin of vent);
<b>HDL</b>	head length (from the tip of snout to the articulation of jaw);
<b>HDW</b>	head width (head width at the commissure of jaws);
<b>SNT</b>	snout length (from the tip of snout to the anterior corner of eye);
<b>IND</b>	internasal distance (distance between nares);
<b>IOD</b>	interorbital distance (minimum distance between upper eyelids);
<b>ED</b>	eye diameter (from the anterior corner of eye to posterior corner of eye);
<b>TD</b>	tympanum diameter (horizontal diameter of tympanum);
<b>HND</b>	hand length (from the proximal border of the outer palmar tubercle to the tip of Finger III);
<b>FTL</b>	foot length (from the distal end of the shank to the tip of Toe IV);
<b>TIB</b>	tibial length (from the outer surface of the flexed knee to the heel).

Sex was identified by examining the nuptial pad and suprabrachial gland. The webbing formula followed Savage (1975).

Geographically and phylogenetically, the new species, *N. leishanensis*, and *N. xiangica* are close to each other. Fourteen adults were measured for comparison,

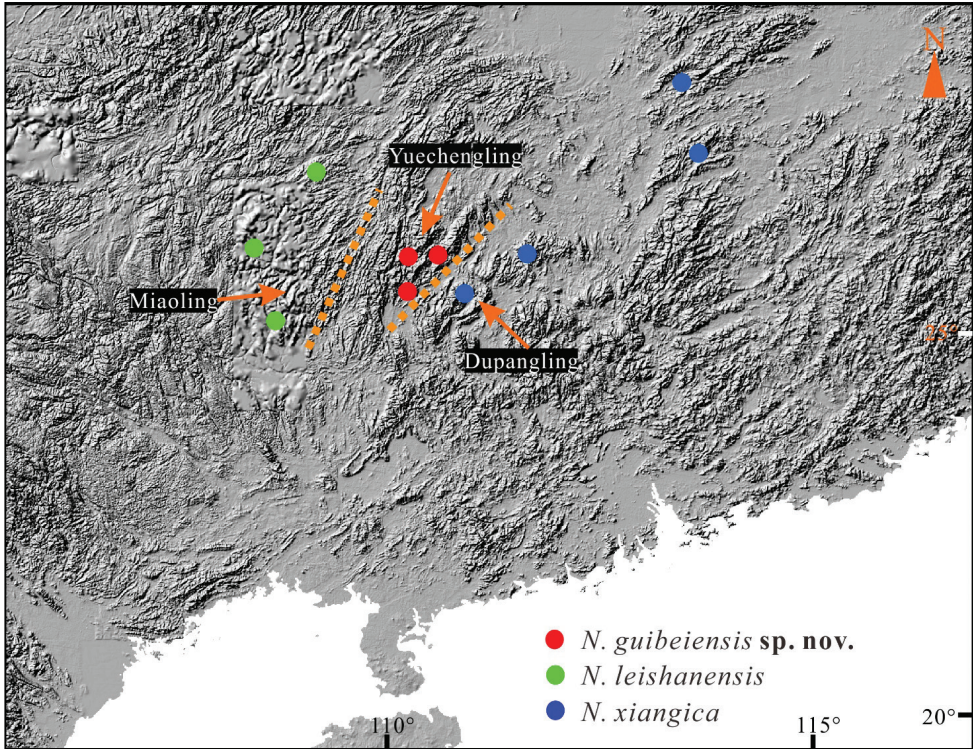


**Figure 1.** Localities of the new species and its sister taxa. The source of the map came from WorldClim (<http://www.worldclim.com/version2>).

whereas the morphological data of *N. leishanensis* and *N. xiangica* came from the references (Li et al. 2019; Lyu et al. 2020a). A principal component analysis (PCA) and the Mann-Whitney *U* tests were performed on SPSS, based on the adult male specimens. To reduce the impact of allometry, the correct value from the ratio of each character to SVL was calculated, then log-transformed for analyzing. The significance level was set at 0.05. Morphological comparison data came from the collected specimens (Appendix 1) and the references in Table 1.

### Phylogenetic analyses

Bayesian inference (BI) and maximum likelihood (ML) methods were used to analyze phylogenetical relationships based on partial 16S ribosomal RNA gene (16S, ~1050 bp) and partial cytochrome oxidase subunit I gene (COI, ~640 bp) sequences analyses. The two mtDNA fragments were amplified and sequenced following Lyu et al. (2019). PCR reaction conditions included 94 °C for 5 min; 35 cycles of denaturing at 94 °C for 35 s, annealing at 55 °C (for 16S)/52 °C (for COI) for 45 s, and extending at 72 °C for 60 s. Sequences were sequenced using an ABI3730 automated DNA sequencer in Sangon Biotech (Shanghai) Co., Ltd (Guangzhou, China). In addition, homologous sequences of *Nidirana* species downloaded from GenBank were included in our phylogenetic analysis (Table 2). These

**Table 1.** Diagnostic characters separating *Nidriana guibetensis* sp. nov. from all congeners. Labial tooth row formula from Dubois (1995).

ID	Species	SVL of males (mm)	SVL of females (mm)	Fingers tips	Lateroventral groove on fingers	Relative length of fingers	Toes tips	Lateroventral groove on toes	Tibio-tarsal articulation	Subgular vocal sacs	Nuptial pad	Spinules on dorsal skin	Nest construction	Tadpole labial tooth row formula	Calling	References
1	<i>N. guibetensis</i> sp. nov.	50.2–63.6	54.6	Dilated	Present except finger I	II < IV < I < III	Dilated	Present	Eye-snout	Present	One on finger I	Absent	Present	?	1–3 notes	This study
2	<i>N. adenopleura</i>	43.1–57.6	47.6–60.7	Dilated	Present except finger I	II < I < IV < III	Dilated	Present	Snout tip or eye-snout	Present	One on finger I	Entire or posterior	Absent	I:1+1/1+1:II or I:0+0/1+1:I	2–5 regular notes	Lyu et al. (2017, 2020b)
3	<i>N. chapuensis</i>	35.5–42.5	41.0–51.8	Dilated	Present except finger I	II < I = IV < III	Dilated	Present	Nostril	Present	Two on finger I	Absent or few above vent	Present	I:1+2/1+1:II	3 notes	Chauyankern et al. (2010)
4	<i>N. dananchina</i>	40.6–51.0	44.0–53.0	Dilated	Absent or rarely present	II < I < IV < III	Dilated	Present	Nostril	Present	One on finger I	Absent	Present	I:1+1/1+1:II or I:1+1/2+2:I	2–5 notes containing a specific first note	Liu (1950); Lyu et al. (2017)
5	<i>N. guangdongensis</i>	50.0–58.4	55.3–59.3	Dilated	Present except finger I	II < I < IV < III	Dilated	Present	Nostril	Present	One on finger I	Entire	Absent	?	2–4 regular notes	Lyu et al. (2020a)
6	<i>N. guangxiensis</i>	40.2–47.6	49.9–51.0	Dilated	Present on fingers III and IV	II < I < IV < III	Dilated	Present	Nostril	Present	One on finger I	Absent	Present	I:1+1/1+1:II	6–11 rapidly repeated regular notes	Lyu et al. (2021)
7	<i>N. hainanensis</i>	32.8–44.4	?	Dilated	Present	II < I < IV < III	Dilated	Present	Nostril	Present	Absent	Absent	Present	?	2–4 fast-repeated double-notes	Fei et al. (2007, 2009)
8	<i>N. leishanensis</i>	49.5–56.4	43.7–55.3	Dilated	Present	II < IV < I < III	Dilated	Present	Eye-snout	Present	Two on fingers I and II	Absent	Absent	I:1+2/1+1:II	1 single note	Li et al. (2019)
9	<i>N. lini</i>	44.1–63.1	57.7–68.6	Dilated	Present except finger I	II < I < IV < III	Dilated	Present	Beyond snout	Present	One on finger I	Posterior	Absent	I:1+1/1+1:II	5–7 notes containing a specific first note	Chou (1999); Lyu et al. (2017)
10	<i>N. mangweni</i>	53.6–59.7	59.7–65.1	Dilated	Present on fingers III and IV	I < II < IV < III	Dilated	Present	Anterior corner of eye	Present	One on finger I	Entire or posterior	Absent	?	2–7 regular notes	Lyu et al. (2020a)

ID	Species	SVL of males (mm)	SVL of females (mm)	Fingers tips	Lateroventral groove on fingers	Relative length of fingers	Toes tips	Lateroventral groove on toes	Tibio-tarsal articulation	Subgular vocal sacs	Nuptial pad	Spinules on dorsal skin	Nest construction	Tadpole labial tooth row formula	Calling	References
11	<i>N. nankunensis</i>	33.3–37.1	37.8–39.5	Dilated	Present except finger I	II < I < IV < III	Dilated	Present	Nostril	Present	One on finger I	Absent or few above vent	Present	I:1+1/1+1:II	13–15 notes containing a specific first note	Lyu et al. (2017)
12	<i>N. occidentalis</i>	44.5–53.0	55.6–61.3	Not dilated	Absent	II < I < IV < III	Not dilated	Absent	Eye	Present	One on finger I	Posterior	Absent	?	3–5 regular notes	Lyu et al. (2020b)
13	<i>N. okinavana</i>	35.5–42.8	44.6–48.8	Dilated	Present except finger I	II < I < IV < III	Dilated	Present	Eye center-near nostril	Absent	Poorly one on finger I	Absent	Present	I:1+1/1+1:II	10–25 fast-repeated notes	Chuaynkern et al. (2010); Lyu et al. (2017)
14	<i>N. pleuraden</i>	46.2–52.3	46.9–61.7	Not dilated	Absent	II < I < IV < III	Not dilated	Absent	Nostril	Present	One on finger I	Posterior	Absent	I:1+1/1+1: II	1–4 regular notes	Lyu et al. (2017, 2020b)
15	<i>N. shiwandashanensis</i>	46.2–50.8	48.3	Dilated	Present	II < IV < I < III	Dilated	Present	Eye	Present	One on finger I	Absent	?	I: 1+1/1+1:II	6–8 double-notes	Chen et al. (2022)
16	<i>N. xiangica</i>	56.3–62.3	53.5–62.6	Dilated	Present	II < I < IV < III	Dilated	Present	Eye-snout	Present	One on finger I	Entire	Absent	?	2–3 notes containing a specific first note	Lyu et al. (2020a)
17	<i>N. yanica</i>	42.1–45.6	?	Dilated	Present	II < I < IV < III	Dilated	Present	Nostril	Present	One on finger I	Absent	? (Probably present)	?	1–3 fast-repeated regular notes	Lyu et al. (2019)
18	<i>N. yueae</i>	41.2–43.5	44.7	Dilated	Absent	II < IV < I < III	Dilated	Present	Eye	Present	One on finger I	Absent	? (Probably absent)	I: 1+1/1+1:II	2–6 notes containing a specific first note	Wei et al. (2020)

**Table 2.** Information for samples used in phylogenetic analyses in this study. Type locality indicated by an asterisk (\*). NNU represents Nanning Normal University; SYS, Sun Yat-sen University; MNHN, Muséum National d’Histoire Naturelle, Paris; NHMG, Natural History Museum of Guangxi; CIB, Chengdu Institute of Biology, Chinese Academy of Sciences.

ID	Species	Locality	Voucher no.	16S	COI	References
1	<i>N. guibeiensis</i> sp. nov.	China: Guangxi: Xing’an: Maoershan (paratype)	NNU 00917	ON985180	ON968962	This study
2	<i>N. guibeiensis</i> sp. nov.	China: Guangxi: Xing’an: Maoershan (paratype)	NNU 00918	ON985181	ON968963	This study
3	<i>N. guibeiensis</i> sp. nov.	China: Guangxi: Xing’an: Maoershan (paratype)	NNU 00919	ON985182	ON968964	This study
4	<i>N. guibeiensis</i> sp. nov.	China: Guangxi: Xing’an: Yanguang (paratype)	NNU 00810	ON985179	ON968961	This study
5	<i>N. guibeiensis</i> sp. nov.	China: Guangxi: Xing’an: Zhongfeng (paratype)	NNU 00694	ON985176	ON968958	This study
6	<i>N. guibeiensis</i> sp. nov.	China: Guangxi: Xing’an: Zhongfeng (paratype)	NNU 00769	ON985177	ON968959	This study
7	<i>N. guibeiensis</i> sp. nov.	China: Guangxi: Xing’an: Zhongfeng (paratype)	NNU 00770	ON985178	ON968960	This study
8	<i>N. guibeiensis</i> sp. nov.	China: Guangxi: Xing’an: Zhongfeng (paratype)	NNU 00867	ON985183	ON968965	This study
9	<i>N. adenopleura</i>	China: Taiwan: Taichung City	SYS a007358	MN946445	MN945201	Lyu et al. (2020a)
10	<i>N. adenopleura</i>	China: Taiwan: Taichung City	SYS a007359	MN946446	MN945202	Lyu et al. (2020a)
11	<i>N. chapensis</i>	Vietnam: Lao Cai: Sapa*	MNHN 2000.4850	KR827711	KR087625	Grosjean et al. (2015)
12	<i>N. daunchina</i>	China: Sichuan: Mt Emei*	SYS a004594	MF807822	MF807861	Lyu et al. (2020a)
13	<i>N. daunchina</i>	China: Sichuan: Mt Emei*	SYS a004595	MF807823	MF807862	Lyu et al. (2020a)
14	<i>N. guangdongensis</i>	China: Guangdong: Yingde City (holotype)	SYS a005767	MN946406	MN945162	Lyu et al. (2020a)
15	<i>N. guangdongensis</i>	China: Guangdong: Yingde City (paratype)	SYS a005768	MN946407	MN945163	Lyu et al. (2020a)
16	<i>N. guangxiensis</i>	China: Guangxi: Mt Daming (paratype)	NHMG 202007001	MZ677222	MZ678729	Lyu et al. (2021)
17	<i>N. guangxiensis</i>	China: Guangxi: Mt Daming (paratype)	NHMG 202007002	MZ677223	MZ678730	Lyu et al. (2021)
18	<i>N. hainanensis</i>	China: Hainan: Mt Diaoluo*	SYS a007669	MN946451	MN945207	Lyu et al. (2020a)
19	<i>N. hainanensis</i>	China: Hainan: Mt Diaoluo*	SYS a007670	MN946452	MN945208	Lyu et al. (2020a)
20	<i>N. leishanensis</i>	China: Guizhou: Mt Leigong*	SYS a007908	MN946453	MN945209	Lyu et al. (2021)
21	<i>N. leishanensis</i>	China: Guizhou: Mt Fanjing	SYS a007195	MN946454	MN945210	Lyu et al. (2021)
22	<i>N. leishanensis</i>	China: Guizhou: Mt Fanjing	SYS a007196	MN946455	MN945211	Lyu et al. (2021)
23	<i>N. leishanensis</i>	China: Guangxi: Mt Jiuwan	NHMG 202007021	MZ677227	MZ678734	Lyu et al. (2021)
24	<i>N. leishanensis</i>	China: Guangxi: Mt Jiuwan	NHMG 202007022	MZ677228	MZ678735	Lyu et al. (2021)
25	<i>N. leishanensis</i>	China: Guangxi: Mt Jiuwan	NHMG 202007023	MZ677229	MZ678736	Lyu et al. (2021)
26	<i>N. leishanensis</i>	China: Guangxi: Mt Jiuwan	NHMG 202007025	MZ677230	MZ678737	Lyu et al. (2021)
27	<i>N. lini</i>	China: Yunnan: Jiangcheng County*	SYS a003967	MF807818	MF807857	Lyu et al. (2017)
28	<i>N. lini</i>	China: Yunnan: Jiangcheng County*	SYS a003968	MF807819	MF807858	Lyu et al. (2017)
29	<i>N. mangveni</i>	China: Zhejiang: Mt Dapan (paratype)	SYS a006310	MN946424	MN945180	Lyu et al. (2020a)
30	<i>N. mangveni</i>	China: Zhejiang: Mt Dapan (paratype)	SYS a006311	MN946425	MN945181	Lyu et al. (2020a)
31	<i>N. nankunensis</i>	China: Guangdong: Mt Nankun (paratype)	SYS a005718	MF807839	MF807878	Lyu et al. (2017)
32	<i>N. nankunensis</i>	China: Guangdong: Mt Nankun (holotype)	SYS a005719	MF807840	MF807879	Lyu et al. (2017)
33	<i>N. occidentalis</i>	China: Yunnan: Mt Gaoligong (paratype)	SYS a003775	MF807816	MF807855	Lyu et al. (2020a)
34	<i>N. occidentalis</i>	China: Yunnan: Mt Gaoligong (holotype)	SYS a003776	MF807817	MF807856	Lyu et al. (2020a)
35	<i>N. okinavana</i>	Japan: Okinawa: Iriomote Island*	Unknown	NC022872	NC022872	Kakehashi et al. (2013)
36	<i>N. pleuraden</i>	China: Yunnan: Kunming City*	SYS a007858	MT935683	MT932858	Lyu et al. (2020b)

ID	Species	Locality	Voucher no.	16S	COI	References
37	<i>N. pleuraden</i>	China: Yunnan: Wenshan City	SYS a007717	MT935671	MT932850	Lyu et al. (2020b)
38	<i>N. shiwandashanensis</i>	China: Guangxi: Shangsi County (holotype)	NNU00238	MZ787977	MZ782098	Chen et al. (2022)
39	<i>N. shiwandashanensis</i>	China: Guangxi: Shangsi County (paratype)	NNU00239	MZ787978	MZ782099	Chen et al. (2022)
40	<i>N. xiangica</i>	China: Hunan: Mt Dawei (paratype)	SYS a006491	MN946433	MN945189	Lyu et al. (2020a)
41	<i>N. xiangica</i>	China: Hunan: Mt Dawei (holotype)	SYS a006492	MN946434	MN945190	Lyu et al. (2020a)
42	<i>N. xiangica</i>	China: Hunan: Mt Dawei (paratype)	SYS a006493	MN946435	MN945191	Lyu et al. (2020a)
43	<i>N. xiangica</i>	China: Hunan: Mt Yangming (paratype)	SYS a007269	MN946436	MN945192	Lyu et al. (2020a)
44	<i>N. xiangica</i>	China: Hunan: Mt Yangming (paratype)	SYS a007270	MN946437	MN945193	Lyu et al. (2020a)
45	<i>N. xiangica</i>	China: Hunan: Mt Yangming (paratype)	SYS a007271	MN946438	MN945194	Lyu et al. (2020a)
46	<i>N. xiangica</i>	China: Hunan: Mt Yangming (paratype)	SYS a007272	MN946439	MN945195	Lyu et al. (2020a)
47	<i>N. xiangica</i>	China: Hunan: Mt Yangming (paratype)	SYS a007273	MN946440	MN945196	Lyu et al. (2020a)
48	<i>N. xiangica</i>	China: Jiangxi: Mt Wugong (paratype)	SYS a002590	MN946441	MN945197	Lyu et al. (2020a)
49	<i>N. xiangica</i>	China: Guangxi: Mt Dupangling	SYS a006568	MN946442	MN945198	Lyu et al. (2020a)
50	<i>N. xiangica</i>	China: Guangxi: Mt Dupangling	SYS a006569	MN946443	MN945199	Lyu et al. (2020a)
51	<i>N. xiangica</i>	China: Guangxi: Mt Dupangling	SYS a006570	MN946444	MN945200	Lyu et al. (2020a)
52	<i>N. yaocia</i>	China: Guangxi: Mt Dayao (paratype)	SYS a007020	MK882276	MK895041	Lyu et al. (2019)
53	<i>N. yaocia</i>	China: Guangxi: Mt Dayao (paratype)	SYS a007021	MK882277	MK895042	Lyu et al. (2019)
54	<i>N. yeae</i>	China: Guizhou: Tongzi County (paratype)	CIB TZ20190608005	MN295228	MN295234	Wei et al. (2020)
55	<i>N. yeae</i>	China: Guizhou: Tongzi County (paratype)	CIB TZ20160714016	MN295231	MN295237	Wei et al. (2020)
56	<i>Babina holsti</i>	Japan: Okinawa*	Unknown	NC022870	NC022870	Kakehashi et al. (2013)
57	<i>Babina subaspena</i>	Japan: Kagoshima: Amami Island*	Unknown	NC022871	NC022871	Kakehashi et al. (2013)

sequences contain all holotypes or paratypes of *Nidirana* species known in China. The BI analysis was implemented using MRBAYES v. 3.1.2 (Ronquist and Huelsenbeck 2003). The best-fit model (GTR+I+G) was chosen using JMODELTEST v. 2.1.2 (Posada 2008) based on Akaike and Bayesian information criteria. Two independent runs with four Markov Chain Monte Carlo simulations were performed for 30 million iterations and sampled every 1000<sup>th</sup> iteration. The first 25% of samples were discarded as burn-in. ML was analyzed on the CIPRES science gateway with 100 rapid bootstrap replicates (Miller et al. 2010) (<https://www.phylo.org/portal2>). Outgroups follow Chen et al. (2022).

## Bioacoustics analysis

Advertisement calls of five individuals were recorded in the fields using a SONY ICX–0471 recorder on 7 May, and 3 and 28 June 2022. The ambient temperature was measured with a digital hygrothermograph. Calls were recorded at 21 °C, 23 °C, and 18 °C. Advertisement calls were analyzed using Raven Pro v. 1.6 (Cornell Laboratory of Ornithology, USA) as per Köhler et al. (2017). The acoustic properties were set to a window size of 512 points, fast Fourier transform, and Hanning window with no overlap. We performed the following measurements: call duration (measured from the beginning to the end of the call), note duration (measured from the beginning to the end of the note), inter-note interval (measured from the end of one note to the beginning of the consecutive note), and dominant frequency (the peak frequency of the call). The published bioacoustics data were obtained from the literature (Table 1).

## Results

PCA results were shown in Fig. 2. The extracted components PC1 eigenvectors accounted for 29.6% of the variance, PC2 for 16.8%, and PC3 for 13.3%. The new specimens can be significantly distinguished from *N. leishanensis* and *N. xiangica*. The results of Mann-Whitney *U* tests implied that the new specimens were significantly different from *N. leishanensis* and *N. xiangica* on many morphometric characters, including HDW, SNT, IND, ED, and FTL for *N. leishanensis*, and SNT, IND, ED, HND, FTL, and TIB for *N. xiangica* (Table 3). Additionally, the new specimens can be easily identified by a series of diagnostic characters, such as relatively larger body size, smooth dorsum with tubercles on the posterior of the back, lateroventral grooves present on all fingers and toes but not on Finger I, and tibiotarsal articulation reaching the level between the eye and nostril (Table 1). ML and BI analyses led to identical topologies based on the two mtDNA fragments (Fig. 3). Phylogenetical trees indicated that our newly collected specimens were strongly clustered into a monophyletic group and sister to *N. leishanensis* with robust support (PP = 0.97, BS = 94).

The call spectrograms of the new specimens are shown in Fig. 4. Three types of calls were recorded: calls with one note (Type A), two notes (Type B), and three notes

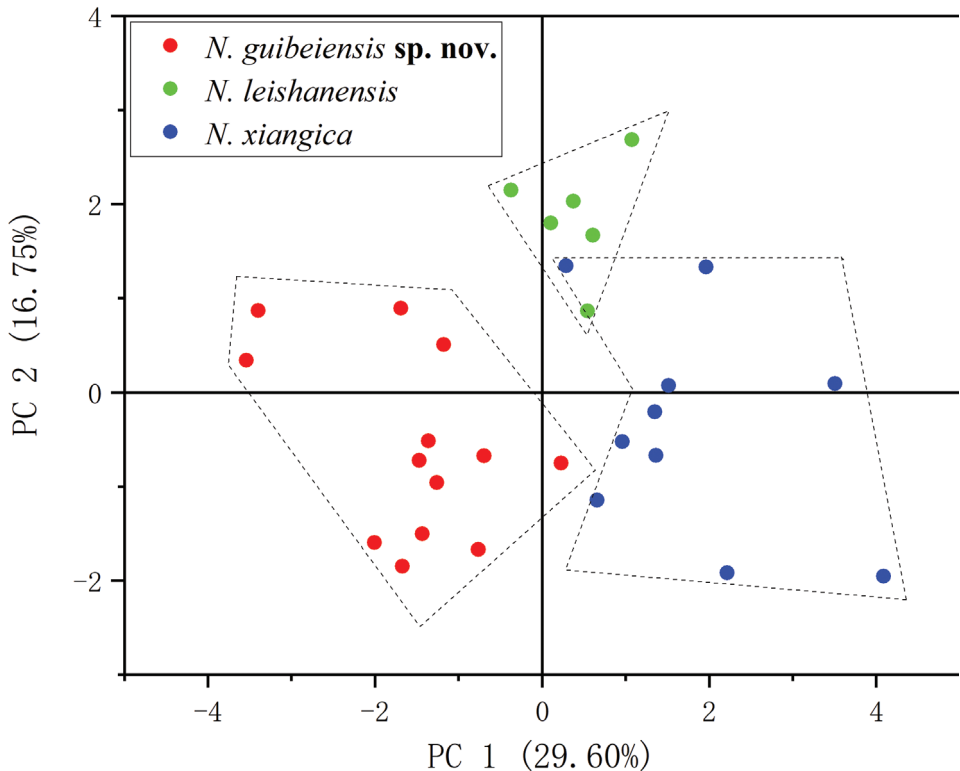


**Figure 2.** Scatter plot of PC1 and PC2 of PCA based on the morphometric measurements, distinguishing *Nidirana guibeiensis* sp. nov., *N. leishanensis*, and *N. xiangica*.

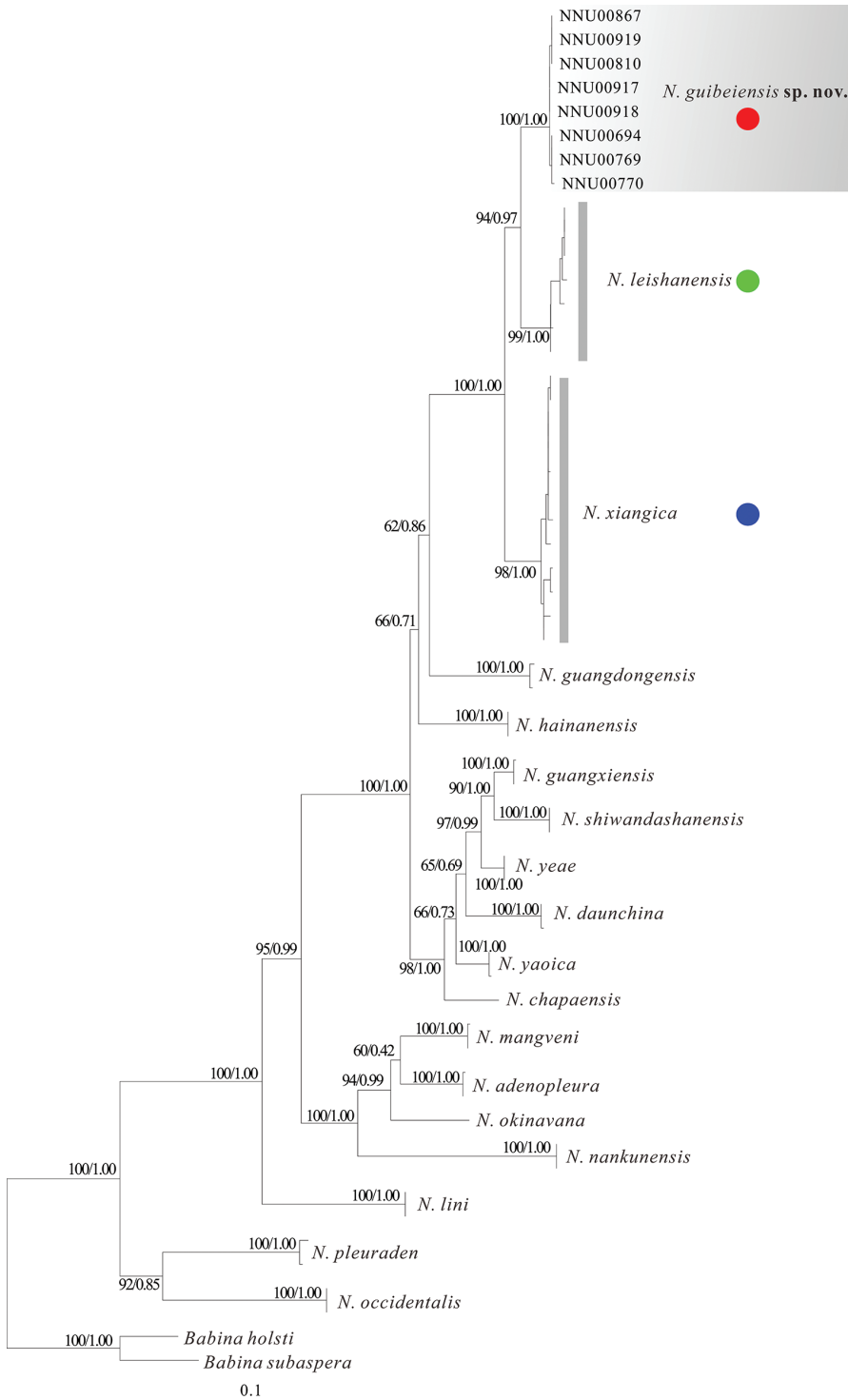


**Figure 3.** Maximum-likelihood tree based on 16S + COI fragments with bootstrap supports/Bayesian posterior probabilities on branches.

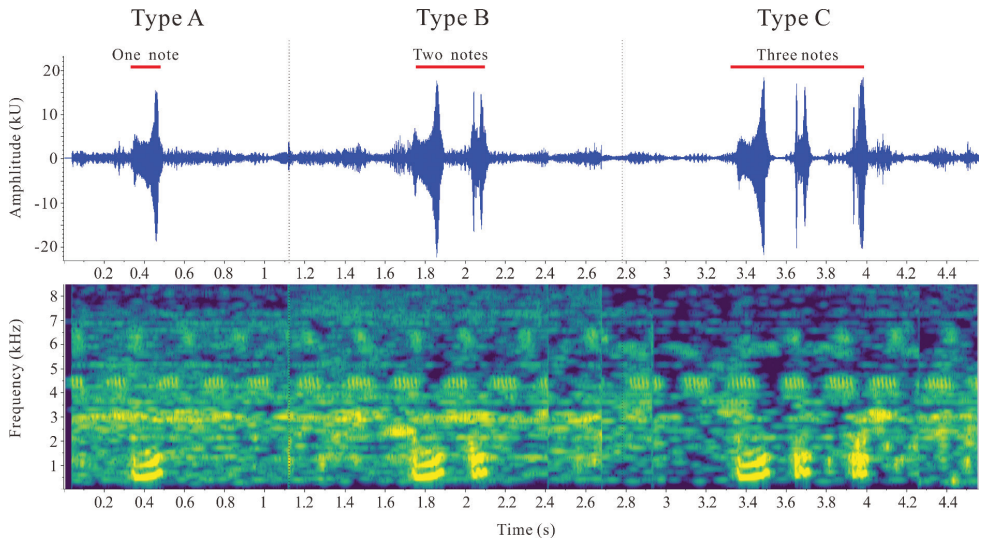


**Figure 4.** Advertisement call spectrograms of *Nidirana guibeiensis* sp. nov.

**Table 3.** Measurements of *Nidirana guibeiensis* sp. nov. (in mm) and morphometric comparisons with *N. leishanensis* and *N. xiangica*. Abbreviations defined in Material and methods. \*  $p$ -values < 0.05, \*\*  $p$ -values < 0.01.

	Male ( $n = 13$ )		Female	$p$ -values from Mann-Whitney $U$ tests	
	Ranging	mean $\pm$ SD	NNU 00694	New species vs <i>N. leishanensis</i>	New species vs <i>N. xiangica</i>
SVL	50.2–63.6	55.2 $\pm$ 3.7	54.6	0.054	0.215
HDL	18.6–22.5	19.9 $\pm$ 1.1	19.8	0.380	0.137
HDW	18.3–23.1	20.1 $\pm$ 1.4	17.3	0.011*	0.321
SNT	7.0–9.5	7.5 $\pm$ 0.7	7.0	0.002**	0.003**
IND	5.3–6.6	6.0 $\pm$ 0.5	5.3	0.028*	0.000**
IOD	4.1–5.6	4.9 $\pm$ 0.4	5.0	0.661	0.121
ED	4.4–6.9	5.6 $\pm$ 0.7	5.4	0.028*	0.000**
TD	4.6–6.3	5.4 $\pm$ 0.5	4.8	0.161	0.094
HND	12.6–15.6	14.0 $\pm$ 1.0	14.3	0.726	0.041*
FTL	26.2–33.4	29.3 $\pm$ 2.0	30.5	0.001**	0.000**
TIB	25.7–29.9	28.4 $\pm$ 1.5	30.8	0.861	0.001**

(Type C). Note number of a call, call duration, note duration, and inter-note duration are listed in Table 4. The newly collected specimens had different call characteristics distinguishing them from the call types of their congeners, a call with notes, call duration, and note duration (Table 4). However, the calls of *N. leishanensis* consist of one strophe with one syllable, and call durations last 330–430 ms. The calls of *N. xiangica* consist of two or three notes, and call durations last 331.9–624.8 ms. The two species above are distinct from the new specimens based on acoustic data (Table 4).

Phylogeny, bioacoustics, and morphology support the recognition of the newly collected specimens from northern Guangxi as a previously undescribed *Nidirana* species, which is described below.

**Table 4.** Vocalization parameters of *Nidirana guibeiensis* sp. nov.

	Type A ( <i>n</i> = 21)	Type B ( <i>n</i> = 37)	Type C ( <i>n</i> = 13)
Notes number of one call	1	2	3
Call duration	155–232, (mean 179.6 ± 24.4) ms	349–471, (mean 383.4 ± 28.6) ms	561–777, (mean 658.6 ± 71.7) ms
First note duration		153–210, (mean 167.4 ± 13.1) ms	160–210, (mean 187.8 ± 18.4) ms
Second note duration		71–90, (mean 79.3 ± 4.2) ms	71–86, (mean 77.2 ± 5.5) ms
Third note duration			75–93, (mean 82 ± 5.3) ms
First inter-note duration		125–171, (mean 136.6 ± 11.3) ms	113–167, (mean 139.5 ± 18.3) ms
Second inter-note duration			142–221, (mean 171.8 ± 24.1) ms

## Taxonomic account

### *Nidirana guibeiensis* Chen, Ye, Peng & Li, sp. nov.

<https://zoobank.org/22E61BF0-A1D2-4E44-83A5-F4EA99A50B78>

Fig. 5

**Holotype.** NNU 00771; adult ♂; CHINA, Guangxi, Ziyuan County, Zhongfeng Town; 110.6882°E, 25.9750°N; Wei-Cai Chen leg., 8 May 2022.

**Paratypes.** NNU 00769–770, 772–773; 4 adult ♂♂; same locality and date as holotype • NNU 00694; 1 adult ♀; same locality as holotype; Gui-Dong Yu leg., 29 April 2022 • NNU 00810; 1 adult ♂; China, Guangxi, Xing'an County, Lingtan Town; 110.5622°E, 25.5907°N; Wei-Cai Chen leg., 9 May 2022 • NNU 00864–867; 4 adult ♂♂; same locality as holotype; Wei-Cai Chen leg., 2 June 2022 • NNU 00917–919; 3 adult ♂♂; Maershan National Nature Reserve; 110.4937°E, 25.8823°N; Wei-Cai Chen, Tong-Ping Su & Gui-Dong Yu leg., 28 June 2022.

**Etymology.** The species name refers to its distribution in northern Guangxi. 'Guibe' means northern Guangxi.

We suggest the English name Guibe Music Frog and the Chinese name Gui Bei Qin Wa (桂北琴蛙).

**Diagnosis.** *Nidirana guibeiensis* sp. nov. differs from its congeners in the combination of the following characteristics: larger body size (SVL 50.2–63.6 mm in males; 54.6 mm in the only sampled female); dorsum smooth with tubercles on the posterior of the back; surfaces of throat, chest, and upper part of the belly with grey clouding, lower part of the belly near immaculate creamy white; dorsal midline with a discrete creamy-white line; lateroventral grooves present on all fingers and toes but not on Finger I; tibiotarsal articulation reaching the level between eye and nostril; a pair of subgular vocal sacs present; three types of calls: one note, two notes, or three notes.

**Description of holotype.** Adult male, SVL 56.3 mm; head length slightly larger than width (HDL/HDW = 1.05); snout oval, significantly protruding beyond lower jaw; canthus rostralis distinct; loreal region concave; nostril oval and closer to snout than eye, laterally opening; a creamy white stripe on upper lip, beginning at the tip of snout along with upper lip and ending above insertion of arm; supratympanic fold visible; IOD/IND = 0.72; eye diameter almost equal to tympanum diameter (ED/



**Figure 5.** The holotype of *Nidirana guibeiensis* sp. nov. (NNU 00771) **A** dorsal view **B** dorsolateral view **C** ventral view **D** ventral view of hand **E** ventral view of foot **F** tubercles on the rear of the back.

TD = 1.02); vomerine teeth oval, closer to each other than to choana; tongue pyriform with a deep notch on posterior; a pair of subgular vocal sacs present. Relative finger lengths: II < IV < I < III; all tips of fingers but Finger I slightly dilated with lateroventral grooves; finger webbing and dermal fringes absent; subarticular tubercles prominent and conical; two palmar tubercles distinct; nuptial pad present on lateral Finger I with velvety spinules, extending from hand base to level of subarticular tubercle. Relative toe lengths: I < II < V < III < IV; all tips of toes slightly dilated, forming elongated and pointed discs with lateroventral grooves; toe webbing formula: I 2 – 2 II 1½ – 3– III 2 – 3+ IV 3+ – 2– V; toes with lateral fringes; subarticular tubercles prominent and oval;

inner metatarsal tubercles elongated, but outer metatarsal tubercles conical; heels not meeting when thighs are held at right angles to body; tibiotarsal articulation reaching the level between eye and nostril. Dorsum smooth with tubercles on the posterior of the back; hindlimbs smooth with several tubercles; dorsolateral fold beginning at the posterior of eye and ending above groin; pineal gland distinct; flanks with suprabrachial glands at each side; peripheral vent with some small tubercles (Fig. 5A–F).

**Color of holotype.** Alive, dorsum moss grey without spots; pineal gland light yellow; dorsal midline with a discrete creamy-white line, beginning at pineal gland and ending at vent; tympanum light brown; presence of a creamy-white linear gland on upper jaw; maxillary gland creamy-white; flank with several black spots and tubercles, and a large grey suprabrachial gland; thigh and tibia with three distinct black bars; surfaces of throat, chest, and upper part of belly with grey clouding, lower part of belly near immaculate creamy white; ventral limbs incarnadine; anterior of base of forelimb with a dark stripe; the anterior and posterior of iris reddish-brown, whereas the upper and lower part of iris brown (Fig. 5A–F). In preservation, dorsal surface faded to deep grey; black spots turned darkish black.

**Variations.** Measurements of type series are listed in Table 3 and Table S1. Paratypes were similar to the holotype in morphology and color pattern. Some had a discrete, rusty dorsal midline, and a rusty line along the dorsolateral folds, and rusty blotches on the flanks (Fig. 6A). Various tubercles on the rear of the back, some denser but some sparse (Fig. 6B). Some had five or six black bars on thigh and tibia (Fig. 6C).

**Ecology and distribution.** *Nidirana guibeiensis* sp. nov. was found in paddy fields or still pools at 300–1 300 m a.s.l. We heard the advertisement calls in the field during the surveys, from April to July. We observed that the new species has nest construction behavior (Fig. 7). The nest was made of rice stems and 20–30 cm in diameter without a covering. Eggs were observed in the nest (Fig. 7). Females were gravid with creamy-yellow eggs with black poles (Fig. 6D). The new species is widespread in northern Guangxi.

**Comparison.** A summary of morphological characteristics is listed in Table 1. *Nidirana guibeiensis* sp. nov. differs from its congeners in the following characteristics: (1) SVL 50.2–63.6 mm in males; (2) dorsum smooth with tubercles on the posterior of the back; (3) surfaces of throat, chest, and upper part of belly with grey clouding, lower part of belly near immaculate creamy white; (4) dorsal midline with a discrete creamy-white line; (5) tibiotarsal articulation reaching the level between eye and nostril; (6) lateroventral grooves present on all fingers and toes but not on Finger I; (7) nuptial pad present on Finger I; (8) a pair of subgular vocal sacs present; (9) a call comprised of one, two, or three notes.

Phylogenetically, *N. guibeiensis* sp. nov. is closest to *N. leishanensis* (Fig. 3). However, *N. guibeiensis* sp. nov. differs from *N. leishanensis* in the absence of dermal fringes on fingers (vs broad lateral fringes on inner sides of Fingers II, III, and IV but absent on Finger I); the presence of lateroventral grooves on all fingers except Finger I (vs lateroventral grooves present on Fingers III and IV); toe webbing formula: I 2 – 2 II 1½ – 3<sup>-</sup> III 2 – 3<sup>+</sup> IV 3<sup>+</sup> – 2<sup>-</sup> V (vs I 1½ – 2 II 1½ – 2½ III 1½ – 3 IV 3½ – 1½ V);

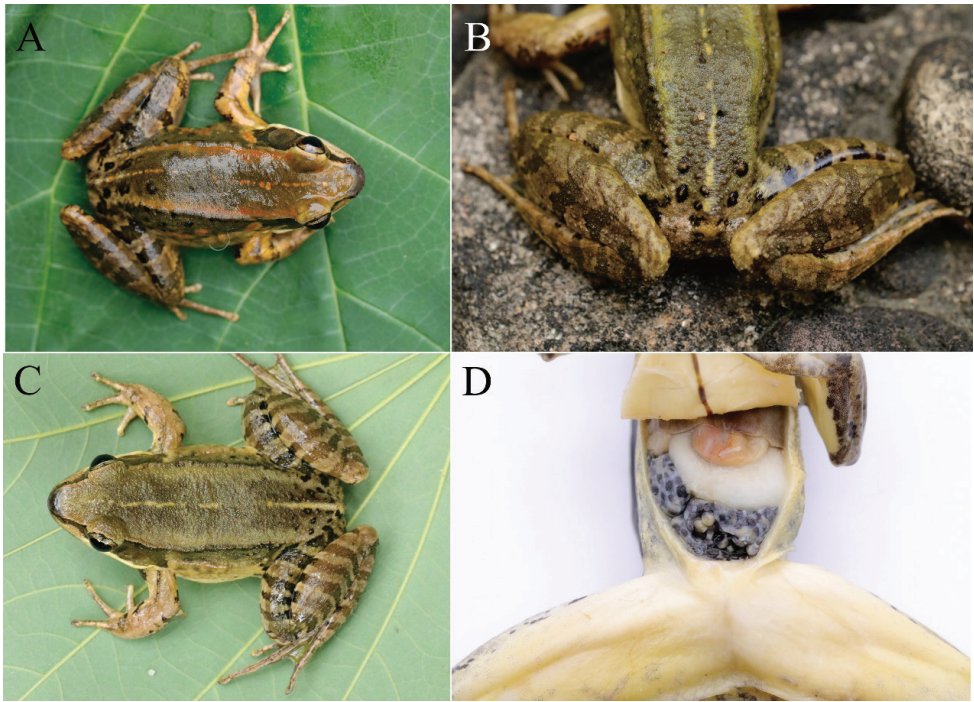


**Figure 6.** *Nidirana guibeiensis* sp. nov. **A** dorsal view of NNU 00769 **B** rough tubercles on the rear of the back (NNU 00865) **C** five bars on thigh and tibia (NNU 00867) **D** female with creamy yellow eggs with pigmented poles (NNU 00694).

dorsum smooth with tubercles on the posterior of the back (vs dorsal skin rough with dense granules but not concentrated on the posterior of the back); heels not meeting when thighs are held at right angles to body (vs heels overlapping); outer metatarsal tubercle present (vs absent); surfaces of throat, chest, and upper part of belly with grey clouding, lower part of belly near immaculate creamy white (vs surface and throat smooth and incarnadine); supratympanic fold present (vs absent); two palmar tubercles distinct (vs three palmar tubercles elliptic, distinct); nuptial pad present on Finger I (vs nuptial pad on the inner side of base of Fingers I and II); a call comprised of one, two, or three notes (vs a call with one strophe with one syllable). The new species has nest construction behavior (vs no nest construction behavior).

*Nidirana guibeiensis* sp. nov. differs from *N. xiangica* in having a dorsal midline with a discrete creamy-white line (vs absent dorsal midline); heels not meeting when thighs are held at right angles to body (vs heels meeting); a smooth dorsum with tubercles on the posterior of the back (vs extremely rough dorsal surface with dense tubercles and white horny spinules on the entire dorsum); supratympanic fold present (vs absent); the anterior and posterior of iris reddish-brown, whereas the upper and lower parts of iris brown (vs upper  $\frac{1}{3}$  iris brownish-white and lower  $\frac{2}{3}$  iris reddish-brown); advertisement calls contained 1–3 notes (vs 2 or 3 notes with a specific first note). Additionally, the new species has nest construction behavior (vs no nest construction behavior).



**Figure 7.** Nests of *Nidirana guibeiensis* sp. nov. with eggs.

Due to the larger body size in males (SVL 50.2–63.6 mm), *N. guibeiensis* sp. nov. differs from males of *N. nankunensis* (SVL 33.3–37.1 mm), *N. chapaensis* (SVL 35.5–42.5 mm), *N. guangxiensis* (SVL 40.2–47.6 mm), *N. hainanensis* (SVL 32.8–44.4 mm), *N. okinavana* (SVL 35.5–42.8 mm), *N. yaoica* (SVL 42.1–45.6 mm), and *N. yae* (SVL 41.2–43.5 mm). Other differences are (Table 1): lateroventral grooves present on all fingers but not on Finger I (vs absent in *N. guangxiensis*, *N. occidentalis*, *N. pleuraden*, and *N. yae*); lateroventral grooves present on all toes (vs absent on all toes in *N. pleuraden* and *N. occidentalis*); tibio-tarsal articulation reaching the level between the eye and nostril (vs beyond the tip of snout in *N. lini*); dorsum smooth with tubercles on the posterior of the back (vs no tubercles on the posterior of the back in *N. chapaensis*, *N. daunchina*, *N. guangdongensis*, *N. guangxiensis*,

*N. hainanensis*, *N. leishanensis*, *N. nankunensis*, *N. okinavana*, *N. shiwandashanensis*, *N. yaoica*, and *N. yeeae*); single nuptial pad present on Finger I (vs absent in *N. hainanensis*; two parts on Finger I in *N. chapaensis*; present on Fingers I and II in *N. leishanensis*).

## Discussion

To date, six recognized *Nidirana* species have been reported from Guangxi, indicating an impressive species diversity. Lyu et al. (2021) and Chen et al. (2022) pointed out that *Nidirana* species have relatively narrow ranges. Rivers and mountains contribute to the speciation of *Nidirana*. Phylogenetically, the new species, *N. leishanensis*, and *N. xiangica* are clustered together. The three species are geographically close but occur in different mountain ranges (Fig. 1). *Nidirana guibeiensis* sp. nov. occurs in the Yuechengling Mountains, *N. leishanensis* in the Miaoling Mountains, and *N. xiangica* in the Dupanling, Dawei, and Yangming mountains. The other three species of *Nidirana* occurring in Guangxi (*N. guangxiensis*, *N. shiwandashanensis* and *N. yaoica*) resemble the abovementioned species but occur in separated mountain ranges (Lyu et al. 2019, 2021; Chen et al. 2022).

The discovery of the new species indicates that the diversity of the genus *Nidirana* is still underestimated. The taxonomic validity of reports of *N. adenopleura* in Guangxi must be reconsidered. In recent years, we have carried out a series of field surveys, but no evidence supports the occurrence of *N. adenopleura* in Guangxi. *Nidirana guibeiensis* sp. nov., which was reported by Mo et al. (2014) as *N. adenopleura*, is a good example of a misidentification of a new *Nidirana* species.

## Acknowledgements

The authors are grateful to the Maoershan National Nature Reserve staff for assistance during fieldwork. The authors also thank to Annemarie Ohler and the anonymous reviewers for their valuable comments on the manuscript. This work was supported by the National Natural Science Foundation of China (32060116) and Guangxi Natural Science Foundation, China (2020GXNSFDA238022).

## References

- AmphibiaChina (2022) The database of Chinese amphibians. Kunming Institute of Zoology (CAS), Kunming, Yunnan. <http://www.amphibiachina.org/> [accessed 15 July 2022]
- Boulenger GA (1909) Descriptions of four new frogs and a new snake discovered by Mr. H. Sauter in Formosa. *Annals and Magazine of Natural History (Series 8)* 4: 492–495. <https://doi.org/10.1080/00222930908692704>
- Chen WC, Peng WX, Li P, Liu YJ (2022) A new species of *Nidirana* (Anura, Ranidae) from southern Guangxi, China. *Asian Herpetological Research* 13(2): 109–116. <https://doi.org/10.16373/j.cnki.ahr.210065>

- Chou WH (1999) A new frog of the genus *Rana* (Anura: Ranidae) from China. *Herpetologica* 55: 389–400.
- Chuaynkern Y, Ohler A, Inthara C, Duengkae P, Makchai S, Salangsingha N (2010) A revision of species in the subgenus *Nidirana* Dubois, 1992, with special attention to the identity of specimens allocated to *Rana adenopleura* Boulenger, 1909, and *Rana chapaensis* (Bourret, 1937) (Amphibia: Anura: Ranidae) from Thailand and Laos. *The Raffles Bulletin of Zoology* 58: 291–310.
- Dubois A (1992) Notes sur la classification des Ranidae (amphibiens anoures). *Bulletin Mensuel de la Societe Linneenne de Lyon* 61(10): 305–352. <https://doi.org/10.3406/linly.1992.11011>
- Dubois A (1995) Keratodont formulae in anuran tadpoles: Proposals for a standardization. *Journal of Zoological Systematics and Evolutionary Research* 33(3–4): I–XV. <https://doi.org/10.1111/j.1439-0469.1995.tb00947.x>
- Fei L, Ye CY, Jiang JP (2007) A new species of Ranidae, *Hylarana (Nidirana) hainanensis*, from China (Amphibia: Anura). *Herpetologica Sinica* 11: 1–4.
- Fei L, Hu SQ, Ye CY, Huang YZ (2009) *Fauna Sinica. Amphibia Vol. 3 Anura*. Science Press, Beijing.
- Frost DR (2021) *Amphibian Species of the World: an Online Reference*. Version 6.1. American Museum of Natural History, New York. <https://doi.org/10.5531/db.vz.0001> [accessed 12 July 2022]
- Grosjean S, Ohler A, Chuaynkern Y, Cruaud C, Hassanin A (2015) Improving biodiversity assessment of anuran amphibians using DNA barcoding of tadpoles. Case studies from Southeast Asia. *Comptes Rendus Biologies* 338(5): 351–361. <https://doi.org/10.1016/j.crvi.2015.03.015>
- Kakehashi R, Kurabayashi A, Oumi S, Katsuren S, Hosono M, Sumida M (2013) Mitochondrial genomes of Japanese *Babina* frogs (Ranidae, Anura): Unique gene arrangements and the phylogenetic position of genus *Babina*. *Genes & Genetic Systems* 88(1): 59–67. <https://doi.org/10.1266/ggs.88.59>
- Köhler J, Jansen M, Rodríguez A, Kok PJR, Toledo LF, Emmrich M, Glaw F, Haddad CFB, Rödel MO, Vences M (2017) The use of bioacoustics in anuran taxonomy: Theory, terminology, methods and recommendations for best practice. *Zootaxa* 4251(1): 1–124. <https://doi.org/10.11646/zootaxa.4251.1.1>
- Li SZ, Wei G, Xu N, Cui JG, Fei L, Jiang JP, Liu J, Wang B (2019) A new species of the Asian music frog genus *Nidirana* (Amphibia, Anura, Ranidae) from southwestern China. *PeerJ* 7: e7157. <https://doi.org/10.7717/peerj.7157>
- Liu CC (1950) Amphibians of western China. *Fieldiana. Zoology Memoirs* 2: 1–400. <https://doi.org/10.5962/bhl.part.4737>
- Lyu ZT, Zeng ZC, Wang J, Lin CY, Liu ZY, Wang YY (2017) Resurrection of genus *Nidirana* (Anura: Ranidae) and synonymizing *N. caldwelli* with *N. adenopleura*, with description of a new species from China. *Amphibia-Reptilia* 38(4): 483–502. <https://doi.org/10.1163/15685381-00003130>
- Lyu ZT, Mo YM, Wan H, Li YL, Pang H, Wang YY (2019) Description of a new species of music frogs (Anura, Ranidae, *Nidirana*) from Mt Dayao, southern China. *ZooKeys* 858: 109–126. <https://doi.org/10.3897/zookeys.858.34363>

- Lyu ZT, Dai KY, Li Y, Wan H, Liu ZY, Qi S, Lin SM, Wang J, Li YL, Zeng YJ, Li PP, Pang H, Wang YY (2020a) Comprehensive approaches reveal three cryptic species of genus *Nidirana* (Anura, Ranidae) from China. *ZooKeys* 914: 127–159. <https://doi.org/10.3897/zookeys.914.36604>
- Lyu ZT, Chen Y, Yang JH, Zeng ZC, Wang J, Zhao J, Wan H, Pang H, Wang YY (2020b) A new species of *Nidirana* from the *N. pleuraden* group (Anura, Ranidae) from western Yunnan, China. *Zootaxa* 4861(1): 43–62. <https://doi.org/10.11646/zootaxa.4861.1.3>
- Lyu ZT, Huang Z, Liao XW, Lin L, Huang Y, Wang YY, Mo YM (2021) A new species of music frog (Anura, Ranidae, *Nidirana*) from Mt Daming, Guangxi, China. *ZooKeys* 1059: 35–56. <https://doi.org/10.3897/zookeys.1059.68140>
- Miller MA, Pfeiffer W, Schwartz T (2010) Creating the CIPRES Science Gateway for inference of large phylogenetic trees. In: Proceedings of the Gateway Computing Environments Workshop (GCE), 14 Nov. 2010, New Orleans, LA, 1–8. <https://doi.org/10.1109/GCE.2010.5676129>
- Mo YM, Wei ZY, Chen WC (2014) Colored Atlas of Guangxi Amphibians. Guangxi Science and Technology Publishing House, Nanning.
- Posada D (2008) jModelTest: Phylogenetic model averaging. *Molecular Biology and Evolution* 25(7): 1253–1256. <https://doi.org/10.1093/molbev/msn083>
- Ronquist FR, Huelsenbeck JP (2003) MrBayes 3: Bayesian phylogenetic inference under mixed models. *Bioinformatics* 19(12): 1572–1574. <https://doi.org/10.1093/bioinformatics/btg180>
- Savage JM (1975) Systematics and distribution of the Mexican and Central American stream frogs related to *Eleutherodactylus rugulosus*. *Copeia* 1975(2): 254–306. <https://doi.org/10.2307/1442883>
- Wei G, Li SZ, Liu J, Cheng YL, Xu N, Wang B (2020) A new species of the music frog *Nidirana* (Anura, Ranidae) from Guizhou Province, China. *ZooKeys* 904: 63–87. <https://doi.org/10.3897/zookeys.904.39161>

## Appendix I

**Table A1.** Specimens examined. Type locality indicated by an asterisk (\*).

Species	Locality	Voucher no.
<i>Nidirana guangxiensis</i>	Damingshan National Nature Reserve, Guangxi, China*	NNU 00213
<i>Nidirana guangxiensis</i>	Damingshan National Nature Reserve, Guangxi, China*	NNU 00214
<i>Nidirana guangxiensis</i>	Damingshan National Nature Reserve, Guangxi, China*	NNU 00215
<i>Nidirana guangxiensis</i>	Damingshan National Nature Reserve, Guangxi, China*	NNU 00216
<i>Nidirana guangxiensis</i>	Damingshan National Nature Reserve, Guangxi, China*	NNU 00217
<i>Nidirana guangxiensis</i>	Damingshan National Nature Reserve, Guangxi, China*	NNU 00218
<i>Nidirana leishanensis</i>	Yuanbaoshan National Nature Reserve, Guangxi, China	NNU 201908032
<i>Nidirana leishanensis</i>	Yuanbaoshan National Nature Reserve, Guangxi, China	NNU 201908033
<i>Nidirana shiwandashanensis</i>	Shiwandashan National Nature Reserve, Guangxi, China*	NNU 00238
<i>Nidirana shiwandashanensis</i>	Shiwandashan National Nature Reserve, Guangxi, China*	NNU 00239
<i>Nidirana shiwandashanensis</i>	Shiwandashan National Nature Reserve, Guangxi, China*	NNU 00605
<i>Nidirana shiwandashanensis</i>	Shiwandashan National Nature Reserve, Guangxi, China*	NNU 00606
<i>Nidirana yaoica</i>	Dayaoshan National Nature Reserve, Guangxi, China*	NNU 201907008
<i>Nidirana yaoica</i>	Dayaoshan National Nature Reserve, Guangxi, China*	NNU 201907009

## Supplementary material I

### Supplementary data

Authors: Wei-Cai Chen, Jian-Ping Ye, Wan-Xiao Peng, Peng Li, Tong-Ping Su, Gui-Dong Yu, Zhi-Ying Cheng

Data type: Morphological.

Explanation note: Measurements of *Nidirana guibeiensis* sp. nov. (in mm). Abbreviations defined in Material and methods. \*= holotype.

Copyright notice: This dataset is made available under the Open Database License (<http://opendatacommons.org/licenses/odbl/1.0/>). The Open Database License (ODbL) is a license agreement intended to allow users to freely share, modify, and use this Dataset while maintaining this same freedom for others, provided that the original source and author(s) are credited.

Link: <https://doi.org/10.3897/zookeys.1135.94371.suppl1>



# Multilocus phylogeny and species delimitation suggest synonymies of two *Lucanus* Scopoli, 1763 (Coleoptera, Lucanidae) species names

Li Yang Zhou<sup>1,2\*</sup>, Zhi Hong Zhan<sup>3\*</sup>, Xue Li Zhu<sup>1,2</sup>, Xia Wan<sup>1,2</sup>

**1** Department of Ecology, School of Resources and Engineering, Anhui University, 111 Jiulong Rd., Hefei 230601, China **2** Anhui Province Key Laboratory of Wetland Ecosystem Protection and Restoration, Anhui University, 111 Jiulong Rd., Hefei, 230601, China **3** Department of Entomology, University of Wisconsin Madison, WI 53706, USA

Corresponding author: Xia Wan ([wanzia@ahu.edu.cn](mailto:wanzia@ahu.edu.cn))

---

Academic editor: Andrey Frolov | Received 20 June 2022 | Accepted 23 November 2022 | Published 14 December 2022

---

<https://zoobank.org/1E8F80E7-EA62-4071-A64F-4DC412181E68>

---

**Citation:** Zhou LY, Zhan ZH, Zhu XL, Wan X (2022) Multilocus phylogeny and species delimitation suggest synonymies of two *Lucanus* Scopoli, 1763 (Coleoptera, Lucanidae) species names. ZooKeys 1135: 139–155. <https://doi.org/10.3897/zookeys.1135.89257>

---

## Abstract

Phylogenetic relationships of four nominal *Lucanus* Scopoli, 1763 species, *L. swinhoei* Parry, 1874, *L. continentalis* Zilioli, 1998, *L. liuyei* Huang & Chen, 2010, and *L. wuyishanensis* Schenk, 1999, are assessed based on mitochondrial (16S rDNA, COI) and nuclear (28S rDNA, Wingless) genes. The genetic distance is 0.0072 between *L. swinhoei* and *L. continentalis*, and 0.0094 between *L. wuyishanensis* and *L. liuyei*. Three species-delimitation approaches (ABGD, PTP, and GMYC) consistently showed *L. swinhoei* + *L. continentalis* and *L. wuyishanensis* + *L. liuyei* as two MOTUs. A new synonymy, *L. liuyei* = *L. wuyishanensis*, is proposed. Synonymy of *L. swinhoei* over *L. continentalis* is confirmed.

## Keywords

genetic distance, Lucanidae, morphology, new synonymy, phylogenetic analysis, species delimitation

---

\* These authors contributed equally to this study.

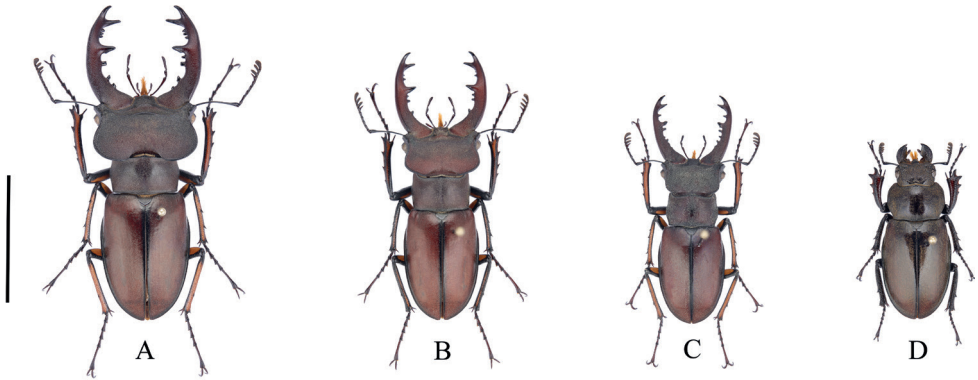
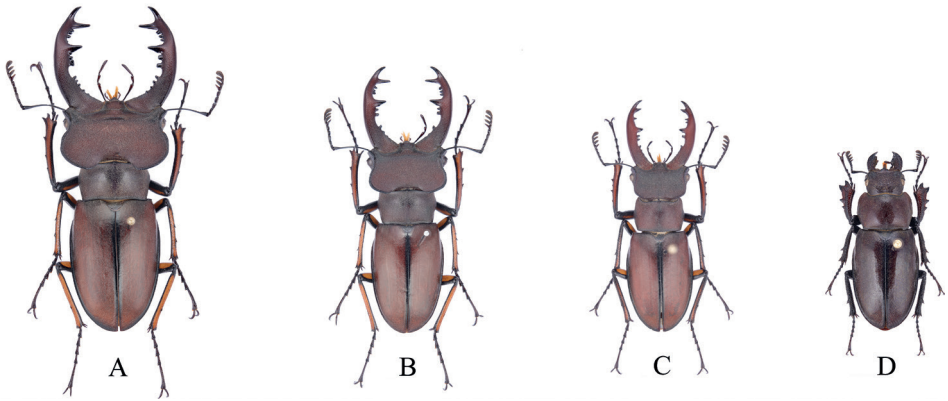
## Introduction

Morphological evidence suggests that the evolution and differences of the mandible of stag-beetles are closely related to environmental heterogeneity (Huang and Lin 2010; Gotoh et al. 2011). Molecular phylogeny also provides evidence for the intraspecific morphological complexity due to environmental heterogeneity in *Lucanus* (Zhou et al. 2019; Ying et al. 2021; Yuan et al. 2021).

The genus *Lucanus* Scopoli, 1763 is recognized as the most typical representative of Lucanidae, and *Lucanus* species (and subspecies) are especially abundant in eastern regions of Asia (including China, India, Laos, Vietnam, and Myanmar), with the majority inhabiting southern China (Wan 2007; Fujita 2010; Huang and Chen 2010; Lin 2017; Chen et al 2020). Hilly topography below 2000 m dominates the central and eastern regions of south China, with many low mountains and valley basins extending from northeast to southwest (Zhou et al. 2006). This unique topography may have hindered gene exchange between species and facilitated population differentiation (Qiu et al. 2011; Zhao et al. 2012; Li et al. 2019). Secondly, sexual dimorphism, male polymorphism, and color pattern polymorphism are significant in *Lucanus*. Due to the above reasons, this genus is phenotypically rich at the intraspecific level, resulting in some taxonomic confusion. Phylogenetic analysis using molecular markers such as mitochondrial and nuclear genes can clarify many morphology-based species taxonomic positions.

*Lucanus wuyishanensis* Schenk, 1999 and *Lucanus liuyei* Huang & Chen, 2010 are typical representatives of *Lucanus*. All collecting data indicate that *L. wuyishanensis* is mainly distributed in southeast China (Zhejiang, Jiangxi, Fujian). Its allied species, *L. liuyei* in south-central China (Guangxi, Guizhou, Hunan), is morphologically similar to *L. wuyishanensis* but has a different geographic distribution. Huang (2006) erroneously treated *L. wuyishanensis* as a synonym of *Lucanus klapperichi*; however, examination of the male genitalia proved that this species should be treated as distinct (Huang and Chen 2010). Similarly, Wan (2007) also believed that the lateral ridges of the head and the major inner tooth are quite different from those of *L. klapperichi*. Additionally, Huang and Chen (2013) observed that *L. liuyei* from Guangxi is closer to *L. wuyishanensis*, from the border area of Jiangxi, Zhejiang, and Fujian, in terms of external morphology, and classified it as a subspecies of *L. liuyei* by comparing their male and female genitalia. However, the specimens collected in Guangxi were identified by Fujita (2010) as *L. wuyishanensis* based on morphological characters. In our opinion, the differences between the two species are insignificant and hardly any diagnostic attribute was found to distinguish them except for existing collecting data showing distribution areas and body size ranges (Fig. 1).

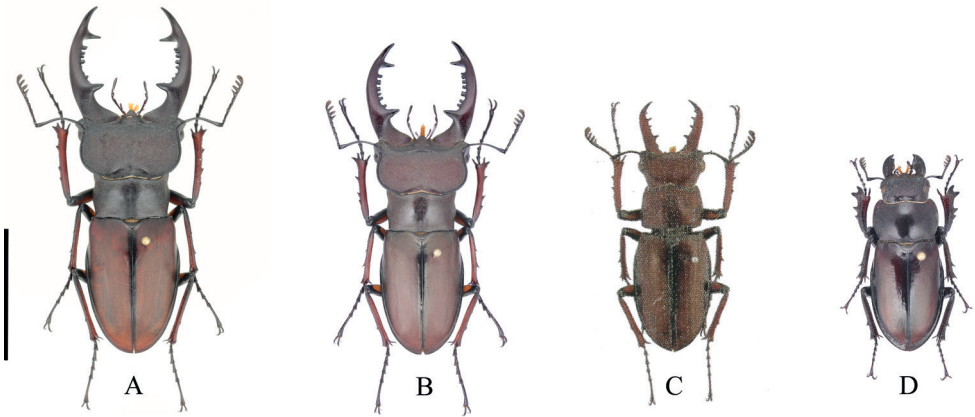
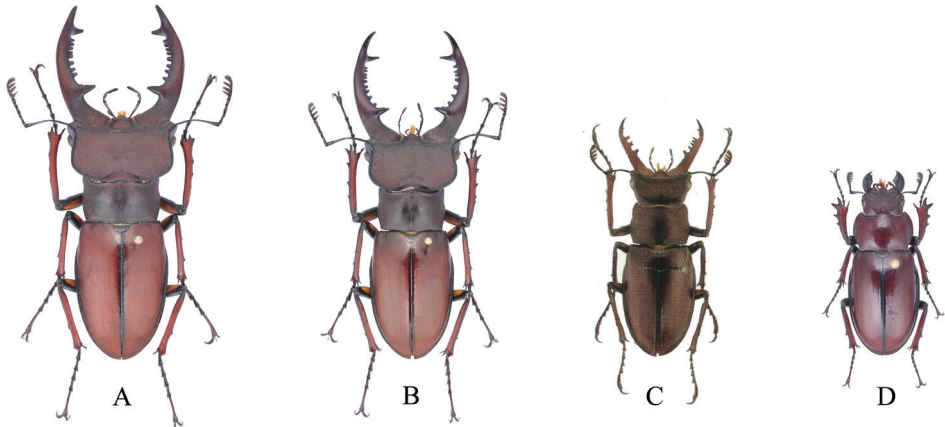
In addition, the taxonomic relationship between *Lucanus swinhoei* Parry, 1874 and *Lucanus continentalis* Zilioli, 1998 has long been controversial. Zilioli (1998) reported that *L. continentalis* is a subspecies of *L. swinhoei*; however, Wan (2007) considered *L. continentalis* as a synonym of *L. swinhoei* based on examination of a

*L. liuyei**L. wuyishanensis*

**Figure 1.** Habitus of *L. wuyishanensis* and *L. liuyei* in dorsal view **A** major male **B** medium male **C** minor male **D** female. All to scale; scale bar: 20.0 mm.

series of specimens. Huang and Chen (2010) compared the inner teeth, the margin of the basal part of the mandible, the labrum, and the geographical distribution of the two species and concluded that they are separate species, with the former mainly distributed in southeastern China and the latter only in Taiwan. Later, Huang and Chen (2017) relegated *L. continentalis* to a subspecies of *L. swinhoei*. So far, the taxonomic positions of *L. swinhoei* have been listed as distinct species, subspecies, or synonyms despite a lack of abundant data to support these modifications (Fig. 2).

This study assesses the taxonomic relationships between the species pairs *L. continentalis* and *L. swinhoei*, and *L. wuyishanensis* and *L. liuyei*, by using multi-locus data, revisiting for the first time the relationships among these four species from a molecular phylogenetic perspective.

*L. continentalis**L. swinhoiei*

**Figure 2.** Habitus of *L. continentalis* and *L. swinhoiei* in dorsal view **A** major male **B** medium male **C** minor male (see Huang and Chen 2010: pl. 35 figs 34–5, 9) **D** female. Scale bar: 20.0 mm.

## Materials and methods

### Sample collection, handling, and storage

All specimens of *Lucanus* were netted or light-trap collected for this study and store in ethanol, including 54 samples of the ingroup (21 *L. wuyishanensis* collected from Zhejiang, Fujian, Jiangxi province; 17 *L. liuyei* from Guangxi, Guizhou, Hunan province; five *L. swinhoiei* from Taiwan; 11 *L. continentalis* from Fujian and Zhejiang province), and 10 samples of the outgroup (one each of *L. parryi* Boileau, 1899, *L. simithii* Parry, 1862, *L. fryi* Boileau, 1911, *L. klapperichi* Bomans, 1989, and six *L. fujianensis* Schenk, 2008). Voucher specimens and their extracted genomic DNA are deposited in the research collection at the Museum of Anhui University, China. (Suppl. material 1).

The map with collection localities was generated using ArcGIS v. 10.3 (<http://www.esri.com/software/arcgis>) based on the geospatial data from the National Geomatics

Center of China (Fig. 3). Photographs of the habitus was taken in .jpg format using a Canon 5D Mark IV with Canon 100 mm f/2.8 macro lens and a twin flash (Figs 1, 2).

### DNA extraction, amplification, and sequencing

The specimens were preserved in 99.7% ethanol at  $-20^{\circ}\text{C}$ . Total genomic DNA was extracted from a small portion of the muscle using DNeasy Blood and Tissue Extraction kit according to the manufacturer's recommendations. The primers used to amplify 28S rDNA and Wingless were adapted from Abouheif and Wray (2002), Ward and Downie (2005), Monaghan et al. (2007), and Wild and Maddison (2008). For COI and 16S rDNA, primers were specifically designed in this study (Table 1).

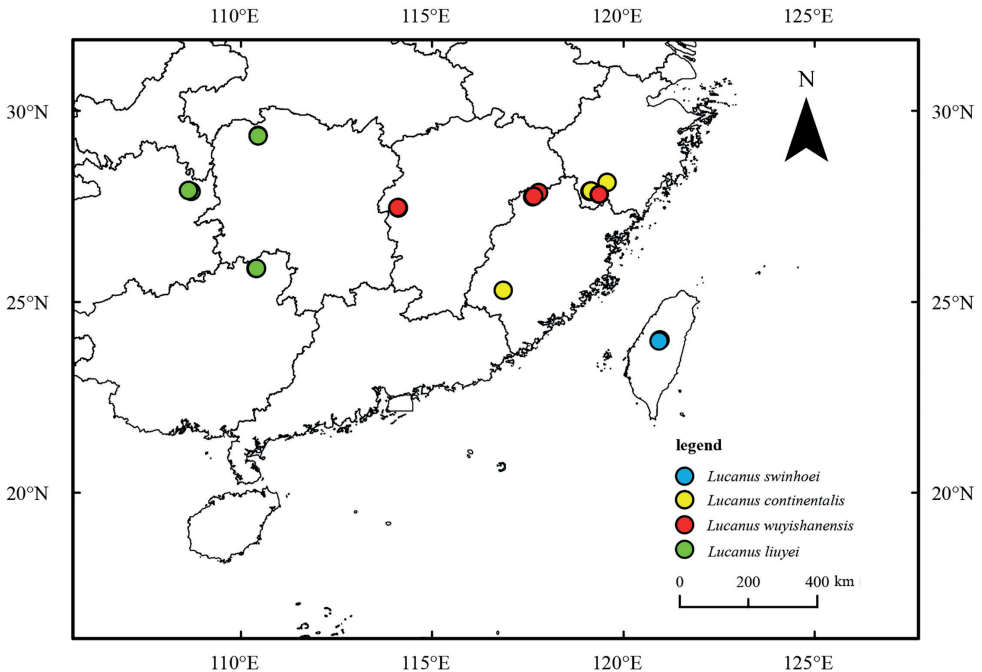


**Figure 3.** Sample collection sites for this study.

**Table 1.** Summary of paired PCR primers in the present study.

Gene	Primer	Sequence (5'–3')	References
COI	LuCOIF1	ATAATCATTGCTGTCCAAC	Present study
	LuCOIR1	TATCTATGTTACAGCRGGRGGT	Present study
16S rDNA	Lu16SF1	CTCGAATTTTRGAGGGC	Present study
	Lu16SR1	AATCCAACATCGAGGTC	Present study
28S rDNA	28SDD	GGGACCCGTCCTTGAACAC	Monaghan et al. 2007
	28SFF	TTACACACTCCTTAGCGGAT	Monaghan et al. 2007
Wing-less	Wg550F	ATGCGTCAGGARTGYAARTGYCAYGGYATGTC	Wild and Maddison 2008
	WgAbRZ	CACTTNACYTCRCARCACCARTG	Wild and Maddison 2008
	Wg578F	TGCACNGTGAARACYTGCTGGATG	Ward and Downie 2005
	WgAbR	ACYTCGCAGCACCARTGGAA	Abouheif and Wray 2002

PCR amplification reactions for the three loci (COI, 16S rDNA, 28S rDNA) were performed in a 25  $\mu$ L volume containing 1  $\mu$ L of each primer (forward and reverse) at 10  $\mu$ M, 2  $\mu$ L of template DNA solution, 12.5  $\mu$ L of 2 $\times$  EasyTaq SuperMix (+ dye), and 8.5  $\mu$ L of sterile double-distilled water to make up the final volume of 25  $\mu$ L. WG was amplified by nested PCR, first PCR containing 1  $\mu$ L of each primer (forward and reverse) at 10  $\mu$ M, 1  $\mu$ L of template DNA solution, 7.5  $\mu$ L of 2 $\times$  EasyTaq SuperMix (+ dye), and 4.5  $\mu$ L of sterile double-distilled water, and finally use the 1  $\mu$ L first amplification product as a template, including 1  $\mu$ L of each primer (forward and reverse) at 10  $\mu$ M, 12.5  $\mu$ L of 2 $\times$  EasyTaq SuperMix (+ dye), and 9.5  $\mu$ L of sterile double-distilled water. The polymerase chain reaction amplifications were performed under the following conditions: initial denaturation at 94  $^{\circ}$ C for 2 min, followed by 35–37 cycles of denaturation at 94  $^{\circ}$ C for 40 seconds, annealing at 52–60  $^{\circ}$ C for 50 seconds, and elongation at 70  $^{\circ}$ C for 1 min, and then a final extension step at 72  $^{\circ}$ C for 7 min, stored at 4  $^{\circ}$ C at room temperature. Amplifications were purified using Template DNA Amplify Kit (Ensure Biologicals).

Sequencing was performed using the ABI PRISM BigDye Terminator v. 3.1 Cycle Sequencing Kit (Life Technologies, USA), and cycle sequencing reactions were performed on ABI PRISM 3730xl automated sequencers (Life Technologies, USA) at Sangon Biotech Company, China. All sequences generated in this study were submitted to GenBank under accession numbers (Suppl. material 1).

## Sequence alignment, genetic distances, and phylogenetic analyses

Sequences of forward and reverse strands were assembled using GENEIOUS PRIME 2019.1.1 (<https://www.geneious.com>) and then aligned using MEGA 11. Genetic divergences among taxa were estimated using MEGA 11 (Kumar et al. 2018) via K2P-distance. The COI gene of *Lucanus* was assembled for genetic distance analyses. Finally, we concatenated alignments using PHYLOSUITE 1.2.1 (Zhang et al. 2020). The concatenated dataset was partitioned according to the Akaike Information Criterion (AIC) with PARTITIONFINDER 2.1.1 (Lanfear et al. 2017) for phylogenetic analyses.

Phylogenetic inferences were conducted using four gene markers based on maximum likelihood inference (**ML**), and Bayesian inference (**BI**). The BI tree was implemented in MRBAYES 3.2.6 (Ronquist et al. 2012). PARTITIONFINDER 2.1.1 was used to determine the best-fit models. Bayesian inference was conducted using MRBAYES 3.2.6 with two simultaneous runs of  $5 \times 10^7$  generations. Samples were drawn every 1,000 Markov Chain Monte Carlo (MCMC) step. The average standard deviation of split frequencies should be less than 0.01, with the initial 25% of trees discarded as burn-in. ML analyses were performed using IQ-TREE webserver (Trifunopoulos and Lam-Tung 2016). The “Auto” option was set under optimal evolutionary models, and the phylogenetic trees were constructed using an ultrafast bootstrap approximation approach with 10,000 replicates. Phylogenetic trees were visualized and edited in FIGTREE 1.4.3 (<http://beast.bio.ed.ac.uk/figtree>).

## Species delimitation

When defining species relationships by using molecular-set data, there are a variety of analytical approaches available. The Automatic Barcode Gap Discovery (**ABGD**) analysis was performed in this study for COI using a web interface (<https://bioinfo.mnhn.fr/abi/public/abgd/abgdweb.html>), which detects a gap in divergence distribution, which corresponds to differences between intraspecific and interspecific distances. When the gap exists, the process works well for species delimitation (Puillandre et al. 2012). An unrooted ML tree was generated in IQ-TREE webserver under the auto options. Poisson Tree Processes (**PTP**) was performed on a single, unrooted tree in the bPTP server (<https://species.h-its.org/>). A total of  $5 \times 10^5$  generations were run with the first 10% as burn-in (Zhang et al. 2013). General Mixed Yule Coalescent model (**GMYC**) analysis was conducted using BEAST 2.6.0 under a relaxed clock Exponential mode and ESS values assessed convergence. A burn-in with 25% was set to obtain an optimal consensus tree. Delimitation approach in the software R with the package 'splits' (available at <http://r-forge.r-project.org/projects/splits>) using the single-threshold method (Pons et al. 2006; Monaghan et al. 2009).

## Abbreviations

<b>ABGD</b>	Automatic Barcode Gap Discovery;
<b>BBP</b>	Bayesian posterior probability;
<b>BI</b>	Bayesian inference;
<b>GMYC</b>	General Mixed Yule Coalescent;
<b>K2P</b>	distance, Kimura 2-parameter distance;
<b>ML</b>	maximum likelihood;
<b>MBL</b>	maximum likelihood bootstrap;
<b>MOTU</b>	molecular operational taxonomic unit;
<b>PCR</b>	Polymerase Chain Reaction;
<b>PTP</b>	Poisson Tree Processes.

## Results

### Morphological comparison

External morphological characteristics of two clades are compared in the table (Suppl. material 2). *Lucanus swinhoei* and *L. continentalis* differ slightly in body size, maintaining an overall range of 27–58 mm. Major males display the following features: mandibles strongly incurved at basal 1/3 and at apex; apical teeth bifurcated, upper branch teeth usually larger or equal in size with lower branch teeth; major mandibular tooth located at basal 1/3, triangular, preceded by more than five inner small teeth. Medium-sized

males have the following features: mandibles strongly incurved at basal 1/3, usually straight at apex; apical teeth bifurcated, upper branch teeth usually equal to or smaller than lower branch teeth; major mandibular tooth located at basal 1/3, triangular, preceded by four or five inner small teeth. Minor males indicate the following features: mandibles weakly incurved at basal 1/3, straight at apex; apical teeth bifurcated, upper branch teeth usually equal to or smaller than lower branch teeth; major mandibular tooth located at basal 1/3, triangular, preceded by fewer than four inner small teeth.

*Lucanus wuyishanensis* and *L. liuyei* differ slightly in body size, maintaining an overall range of 28–53 mm. Major males indicate the following features: mandible weakly incurved at basal 1/3, straight at the middle then strongly incurved at apical 1/4; the major inner mandibular tooth located 2/3 from the apical mandibular fork, sharp, triangular protruding forward and inflated on both sides, four separated small inner mandibular teeth attached below the major inner mandibular tooth, four or five unclear, minor inner mandibular teeth continuously located along the midlength of basal mandibles; four small inner mandibular teeth densely distributed between the major tooth and the apical fork. Medium-sized males indicate the following features: major inner mandibular tooth somewhat triangular, weakly inflated on both sides; more than four unclear, minor inner mandibular teeth continuously located along the midlength of basal mandibles, and more than four small inner mandibular teeth densely distributed between the major tooth and the apical fork. Minor males indicate the following features: major inner mandibular tooth weakly developed, single-point and not triangular; less than two separated small inner mandibular teeth attached below the major inner mandibular tooth; more than three unclear, minor inner mandibular teeth continuously located on 1/2 of basal mandible; more than two small inner mandibular teeth densely distributed between the major tooth and the apical fork.

## Phylogenetic analyses

A concentrated matrix with 2489 aligned positions for data was obtained comprising COI, 16S rDNA, 28S rDNA, and Wingless genes. The phylogenetic analyses using both BI and ML inferences recovered overall a consistent topology (Fig. 4). As outgroups, *L. smithii*, *L. fryi*, and *L. parryi* were separated from other species with high support, forming an independent clade. In addition, the clade *L. klapperichi* was sister to the clade (*L. liuyei* + *L. wuyishanensis*) (BPP = 1, MLB = 94). The clade *L. fujianensis* was sister to the clade (*L. swinhoei* + *L. continentalis*) (BPP = 1, MLB = 100). Nested structures of *L. liuyei* and *L. wuyishanensis* occur in all geographic populations.

## Genetic distance

Genetic distances (K2P-distances) were calculated for all taxa using COI genes (Table 2). The results showed that the average genetic distance between *L. wuyishanensis* and *L. liuyei* populations in each collection area was a low mean range (0.0067–0.0110)

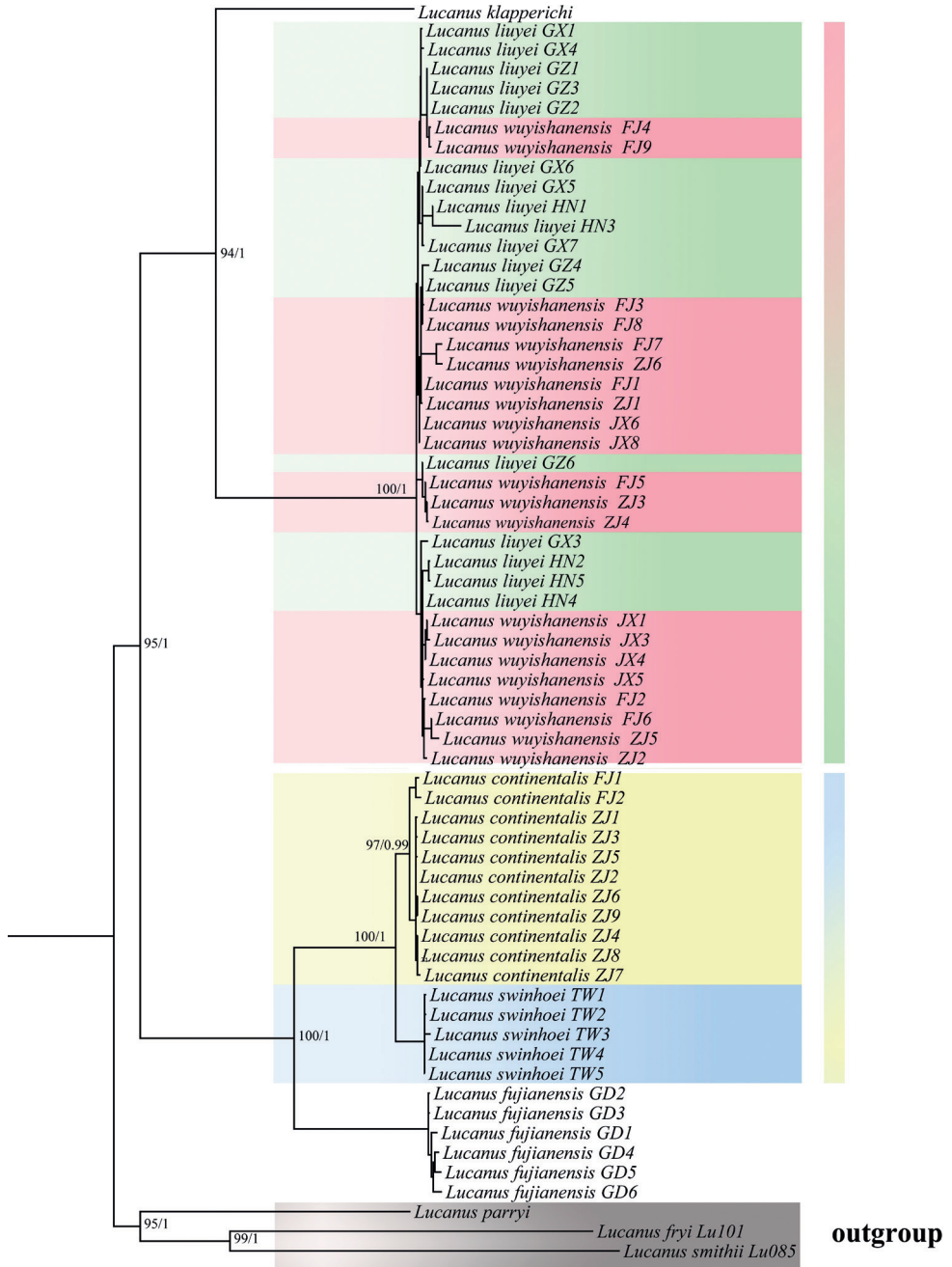


**Figure 4.** Phylogenetic inferences based on four genes (COI, 16S rDNA, Wingless, and 28S rDNA) by maximum-likelihood inference (MLI) and Bayesian inference (BI) with posterior probability. Both posterior probabilities of MLI (above/left of branch) and bootstrapping values of BI (below/right of branch) are shown at nodes.

(Suppl. material 3) and mean genetic distance of 0.0094 in all taxa (Table 2); the mean genetic distance between *L. swinhoei* and *L. continentalis* was 0.0072 (Table 2). The numbers were lower than the minimum mean genetic distances of 0.1592 among interspecific taxa and far less than the mean genetic distance of 0.2090 between inter-species of *Lucanus* (Lin 2017).

## Species delimitation

Species delimitation is shown in Fig. 5. Analysis of COI gene by all methods (ABGD, PTP, and GMYC) resulted in two molecular MOTUs, *L. wuyishanensis* + *L. liuyei* and *L. swinhoei* + *L. continentalis* (Fig. 5). For the concatenated dataset, all three methods suggested that *L. wuyishanensis* + *L. liuyei* were one MOTU, whereas GMYC divided *L. swinhoei* and *L. continentalis* into two MOTUs.

## Taxonomic account

### *Lucanus swinhoei* Parry, 1897

*Lucanus swinhoei* Parry, 1874: 370.

*Lucanus continentalis* Zilioli, 1998: 145, synonymy by Wan (2007).

**Material examined.** CHINA • 1 male; Zhejiang Province, Yunhe County; 18 Jul. 2019; ZH Zhan leg. • 3 males; same locality as for preceding; 5 Jul. 2021 • 3 males; Zhejiang Province, Baishanzu County; 23 Jul. 2015 • 2 males; Zhejiang Province, Longquan County; 6 Jul. 2019 • 1 male; Fujian Province, Shanghang County; 12 Jul. 2021; LY Zhou leg. 1 male; same locality as for preceding; 22 Jul. 2011; Q Zhang and YY Cao leg. • 2 males; Taiwan Island, Nantou County; 12 Jun. 2019; JZ Lin leg. • 2 males; same locality as for preceding; 6 Jun. 2020.

**Diagnosis.** Males of *L. swinhoei* could be distinguished from related species by following characters: 1) mandibles incurved at basal 1/3, straight along the midlength and incurved apically; 2) apical teeth bifurcated; major mandibular tooth located at basal 1/3, triangular, not flat on both sides; 3) elytra metallic luster at disc and along

**Table 2.** The mean genetic distances among studied species (K2P-distances).

	<i>L. liuyei</i>	<i>L. wuyishanensis</i>	<i>L. continentalis</i>	<i>L. swinhoei</i>	<i>L. fujianensis</i>	<i>L. klapperichi</i>	<i>L. fryi</i>	<i>L. smithii</i>	<i>L. parryi</i>
<i>L. liuyei</i>									
<i>L. wuyishanensis</i>	0.0094								
<i>L. continentalis</i>	0.1949	0.1924							
<i>L. swinhoei</i>	0.1906	0.1872	0.0072						
<i>L. fujianensis</i>	0.2131	0.2142	0.1617	0.1592					
<i>L. klapperichi</i>	0.1946	0.1977	0.1925	0.1872	0.1929				
<i>L. fryi</i>	0.2067	0.2086	0.2321	0.2280	0.1885	0.1955			
<i>L. smithii</i>	0.2246	0.2245	0.2150	0.2176	0.2230	0.2434	0.1962		
<i>L. parryi</i>	0.2280	0.2306	0.2193	0.2164	0.2054	0.1840	0.1774	0.1987	

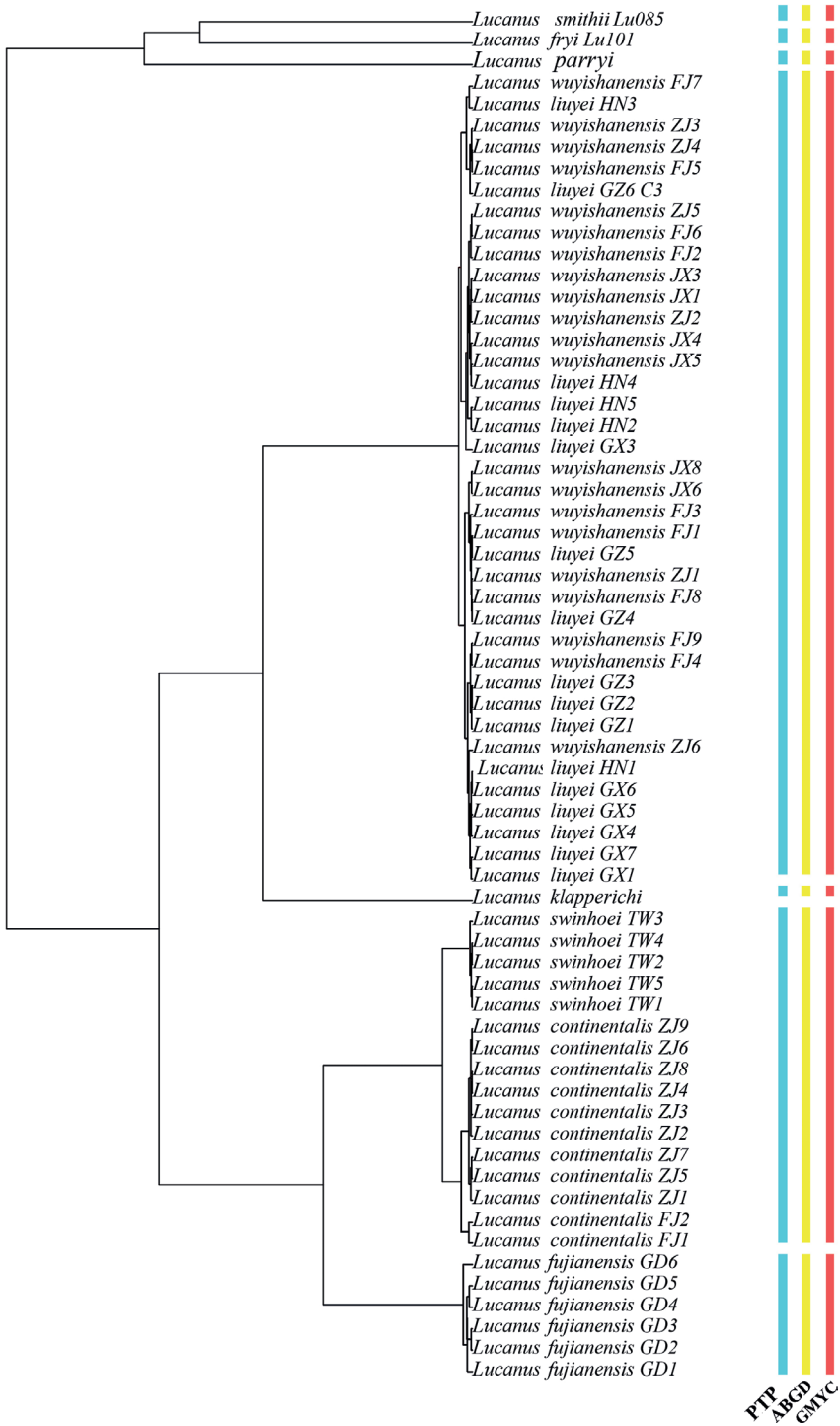


**Figure 5.** Delimitation of the studied *Lucanus* species based on COI. Columns are taxonomic identification based on three molecular delimitation methods: ABGD, PTP, and GMYC. The phylogenetic tree is based on the GMYC analysis.

the suture, reddish to brownish; less punctate and without any yellowish setae. The females of most species in *Lucanus* are not easy to distinguish due to their significant similarities in morphology. Typical female of *L. swinhoei* could be identified by the following subtle differences: elytra without a marked pubescence, metasternum not densely hairy and the canthi not markedly outside of the eyes.

**Distribution.** China (Zhejiang, Fujian, Taiwan Island).

### *Lucanus wuyishanensis* Schenk, 1999

*Lucanus wuyishanensis* Schenk, 1999: 114.

*Lucanus liuyei* Huang & Chen, 2010: 93–94, syn. nov.

**Material examined.** CHINA • 2 males; Jiangxi Province, Pingxiang County; 15 Jun. 2017; ZH Zhan leg. • 4 males; Jiangxi Province, same locality as for preceding; 03 Jun. 2021; Q Qi leg. • 6 males; Zhejiang Province, Mount Longquanshan; 18 Jul. 2019. • 1 male; Fujian Province, Mount Wuyishan; 18 Jul. 2011. • 2 males; Fujian Province, Mount Wuyishan; 14 Jul. 2011; Q Zhang and YY Cao leg. • 4 males; Fujian Province, same locality as for preceding; 12 Jun. 2020; ZH Zhan leg. • 2 males; Fujian Province, same locality as for preceding; 20 Jun. 2021; ZL Zhou leg. • 1 male; Guangxi Province, Mount Maoershan; 20 Jul. 2011. • 3 males; same locality as for preceding; 20 Jul. 2017; Q Qi leg. • 2 male, 1 female; same locality as for preceding; 20 Jul. 2021; ZH Zhan leg. • 2 male, 2 female; Guizhou Province, Mount Fanjingshan; 20 Jun. 2017; ZH Zhan leg. • 2 males; same locality as for preceding; 08 Jul. 2015; LX Zhu leg. • 1 male; Hunan Province, Zhangjiajie County; 20 Jun. 2015 • 4 males; same locality as for preceding; 21 May 2019; ZH Zhan leg.

**Diagnosis.** Males of *L. wuyishanensis* could be distinguished from related species by the following characters: 1) mandibles weakly incurved at basal 1/3, straight extending to the mid-length and strongly incurved at 1/4 anteriorly; 2) two separated, small, inner mandibular teeth attached below the major inner mandibular tooth; 2–4 small inner mandibular teeth densely distributed between the major tooth and the apical fork; 3) elytra reddish to brownish, usually bicolored with head and pronotum; oval, widest at the apical 1/4, strongly narrow at basal. Females of *L. wuyishanensis* are also similar in appearance to those of other *Lucanus* members. There are the following slight differences: dorsal surface covered with a vestiture of small and significant, yellowish-amber setae; head surface punctate heavily, mandible snout, strongly incurved anteriorly.

**Distribution.** China (Sichuan, Guangxi, Guizhou, Fujian, Hunan, Jiangxi).

### Discussion

Phylogenetic inferences by applying ML and BI analyses showed consistent patterns, which show that the *Lucanus klapperichi* clade is sister to the clade (*L. wuyishanensis* + *L. liuyei*) (MLB = 94%, BPP = 1). *Lucanus wuyishanensis* and

*L. liuyei* collected from different provinces were all clustered in a highly supported clade. The subclade *L. swinhoi* + *L. continentalis* is nested in the same clade (MLB = 100%, BPP = 1; Fig. 4). The K2P genetic distances between *L. wuyishanensis* and *L. liuyei* were (0.0067–0.0110 mean genetic distance of 0.0094), indicating that two forms belong to one species. The K2P distance between *L. swinhoi* and *L. continentalis* (0.0072) suggests that the former most likely represents an island population of the latter, similar to the forms distributed on Hainan Island (Zhou et al. 2019). Three species-delimitation approaches (ABGD, PTP, and GMYC) based on the COI gene also consistently showed *L. swinhoi* + *L. continentalis* and *L. wuyishanensis* + *L. liuyei* as two MOTUs (Fig. 5). Based on the concatenated dataset analysis, three methods suggested *L. wuyishanensis* and *L. liuyei* were one MOTU, whereas GMYC divided *L. swinhoi* and *L. continentalis* into two MOTUs. GMYC typically over-splits species, owing to low genetic diversity across lineages and overlap of interspecific and intraspecific divergences, as well as a lack of reciprocal monophyly within sister clades (Talavera et al. 2013; Pentinsaari et al. 2016; Stokkan et al. 2018; Yuan et al. 2021).

The genus *Lucanus* is susceptible to several pressures, such as habitat selection, sexual selection, and food resources, and only occurs in wooded alpine areas above 800 m with more demanding environmental conditions and tiny ecological niches (Switala et al. 2014; Chen et al. 2020). Hilly topography with below 2000 m dominates the central and eastern regions of south China, with many low mountains and valley basins extending from the northeast to the southwest (Zhou et al. 2006). Therefore, we think that the small phenotypic differences previously examined are attributable to phenotypic divergence due to geographic and climatic variables.

All our results indicate that *L. continentalis* is a junior subjective synonym of *L. swinhoi* and that *L. liuyei* as a junior subjective synonym of *L. wuyishanensis*. It is also clear, that in case of closely related species of the genus, an integrative approach utilizing both morphological and molecular data should be used. Molecular data can provide insight into the status of the forms with weak morphological differences. It is especially important for *Lucanus* and majority of other stag beetles because molecular traits are not prone to allometric variability.

## Acknowledgements

We express our heartfelt gratitude to the Insect Evolution Research Group at Anhui University, especially JiaoJiao Yuan, MiaoMiao Wang, and Yingying, for their valuable and insightful suggestions. This work was supported by research grants from the National Natural Science Foundation of China (no. 31872276 and 31572311).

## References

Abouheif E, Wray GA (2002) Evolution of the gene network underlying wing polyphenism in *Ants*. *Science* 297(5579): 249–252. <https://doi.org/10.1126/science.1071468>

- Chen D, Cao LJ, Zhao JL, Wan X, Wei SJ (2020) Geographic patterns of *Lucanus* (Coleoptera: Lucanidae) species diversity and environmental determinants in China. *Ecology and Evolution* 10(23): 13190–13197. <https://doi.org/10.1002/ece3.6911>
- Fujita H (2010) *The Lucanid Beetles of the World*. Mushi-sha, Tokyo, 472 pp.
- Gotoh H, Cornette R, Koshikawa S, Okada Y, Lavine LC, Emlen DJ, Miura T (2011) Juvenile hormone regulates extreme mandible growth in male stag beetles. *PLoS ONE* 6(6): e21139. <https://doi.org/10.1371/journal.pone.0021139>
- Huang H (2006) New descriptions and notes on Chinese stag-beetles, with discovery of the second species of *Noseolucanus* from SE Tibet. *Coleoptera* 10: 11–34.
- Huang H, Chen CC (2010) *Stag Beetles of China I*. Formosa Ecological Company, Taiwan, 288 pp.
- Huang H, Chen CC (2013) *Stag Beetles of China II*. Formosa Ecological Company, Taiwan, 716 pp.
- Huang H, Chen CC (2017) *Stag Beetles of China III*. Formosa Ecological Company, Taiwan, 524 pp.
- Huang JP, Lin CP (2010) Diversification in subtropical mountains: Phylogeography, Pleistocene demographic expansion, and evolution of polyphenic mandibles in Taiwanese stag beetle, *Lucanus formosanus*. *Molecular Phylogenetics and Evolution* 57(3): 1149–1161. <https://doi.org/10.1016/j.ympev.2010.10.012>
- Kumar S, Stecher G, Li M, Knyaz C, Tamura K (2018) MEGA X: Molecular Evolutionary Genetics Analysis across computing platforms. *Molecular Biology and Evolution* 35(6): 1547–1549. <https://doi.org/10.1093/molbev/msy096>
- Lanfear R, Frandsen PB, Wright AM, Senfeld T, Calcott B (2017) PartitionFinder 2: New methods for selecting partitioned models of evolution for molecular and morphological phylogenetic analyses. *Molecular Biology and Evolution* 34: 772–773. <https://doi.org/10.1093/molbev/msw260>
- Li H, Kong L, Wang K, Zhang S, Motokawa M, Wu Y, Wang WQ, Li Y (2019) Molecular phylogeographic analyses and species delimitations reveal that *Leopoldamys edwardsi* (Rodentia: Muridae) is a species complex. *Integrative Zoology* 14(5): 494–505. <https://doi.org/10.1111/1749-4877.12378>
- Lin ZQ (2017) *Molecular phylogeny of Lucanus Scopoli (Coleoptera: Lucanidae)*. Masters thesis, Anhui University, Hefei, China.
- Monaghan MT, Inward DJG, Hunt T, Vogler AP (2007) A molecular phylogenetic analysis of the Scarabaeinae (dung beetles). *Molecular Phylogenetics and Evolution* 45(2): 674–692. <https://doi.org/10.1016/j.ympev.2007.06.009>
- Monaghan MT, Wild R, Elliot M, Fujisawa T, Balke M, Inward DJG, Lees DC, Ranivosolo R, Eggleton P, Barraclough TG, Vogler AP (2009) Accelerated species inventory on Madagascar using coalescent-based models of species delineation. *Systematic Biology* 58(3): 298–311. <https://doi.org/10.1093/sysbio/syp027>
- Pentinsaari M, Vos R, Mutanen M (2016) Algorithmic single-locus species delimitation: Effects of sampling effort, variation and nonmonophyly in four methods and 1870 species of beetles. *Molecular Ecology Resources* 17(3): 393–404. <https://doi.org/10.1111/1755-0998.12557>

- Pons J, Barraclough TG, Gomez-Zurita J, Cardoso A, Duran DP, Hazell S, Kamoun S, Sumlin WD, Vogler AP (2006) Sequence-based species delimitation for the DNA taxonomy of undescribed insects. *Systematic Biology* 55(4): 595–609. <https://doi.org/10.1080/10635150600852011>
- Puillandre N, Modica MV, Zhang Y, Sirovich L, Boisselier MC, Cruaud C, Holford M, Samadi S (2012) Large-scale species delimitation method for hyperdiverse groups. *Molecular Ecology* 21: 2671–2691. <https://doi.org/10.1111/j.1365-294X.2012.05559.x>
- Qiu YX, Fu CX, Comes HP (2011) Plant molecular phylogeography in China and adjacent regions: Tracing the genetic imprints of Quaternary climate and environmental change in the world's most diverse temperate flora. *Molecular Phylogenetics and Evolution* 59(1): 225–244. <https://doi.org/10.1016/j.ympev.2011.01.012>
- Ronquist F, Teslenko M, van der Mark P, Ayres DL, Darling A, Hohna S, Larget B, Liu L, Suchard MA, Huelsenbeck JP (2012) MrBayes 3.2: Efficient Bayesian phylogenetic inference and model choice across a large model space. *Systematic Biology* 61(3): 539–542. <https://doi.org/10.1093/sysbio/sys029>
- Stokkan M, Jurado-Rivera JA, Oromí P, Juan C, Jaume D, Pons J (2018) Species delimitation and mitogenome phylogenetics in the subterranean genus *Pseudoniphargus* (Crustacea: Amphipoda). *Molecular Phylogenetics and Evolution* 127: 988–999. <https://doi.org/10.1016/j.ympev.2018.07.002>
- Switala AK, Sole CL, Scholtz CH (2014) Phylogeny, historical biogeography and divergence time estimates of the genus *Colophon* Gray (Coleoptera: Lucanidae). *Invertebrate Systematics* 28(3): 326–336. <https://doi.org/10.1071/IS13054>
- Talavera G, Dincă V, Vila R (2013) Factors affecting species delimitations with the GMYC model: Insights from a butterfly survey. *Methods in Ecology and Evolution* 4(12): 1101–1110. <https://doi.org/10.1111/2041-210X.12107>
- Trifinopoulos JN, Lam-Tung A (2016) W-IQ-TREE: A fast online phylogenetic tool for maximum likelihood analysis. *Nucleic Acids Research* 44(W1): W232–W235. <https://doi.org/10.1093/nar/gkw256>
- Wan X (2007) Study on the systematics of Lucanidae from China (Coleoptera: Scarabaeoidea). PhD thesis, Institute of Zoology Chinese Academy of Sciences, Beijing.
- Ward PS, Downie DA (2005) The ant subfamily Pseudomyrmecinae (Hymenoptera: Formicidae): phylogeny and evolution of big-eyed arboreal ants. *Systematic Entomology* 30(2): 310–335. <https://doi.org/10.1111/j.1365-3113.2004.00281.x>
- Wild AL, Maddison DR (2008) Evaluating nuclear protein-coding genes for phylogenetic utility in beetles. *Molecular Phylogenetics and Evolution* 48(3): 877–891. <https://doi.org/10.1016/j.ympev.2008.05.023>
- Ying Y, Zhan ZH, Wan X (2021) New color patterns and new synonym of *Odontolabis sinensis* (Westwood, 1848) (Coleoptera: Lucanidae): insights from a multilocus phylogeny and species delimitation. *Zootaxa* 4926(2): 263–275. <https://doi.org/10.11646/zootaxa.4926.2.6>
- Yuan JJ, Chen D, Wan X (2021) A multilocus assessment reveals two new synonymies for East Asian *Cyclommatus* stag beetles (Coleoptera, Lucanidae). *ZooKeys* 1021: 65–79. <https://doi.org/10.3897/zookeys.1021.58832>

- Zilioli M (1998) Note on some new stag-beetles *Lucanus* from Vietnam and China. *Coleopteres* 4(11): 137–147.
- Zhang J, Kapli P, Pavlidis P, Stamatakis A (2013) A general species delimitation method with applications to phylogenetic placements. *Bioinformatics* 29(22): 2869–2876. <https://doi.org/10.1093/bioinformatics/btt499>
- Zhang D, Gao F, Jakovlic I, Zou H, Zhang J, Li WX, Wang GT (2020) PhyloSuite: An integrated and scalable desktop platform for streamlined molecular sequence data management and evolutionary phylogenetics studies. *Molecular Ecology Resources* 20(1): 348–355. <https://doi.org/10.1111/1755-0998.13096>
- Zhao N, Dai CY, Wang WJ, Zhang RY, Qu YH, Song G, Chen K, Yang XJ, Zou FS, Lei FM (2012) Pleistocene climate changes shaped the divergence and demography of Asian populations of the great tit *Parus major*: Evidence from phylogeographic analysis and ecological niche models. *Journal of Avian Biology* 43(4): 297–310. <https://doi.org/10.1111/j.1600-048X.2012.05474.x>
- Zhou XM, Sun T, Shen WZ, Shu LS, Niu YL (2006) Petrogenesis of Mesozoic granitoids and volcanic rocks in South China: A response to tectonic evolution. *Episodes* 29(1): 26–33. <https://doi.org/10.18814/epiiugs/2006/v29i1/004>
- Zhou SJ, Chen YJ, Liu J, Wan X (2019) Junior synonym of *Prosopocoilus blanchardi* (Coleoptera: Lucanidae) proposed by the integrated taxonomic approach. *Journal of Entomological Science* 54(4): 430–442. <https://doi.org/10.18474/JES18-135>

## Supplementary material I

### A list of specimens' voucher information and GenBank accession numbers used in this study

Author: Li Yang Zhou

Data type: occurrences, phylogenetic (excel document)

Explanation note: The table contains the name of the organism, the sample storage number, the location of the sample collection, latitude and longitude, and GenBank accession numbers.

Copyright notice: This dataset is made available under the Open Database License (<http://opendatacommons.org/licenses/odbl/1.0/>). The Open Database License (ODbL) is a license agreement intended to allow users to freely share, modify, and use this Dataset while maintaining this same freedom for others, provided that the original source and author(s) are credited.

Link: <https://doi.org/10.3897/zookeys.1135.89257.suppl1>

## **Supplementary material 2**

### **Morphological comparisons between phylogenetic clades**

Author: Li Yang Zhou

Data type: morphological (word document)

Copyright notice: This dataset is made available under the Open Database License (<http://opendatacommons.org/licenses/odbl/1.0/>). The Open Database License (ODbL) is a license agreement intended to allow users to freely share, modify, and use this Dataset while maintaining this same freedom for others, provided that the original source and author(s) are credited.

Link: <https://doi.org/10.3897/zookeys.1135.89257.suppl2>

## **Supplementary material 3**

### **The mean genetic distance among populations in each collection area (K2P-distances)**

Author: Li Yang Zhou

Data type: genetic distance (word document)

Explanation note: Interspecific pairwise comparison using K2P-distances based on COI among populations in each collection area.

Copyright notice: This dataset is made available under the Open Database License (<http://opendatacommons.org/licenses/odbl/1.0/>). The Open Database License (ODbL) is a license agreement intended to allow users to freely share, modify, and use this Dataset while maintaining this same freedom for others, provided that the original source and author(s) are credited.

Link: <https://doi.org/10.3897/zookeys.1135.89257.suppl3>



# DNA barcoding of *Scomberomorus* (Scombridae, Actinopterygii) reveals cryptic diversity and misidentifications

Xiao-Shu Zeng<sup>1\*</sup>, Cheng-He Sun<sup>1\*</sup>, Xiao-Ying Huang<sup>1</sup>, Ye-Ling Lao<sup>1</sup>,  
Jin-Long Huang<sup>1</sup>, Sha Li<sup>2,3</sup>, Qun Zhang<sup>1</sup>

**1** Department of Ecology and Institute of Hydrobiology, Jinan University, Guangzhou 510632, China

**2** Chinese Sturgeon Research Institute, China Three Gorges Corporation, Yichang 443100, Hubei, China

**3** Hubei Key Laboratory of Three Gorges Project for Conservation of Fishes, Yichang 443100, Hubei, China

Corresponding author: Qun Zhang ([tzhang@jnu.edu.cn](mailto:tzhang@jnu.edu.cn))

---

Academic editor: Nina Bogutskaya | Received 18 August 2022 | Accepted 15 November 2022 | Published 14 December 2022

---

<https://zoobank.org/992FEA9A-5FF1-4DFA-B138-D91EC26EE6FD>

---

**Citation:** Zeng X-S, Sun C-H, Huang X-Y, Lao Y-L, Huang J-L, Li S, Zhang Q (2022) DNA barcoding of *Scomberomorus* (Scombridae, Actinopterygii) reveals cryptic diversity and misidentifications. ZooKeys 1135: 157–170. <https://doi.org/10.3897/zookeys.1135.93631>

---

## Abstract

The genus *Scomberomorus* is economically important; however, the taxonomic status and phylogenetic relationships in this genus are not clearly resolved, making it difficult to effectively protect and exploit fish resources. To clarify the taxonomic status of *Scomberomorus* species, mitochondrial cytochrome c oxidase I (COI) gene sequences of 150 samples were analyzed. The average genetic distance among 14 species was approximately 11 times greater than the distances within species, in accordance with the ‘10× rule’ of species identification. Five of the 14 species did not form monophyletic clades based on a Bayesian inference gene tree. The application of four DNA-based species delimitation methods (automatic barcode gap discovery, barcode index numbers, Poisson tree process, and the K/θ method) yielded several key results. (1) Cryptic species were detected within *Scomberomorus commerson*. (2) A *Scomberomorus queenslandicus* sample from Australia was misidentified as *S. commerson* in the Barcode of Life Data System (BOLD). (3) Specimens originally identified as *Scomberomorus guttatus* was differentiated into four OTUs or species, two in the Yellow, South China, and Java seas, and two in geographically distant areas, one each in the Arabian Sea and the Bay of Bengal. (4) Six specimens from South Africa originally identified as *S. plurilineatus* most likely do not belong to the species. (5) Specimens identified as *S. maculatus* and *S. regalis* were conspecific; however, introgression cannot be ruled out. Our findings

---

\* These authors contribute equally to this work.

revealed cryptic diversity and difficulties in morphological identification of species in the genus *Scomberomorus*. This study provides scientifically based support for the conservation of germplasm resources of the genus *Scomberomorus*.

### Keywords

COI, conservation, cryptic species, DNA-based species delimitation, mackerel, phylogeny

## Introduction

DNA barcoding provides a complementary approach to morphological species identification (Hebert et al. 2003a). The approximately 650 bp sequence at the 5' end of the animal cytochrome c oxidase I (COI) is a standard DNA barcoding region for delineating species (Hebert et al. 2003a; Vences et al. 2005). Hebert et al. (2003b, 2004) proposed the '10× rule' of species identification and concluded that intraspecific COI genetic distances are generally less than 2% based on an analysis of 13320 species in 11 phyla. Numerous studies (e.g., Zemplak et al. 2009; Pereira et al. 2013; Kneibelsberger et al. 2015; Neves et al. 2020) have suggested that the COI gene is effective for differentiating among fish species and could be used for resolving synonymy, heteronymy, and identifying cryptic species.

The genus *Scomberomorus* belongs to the family Scombridae, one of the most popular and familiar food fish in the world (Yemmen and Gargouri 2022), composed of 18 species (Collette et al. 2001). They are rich in protein and highly unsaturated fatty acids and therefore possess high nutritional value (Lou et al. 2000). The biological characteristics and trends in the unit production of *Scomberomorus* fishes indicate that their resources are in a state of decline, and this can be attributed to overfishing and marine environmental pollution (Zheng et al. 2014). Therefore, research focused on the conservation of fish germplasm resources in the genus *Scomberomorus* is urgently needed.

Species identification in the genus *Scomberomorus* is mostly based on morphology (Collette and Russo 1985; Collette et al. 2001; Zhang et al. 2013a) and molecular data (e.g., Hoolihan et al. 2006; Habib and Sulaiman 2016; Mansourkiaei et al. 2016). Morphological identification mainly depends on the lateral line, pattern, and body color (Collette and Nauen 1983). However, the phenotype changes with growth, the color fades during preservation, and sexual dimorphism has been discovered (Collette and Nauen 1983) in some species of this genus, all of which make morphological identification difficult.

Previous molecular studies of the genus *Scomberomorus* have mostly focused on a few species within the genus (e.g., Habib and Sulaiman 2016; Mansourkiaei et al. 2016), and few studies (Banford et al. 1999; Jeena et al. 2022) have evaluated the whole genus. Owing to this lack of species representation, relationships within the *Scomberomorus* are unclear (Bayona-Vásquez et al. 2018). In this study, we conducted a DNA barcoding study of 150 specimens from the genus *Scomberomorus* to clarify their identification and provide scientific support for the conservation of germplasm resources.

## Materials and methods

### Ethical statement

The collection and sampling of specimens were reviewed and approved by the Animal Ethics Committee of Jinan University. All specimens used in this study were collected in accordance with Chinese laws. All experiments were performed to ensure optimal animal welfare and care.

### Sample collection and morphological identification

Samples were collected from 11 locations in the coastal waters of China and 116 homologous sequences were downloaded from GenBank and the Barcode of Life Data System (BOLD). The collected information is shown in Fig. 1 and Suppl. material 1: table S1. All specimens preserved in 95% ethanol in Department of Ecology and Institute of Hydrobiology, Jinan University were identified based on morphological characters known in literature (Institute of Zoology et al. 1962; Collette and Russo 1985). For 116 homologous sequences downloaded from GenBank and BOLD, samples were morphologically identified according to the original publications (Suppl. material 1: table S1), excluding directly submitted sequences.

### DNA extraction, amplification, and sequencing

Muscle tissue samples collected in our laboratory were extracted for the determination of COI sequences. DNA was extracted using a modified phenol/chloroform method (Le et al. 2010). PCR amplification was performed according to the method described by Ward et al. (2005). Universal primers FishF1 (5'-TCA ACC AAC CAC AAA GAC ATT GGC AC-3') and FishR1 (5'-TAG ACT TCT GGG TGG CCA AAG AAT CA-3') were used. The 20  $\mu$ L polymerase chain reaction (PCR) mixtures contained 7  $\mu$ L of sterilized ultrapure water, 10  $\mu$ L of PCR Mix, 1  $\mu$ L of each primer, and 1  $\mu$ L of the DNA template. The reaction conditions were as follows: pre-denaturation at 95 °C for 5 min, denaturation at 94 °C for 40 s, annealing at 54 °C for 40 s, extension at 72 °C for 50 s, for 35 cycles, and a final extension at 72 °C for 10 min. PCR products were detected by 1% agarose gel electrophoresis, purified, and sequenced by BGI Genomics Co., Ltd. (Shenzhen, China). DNA extraction, amplification, and sequencing of the downloaded homologous sequences were also performed according to GenBank and BOLD.

### Data analyses

The sequencing peaks were visualized using Chromas 2.6.6 (Technelysium Pty Ltd., South Brisbane, Queensland, Australia 2018) and the sequences were manually calibrated using Bioedit 7.2.5 (Hall 1999). Sequence characteristics were analyzed using

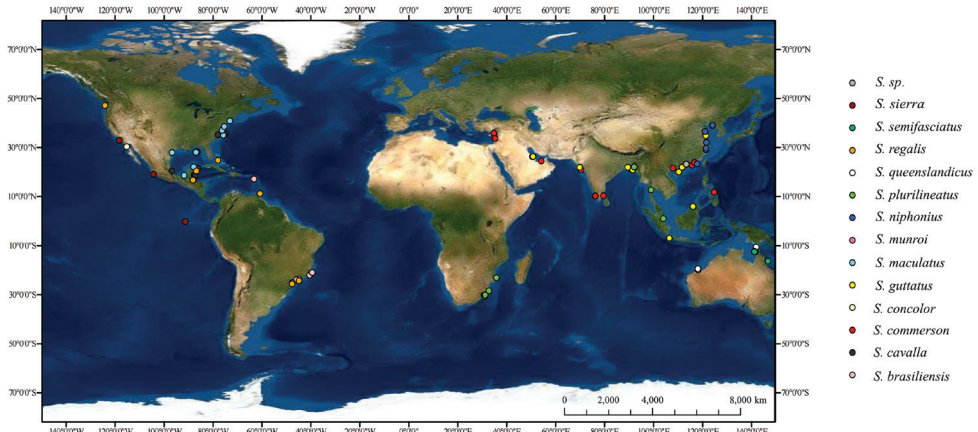


**Figure 1.** Localities of 150 samples in this study. One dot may represent more than one specimen.

MEGA 7.0 (Kumar et al. 2016), and various indices, such as base composition, variable sites (including parsimony-informative sites and singleton sites), and the transition-to-transversion ratio, were calculated.

All genetic distances were calculated based on Kimura two parameter (K2P) (Nei and Kumar 2000) distances using MEGA 7.0 (Kumar et al. 2016). A comparative analysis of all individuals within the same species was used to calculate the genetic distances between samples within each species, and these results were combined with the interspecific genetic distances to plot the barcode gap map of 14 species.

The COI gene sequences were tested for saturation using DAMBE 7.3.5 (Xia and Xie 2001). Based on the K2P substitution model, a neighbor-joining tree (NJ tree) was constructed, branch support was evaluated by 1000 repetitions of sampling, and genetic distances between and within clades were calculated. The construction of the Bayesian inference gene tree (BI tree) was performed using PhyloSuite v. 1.2.2 (Zhang et al. 2020). ModelFinder was used to select the best-fit partitioning model using the BIC criterion (Kalyanamoorthy et al. 2017). BI phylogenies were inferred using MrBayes 3.2.6 (Ronquist et al. 2012) under the HKY+I+G+F model (two parallel runs, 2000000 generations), in which the initial 25% of sampled data were discarded as burn-in. FigTree v. 1.4.4 (Rambaut 2009) was used to visualize and edit the BI tree.

We employed four species delimitation methods: (1) Automatic Barcode Gap Discovery (ABGD) (Puillandre et al. 2012); (2) Barcode Index Numbers (BIN) (Ratnasingham and Hebert 2013) implemented in BOLD to obtain operational taxonomic units (OTUs); (3) Poisson tree processes (PTP) (Zhang et al. 2013b) implemented in the bPTP server (<https://species.h-its.org/ptp/>) with the BI tree as the input file; (4) the  $K/\theta$  method: for species morphologically identified as conspecific, the mean pairwise distance within each clade ( $\theta$ ) and the minimum pairwise distance between clades ( $K$ ) in the phylogenetic tree were recorded. Clades with  $K/\theta \geq 4$  are considered reciprocally monophyletic with  $\geq 95\%$  probability (Birky et al. 2010).

## Results

### Sequence analysis

The COI gene sequences had an average length of 648 bp (567–652 bp) in 150 samples from 14 species in the genus *Scomberomorus*, and there were no base insertions or deletions. There were 453 conserved bases, accounting for 69.48% of the total number of bases, and 199 variable bases, accounting for 30.52% of the total number of bases, including 191 parsimony-informative sites and eight singleton bases. The A+T content (53.3%) was higher than the C+G content (46.7%), indicating an AT bias. The transition-to-transversion ratio was 3.1. A saturation analysis (Suppl. material 1: table S2) indicated that the base mutations did not reach saturation and were suitable for phylogenetic analyses.

### Genetic distances and barcoding gaps

The intraspecific genetic distances of 14 species of the genus *Scomberomorus* were 0%–6.0%, with an average genetic distance of 1.18%. The interspecific genetic distances were 0.3%–17.4%, with an average genetic distance of 13.0%, which was approximately 11 times higher than estimates within species. Furthermore, 79% of intraspecific genetic distances were within the range of 0%–2%. The barcoding gap map (Fig. 2) showed that the maximum intraspecific genetic distances for *S. commerson*

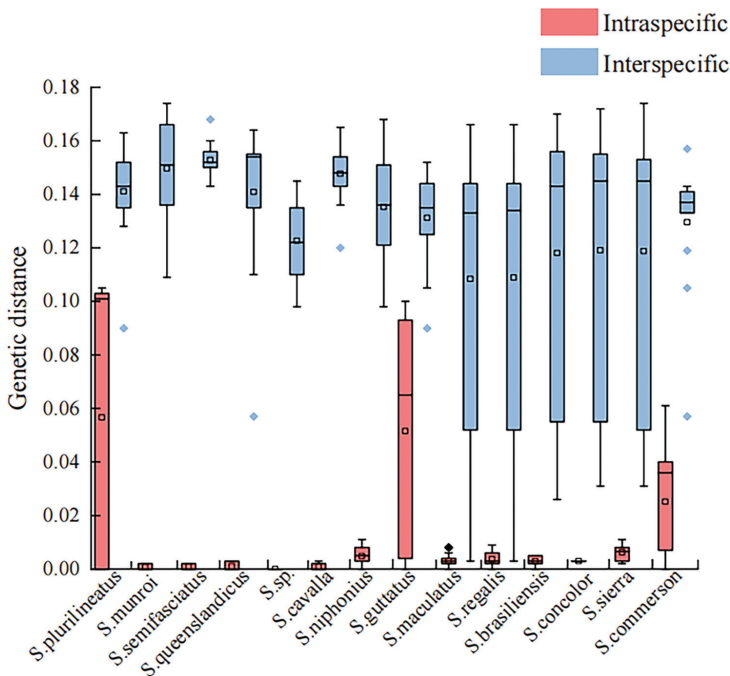


**Figure 2.** DNA barcoding gaps of 14 *Scomberomorus* species

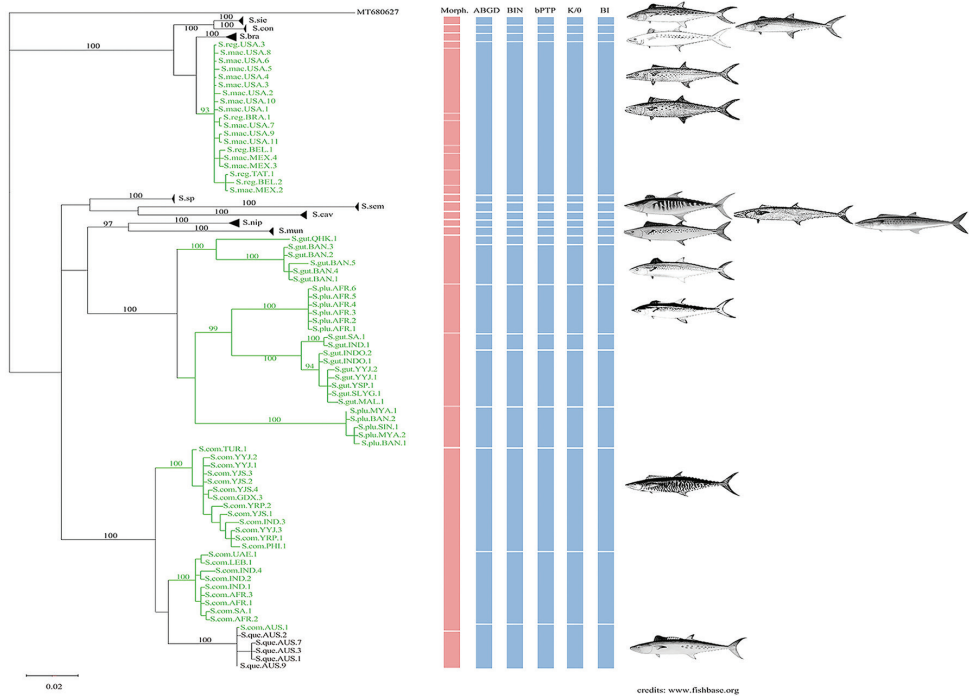


**Figure 3.** Bayesian inference (BI) tree based on the COI sequences of 14 *Scomberomorus* species. The green clades represent five species for which the species delimitation result is different based on morphology and the BI tree: *S. commerson*, *S. guttatus*, *S. plurilineatus*, *S. regalis*, and *S. maculatus*. Images of the genus *Scomberomorus* on the right from top to bottom are: *S. sierra*, *S. concolor*, *S. brasiliensis*, *S. regalis*, *S. maculatus*, *S. semifasciatus*, *S. cavalla*, *S. niphonius*, *S. munroi*, *S. guttatus*, *S. plurilineatus*, *S. commerson*, and *S. queenslandicus*. MT680627 is the outgroup. Numbers near the branches are bootstrap values.

(Lacepède, 1800), *S. guttatus* (Bloch & Schneider, 1801), *S. plurilineatus* Fourmanoir, 1966, *S. regalis* (Bloch, 1793), and *S. maculatus* (Mitchill, 1815) were not clearly different from the minimum interspecific genetic distances. In particular, the intraspecific genetic distances for *S. plurilineatus*, *S. guttatus*, and *S. commerson* were 6%, 5.2%, and 2.6%, respectively, and the interspecific genetic distance between *S. maculatus* and *S. regalis* was 0.3%. The remaining nine species had intraspecific distances of less than 2% and interspecific distances greater than 2%, forming clear DNA barcoding gaps.

### Phylogenetic clustering analysis

A BI tree (Fig. 3) and a NJ tree (Suppl. material 1: fig. S1) exhibited similar topologies. All specimens in the BI tree formed 18 clades. The average genetic distance between clades was 12.97% (2.3%–17.4%), which was 48 times higher than the average genetic distance within clades of 0.27% (0%–0.75%). *S. commerson* formed two clades with 100 bootstrap values separated by a genetic distance of 3.9% in the BI tree. One *S. commerson* sample from Australia was assigned to a lineage with *S. plurilineatus*

samples from Australia. *S. plurilineatus* and *S. guttatus* clustered together in one large clade, and *S. guttatus* formed three clades with 100, 100, and 94 bootstrap values in the BI tree. Together with the sample from Haikou, Hainan, China, *S. guttatus* was divided into four small clades with an inter-clade genetic distance of 7.48%, which was 31 times higher than the average intra-clade genetic distance (0.24%). *S. maculatus* formed a clade with *S. regalis* with 93 bootstrap value in the BI tree, and the genetic distance within the clade was only 0.3%. All other species formed monophyletic groups.

### DNA-based species delimitation

Four DNA-based species delimitation methods yielded consistent results (Fig. 3). All methods supported the division of 14 species into 18 hypothetical species by classifying *S. commerson* into two hypothetical species, *S. guttatus* into four hypothetical species, and *S. plurilineatus* into two hypothetical species and combining *S. regalis* with *S. maculatus*.

In the ABGD analysis (Suppl. material 1: fig. S2), a good barcode gap was observed when a priori intraspecific divergence was 0.0046, and this barcode gap strongly supported the division of taxa into 18 groups. The BIN analysis (Suppl. material 1: table S3) divided the 150 samples into 18 OTUs in which the genetic distance between the OTU and the nearest OTU (NN Dist) was greater than the internal maximum genetic distance (Max), indicating apparent divergence. In the bPTP analysis (Table 1), combined with the results based on morphological characters, the divisions based on bPTP (ML) were selected as the species definitions. A map (Fig. 4) of new clades of *S. guttatus* (OTU-10, OTU-11, OTU-13, and OTU-14) and *S. commerson* (OTU-16 and OTU-17) was obtained based on the bPTP results. In the K/θ method (Suppl. material 1: table S4), the clades with  $\theta = 0$  and the clade with only one sample (clade 10 in the BI tree) were considered separate OTUs; therefore, 18 OTUs were obtained.

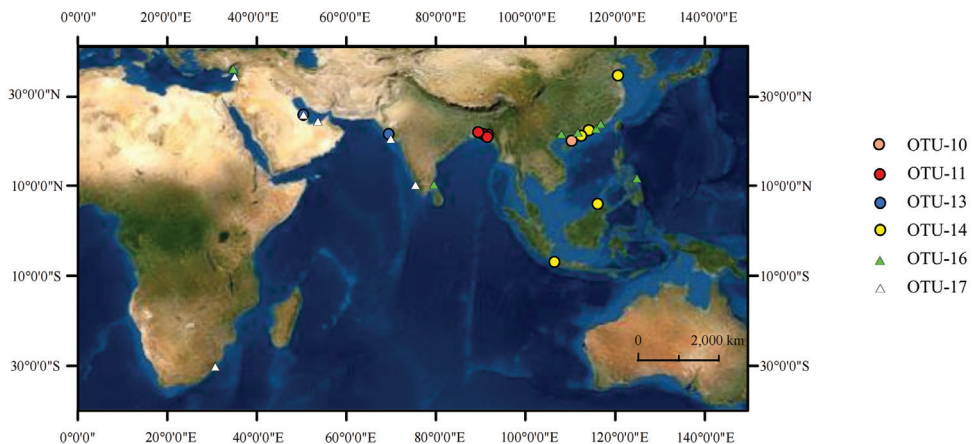


**Figure 4.** Localities of new clades of *S. guttatus* (OTU-10, OTU-11, OTU-13, and OTU-14) and *S. commerson* (OTU-16 and OTU-17) based on the bPTP results.

**Table 1.** Results for 14 *Scomberomorus* species based on a bPTP analysis.

Morphological species	OTU	Number	Catalog number
<i>S. sierra</i>	OTU-1	4	S.sie.ECU.1, S.sie.MEX.1–2, S.sie.USA.1
<i>S. concolor</i>	OTU-2	2	S.con.MEX.1, S.con.MEX.2
<i>S. brasiliensis</i>	OTU-3	14	S.bra.NET.1, S.bra.BRA.1–13
<i>S. maculatus</i> and <i>S. regalis</i>	OTU-4	28	S.mac.USA.1–11, S.mac.MEX.1–5, S.reg.BRA.1–3, S.reg.BEL.1–3, S.reg.TAT.1, S.reg.BAH.1, S.reg.MEX.1, S.reg.USA.1–3
<i>S. sp</i>	OTU-5	3	S.sp.YSP.1–3
<i>S. semifasciatus</i>	OTU-6	5	S.sem.AUS.1–5
<i>S. cavalla</i>	OTU-7	12	S.cav.USA.1–2, S.cav.MEX.1–7, S.cav.ALT.1, S.cav.USA.3–4
<i>S. niphonius</i>	OTU-8	14	S.nip.SLS.1–4, S.nip.LYK.1–3, S.nip.YRP.1–2, S.nip.LDG.1–3, S.nip. ZSM.1, S.nip.ZZS.1
<i>S. munroi</i>	OTU-9	6	S.mun.AUS.1–6
<i>S. guttatus</i>	OTU-10	1	S.gut.QHK.1
	OTU-11	5	S.gut.BAN.1–5
	OTU-12	6	S.plu.AFR.1–6
	OTU-13	2	S.gut.IND.1, S.gut.SA.1
<i>S. plurilineatus</i>	OTU-14	9	S.gut.INDO.1–2, S.gut.MAL.1, S.gut.SCS.1, S.gut.SLYG.1, S.gut. YSP.1–2, S.gut.YYJ.1–2
	OTU-15	5	S.plu.MYA.1–2, S.plu.BAN.1–2, S.plu.SIN.1
<i>S. commerson</i>	OTU-16	15	S.com.IND.3, S.com.PHI.1, S.com.GDX.1–3, S.com.YYJ.1–3, S.com. YRP.1–2, S.com.YJS.1–4, S.com.TUR.1
	OTU-17	9	S.com.AFR.1–3, S.com.SA.1, S.com.IND.1–2, S.com.IND.4, S.com. LEB.1, S.com.UAE.1
<i>S. queenslandicus</i>	OTU-18	10	S.com.AUS.1, S.que.AUS.1–9

## Discussion

According to the ‘10× rule’ of species identification and 2% threshold (Hebert et al. 2003b, 2004), taxonomic uncertainty was discovered in the samples of *S. commerson*, *S. guttatus*, *S. plurilineatus*, *S. maculatus*, and *S. regalis* on the basis of genetic distances. Phylogenetic trees and four DNA molecular definition methods all support the classification of 14 morphological species into 18 hypothetical species.

### Taxonomic identification of *S. commerson* and *S. queenslandicus* individuals

Intraspecific genetic distance in *S. commerson* (2.6%) was slightly greater than the threshold of 2%; *S. commerson* samples were assigned to three lineages in the phylogenetic trees. The samples from Australia were mixed with *S. queenslandicus* (Munro, 1943) on a single clade. Both species are distributed in Australia (Collette and Nauen 1983; Collette et al. 2001; Kuitert 2021). The adult color pattern in the two species differ: *S. commerson* has many thin, wavy, vertical stripes on the side of the body, while *S. queenslandicus* adults have about three indistinct rows of bronze-grey blotches on the sides (Collette and Nauen 1983). Adult *S. commerson* (generally 120 cm in length) is larger than *S. queenslandicus* (generally 80 cm in length), and juvenile *S. commerson* often have blotches. Therefore, we assumed that *S. commerson* from Australia in the BOLD was misidentified and was actually *S. queenslandicus*; however, further identi-

fication and determination were impossible because the corresponding image was not available in the database.

The bootstrap values for the other two clades of *S. commerson* were 100 in the BI tree. The samples in this study and the three samples from India, the Philippines, and Turkey were assigned to the same clade, and the remaining samples belonged to a separate clade. The two clades did not show obvious geographical clustering (Fig. 4), and the genetic distance between clades was 3.9% (greater than the 2% threshold). Vineesh et al. (2018) detected at least three genetically distinct populations of *S. commerson* in the Indian Ocean region. Johnson et al. (2021) studied the genetic population structure and phylogenetic relationships in the coastal waters of northern Tanzania and concluded that *S. commerson* is a single mixed population with high genetic diversity. In this study, the splitting of *S. commerson* into two clades in the molecular phylogenetic trees without obvious geographical clustering may be explained by the migratory behavior of the mackerels and the easy dispersal of their larvae over a wide area by ocean currents (Hoolihan et al. 2006), leading to secondary contact after differentiation. Therefore, cryptic species may exist in this lineage.

### Taxonomic identification of *S. guttatus* and *S. plurilineatus* individuals

The intraspecific genetic distance in *S. guttatus* was 5.2%, which was significantly greater than the 2% threshold. Four clades were formed in the phylogenetic trees, and the genetic distances between the clades were greater than 2% in the phylogenetic trees. The inter-clade genetic distance (7.48%) was 31 times higher than the average intra-clade genetic distance (0.24%), which was in accordance with the '10× rule' of species identification (Hebert et al. 2003b, 2004). Except for the sample from Haikou, Hainan, China, the other three clades clustered according to geographical distributions. The first clade consisted of individuals from the Bay of Bengal, the second clade consisted of individuals from the Arabian Gulf and Arabian Sea, and the third clade consisted of individuals from the Yellow Sea, South China Sea, and Java Sea (Fig. 4). Yu et al. (2021) conducted a DNA barcoding analysis of *Jaydia smithi* (Kotthaus, 1970) and found that the Chinese and Mediterranean populations could be divided into two groups, with an average genetic distance between the two groups of 0.044, suggesting the presence of cryptic species. Chen et al. (2017) found that the genetic distance between two *Terapon puta* (Cuvier, 1829) groups was 5% in the western Pacific and Indo-Mediterranean and suggested that the species might be divided into two subspecies or even two species. Luo et al. (2021) found that the average intraspecific genetic distance of *Lateolabrax* spp. was 3.91%, and two clades corresponding to populations in China and Japan were found in the NJ tree; the average inter-clade genetic distance (6.98%) was 14.2 times higher than the average intra-clade genetic distance (0.49%), supporting the division into two species, *L. japonicus* and *L. maculatus*. A study of *S. guttatus* from the South China Sea (Ye 2012) revealed that 19 individuals formed two major clades and suggested that the group originated from two different maternal ancestors. These findings are highly similar to the results of the present study, in which samples from the South China Sea clustered into two clades. Our data indicate that *S. guttatus* complex involves four OTUs or even four species.

*S. plurilineatus* formed two distant clades in the phylogenetic trees, one of which mixed with *S. guttatus*. The name *S. guttatus* has been misapplied to *S. plurilineatus* (Collette and Nauen 1983); therefore, six specimens of *S. plurilineatus* from South Africa might have been misidentified. According to a previous publication (Steinke et al. 2016), three specimens (JF494458–JF494460) were adults and morphological identification was performed; however, specimen images were not available in GenBank or BOLD. The other three specimens (DSL600-10, DSL1283-11, and DSL1287-11) were larvae and images of juvenile and fish eggs were obtained; however, it was not possible to accurately identify them based on the images alone.

### Taxonomic identification of *S. maculatus* and *S. regalis* individuals

The interspecific genetic distance between *S. maculatus* and *S. regalis* was 0.3% and the taxa were mixed on a single clade of the phylogenetic trees. According to FishBase (<https://fishbase.org/>) and the localities of samples in this study (Fig. 1), *S. maculatus* and *S. regalis* are both distributed in the western Atlantic Ocean, and *S. regalis* has a wider range. Banford et al. (1999) found little difference between the mitochondrial genomes of *S. maculatus* and *S. regalis* and hypothesized that the hybridization with *S. regalis* resulted in the introgressive loss of the *S. maculatus* mtDNA genome. Based on the 2% threshold and with reference to the geographic distributions of the two species, we speculated that *S. maculatus* and *S. regalis* are the same species. However, it is possible that introgressive hybridization affected the results, and we cannot exclude the possibility that the two are actually separate species.

The discovery of cryptic species in this study expands current estimates of biodiversity and allows better precautionary and scientific management, which is important to plan reasonable conservation strategies (Loxdale et al. 2016). However, owing to the wide geographical distribution of the samples, it was difficult to obtain representative samples for comparison, leading to the potential for species misidentification. In addition, the maternally inherited mitochondrial COI does not reflect bi-parentally inherited nuclear genome information, making it difficult to distinguish introgressive hybridization. Therefore, future studies of species identification should combine morphometric, nuclear genetic markers, and biological analyses to further clarify the taxonomic status of the genus *Scomberomorus* so as not to destroy the available resources (Wuketits 1997).

### Acknowledgements

We would like to thank Editage ([www.editage.cn](http://www.editage.cn)) for English language editing.

The present study was supported by the National Key R&D Program of China (Grant number 2018YFD0900802); Fishery resources survey of Guangxi Zhuang Autonomous Region (GXZC2022-G3-001062-ZHZB); Director's Fund of the Hubei Key Laboratory of Three Gorges Project for Conservation of Fishes, China Three Gorges Corporation (0704157) and the Outstanding Innovative Talents Cultivation Funded Programs for Doctoral Students of Jinan University (Project number 2021CXB022).

## References

- Banford HM, Bermingham E, Collette BB, McCafferty SS (1999) Phylogenetic systematics of the *Scomberomorus regalis* (Teleostei: Scombridae) species group: molecules, morphology and biogeography of Spanish mackerels. *Copeia* 1999(3): 596–613. <https://doi.org/10.2307/1447593>
- Bayona-Vásquez NJ, Glenn TC, Domínguez-Domínguez O, Uribe-Alcocer M, Díaz-Jaimes P (2018) Mitochondrial genomes of the Pacific sierra mackerel *Scomberomorus sierra* and the Monterey Spanish mackerel *Scomberomorus concolor* (Perciformes, Scombridae). *Conservation Genetics Resources* 10(3): 471–474. <https://doi.org/10.1007/s12686-017-0851-9>
- Birky Jr CW, Adams J, Gemmel M, Perry J (2010) Using population genetic theory and DNA sequences for species detection and identification in asexual organisms. *PLoS ONE* 5(5): e10609. <https://doi.org/10.1371/journal.pone.0010609>
- Chen L, Huang BY, Xue D (2017) DNA barcoding of Terapontidae and taxonomic status of a new record of *Terapon puta* in coastal waters of China. *Marine Fisheries* 39(2): 121–130. <https://doi.org/10.13233/j.cnki.mar.fish.2017.02.001> [in Chinese]
- Collette BB, Nauen CE (1983) An annotated and illustrated catalogue of Tunas, Mackerels, Bonitos and related species known to date. FAO Species Catalogue. Vol. 2. Scombrids of the world. FAO Fisheries Synopsis 125(2).
- Collette BB, Russo JL (1985) Morphology, systematics, and biology of the Spanish Mackerels (*Scomberomorus*, Scombridae). *Fish Bulletin* 82(4): 545–692.
- Collette BB, Reeb C, Block BA (2001) Systematics of the tunas and mackerels (Scombridae). *Fish Physiology* 19: 1–33. [https://doi.org/10.1016/S1546-5098\(01\)19002-3](https://doi.org/10.1016/S1546-5098(01)19002-3)
- Habib A, Sulaiman Z (2016) High genetic connectivity of narrow-barred Spanish mackerel (*Scomberomorus commerson*) from the South China, Bali and Java Seas. *Zoology and Ecology* 26(2): 93–99. <https://doi.org/10.1080/21658005.2016.1161121>
- Hall TA (1999) Bioedit: A user-friendly biological sequence alignment program for windows 95/98/nt. *Nucleic Acids Symposium Series* 41(41): 95–98. <https://doi.org/10.1021/bk-1999-0734.ch008>
- Hebert PDN, Cywinska A, Ball SL, DeWaard JR (2003a) Biological identifications through DNA barcodes. *Proceedings of the Royal Society of London, Series B, Biological Sciences* 270(1512): 313–321. <https://doi.org/10.1098/rspb.2002.2218>
- Hebert PDN, Ratnasingham S, DeWaard JR (2003b) Barcoding animal life: cytochrome c oxidase subunit 1 divergences among closely related species. *Proceedings of the Royal Society of London, Series B: Biological Sciences* 270(suppl\_1): S96–S99. <https://doi.org/10.1098/rsbl.2003.0025>
- Hebert PDN, Stoeckle MY, Zemplak TS, Francis CM, Godfray C (2004) Identification of birds through DNA barcodes. *PLoS Biology* 2(10): e312. <https://doi.org/10.1371/journal.pbio.0020312>
- Hoolihan JP, Anandh P, van Herwerden L (2006) Mitochondrial DNA analyses of narrow-barred Spanish mackerel (*Scomberomorus commerson*) suggest a single genetic stock in the ROPME sea area (Arabian Gulf, Gulf of Oman, and Arabian Sea). *ICES Journal of Marine Science* 63(6): 1066–1074. <https://doi.org/10.1016/j.icesjms.2006.03.012>

- Institute of Zoology, Chinese Academy of Sciences, Institute of Oceanology, Chinese Academy of Sciences, Shanghai Ocean University (1962) Fish of the South China Sea. Science Press, Beijing. [in Chinese]
- Jena NS, Rahuman S, Roul SK, Azeez PA, Vinothkumar R, Manas HM, Nesnas EA, Rathinam AMM, Surya S, Rohit P, Abdussamad EM, Gopalakrishnan A (2022) Resolved and Redeemed: A New Fleck to the Evolutionary Divergence in the Genus *Scomberomorus* Lacépède, 1801 (Scombridae) With Cryptic Speciation. *Frontiers in Marine Science* 9: e888463. <https://doi.org/10.3389/fmars.2022.888463>
- Johnson MG, Mgaya YD, Shaghude YW (2021) Analysis of the genetic stock structure and phylogenetic relationship of narrow-barred Spanish mackerel *Scomberomorus commerson* (Lacépède, 1800) along the northern Tanzanian coastal waters using mitochondrial DNA. *Regional Studies in Marine Science* 46: e101862. <https://doi.org/10.1016/j.rsma.2021.101862>
- Kalyaanamoorthy S, Minh BQ, Wong TK, Von Haeseler A, Jermiin LS (2017) ModelFinder: Fast model selection for accurate phylogenetic estimates. *Nature Methods* 14(6): 587–589. <https://doi.org/10.1038/nmeth.4285>
- Kneibelsberger T, Dunz AR, Neumann D, Geiger MF (2015) Molecular diversity of Germany's freshwater fishes and lampreys assessed by DNA barcoding. *Molecular Ecology Resources* 15(3): 562–572. <https://doi.org/10.1111/1755-0998.12322>
- Kuiter RH (2021) A Guide to Sea Fishes of Australia. Reed New Holland, Chatswood.
- Kumar S, Stecher G, Tamura K (2016) MEGA7: Molecular Evolutionary Genetics Analysis Version 7.0 for Bigger Datasets. *Molecular Biology and Evolution* 33(7): 1870–1874. <https://doi.org/10.1093/molbev/msw054>
- Le XL, Zhang Q, Zhao S (2010) A fast and efficient method for isolation of genomic DNA from fish specimens. *Shengwu Jishu Tongbao* 20(2): 202–204. <https://doi.org/10.13560/j.cnki.biotech.bull.1985.2010.02.014> [in Chinese]
- Lou YJ, Yang WG, Wang Y, Qiu DH, Dong MM (2000) Development of Spanish mackerel convenience food. *Food Science and Technology* 25(06): 31. <https://doi.org/10.13684/j.cnki.spkj.2000.06.017> [in Chinese]
- Loxdale HD, Davis BJ, Davis RA (2016) Known knowns and unknowns in biology. *Biological Journal of the Linnean Society* 117(2): 386–398. <https://doi.org/10.1111/bij.12646>
- Luo C, Zhang Q, Huang ZJ, Zhang YN (2021) DNA barcoding of some common coastal fishes from Japan and China. *Marine Fisheries* 43(01): 1–11. <https://doi.org/10.3724/SPJ.1004-2490.2021.0101> [in Chinese]
- Mansourkiaei A, Mostafavi PG, Fatemi SMR, Kaymaram F, Nazemi A (2016) Phylogenetic relationships of *Scomberomorus commerson* using sequence analysis of the mtDNA D-loop region in the Persian Gulf, Oman Sea and Arabian Sea. *international aquatic research* 8(2): 137–148. <https://doi.org/10.1007/s40071-016-0129-y>
- Nei M, Kumar S (2000) Molecular evolution and phylogenetics. Oxford University Press, USA.
- Neves JM, Almeida JP, Sturaro MJ, Fabre NN, Pereira RJ, Mott T (2020) Deep genetic divergence and paraphyly in cryptic species of *Mugil* fishes (Actinopterygii: Mugilidae). *Systematics and Biodiversity* 18(2): 116–128. <https://doi.org/10.1080/14772000.2020.1729892>

- Pereira LH, Hanner R, Foresti F, Oliveira C (2013) Can DNA barcoding accurately discriminate megadiverse Neotropical freshwater fish fauna? *BMC Genetics* 14(1): 1–14. <https://doi.org/10.1186/1471-2156-14-20>
- Puillandre N, Lambert A, Brouillet S, Achaz G (2012) ABGD, Automatic Barcode Gap Discovery for primary species delimitation. *Molecular Ecology* 21(8): 1864–1877. <https://doi.org/10.1111/j.1365-294X.2011.05239.x>
- Rambaut A (2009) FigTree version 1.4.4. Computer program distributed by the author. <http://tree.bio.ed.ac.uk/software/figtree/>
- Ratnasingham S, Hebert PDN (2013) A DNA-based registry for all animal species: The Barcode Index Number (BIN) system. *PLoS ONE* 8(7): e66213. <https://doi.org/10.1371/journal.pone.0066213>
- Ronquist F, Teslenko M, Van Der Mark P, Ayres DL, Darling A, Höhna S, Huelsenbeck JP (2012) MrBayes 3.2: Efficient Bayesian phylogenetic inference and model choice across a large model space. *Systematic Biology* 61(3): 539–542. <https://doi.org/10.1093/sysbio/sys029>
- Steinke D, Connell AD, Hebert PD (2016) Linking adults and immatures of South African marine fishes. *Genome* 59(11): 959–967. <https://doi.org/10.1139/gen-2015-0212>
- Technelysium Pty Ltd., South Brisbane, Queensland, Australia (2018) Chromas version 2.6.6.
- Vences M, Thomas M, Bonett RM, Vieites DR (2005) Deciphering amphibian diversity through DNA barcoding: Chances and challenges. *Philosophical Transactions of the Royal Society B: Biological Sciences* 360(1462): 1859–1868. <https://doi.org/10.1098/rstb.2005.1717>
- Vineesh N, Divya PR, Kathirvelpandian A, Mohitha C, Shanis CPR, Basheer VS, Gopalakrishnan A (2018) Four evolutionarily significant units among narrow-barred Spanish mackerel (*Scomberomorus commerson*) in the Indo-West Pacific region. *Marine Biodiversity* 48(4): 2025–2032. <https://doi.org/10.1007/s12526-017-0714-3>
- Ward RD, Zemlak TS, Innes BH, Last PR, Hebert PDN (2005) DNA barcoding Australia's fish species. *Philosophical Transactions of the Royal Society B: Biological Sciences* 360(1462): 1847–1857. <https://doi.org/10.1098/rstb.2005.1716>
- Wuketits FM (1997) The status of biology and the meaning of biodiversity. *Naturwissenschaften* 84(11): 473–479. <https://doi.org/10.1007/s001140050431>
- Xia X, Xie Z (2001) DAMBE: Software package for data analysis in molecular biology and evolution. *The Journal of Heredity* 92(4): 371–373. <https://doi.org/10.1093/jhered/92.4.371>
- Ye HW (2012) The South China Sea Spotted Mackerel Population Genetic Diversity Research. *Beijing Agriculture* (12): 138–139. [in Chinese]
- Yemmen C, Gargouri M (2022) Potential hazards associated with the consumption of Scombridae fish: Infection and toxicity from raw material and processing. *Journal of Applied Microbiology* 132(6): 4077–4096. <https://doi.org/10.1111/jam.15499>
- Yu ZS, Song N, Motomura H, Gao T (2021) Taxonomic revision of the cardinalfish genus *Jaydia* in China. *Biodiversity Science* 29(7): 971–979. <https://doi.org/10.17520/biods.2020320> [in Chinese]
- Zemlak TS, Ward RD, Connell AD, Holmes BH, Hebert PDN (2009) DNA barcoding reveals overlooked marine fishes. *Molecular Ecology Resources* 9: 237–242. <https://doi.org/10.1111/j.1755-0998.2009.02649.x>

- Zhang C, Ye Z, Panhwar SK, Shen W (2013a) Stock discrimination of the Japanese Spanish mackerel (*Scomberomorus niphonius*) based on the otolith shape analysis in the Yellow Sea and Bohai Sea. *Journal of Applied Ichthyology* 29(2): 368–373. <https://doi.org/10.1111/jai.12084>
- Zhang J, Kapli P, Pavlidis P, Stamatakis A (2013b) A general species delimitation method with applications to phylogenetic placements. *Bioinformatics* 29(22): 2869–2876. <https://doi.org/10.1093/bioinformatics/btt499>
- Zhang D, Gao F, Jakovčić I, Zou H, Zhang J, Li WX, Wang GT (2020) PhyloSuite: An integrated and scalable desktop platform for streamlined molecular sequence data management and evolutionary phylogenetics studies. *Molecular Ecology Resources* 20(1): 348–355. <https://doi.org/10.1111/1755-0998.13096>
- Zheng YJ, Li JS, Zhang QY, Hong WS (2014) Research progresses of resource biology of important marine pelagic food fishes in China. *Shuichan Xuebao* (01): 149–160. <https://doi.org/10.3724/SP.J.1231.2014.48799> [in Chinese]

## Supplementary material I

### DNA barcoding of *Scomberomorus* (Scombridae, Actinopterygii) reveals cryptic diversity and misidentifications

Authors: Xiao-Shu Zeng, Cheng-He Sun<sup>1</sup>, Xiao-Ying Huang, Ye-Ling Lao, Jin-Long Huang, Sha Li, Qun Zhang

Data type: Data and image (word file).

Explanation note: Specimen information of *Scomberomorus* in this study. Test of the substitution saturation of COI gene sequences of the genus *Scomberomorus*. Results of 14 *Scomberomorus* species based on the BIN analysis. Results of 14 *Scomberomorus* species based on the K/θ method. NJ tree based on the COI sequences of 14 *Scomberomorus* species. The green clades represent five species for which the species delimitation result is different based on morphology and the NJ tree: *S. commerson*, *S. guttatus*, *S. plurilineatus*, *S. regalis*, and *S. maculatus*. MT680627 is the outgroup. Numbers near the branches are bootstrap values. ABGD analysis of the genus *Scomberomorus*.

Copyright notice: This dataset is made available under the Open Database License (<http://opendatacommons.org/licenses/odbl/1.0/>). The Open Database License (ODbL) is a license agreement intended to allow users to freely share, modify, and use this Dataset while maintaining this same freedom for others, provided that the original source and author(s) are credited.

Link: <https://doi.org/10.3897/zookeys.1135.93631.suppl1>

# A new species of *Chrysotus* Meigen (Diptera, Dolichopodidae) from soybean fields in South Dakota, USA

Justin B. Runyon<sup>1</sup>, Eric Beckendorf<sup>2</sup>, Louis S. Hesler<sup>2</sup>

**1** Rocky Mountain Research Station, USDA Forest Service, 1648 S. 7<sup>th</sup> Avenue, Bozeman, Montana 59717, USA **2** North Central Agricultural Research Laboratory, USDA Agricultural Research Service, 2923 Medary Avenue, Brookings, South Dakota 57006, USA

Corresponding author: Justin B. Runyon ([justin.runyon@usda.gov](mailto:justin.runyon@usda.gov))

---

Academic editor: Marija Ivković | Received 17 September 2022 | Accepted 2 November 2022 | Published 14 December 2022

---

<https://zoobank.org/6A4AD3D3-E710-44A7-81D4-1A1C6CD32F5C>

---

**Citation:** Runyon JB, Beckendorf E, Hesler LS (2022) A new species of *Chrysotus* Meigen (Diptera, Dolichopodidae) from soybean fields in South Dakota, USA. ZooKeys 1135: 171–180. <https://doi.org/10.3897/zookeys.1135.95026>

---

## Abstract

A new long-legged fly species, *Chrysotus soya* **sp. nov.** (Diptera: Dolichopodidae), is described and illustrated from specimens collected in soybean fields near Brookings, South Dakota, USA. The abundance of this species in soybeans suggests it plays an important role as a beneficial predator.

## Keywords

Diaphorinae, egg, natural enemy, Nearctic, new species

## Introduction

The genus *Chrysotus* Meigen (Diptera: Dolichopodidae: Diaphorinae) has a worldwide distribution with about 300 described species (Yang et al. 2006), of which 111 species are known to occur in America north of Mexico (Pollet et al. 2004; Runyon and Capelari 2018). Adults of *Chrysotus* species are found in a variety of habitats, but frequently on foliage of low plants and on humid or moist soils. Larvae are poorly known, but likely occur in mud, damp soil, or leaf litter (Pollet and Brooks 2008). Like most other Dolichopodidae, adults and larvae of *Chrysotus* are generalist predators that feed on other invertebrates including aphids, leafhoppers, and thrips (Rathman et al. 1988;

Ulrich 2004). Dolichopodidae are often abundant in agroecosystems, and the beneficial role they play as natural enemies of crop pests is increasingly appreciated (Kautz and Gardiner 2019; Harterreiten-Souza et al. 2020; Krey et al. 2020).

In 2016 and 2017, we collected large numbers of an undescribed species of *Chrysotus* on red sticky traps during a study comparing pest and beneficial insect levels between soybean pest management systems in eastern South Dakota, USA (L. Hessler and E. Beckendorf, unpublished data). However, we were unable to remove these specimens from the sticky cards in satisfactory condition for description. In 2021, we re-sampled these soybean fields using red pan traps to obtain suitable specimens, which are described herein. Two specimens of this species were also found in eastern Montana, collected in colored pan traps as part of the ongoing inventory of wild bees in Montana. The purpose of this paper is to describe this new species of *Chrysotus* and provide a name so that it may be used in forthcoming publications on crop management effects on natural enemies in soybeans.

## Materials and methods

This study is based on specimens collected in 2021 using red pan traps filled with a 50/50 propylene glycol/water mixture and placed in soybean fields at the USDA Agricultural Research Service (ARS), North Central Agricultural Research Laboratory (NCARL) in Brookings, South Dakota, USA. Two additional specimens were collected in 2019 and 2020 in eastern Montana using yellow, white, and blue pan traps deployed for the ongoing inventory of wild bees of Montana at Montana State University. Specimens were transferred to 70% ethanol and dry mounted on pins using hexamethyldisiloxane (HMDS) (Brown 1993). Material from this work is housed in the following institutions: Montana Entomology Collection (MTEC), Montana State University, Bozeman, USA; National Museum of Natural History, Smithsonian Institution (USNM), Washington, D.C., USA; U.S. Department of Agriculture, Agricultural Research Service, North Central Agricultural Research Laboratory (NCARL), Brookings, South Dakota, USA.

Label data for the primary type are cited verbatim. Labels are listed from the top label down with data from each label in quotation marks and separated by a semicolon. Lines of text on labels are delimited by a slash (/) and annotations are placed in square brackets (i.e., [ ]).

The morphological nomenclature follows Cumming and Wood (2017). Homologies of the male and female terminalia follow Capellari (2018). To examine male and female terminalia using a compound microscope, specimens were macerated in 85% lactic acid by heating in a microwave oven for three to four 20-second intervals, prior to being transferred to glycerin on a depression slide for illustration. The male postabdomen on intact specimens is rotated approximately 180° and lateroflexed to the right, but in descriptions “dorsal” and “ventral” refer to the true morphological positions prior to genitalic rotation and flexion (e.g., in

lateral view, top of the page is ventral while the bottom is dorsal). Measurements of the leg segments are representative ratios given according to the formula: tibia, tarsomeres 1, 2, 3, 4, and 5.

## Results

Family Dolichopodidae, Latreille, 1809

Subfamily Diaphorinae Schiner, 1864

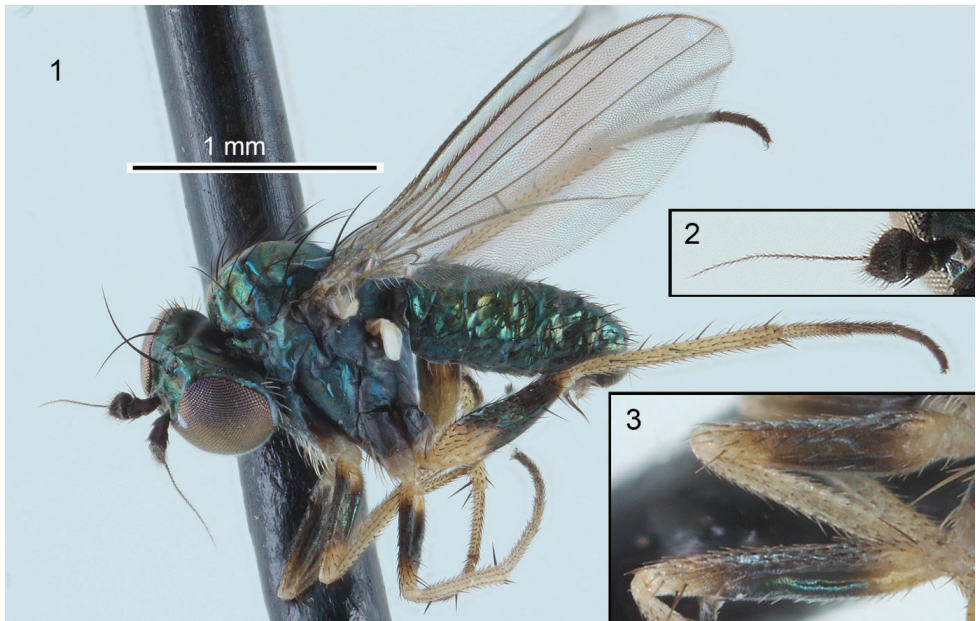
Genus *Chrysotus* Meigen, 1824

*Chrysotus soya* Runyon sp. nov.

<https://zoobank.org/6D62898C-990C-4547-B3EA-9D8835489A15>

Figs 1–8

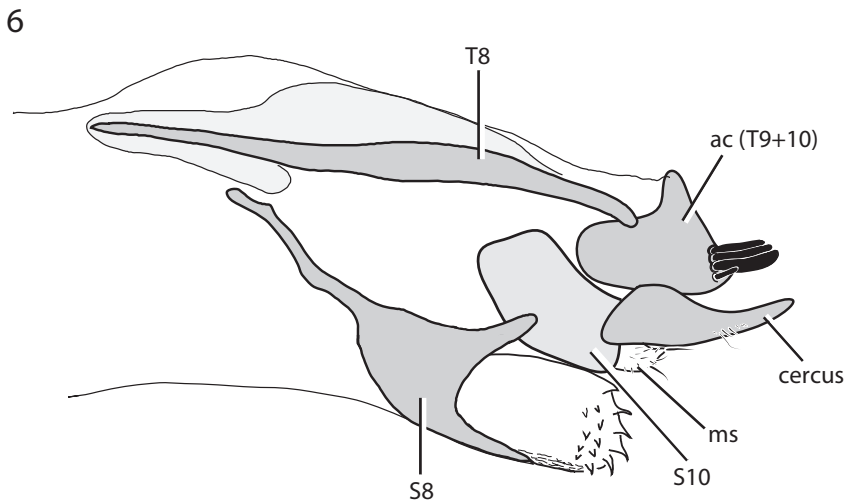
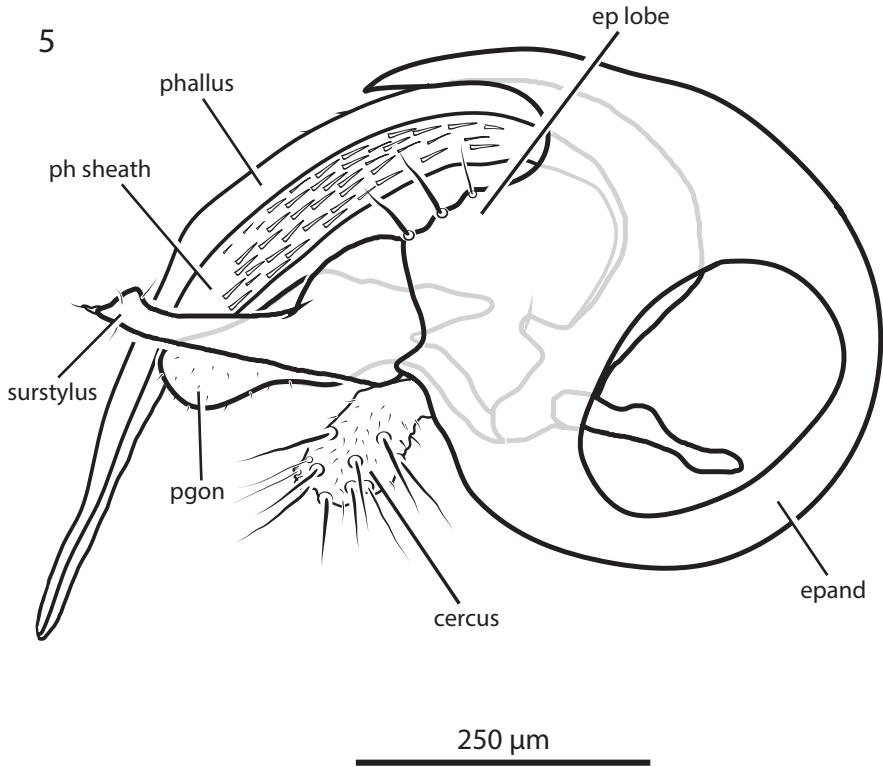
**Type material.** *Holotype*, ♂ labelled: “SOUTH DAKOTA: Brookings Co/ North Central Ag[ricultural] Res.[earch] Lab/ soybean, 44.3388°, -96.7924°/ 11 Aug 2021, red pan traps/ L. Hesler & E. Beckendorf”; “HOLOTYPE/ ♂ *Chrysotus/ soya/* Runyon [red label]” (USNM, type number USNMENT01828501). *Paratypes*: SOUTH DAKOTA: 4 ♂, 57 ♀, same data as holotype (USNM, MTEC, NCARL). MONTANA: 1 ♂, Dawson Co., 1.5 km southwest of Glendive, 47.093354°N, 104.72388°W, 625 m, 10 July 2019,



**Figures 1–3.** Habitus, antenna, and fore and mid femora of the male holotype of *Chrysotus soya* sp. nov. **1** habitus, left lateral view **2** antenna, medial view **3** fore (top) and mid (bottom) femora, posterior view.



**Figure 4.** Female habitus of *Chrysotus soya* sp. nov. In some specimens the dark coloration on the fore and mid femora is reduced, and in a few specimens, the fore and mid femora are entirely yellow.



**Figures 5, 6.** Male and female terminalia of *Chrysotus soya* sp. nov., left lateral view **5** hypopygium of male **6** ovipositor of female. Abbreviations: ac – acanthophorite; epand – epandrium; ep lobe – epandrial lobe; ms – membranous swelling; pgon – postgonite; ph sheath – sheath of phallus; s – sternite; t – tergite.

bee bowls, J. Brower (MTEC); 1 ♀, Sheridan Co., N Westby Road, 48.88642°N, 104.06082°W, 644 m, 29–30 August 2020, bee bowls, Z. Pritchard & J. Botti (MTEC).

**Diagnosis.** Males of *Chrysotus soya* sp. nov. can be distinguished from other known New World species of *Chrysotus* by the following combination of characters: eyes contiguous below antenna; antenna entirely black (Fig. 2); palpus yellow, small, oval; calypteral setae and halteres white; legs lacking male secondary sexual characteristics; and the distinct coloration of the femora (dark brown, except base and apex of fore and mid femora and nearly basal half of hind femora yellow; Figs 1, 3) with tibiae entirely yellow. In Van Duzee (1924), *C. soya* sp. nov. fits in the *C. choricus* species group and keys to *C. parvicornis* Van Duzee (= *C. exiguus* Van Duzee), but the latter species has dark femora with only the extreme tips yellow. In Robinson (1964), *C. soya* sp. nov. keys to *C. flavicauda* Van Duzee, but this species differs in having black calypteral setae and a yellowish hypopygium.

**Description. Male** (Figs 1–3, 5): body length 1.9–2.0 mm; wing length 1.7–1.8 mm. **Head:** eyes contiguous below, with anterior ommatidia slightly enlarged; upper face narrowly triangular, metallic green with dense light brown pruinosity along eye margins. Frons metallic green with bronze reflections and sparse light brown pruinosity. Postcranium metallic green with stronger bronze reflections and brown pruinosity. Palpus small, oval, light yellow, with 2–3 yellow to light brown setae. Proboscis small, brown with fine brown hairs along margin. Antenna (Fig. 2) entirely black; scape short, funnel-shaped; pedicel subequal in length to scape, spheroidal with subapical circlet of setulae; postpedicel reniform, 1.5 × wider than long, with a small point below insertion of arista-like stylus; arista-like stylus inserted just lateral to apex, length about 2× combined length of scape, pedicel and postpedicel. Postocular setae white with uppermost setae grading to dark brown. **Thorax:** scutum and scutellum metallic green-blue with strong bronze reflections and sparse light brown pruinosity; about 6 pairs of biseriata acrostichal setae in offset rows; 6 pairs of dorsocentral setae, anterior-most pair small; scutellum with 1 pair of large marginal setae and 1 pair of small lateral setae. Pleuron metallic bluish green with dense gray pruinosity; 2–3 pale setae on lower proepisternum. **Legs** (Figs 1, 3): coxae concolorous with pleuron but often slightly browner, with yellow apices; fore coxa with white to yellow-white setae; setae of mid coxa usually white but light brown in one specimen; hind coxa bare except for white to light brown anterodorsal seta. Trochanters yellow. Fore and mid femora yellow at base and apex, with broad dark brown band with green-blue reflections around middle; hind femur yellow with approximately apical half dark brown with green-blue reflections, dark coloration extending further towards base dorsally and ventrally; hind femur with 2–3 distinct anteroventral setae near tip. Tibiae entirely yellow; fore tibia with small anterodorsal seta near 1/4; mid tibia with large anterodorsal seta near 1/4 and 1/2, 2–3 indistinct posterodorsal setae on basal half, and apical ring of 4 setae with ventral seta strongest; hind tibia with anterodorsal seta near 1/4 and 1/2, 4–5 smaller posterodorsal setae, and apical ring of 4 setae. Tarsi unmodified, yellow with distal tarsomeres becoming brown, all legs with small claws and very small pulvilli. Ratios of tibia:tarsomeres for foreleg: 20–10–5–4–3–4; for midleg: 26–14–6–5–4–4; for

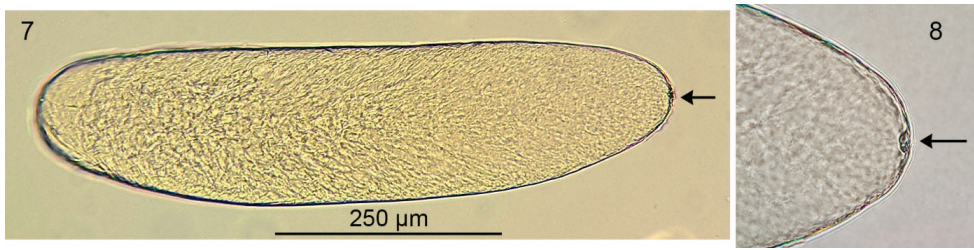
hindleg: 24–8–6–4–3–2. **Wing** (Fig. 1): hyaline, narrowly elliptical, without anal lobe. Vein  $R_{2+3}$  nearly straight and slightly but evenly diverging from  $R_{4+5}$ . Veins  $R_{4+5}$  and  $M_1$  slightly diverging before to just beyond crossvein dm-cu, then nearly parallel in apical fourth of wing. Vein  $M_1$  ending before wing apex. Crossvein dm-cu placed near 2/5 of wing length, about one-fifth as long as last part of  $CuA_1$ . Calypter white with white setae. Halter stem yellow, knob white. **Abdomen**: cylindrical, only slightly tapering to apex. Tergites dark metallic green-blue with bronze reflections and sparse gray pruinosity, with dark brown to black setae; tergite 6 with numerous setae. Sternites concolorous with tergites; basal sternites with whitish setae, distal sternites with brown to black setae; sternite 8 covering hypopygial foramen, with small setae. Hypopygium (Fig. 5) partially embedded in tip of abdomen. Hypopygial foramen left lateral. Epandrium dark brown, ventral two-thirds shiny, dorsal one-third covered with minute pale setulae; ventroapical epandrial lobe rather flattened, with 3 broad lobes each bearing a pale seta. Surstylus shining brown, broadened ventrally near base; in lateral view, narrowed apically with slightly broadened and shallowly bilobed apex; in ventral view, spatulate; with apical small pale seta and 2–3 smaller subapical setulae. Cercus pale brown with numerous pale hairs and setae. Phallus narrow with sharply pointed apex; encircled by external membranous sheath that is expanded dorsally, this expanded area contains numerous narrowly-triangular spicules. Postgonites rather large, broadly rounded and covered with sparse microtrichia apically.

**Female** (Figs 4, 6): body length 2.2–2.8 mm, wing length 2.0–2.5 mm. Similar to male except as follows: **Head**: face wide (width subequal to width of postpedicel), nearly parallel-sided, covered with dense light gray pruinosity which becomes yellowish along eyes. Palpi larger, yellow with base brownish, covered with yellow microtrichia and about five yellow to light brown setae. Postpedicel slightly shorter and wider (2.0× wider than long). **Legs**: fore and mid femora with dark brown banding often reduced to nearly absent (in a few specimens, the fore and mid femora are entirely yellow). **Abdomen**: broader, more abruptly tapering to apex. Terminalia (Fig. 6) typical for *Chrysotus* species (Capellari 2018). Acanthophorites (syntergites 9+10) each with four spines. **Eggs** (Figs 7, 8): one dissected female contained seven eggs within the abdomen. These eggs were light yellow in color, elongate oval in shape, and of uniform size: approximate length 650  $\mu\text{m}$ , width 170  $\mu\text{m}$ . Chorion smooth and shiny. Yolk homogenous and evenly distributed throughout the cytoplasm. Micropyle located at the anterior tip. No other structures (e.g., aeropyles, nucleus) could be detected using light microscopy.

**Etymology.** The specific epithet *soya* is derived from soya bean, a common name of soybean, *Glycine max*, and should be regarded as a noun in apposition.

**Distribution.** Montana, South Dakota.

**Remarks.** A heavily female-biased sex ratio of approximately 10:1 (females:males) was found in specimens of *Chrysotus soya* sp. nov. collected in South Dakota soybean fields. This skewed sex ratio occurred in both sets of specimens used in this study, those collected in red pan traps in 2021 (57 females, 5 males), and those collected on red sticky traps in 2016–2017 (1978 females, 218 males). Whether this reflects the true sex ratio is unclear, as females could be more attracted to red color than males.



**Figures 7, 8.** Egg extracted from abdomen of female *Chrysotus soya* sp. nov. **7** egg, lateral view **8** anterior tip of egg. Arrows indicate the micropyle.

## Discussion

*Chrysotus soya* sp. nov. was abundant in soybean fields in eastern South Dakota, and in fact, was the most abundant predatory insect found in these fields (L. Hesler and E. Beckendorf, unpublished data). Because *Chrysotus* species are generalist predators of other arthropods, this suggests that *C. soya* sp. nov. could play a role in pest management. For example, aphids are a frequently reported prey of adult Dolichopodidae (Ulrich 2004) and could contribute to the management of the soybean aphid (*Aphis glycines* Matsumura), the most important arthropod pest of soybeans in North America (Ragsdale et al. 2011). It is estimated that some adult Dolichopodidae could consume one aphid per minute (Rathman et al. 1988) and have the capacity to reduce aphid populations by 50% in wheat fields in Brazil (Bortolotto et al. 2022). Moreover, adult dolichopodids are reported to prey on other insects of economic importance, including caterpillars, leafhoppers, leaf miners, and thrips (Ulrich 2004).

The specimens collected in Montana offer insight into the native habitat of *C. soya* sp. nov. Both Montana specimens were collected in prairie habitat, close to a pond or river. This species is uncommon in Montana – just two specimens were found despite intensive sampling (using yellow, blue, and white pan traps) throughout Montana from 2019–2021. This suggests that *C. soya* sp. nov. naturally occurs in low abundance in grassland habitat in the Northern Great Plains and is able to thrive in the conditions created in at least some soybean fields.

The occurrence of large numbers of *C. soya* sp. nov. in soybean fields provides an opportunity to learn more about this species, and the biology of Dolichopodidae, in general. Of particular interest is documenting what adults are feeding on, and assessing the role they might play in controlling pest species. Despite being widely abundant in agriculture, little is understood about the likely benefits Dolichopodidae provide to growers (Kautz and Gardiner 2019). *Chrysotus soya* sp. nov. could serve as a model to fill this knowledge gap, increase appreciation of dolichopodids, and promote their conservation. Determining the distribution and abundance of *C. soya* sp. nov. in soybeans (and other crops) across the midwestern U.S. and Canada is of clear importance. Lastly, can the larvae be found (likely in soil), and what do they feed on? It is possible that soybean fields are too disturbed for larvae which could develop in soils of nearby

native or fallow vegetation with adults emerging and moving into fields to feed and mate. Surprisingly little is known about the larvae of most Dolichopodidae, and the discovery and study of larvae of *C. soya* could contribute significantly to our understanding of the biology of these flies.

## Acknowledgements

We thank Casey Delphia (Montana State University) for help taking photos. This research was supported in part by the USDA Forest Service, Rocky Mountain Research Station, and the USDA ARS North Central Agricultural Research Laboratory. The findings and conclusions in this publication are those of the authors and should not be construed to represent any official USDA or U.S. Government determination or policy.

## References

- Bortolotto OC, Hoshino AT, Silva KCK, Capellari RS, Menezes ADO Junior (2022) Dolichopodidae abundance in different cover crop species. *Ciência Rural* 52(5): e20201062. <https://doi.org/10.1590/0103-8478cr20201062>
- Brown BV (1993) A further chemical alternative to critical-point-drying for preparing small (or large) flies. *Fly Times* 11: 10.
- Capellari RS (2018) Gynandromorphs in *Chrysotus spectabilis* (Diptera: Dolichopodidae) and considerations for sclerite homology for the Diptera *Terminalia*. *Journal of Insect Biodiversity* 7(3): 51–57. <https://doi.org/10.12976/jib/2018.07.3.2>
- Cumming JM, Wood DM (2017) [Chapter] 3. Adult morphology and terminology. In: Kirk-Spriggs AH, Sinclair BJ (Eds) *Manual of Afrotropical Diptera*. Vol. 1. Introductory chapters and keys to Diptera families. Suricata 4. South African National Biodiversity Institute, Pretoria, 89–133.
- Harterreiten-Souza ÉS, Pujol-Luz JR, Capellari RS, Bickel D, Sujii ER (2020) Diversity and spatial distribution of predacious Dolichopodidae (Insecta: Diptera) on organic vegetable fields and adjacent habitats in Brazil. *The Florida Entomologist* 103(2): 197–205. <https://doi.org/10.1653/024.103.0207>
- Kautz AR, Gardiner MM (2019) Agricultural intensification may create an attractive sink for Dolichopodidae, a ubiquitous but understudied predatory fly family. *Journal of Insect Conservation* 23(3): 453–465. <https://doi.org/10.1007/s10841-018-0116-2>
- Krey KL, Cooper WR, Renkema JM (2020) Revealing the diet of generalist insect predators in strawberry fields: Not only pests, but other predators beware. *Environmental Entomology* 49(6): 1300–1306. <https://doi.org/10.1093/ee/nvaa125>
- Pollet M, Brooks SE (2008) Long-Legged Flies (Diptera: Dolichopodidae). In: Capinera JL (Ed.) *Encyclopedia of Entomology*. 2<sup>nd</sup> Edn. Springer, Dordrecht, 2232–2241. [https://doi.org/10.1007/978-1-4020-6359-6\\_2087](https://doi.org/10.1007/978-1-4020-6359-6_2087)

- Pollet MAA, Brooks SE, Cumming JM (2004) Catalog of the Dolichopodidae (Diptera) of America north of Mexico. *Bulletin of the American Museum of Natural History* 283: 1–114. [https://doi.org/10.1206/0003-0090\(2004\)283<0001:COTDDO>2.0.CO;2](https://doi.org/10.1206/0003-0090(2004)283<0001:COTDDO>2.0.CO;2)
- Ragsdale DW, Landis DA, Brodeur J, Heimpel GE, Desneux N (2011) Ecology and management of the soybean aphid in North America. *Annual Review of Entomology* 56(1): 375–399. <https://doi.org/10.1146/annurev-ento-120709-144755>
- Rathman RJ, Brunner JF, Hulbert SJ (1988) Feeding by *Medetera* species (Diptera: Dolichopodidae) on aphids and eriophyid mites on apple, *Malus domestica* (Rosaceae). *Proceedings of the Entomological Society of Washington* 90: 510–512.
- Robinson H (1964) A synopsis of the Dolichopodidae (Diptera) of the southeastern United States and adjacent regions. *Miscellaneous Publications of the Entomological Society of America* 4: 103–192.
- Runyon JB, Capellari RS (2018) Palpi aplenty: new species in the *Chrysotus longipalpus* species group (Diptera: Dolichopodidae). *Zootaxa* 4399(4): 579–585. <https://doi.org/10.11646/zootaxa.4399.4.8>
- Ulrich H (2004) Predation by adult Dolichopodidae (Diptera): A review of literature with an annotated prey-predator list. *Studia Dipterologica* 11: 369–403.
- Van Duzee MC (1924) A revision of the North American species of the dipterous genus *Chrysotus*. *Bulletin of the Buffalo Society of Natural Sciences* 13: 3–53.
- Yang D, Zhu Y, Wang M, Zhang L (2006) *World Catalog of Dolichopodidae (Insecta: Diptera)*. China Agricultural University Press, Beijing, 704 pp.

# Two new species and two new records of *Homidia* (Collembola, Entomobryidae) from China

Mei-dong Jing<sup>1</sup>, Yi-tong Ma<sup>1</sup>

<sup>1</sup> School of Life Sciences, Nantong University, Nantong, Jiangsu 226000, China

Corresponding author: Yi-tong Ma ([mayitong@ntu.edu.cn](mailto:mayitong@ntu.edu.cn))

---

Academic editor: Louis Deharveng | Received 22 June 2022 | Accepted 25 October 2022 | Published 15 December 2022

<https://zoobank.org/18798B62-4F1F-4026-91F1-D773E0176082>

---

**Citation:** Jing M-d, Ma Y-t (2022) Two new species and two new records of *Homidia* (Collembola, Entomobryidae) from China. ZooKeys 1135: 181–212. <https://doi.org/10.3897/zookeys.1135.89373>

---

## Abstract

*Homidia*, one of the largest genera of the family Entomobryidae, is widely distributed in China. To date, 46 species of this genus are present in China and account for approximately 60% of all known species of the genus. In the present paper, two new species of *Homidia* are described from China: *H. acutus* **sp. nov.** and *H. changensis* **sp. nov.** The former is discriminated by the brown to blue-violet pigment present on whole dorsal body and by pointed tenent hairs. The latter is characterised by having only scattered traces of brown pigment on tergites, and by the special macrochaetal formula of coxae. Additionally, two known species of the genus, *H. linhaiensis* Shi, Pan & Qi, 2009 and *H. socia* Denis, 1929, are reported from Jiangxi Province for the first time, and some of their taxonomic characters are described. A key to the Chinese species of the genus is provided.

## Keywords

Chaetotaxy, Entomobryinae, Jiangxi, taxonomy

## Introduction

*Homidia* was established as a subgenus of *Entomobrya* by Börner (1906) based on the presence of inner spines at the base of the dens in adults. Denis (1929) considered the character significant enough to raise *Homidia* to generic level. The genus is also characterised by the presence of “eyebrow” macrochaetae on the anterior part of Abd. IV in adults, the absence of scales, and a bidentate mucro with the subapical tooth much larger than the apical one.

Colour pattern plays a key role in classification of *Homidia* because intraspecific variability is very low. However, some species, such as *H. sauteri*, *H. similis*, *H. sinensis*, and *H. socia*, are widespread and some intraspecific variability of colour pattern from different regions may be sometimes present. Chaetotaxy is also very useful in species identification, especially that of Abd. I, IV, and labium basis.

The first person to study the Chinese *Homidia* was the Frenchman J. R. Denis, who reported *Homidia sauteri* (Börner, 1909) from Yunnan Province in 1928. To date, 46 species have been described or reported from China among a total of 75 species worldwide (Bellinger et al. 1996–2022, Table 1). These species are mainly distributed in the eastern region of China, especially Zhejiang Province (Fig. 1).

**Table 1.** Species checklist of *Homidia* recorded from China.

Species name	Distribution
<i>H. acutus</i> sp. nov.	Jiangxi*
<i>H. anhuiensis</i> Li & Chen, 1997	Anhui
<i>H. apigmenta</i> Shi, Pan & Zhang, 2010	Fujian
<i>H. breviseta</i> Pan, 2022	Xizang
<i>H. changensis</i> sp. nov.	Jiangxi*
<i>H. chroma</i> Pan & Yang, 2019	Guangdong
<i>H. dianbaiensis</i> (Lin, 1985)	Guangdong
<i>H. emeiensis</i> Jia, Chen & Christiansen, 2004	Sichuan
<i>H. fascia</i> Wang & Chen, 2001	Jiangsu
<i>H. formosana</i> Uchida, 1943	Taiwan; Zhejiang
<i>H. hangzhouensis</i> Pan & Ma, 2021	Zhejiang
<i>H. hexaseta</i> Pan, Shi & Zhang, 2011	Zhejiang
<i>H. huashanensis</i> Jia, Chen & Christiansen, 2005	Shaanxi
<i>H. jordanae</i> Pan, Shi & Zhang, 2011	Zhejiang
<i>H. laba</i> Christiansen & Bellinger, 1992	Zhejiang
<i>H. latifolia</i> Chen & Li, 1999	Zhejiang
<i>H. lei</i> Chen & Li, 1997	Jiangxi
<i>H. leniseta</i> Pan & Yang, 2019	Guangdong
<i>H. linhaiensis</i> Shi, Pan & Qi, 2009	Jiangxi*; Zhejiang
<i>H. maijiensis</i> Zhou & Ma, 2022	Gansu
<i>H. mediofascia</i> Shi, Pan & Bai, 2009	Shaanxi
<i>H. nigrifascia</i> Ma & Pan, 2017	Guizhou
<i>H. nigrocephala</i> Uchida, 1943	Taiwan
<i>H. obliquistria</i> Ma & Pan, 2017	Guizhou
<i>H. pentachaeta</i> Li & Christiansen, 1997	Jiangsu
<i>H. phjongjangica</i> Szeptycki, 1973	Jilin; Zhejiang
<i>H. polyseta</i> Chen, 1998	Hunan
<i>H. pseudofascia</i> Pan, Zhang & Li, 2015	Jiangsu
<i>H. pseudosinensis</i> Shi & Pan, 2012	Fujian
<i>H. qimenensis</i> Yi & Chen, 1999	Anhui; Fujian; Guangxi; Jiangxi; Zhejiang
<i>H. quadriseta</i> Pan, 2018	Zhejiang
<i>H. quadrimaculata</i> Pan, 2015	Zhejiang
<i>H. sauteri</i> (Börner, 1909)	Shanxi; Yunnan; Zhejiang
<i>H. sichuanensis</i> Jia, Zhang & Jordana, 2010	Sichuan; Guangdong; Guangxi; Guizhou; Xizang
<i>H. similis</i> Szeptycki, 1973	Zhejiang
<i>H. sinensis</i> Denis, 1929	Beijing; Fujian; Yunnan; Zhejiang; Xizang
<i>H. socia</i> Denis, 1929	Anhui; Fujian; Guangxi; Jiangsu; Jiangxi*; Taiwan; Zhejiang
<i>H. taibaiensis</i> Yuan & Pan, 2013	Shaanxi

Species name	Distribution
<i>H. tiantaiensis</i> Chen & Lin, 1998	Zhejiang
<i>H. tibetensis</i> Chen & Zhong, 1998	Xizang
<i>H. transitoria</i> Denis, 1929	Fujian
<i>H. triangulimacula</i> Pan & Shi, 2015	Zhejiang
<i>H. unichaeta</i> Pan, Shi & Zhang, 2010	Zhejiang
<i>H. wanensis</i> Pan & Ma, 2021	Anhui
<i>H. xianjuensis</i> Wu & Pan, 2016	Zhejiang
<i>H. yandangensis</i> Pan, 2015	Zhejiang
<i>H. zhangji</i> Pan & Shi, 2012	Zhejiang
<i>H. ziguiensis</i> Jia, Chen & Christiansen, 2003	Hubei

Notes: \* described or reported in this paper.



**Figure 1.** Distribution of all Chinese species of *Homidia* (the number in each region represents the number of the species reported from this province). Scale bar: 1000 km.

## Materials and methods

Specimens were collected with an aspirator and stored in 99% alcohol. They were mounted on glass slides in Marc André II solution, and were studied with a Leica DM2500 phase contrast microscope. Photographs were taken with a Leica DFC300

FX digital camera mounted on the microscope and a ZEISS Gemini SEM 300. They were enhanced with Photoshop CS2 (Adobe Inc.). The nomenclature of the dorsal macrochaetotaxy of head and interocular chaetae are described following Szeptycki (1973) and Mari Mutt (1986). Labial chaetae are designated following Gisin (1964) and tergal chaetae of the body after Szeptycki (1979).

## Abbreviations

<b>Abd</b>	abdominal segment;
<b>Ant</b>	antennal segment;
<b>asl</b>	above sea level;
<b>mac</b>	macrochaeta(e);
<b>ms</b>	specialised microchaeta(e);
<b>NTU</b>	Nantong University;
<b>sens</b>	specialised ordinary chaeta(e);
<b>Th</b>	thoracic segment.

## Taxonomic account

### *Homidia acutus* sp. nov.

<https://zoobank.org/C2B263A9-3D3D-4BEE-A1AF-2B04559281E6>

Figs 2–40, Table 2

**Type material.** *Holotype*. 1♀ on slide, CHINA, Jiangxi Province, Pingxiang City, Luxi County, Gate of Wugong Mountain, 27°29'27"N, 114°07'33"E, 393 m asl, sample number 1229, collected by Y-T Ma, 7-XI-2020, deposited in NTU. *Paratypes*. 3♀ on slides, same data as holotype.

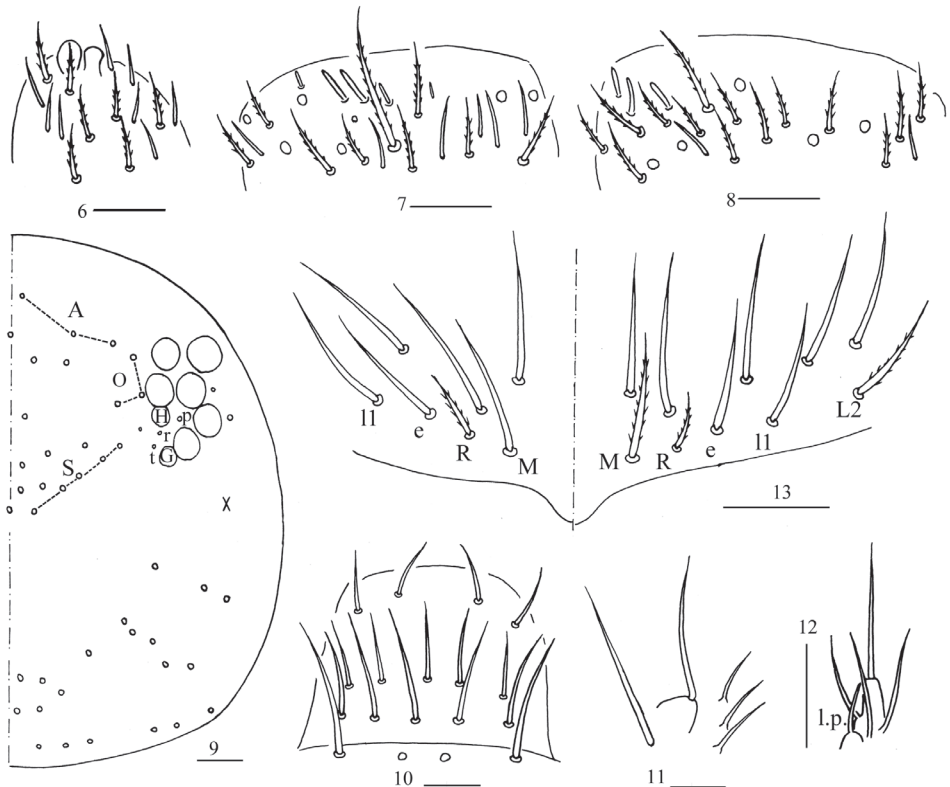
**Descriptions.** *Size*. Body length up to 2.05 mm.

**Colouration.** Ground colour pale white to pale yellow. Eye patches dark blue. Brown to blue-violet pigment present on whole dorsal body, antennae, legs, ventral tube, and manubrium. Some unpigmented irregular stripes or spots present on dorsal side of body (Figs 2–5).

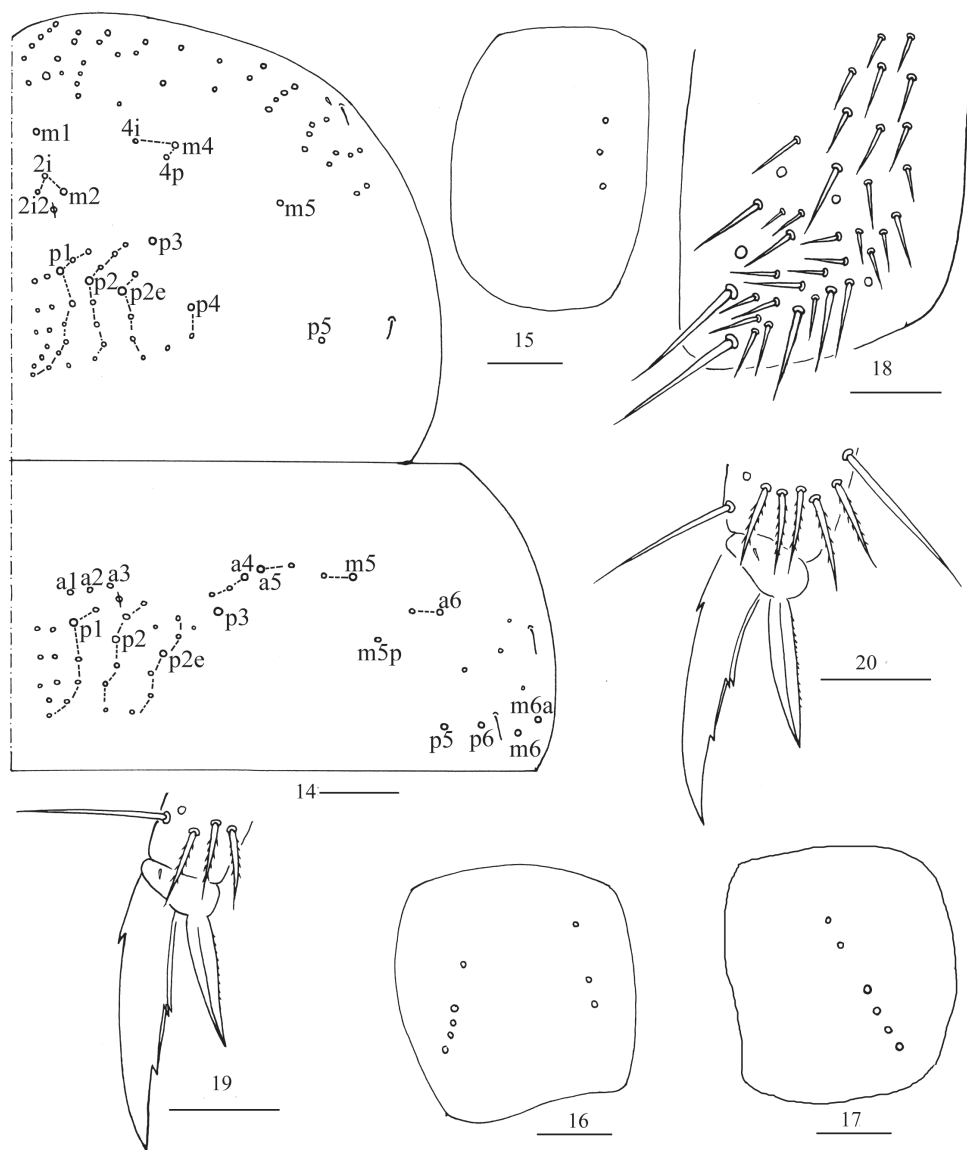
**Head.** Antenna 0.46–0.58× body length; antennal segment ratio I: II: III: IV = 1: 1.35–1.67: 1.20–1.33: 1.88–1.93. Apical bulb of Ant. IV bilobed (Fig. 6). Ant. III organ with two rod-like chaetae (Fig. 7). Ant. II with three distal rod-like chaetae (Fig. 8). Eyes 8 + 8, G and H smaller than others; interocular chaetae with p, r, and t. Dorsal cephalic chaetotaxy with three antennal (A), three ocellar (O) and five sutural (S) mac (Fig. 9). Labral chaetae as 4/5, 5, 4, all smooth; labral papillae absent (Fig. 10). Basal chaeta of maxillary outer lobe thin, subequal to apical one; sublobal plate with three smooth chaeta-like processes (Fig. 11). Lateral process (l.p.) of labial papilla E differentiated, as thick as normal chaeta, with tip almost reaching apex of papilla E (Fig. 12). Chaetal formula of labial base as MRel<sub>1</sub>L<sub>2</sub>, chaetae e and l<sub>1</sub> smooth, others ciliate, M of one side smooth in one individual, R/M as 0.45–0.60 (Fig. 13).



**Figures 2–5.** Habitus of *Homidia acutus* sp. nov. **2** lateral view **3, 4** dorsal view **5** ventral view. Scale bars: 500  $\mu\text{m}$ .

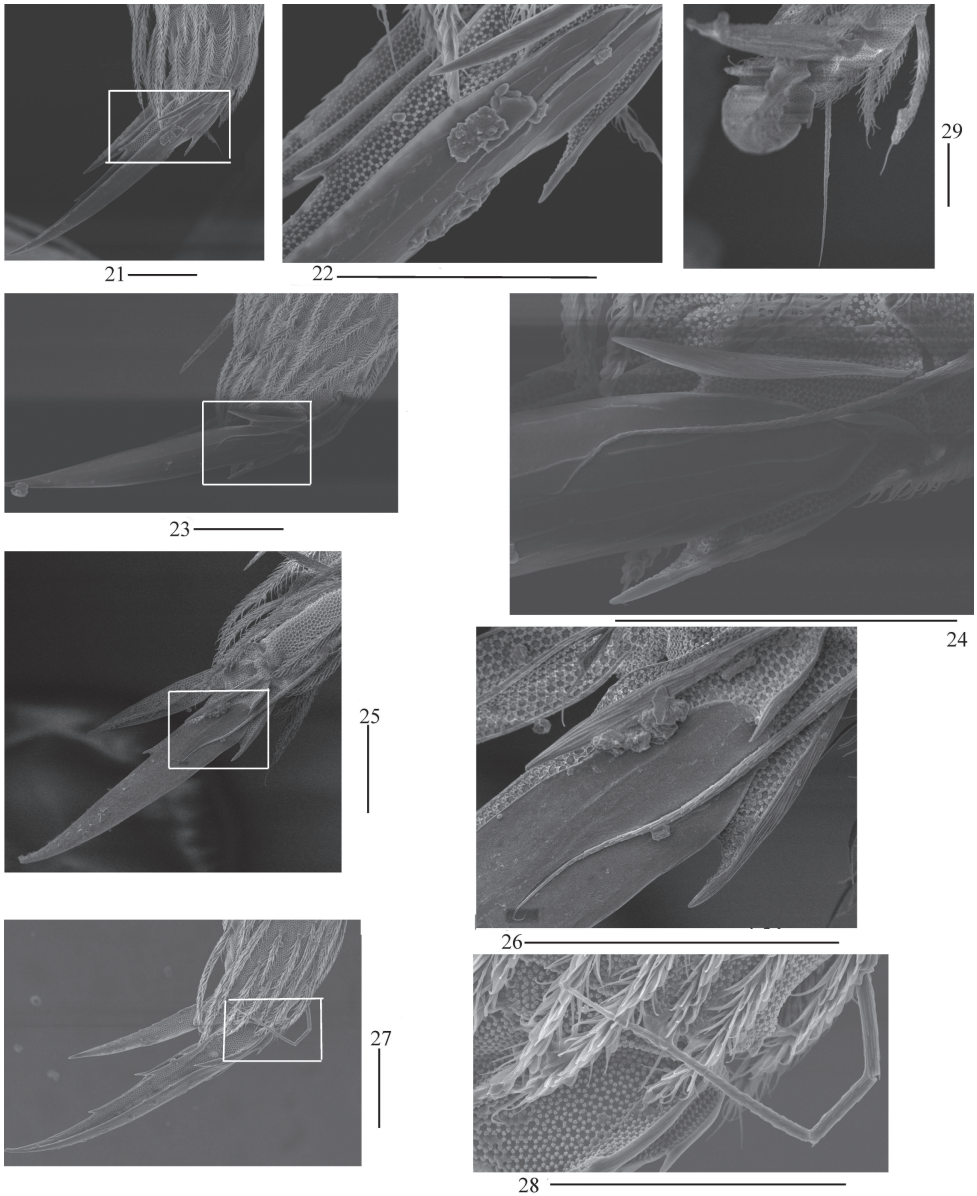


**Figures 6–13.** *Homidia acutus* sp. nov. **6** apex of Ant. IV **7** Ant. III organ **8** distal Ant. II **9** dorsal chaetotaxy of head **10** labrum **11** maxillary palp and outer lobe **12** labial palp E **13** labial base E. Scale bars: 20  $\mu\text{m}$ .



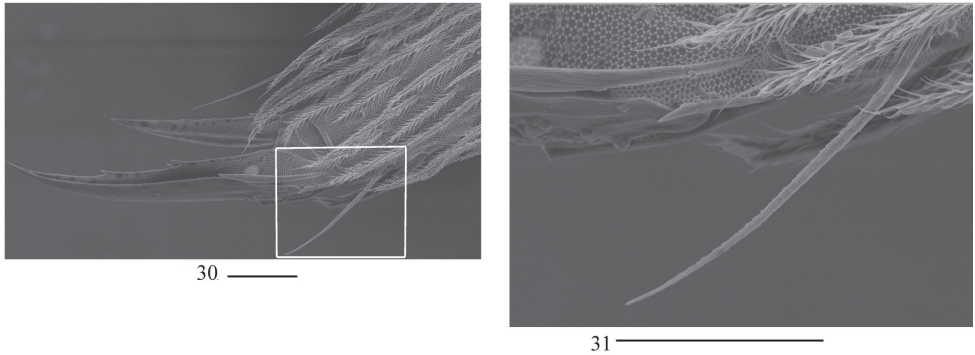
**Figures 14–20.** *Homidia acutus* sp. nov. **14** cchaetotaxy of Th. II–III **15–17** coxal chaetotaxy of fore, middle and hind leg **18** trochanteral organ **19, 20** fore and hind foot complex. Scale bar: 50  $\mu\text{m}$  (**14**); 20  $\mu\text{m}$  (**15–20**).

**Thorax.** Th. II with four medio-medial (m1, m2, m2i, m2i2), three medio-sublateral (m4, m4i, m4p), 35–38 posterior mac, one ms and two sens (ms antero-internal to sens). Th. III with 40–49 mac and two sens (Fig. 14). Pseudopores on coxae not clearly seen; coxal macrochaetal formula as 4/4+1, 3/4+2 (Figs 15–17). Trochanteral organ with 40 smooth chaetae (Fig. 18). All tenent hairs pointed and



**Figures 21–29.** SEM photomicrographs of *Homidia acutus* sp. nov. **21, 23, 25** fore foot complex of three individuals **22, 24, 26** magnifications of white rectangles of **21, 23, 25** respectively **27, 29** middle foot complex of two individuals **28** magnification of white rectangle of **27**. Scale bars: 20 μm.

shorter than inner edge of unguis. Unguis with three inner teeth, basal pair located at 0.39–0.42 distance from base of inner edge of unguis, distal unpaired tooth at 0.64–0.70 distance from base; unguiculus lanceolate, outer edge slightly serrate (Figs 19–31).



**Figures 30, 31.** SEM photomicrographs of *Homidia acutus* sp. nov. **30** hind foot complex **31** magnification of white rectangle of **30**. Scale bars: 20 μm.

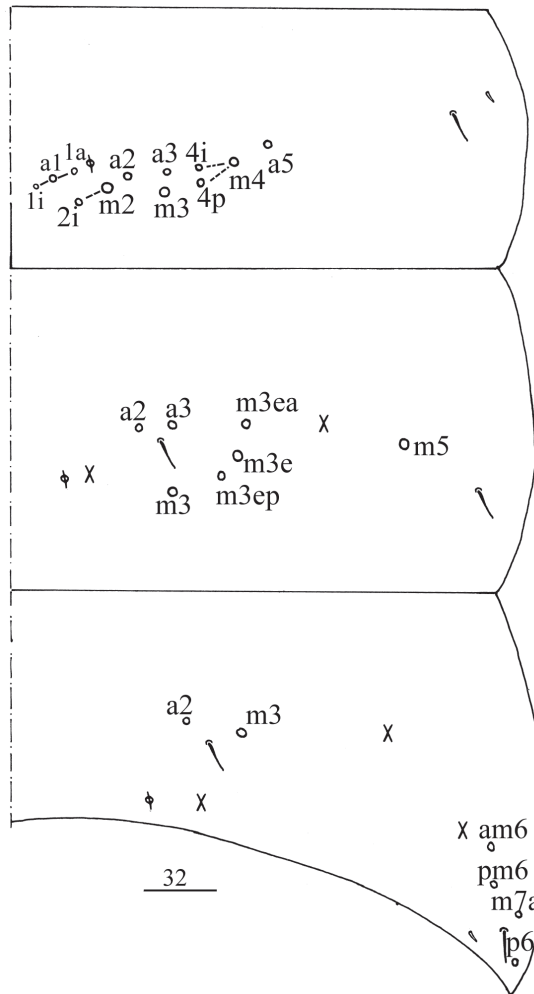


**Figure 32.** Chaetotaxy of Abd. I–III of *Homidia acutus* sp. nov. Scale bar: 50 μm.

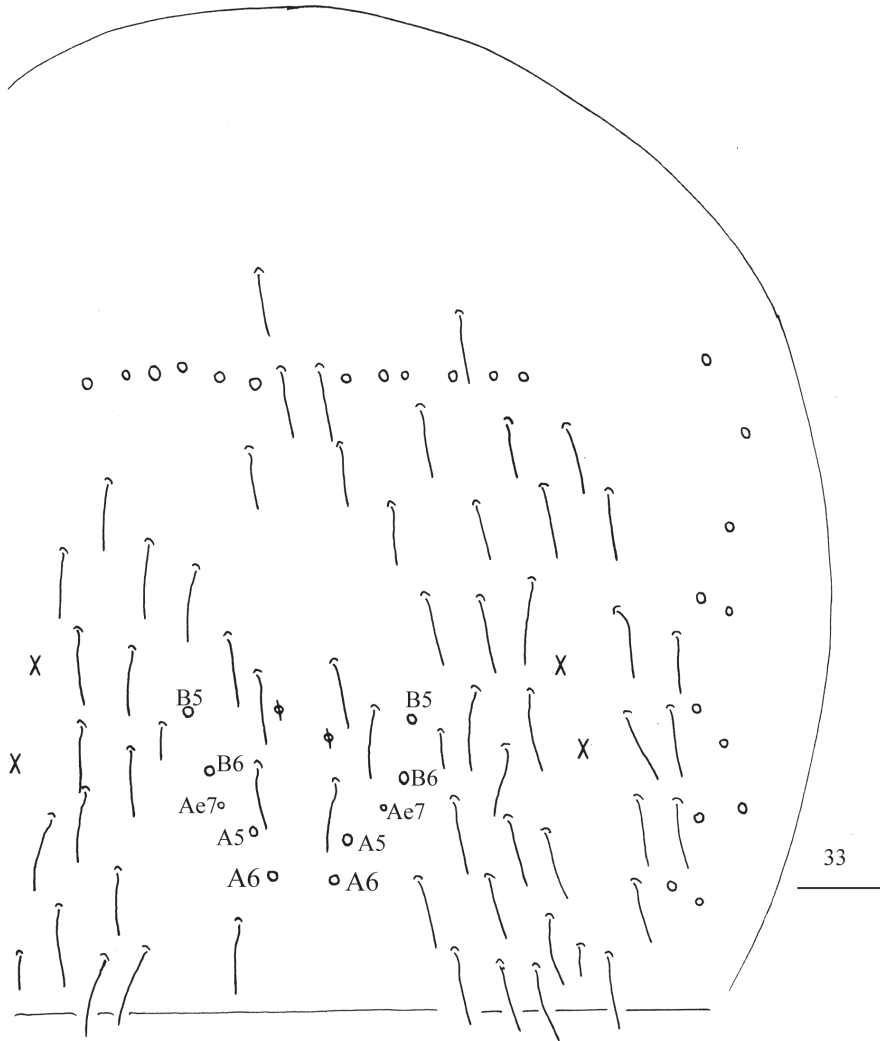
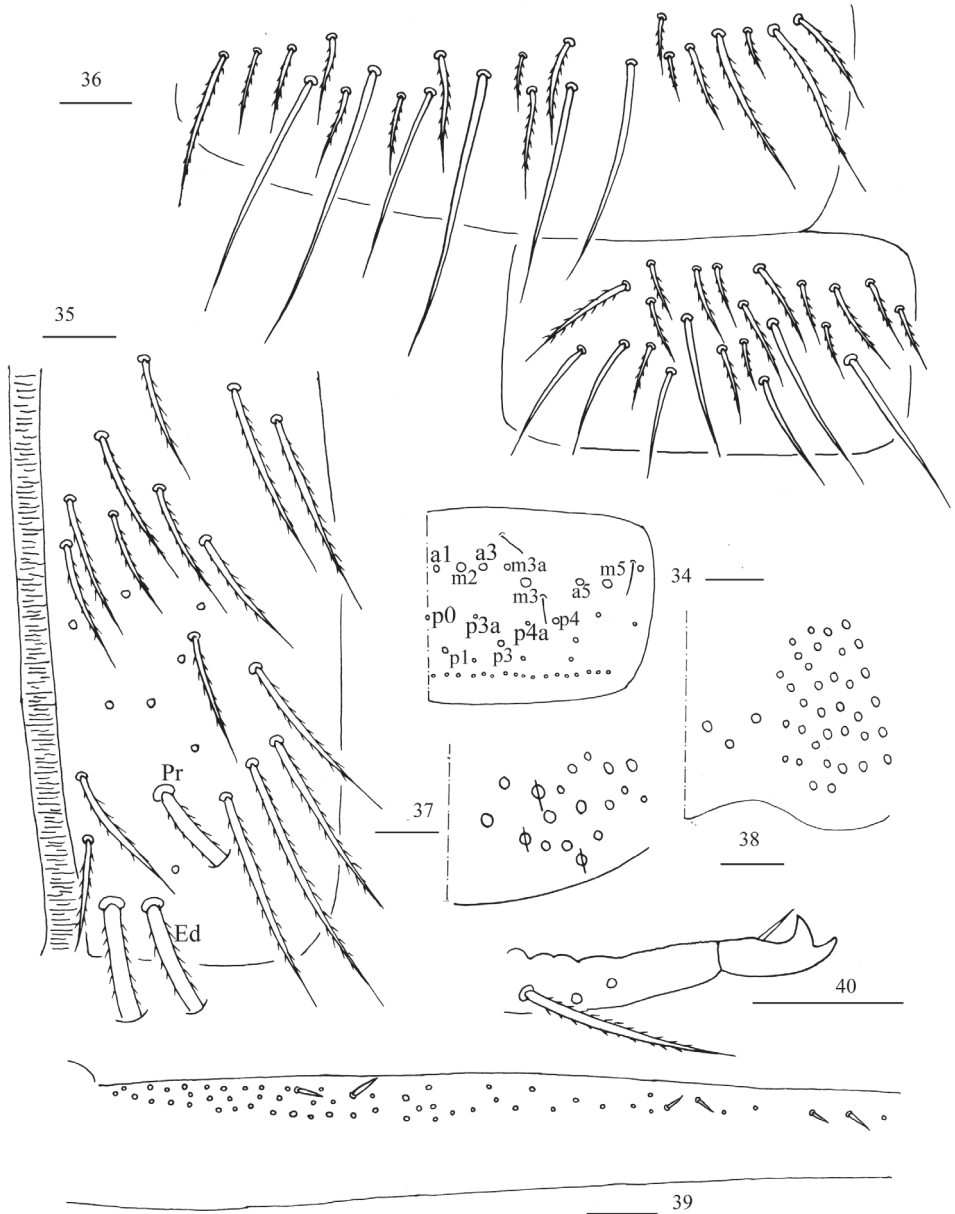


**Figure 33.** Chaetotaxy of Abd. IV of *Homidia acutus* sp. nov. Scale bar: 50  $\mu$ m.

**Abdomen.** Range of Abd. IV length as 5.00–7.50 $\times$  as dorsal axial length of Abd. III. Abd. I with 11 or 12 (a1a, a1–3, a5, m2–4, m2i, m4i, m4p, a1i sometimes present) mac, ms antero-external to sens. Abd. II with six (a2, a3, m3, m3e, m3ea, m3ep) central, one (m5) lateral mac and two sens. Abd. III with two (a2, m3) central and four (am6, pm6, m7a, p6) lateral mac, one ms and two sens (Fig. 32). Abd. IV with two normal sens and approximately half length of elongate sens; anteriorly with six mac arranged in irregular transverse row, posteriorly with five central mac (A5, A6, B5, B6, Ae7), laterally with 12 or 13 mac (Fig. 33). Abd. V with three sens, middle one posterior to m3 (Fig. 34). Anterior face of ventral tube with 27–32 ciliate chaetae, 3+3 of them as mac, line connecting proximal (Pr) and external-distal (Ed) mac oblique



**Figures 34–40.** *Homidia acutus* sp. nov. **34** chaetotaxy of Abd. V **35** anterior face of ventral tube **36** posterior face and lateral flap of ventral tube **37** manubrial plaque **38** ventro-apical part of manubrium **39** proximal section of dens (circles also representing spines) **40** mucro. Scale bars: 20  $\mu$ m.

to median furrow (Fig. 35); posterior face with six distal smooth and numerous ciliate chaetae; lateral flap with seven smooth and 10–15 ciliate chaetae (Fig. 36). Manubrial plate dorsally with 13–15 ciliate chaetae and three pseudopores (Fig. 37); ventrally

**Table 2.** Comparison between *H. acutus* sp. nov. and *H. zhangii*.

Characters	<i>H. acutus</i> sp. nov.	<i>H. zhangii</i>
Tip of tenent hairs	pointed	clavate
Mac m5 on Th. II	present	absent
Centro-posterior mac on Abd. IV	5 (A5, A6, B5, B6, Ae7)	3(4) (A6, B6, Ae7. B5 sometimes absent)
Inner teeth on unguis	3	4
Relative position of ms to sens on Abd. I	antero-external	antero-internal
Relative position of middle sens to m3 on Abd. V	postero-external	antero-external

with 32–38 ciliate chaetae on each side (Fig. 38). Dens with 32–59 smooth inner spines (Fig. 39). Mucro bidentate with subapical tooth larger than apical one; tip of basal spine reaching apex of subapical tooth; distal smooth section of dens almost equal to mucro in length (Fig. 40).

**Ecology.** In the leaves litter of *Phyllostachys edulis*.

**Etymology.** The name of the species is derived from the Latin *acutus* = pointed, which refers to the tip of tenent hairs.

**Remarks.** The new species is characterised by pointed tip of tenent hairs and this character can be used to distinguish it from all known species of *Homidia*. It is similar to *H. zhangii* Pan & Shi, 2012 in colour pattern and labium, but there are some differences between them, such as tenent hairs, posterior chaetotaxy of Abd. IV, and other characters. The detailed character comparisons are listed in Table 2.

### *Homidia changensis* sp. nov.

<https://zoobank.org/7A88BCD3-07D5-40B4-8E44-BE1F21AD6FC8>

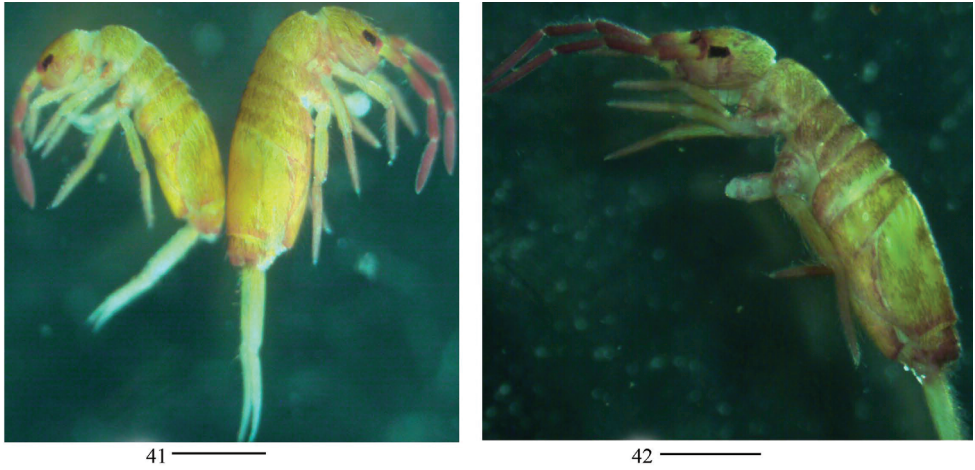
Figs 41–64, Table 3

**Type material. Holotype.** 1♀ on slide, CHINA, Jiangxi Province, Nanchang City, Xinjian District, Jiuxi, 28°47'56"N, 115°45'11"E, 168 m asl, sample number 1243, collected by Y-T Ma, 12-XI-2020, deposited in NTU. **Paratypes.** 2♀ on slides, same data as holotype.

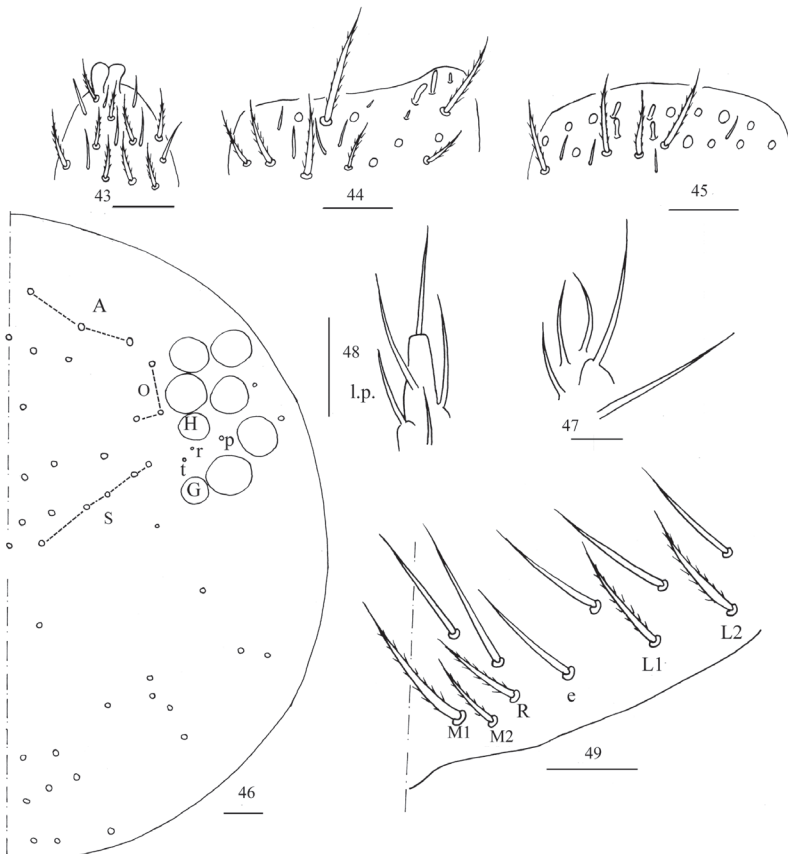
**Description. Size.** Body length up to 2.33 mm.

**Colouration.** Ground colour yellow. Ant. II–IV and distal part of Ant. I brown. Eye patches dark blue. Coxae, tibiotarsi, posterior part of Abd. IV and Abd. V with scattered brown pigment (Figs 41, 42).

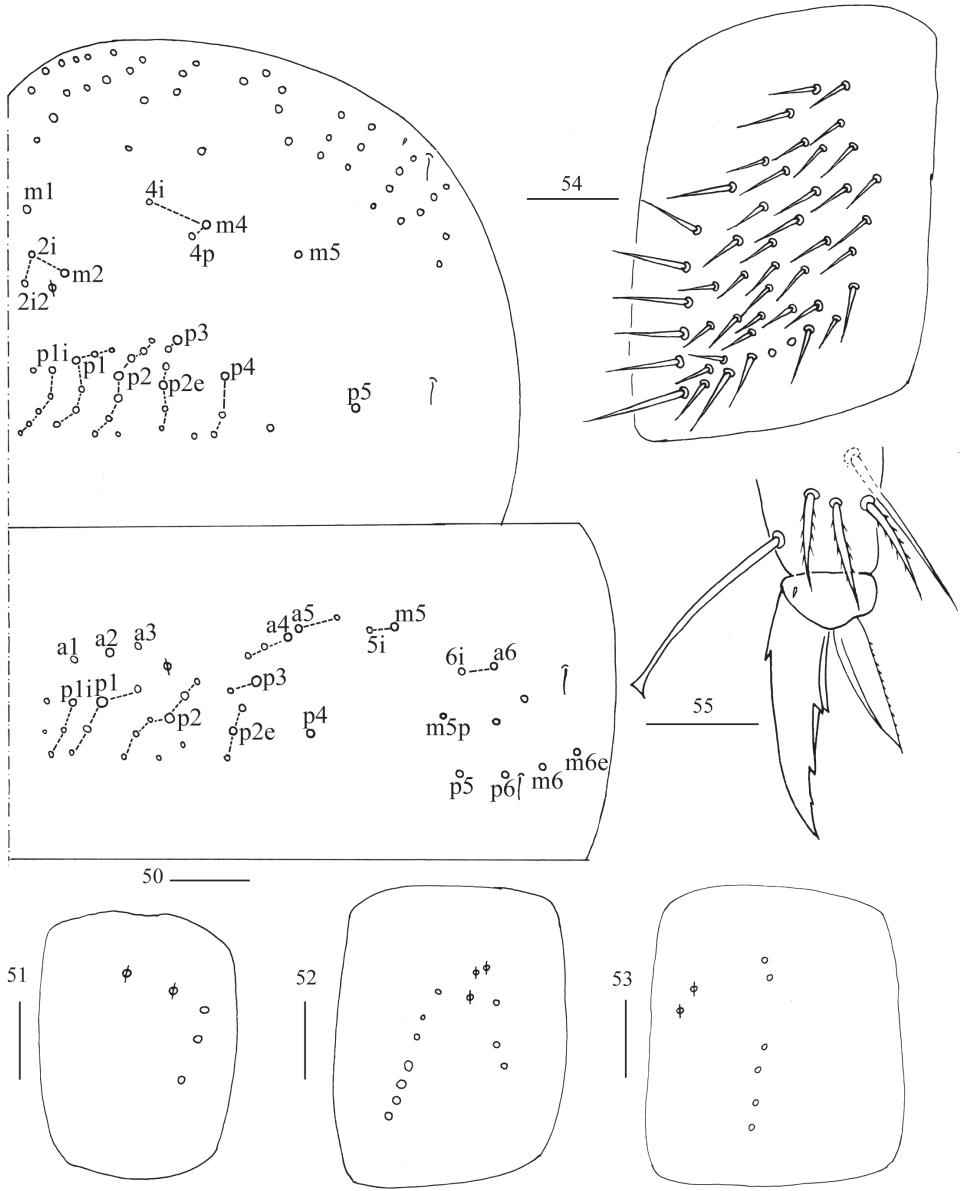
**Head.** Antenna 0.50–0.57× body length; antennal segment ratio I: II: III: IV = 1: 1.33–1.50: 1.17–1.30: 1.90–2.00. Apical bulb of Ant. IV bilobed (Fig. 43). Ant. III organ with two rod-like chaetae (Fig. 44). Ant. II with four distal rod-like chaetae (Fig. 45). Eyes 8 + 8, G and H smaller than others; interocular chaetae with p, r, and t. Dorsal cephalic chaetotaxy with three antennal (A), three ocellar (O) and five sutural (S) mac (Fig. 46). Basal chaeta of maxillary outer lobe thin, subequal to apical one; sublobal plate with three smooth chaeta-like processes (Fig. 47). Lateral process (l.p.) of labial papilla E differentiated, as thick as normal chaeta, with tip almost reaching



**Figures 41, 42.** Habitus of *Homidia changensis* sp. nov. Scale bars: 500 µm.



**Figures 43–49.** *Homidia changensis* sp. nov. **43** apex of Ant. IV **44** Ant. III organ **45** distal Ant. II **46** dorsal chaetotaxy of head **47** maxillary palp and outer lobe **48** labial palp **E 49** labial base. Scale bars: 20 µm.



**Figures 50–55.** *Homidia changensis* sp. nov. **50** chaetotaxy of Th. II–III **51–53** coxal chaetotaxy of fore, middle and hind leg **54** trochanteral organ **55** hind foot complex. Scale bar: 50  $\mu\text{m}$  (**50**); 20  $\mu\text{m}$  (**51–55**).

apex of papilla E (Fig. 48). Chaetal formula of labial base as  $M_1M_2ReL_1L_2$ , chaeta e smooth, others ciliate,  $R/M_1$  as 0.63–0.70 (Fig. 49).

**Thorax.** Th. II with four medio-medial (m1, m2, m2i, m2i2), three medio-sublateral (m4, m4i, m4p), 32–38 posterior mac, one ms and two sens (ms antero-internal

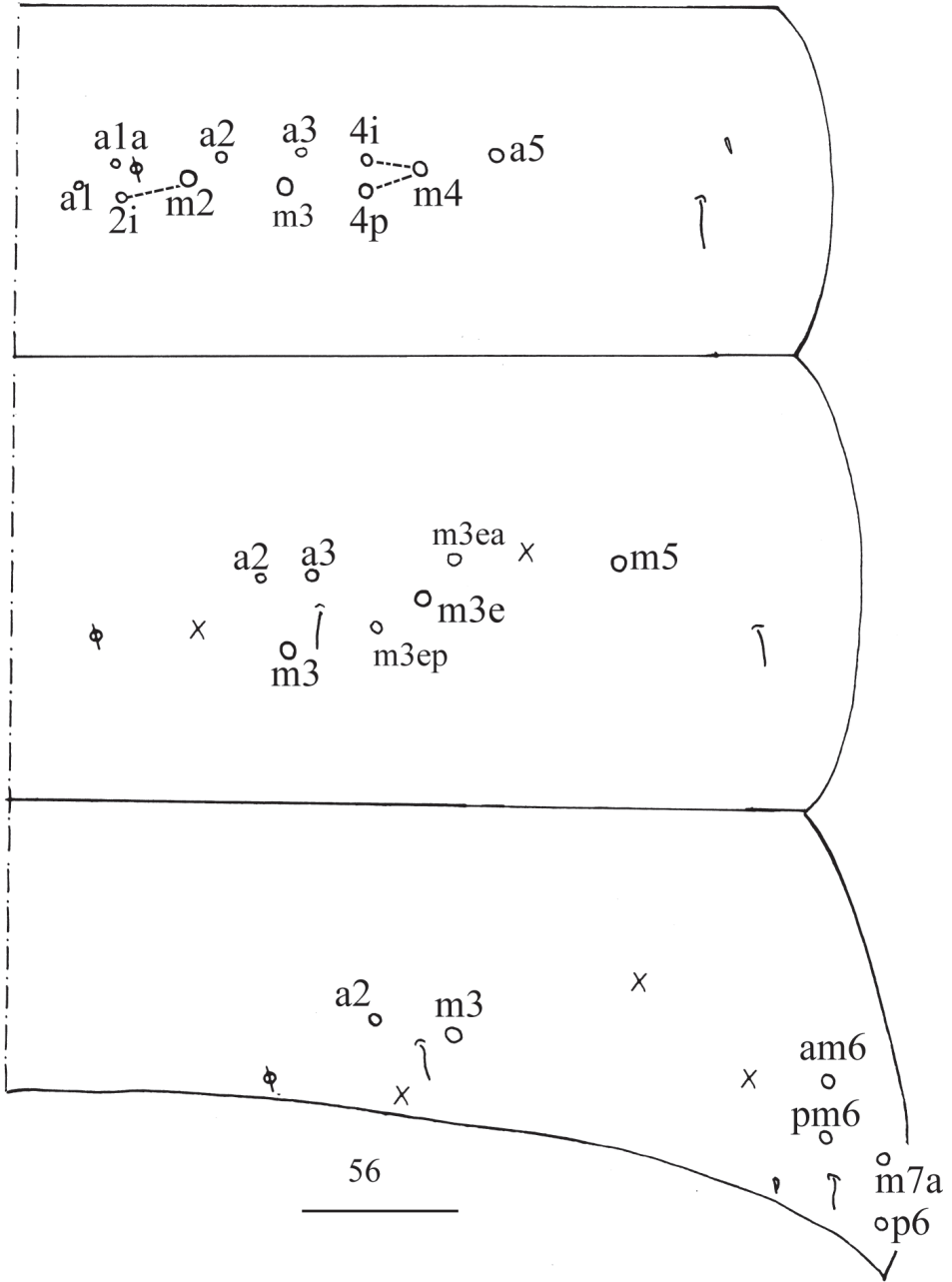


**Figure 56.** Chaetotaxy of Abd. I–III of *Homidia changensis* sp. nov. Scale bar: 50  $\mu$ m.

to sens). Th. III with 38–47 mac and two sens (Fig. 50). Pseudopores on coxa I–III as 2, 3, 2, respectively; coxal macrochaetal formula as 3/4+3(4), 3/4+2 (Figs 51–53). Trochanteral organ with 45–48 smooth chaetae (Fig. 54). Tenent hairs clavate and

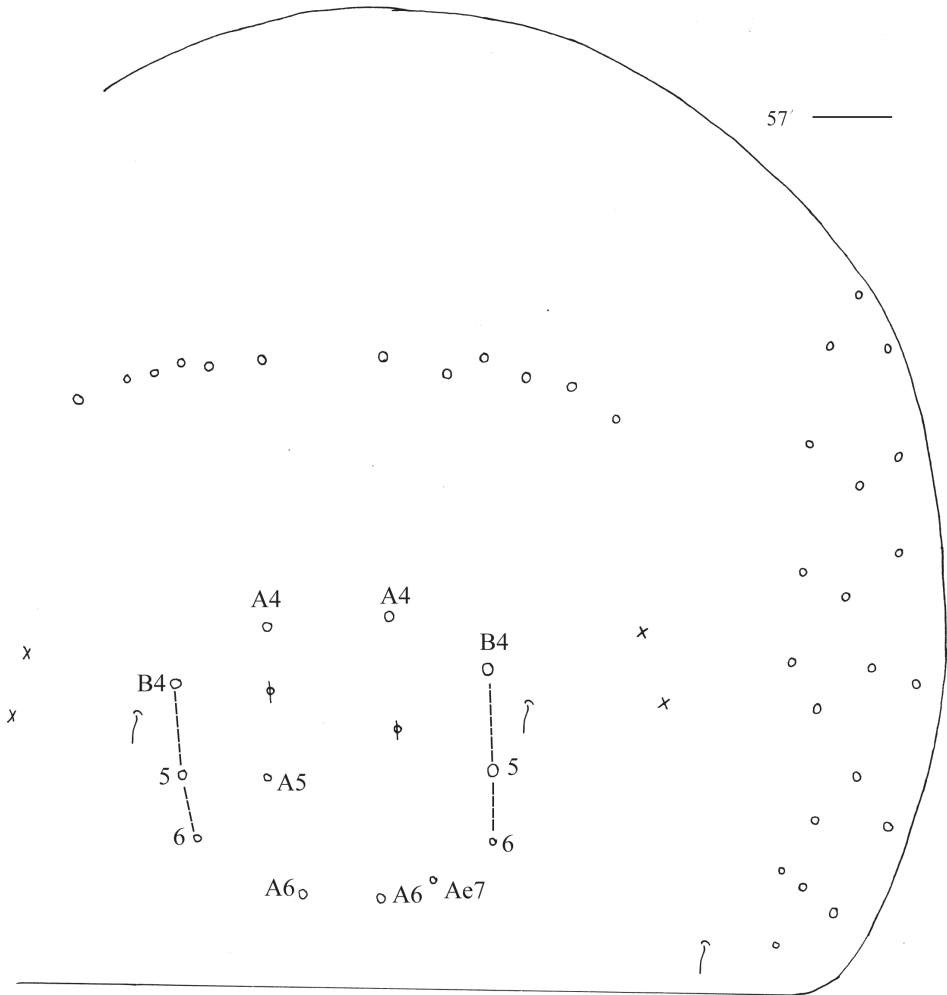
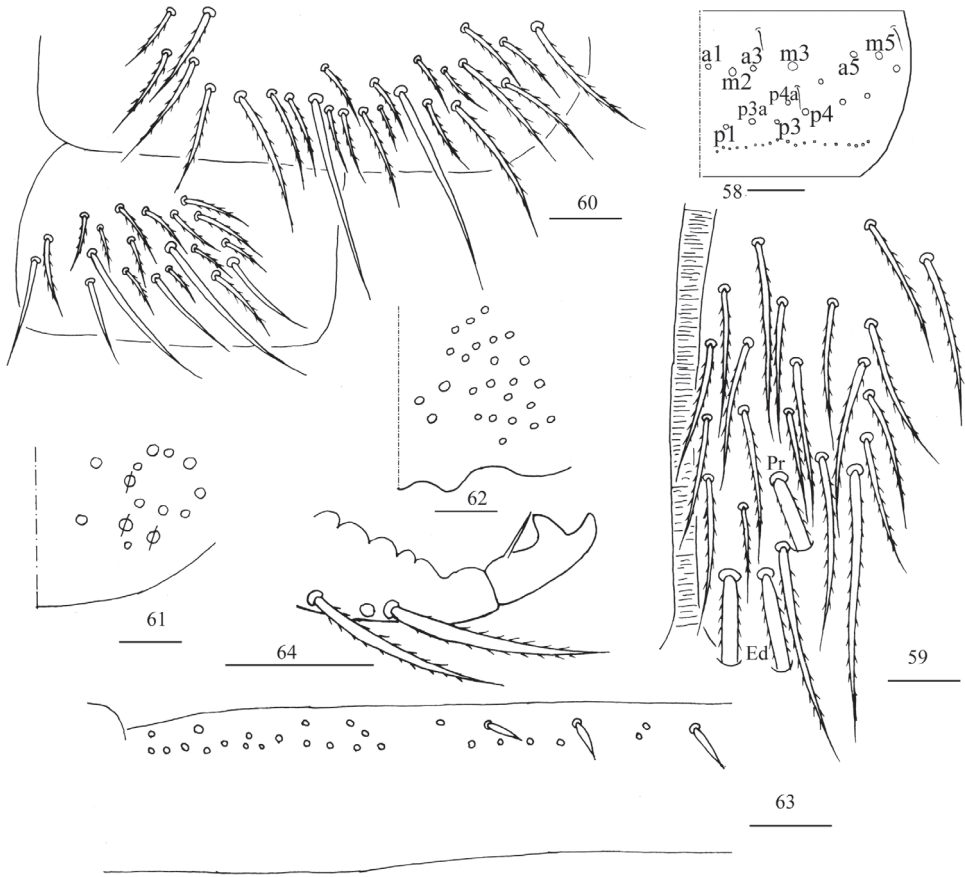


**Figure 57.** Chaetotaxy of Abd. IV of *Homidia changensis* sp. nov. Scale bar: 50  $\mu$ m.

almost equal to inner edge of unguis. Unguis with four inner teeth, basal pair located at 0.31–0.41 distance from base of inner edge of unguis, distal unpaired teeth at 0.63–0.71 and 0.83–0.84 distance from base; unguiculus lanceolate, outer edge slightly serrate (Fig. 55).

**Abdomen.** Range of Abd. IV length as 6.03–10.40 $\times$  as dorsal axial length of Abd. III. Abd. I with 11 (a1a, a1–3, a5, m2–4, m2i, m4i, m4p) mac, ms antero-external to sens. Abd. II with six (a2, a3, m3, m3e, m3ea, m3ep) central, one (m5) lateral mac and two sens. Abd. III with two (a2, m3) central and four (am6, pm6, m7a, p6) lateral mac, one ms and two sens (Fig. 56). Abd. IV with two normal sens; anteriorly with six or seven mac arranged in irregular transverse row, posteriorly with 5–7 (A4, A6, B4–6, A5 and Ae7 sometimes present) central mac, laterally with 20–22 mac (Fig. 57).



**Figures 58–64.** *Homidia changensis* sp. nov. **58** chaetotaxy of Abd. V **59** anterior face of ventral tube **60** posterior face and lateral flap of ventral tube **61** manubrial plaque (a circle with a slash means a pseudopore) **62** ventro-apical part of manubrium **63** proximal section of dens (circles also representing spines) **64** mucro. Scale bars: 20  $\mu$ m.

Abd. V with three sens, middle one posterior to m3 (Fig. 58). Anterior face of ventral tube with 24–27 ciliate chaetae, 3+3 of them as mac, line connecting proximal (Pr) and external-distal (Ed) mac oblique to median furrow (Fig. 59); posterior face with two or four distal smooth and numerous ciliate chaetae; lateral flap with six smooth and 14–16 ciliate chaetae (Fig. 60). Manubrial plaque dorsally with 11 or 12 ciliate chaetae and 2–4 pseudopores (Fig. 61); ventrally with 25–28 ciliate chaetae on each side (Fig. 62). Dens with 16–28 smooth inner spines (Fig. 63). Mucro bidentate with subapical tooth larger than apical one; tip of basal spine reaching apex of subapical tooth; distal smooth section of dens shorter than mucro in length (Fig. 64).

**Ecology.** In the leaves litter of *Phyllostachys edulis*.

**Etymology.** Named after its locality: Nanchang City, which is abbreviated as Chang.

**Table 3.** Comparison between *H. changensis* sp. nov. and similar species.

Characters	<i>H. changensis</i> sp. nov.	<i>H. huashanensis</i>	<i>H. jordanai</i>	<i>H. unichaeta</i>	<i>H. koreana</i>
Ground colour	yellow	hazel	pale yellow	pale to yellowish	brown
Length ratio of antenna to body	0.50–0.57	0.67	1.00	0.80–1.00	unknown
Chaetal formula of labial base	M <sub>1</sub> M <sub>2</sub> ReL <sub>1</sub> L <sub>2</sub>	MRE(c)L <sub>1</sub> L <sub>2</sub>	MReL <sub>1</sub> L <sub>2</sub>	MRel <sub>1</sub> L <sub>2</sub>	MReL <sub>1</sub> L <sub>2</sub>
Chaetae a1, a1a on Abd. I	present	present	absent	a1 rarely present, a1a absent	absent
Central mac on Abd. III	2	2	1	2	2
Centro-posterior mac on Abd. IV	5–7	7–9	2(3)	1	6
Dental spines	16–28	80–114	20–40	19–23	40–50

**Remarks.** The new species is characterised by its colour pattern and coxal macrochaetotaxy, and can be easily distinguished from all known species of *Homidia*. It is similar to the Chinese species *H. huashanensis* Jia, Chen & Christiansen, 2005, *H. jordanai* Pan, Shi & Zhang, 2011, and *H. unichaeta* Pan, Shi & Zhang, 2010 and the Korean species *H. koreana* Lee & Lee, 1981 in colour pattern, but significant differences exist between these species, such as chaetotaxy on Abd. I and IV and number of dental spines (Table 3).

### *Homidia linhaiensis* Shi, Pan & Qi, 2009

Figs 65–75

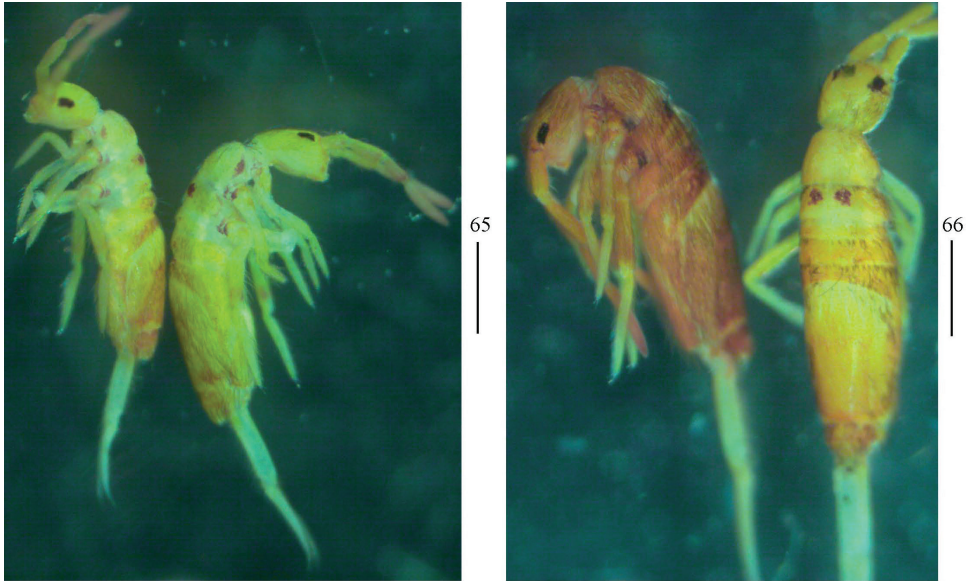
*Homidia linhaiensis* Shi, Pan & Qi, 2009: 63.

**Examined specimens.** 2♀ on slides, CHINA, Jiangxi Province, Pingxiang City, Luxi Town, Shankouyan Park, 27°36'55"N, 114°01'39"E, 144 m asl, sample number 1231, collected by Y-T Ma, 7-XI-2020, in the rotten leaves of *Salix babylonica*; 5♀ on slides, CHINA, Jiangxi Province, Nanchang City, Xinjian District, Shizifeng Park, 28°48'48"N, 115°43'15"E, 193 m asl, sample number 1241, collected by Y-T Ma, 12-XI-2020, in the leaves litter of *Phyllostachys edulis*; 2♀ on slides, CHINA, Jiangxi Province, Shangrao City, Yunbifeng Park, 28°27'47"N, 117°58'55"E, 101 m asl, sample number 1246, collected by Y-T Ma, 14-XI-2020, in the leaves litter of *Phyllostachys edulis*.

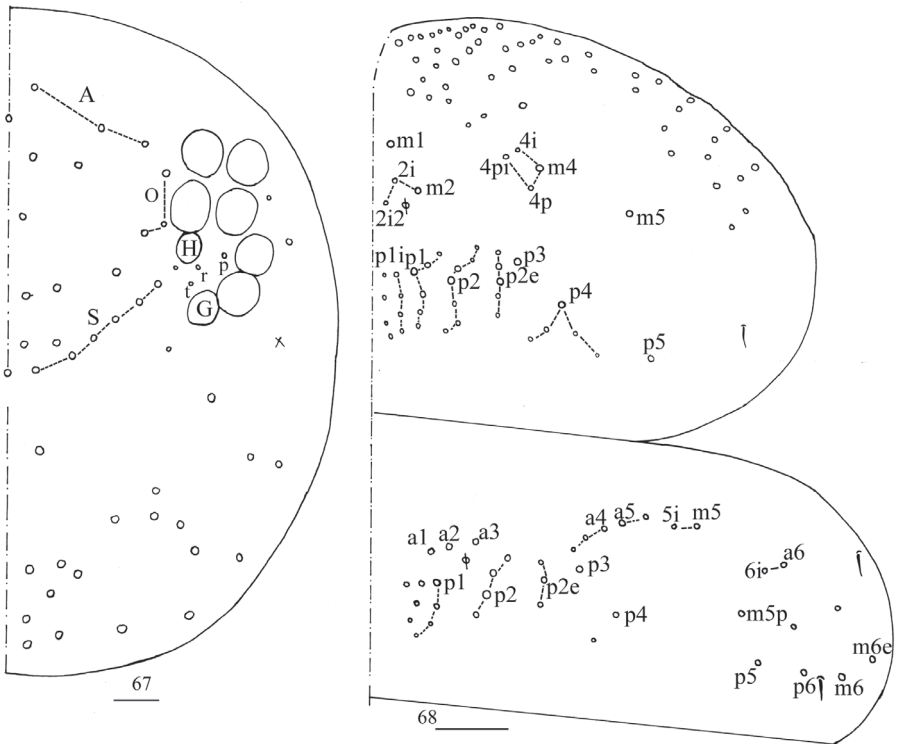
**Description. Size.** Body length up to 2.00 mm.

**Colouration.** Ground colour yellow. Ant. III & IV with scattered blue pigment. Eye patches dark blue. Th. III with a pair of dark blue spots and coxae and lateral of Th. II also with blue pigment (Figs 65, 66).

**Head.** Antenna 0.44–0.59× body length; antennal segment ratio I: II: III: IV = 1: 1.30–1.47: 1.21–1.33: 2.13–2.51. Eyes 8 + 8, interocular chaetae with p, r, and t. Dorsal cephalic chaetotaxy with three antennal (A), three ocellar (O) and six sutural



**Figures 65, 66.** Habitus of *Homidia linbaiensis*. Scale bars: 500  $\mu$ m.



**Figures 67, 68.** *Homidia linbaiensis* **67** dorsal chaetotaxy of head **68** chaetotaxy of Th. II–III. Scale bars: 20  $\mu$ m (**67**); 50  $\mu$ m (**68**).

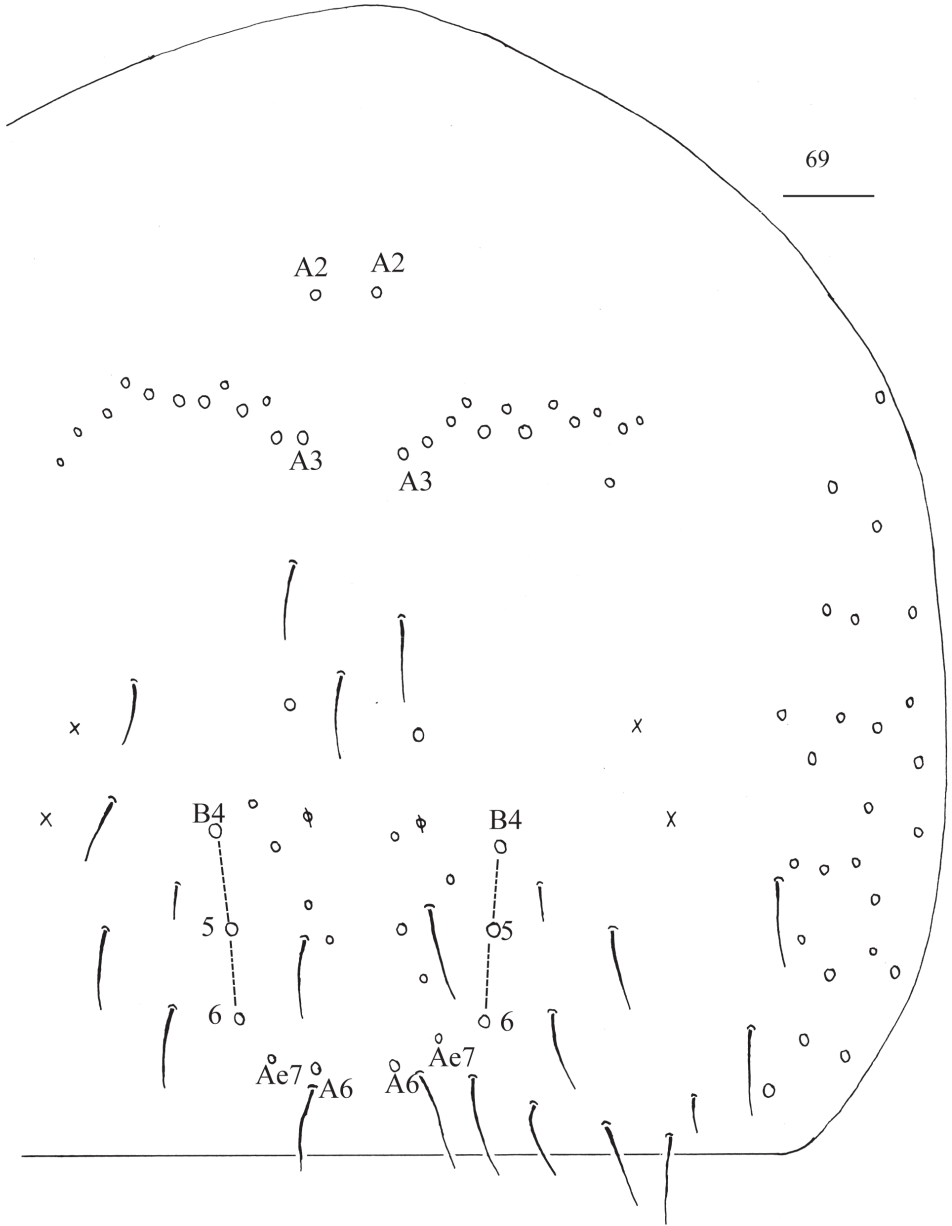
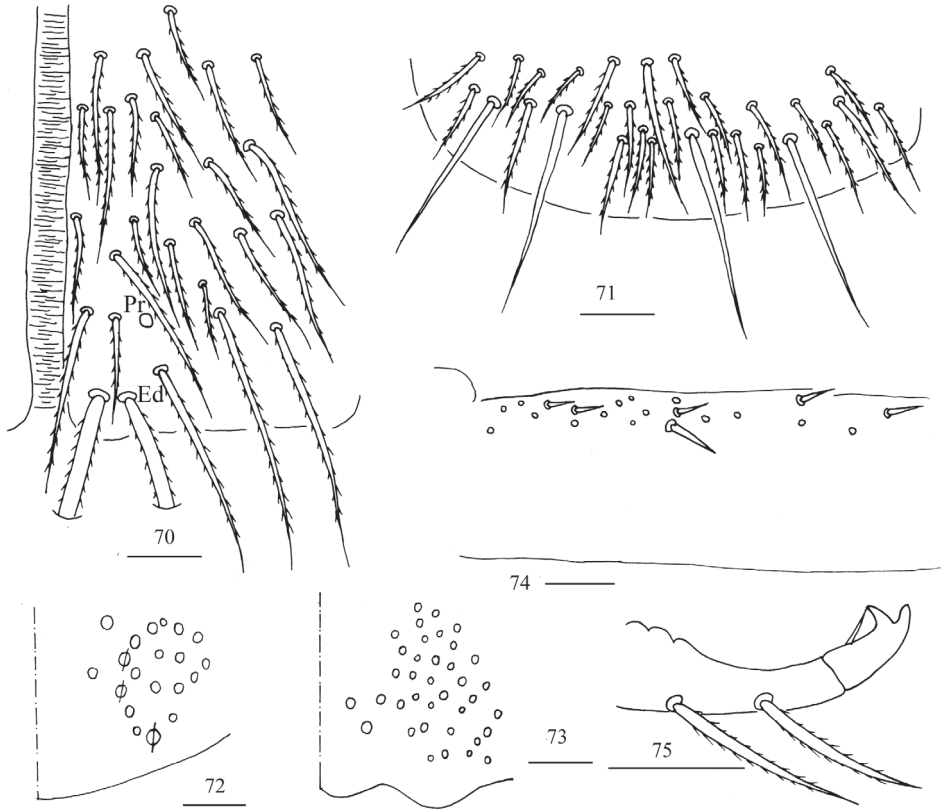


**Figure 69.** Chaetotaxy of Abd. IV of *Homidia linhaiensis*. Scale bar: 50  $\mu\text{m}$ .

(S) mac (Fig. 67). Chaetal formula of labial base as  $\text{MR}e_1L_2$ , chaetae  $e$  and  $l_1$  smooth, others ciliate, R/M as 0.56.

**Thorax.** Th. II with four medio-medial ( $m_1, m_2, m_{2i}, m_{2i2}$ ), four medio-sublateral ( $m_4, m_{4i}, m_{4p}, m_{4pi}$ ), 33 posterior mac. Th. III with 36–39 mac and two sens (Fig. 68).



**Figures 70–75.** *Homidia linhaiensis* **70** anterior face of ventral tube **71** posterior face of ventral tube **72** manubrial plaque **73** ventro-apical part of manubrium **74** proximal section of dens (circles also representing spines) **75** mucro. Scale bars: 20  $\mu$ m.

**Abdomen.** Range of Abd. IV length as 6.28–9.32 $\times$  as dorsal axial length of Abd. III. Abd. I with 10 (a2, a3, a5, m2–5, m2i, m4i, m4p) mac, ms antero-internal to sens. Abd. II with six (a2, a3, m3, m3e, m3ea, m3ep) central, one (m5) lateral mac and two sens. Abd. III with two (a2, m3) central and five (am6, pm6, m7a, p6, p7) lateral mac, one ms and two sens. Abd. IV anteriorly with 9–13 mac arranged in irregular transverse row, A2 always present and anterior to transverse row; posteriorly with 10–16 central mac, laterally with 23–27 mac (Fig. 69). Anterior face of ventral tube with 24–28 ciliate chaetae, 3+3 of them as mac, line connecting proximal (Pr) and external-distal (Ed) mac oblique to median furrow (Fig. 70); posterior face with four distal smooth and numerous ciliate chaetae (Fig. 71). Manubrial plaque dorsally with 14–17 ciliate chaetae and three pseudopores (Fig. 72); ventrally with 37 ciliate chaetae on each side (Fig. 73). Dens with 12–21 smooth inner spines (Fig. 74). Mucro bidentate with subapical tooth larger than apical one; tip of basal spine reaching apex of subapical tooth; distal smooth section of dens almost equal to than mucro in length (Fig. 75).

**Remarks.** This species was first described from Zhejiang Province by Shi et al. (2009) and can be easily distinguished from other known species of the genus by two small blue spots on Th. III, five mac on Abd. III laterally, presence of A2 on Abd. IV. The characters of our specimens agree well with the original description in chaetotaxy of body, labium, colour pattern, and other characters, but there are five smooth chaetae on posterior face of ventral tube from Zhejiang and four smooth chaetae from that from Jiangxi. In fact, the number of smooth chaetae on posterior face of ventral tube may varies intraspecifically from two to five in some species of the genus. Chaetotaxy of manubrial plaque is added here.

**Distribution.** China (Jiangxi, Zhejiang).

***Homidia socia* Denis, 1929**

Figs 76–86

*Homidia socia* Denis, 1929: 310.

**Examined specimens.** 3♀ on slides, CHINA, Jiangxi Province, Nanchang City, Xinjian District, Jiuxi, 28°47'56"N, 115°45'11"E, 168 m asl, sample number 1243, collected by Y-T Ma, 12-XI-2020.

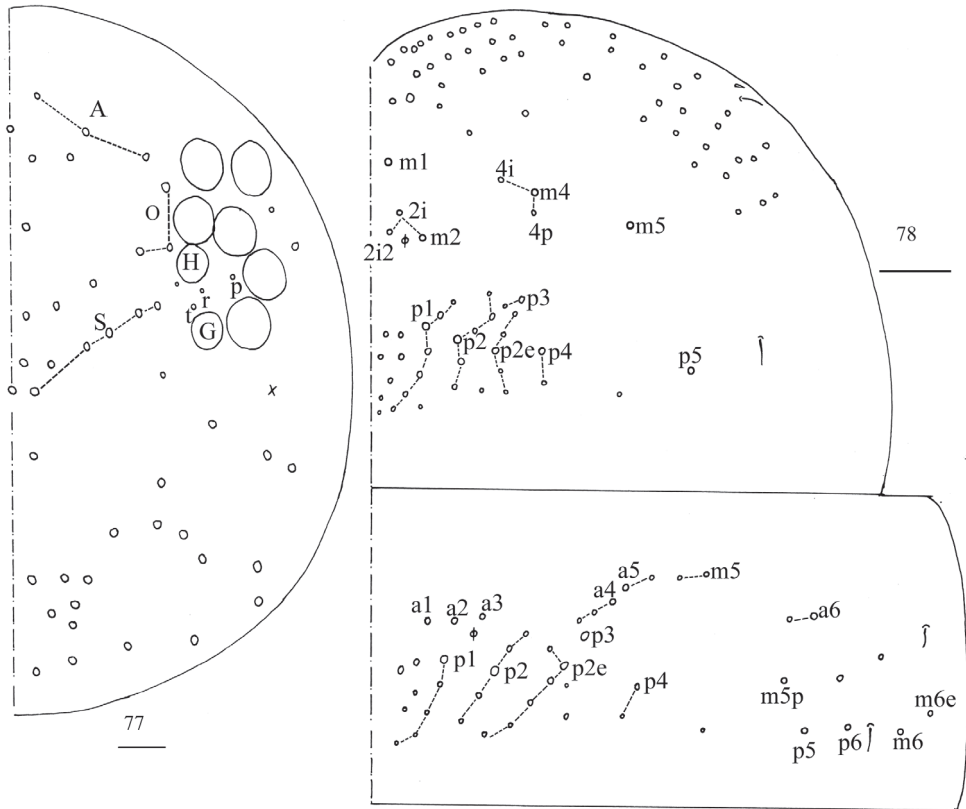
**Description. Size.** Body length up to 2.16 mm.

76

---



**Figure 76.** Habitus of *Homidia socia* Scale bar: 500  $\mu$ m.



**Figures 77, 78.** *Homidia socia* **77** dorsal chaetotaxy of head **78** chaetotaxy of Th. II–III. Scale bars: 20 μm (**77**); 50 μm (**78**).

**Colouration.** Ground ground colour pale yellow. Ant. I–IV with scattered blue pigment. Eye patches dark blue. A pair of longitudinal blue stripes present along lateral side of head to Abd. III. Medial longitudinal narrow stripe present from Th. II to Abd. III. Abd. V with blue pigment (Fig. 76).

**Head.** Antenna 0.52–0.66× body length; antennal segment ratio I: II: III: IV = 1: 1.28–1.40: 1.00–1.20: 1.67–2.11. Eyes 8 + 8, G and H smaller than others, interocular chaetae with p, r, and t. Dorsal cephalic chaetotaxy with three antennal (A), three ocellar (O) and five sutural (S) mac (Fig. 77). Chaetal formula of labial base as MREL1L2, all ciliate, R/M as 0.67–0.72.

**Thorax.** Th. II with four medio-medial (m1, m2, m2i, m2i2), three medio-sublateral (m4, m4i, m4p), 30–33 (24) posterior mac. Th. III with 41–45 mac and two sens (Fig. 78). Pseudopores on coxa I–III as 2, 3, 2, respectively; coxal macrochaetal formula as 3/4+3, 3/4+2. Trochanteral organ with 39 smooth chaetae. Tenent hairs clavate and almost equal to inner edge of unguis. Unguis with four inner teeth, basal pair located at 0.38–0.45 distance from base of inner edge of unguis, distal unpaired

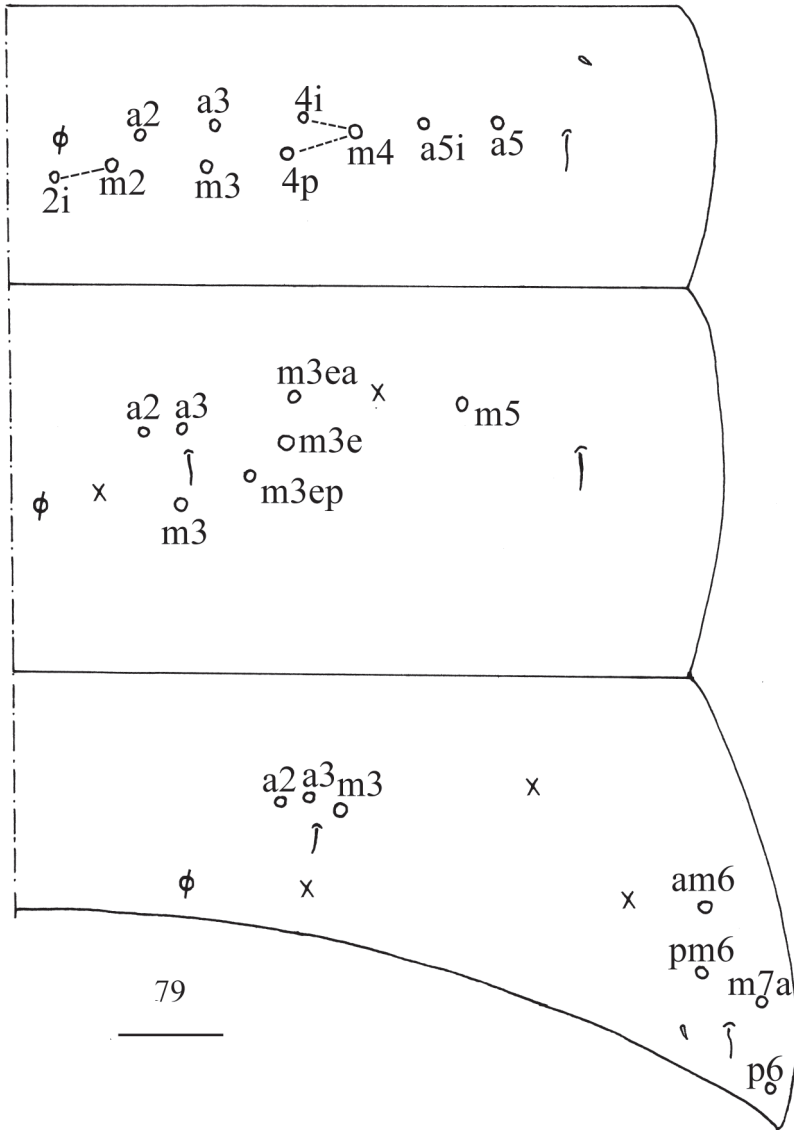


**Figure 79.** Chaetotaxy of Abd. I–III of *Homidia socia*. Scale bar: 50  $\mu\text{m}$ .

teeth at 0.65–0.67 and 0.80–0.85 distance from base; unguiculus lanceolate, outer edge slightly serrate.

**Abdomen.** Range of Abd. IV length as 6.25–10.12 $\times$  as dorsal axial length of Abd. III. Abd. I with 10 (a2, a3, a5, a5i, m2–5, m2i, m4i, m4p) mac, ms antero-external to sens. Abd. II with six (a2, a3, m3, m3e, m3ea, m3ep) central, one (m5) lateral mac, and two sens. Abd. III with two or three (a2, m3, a3 sometimes absent) central and four (am6, pm6, m7a, p6) lateral mac, one ms, and two sens (Fig. 79). Abd. IV

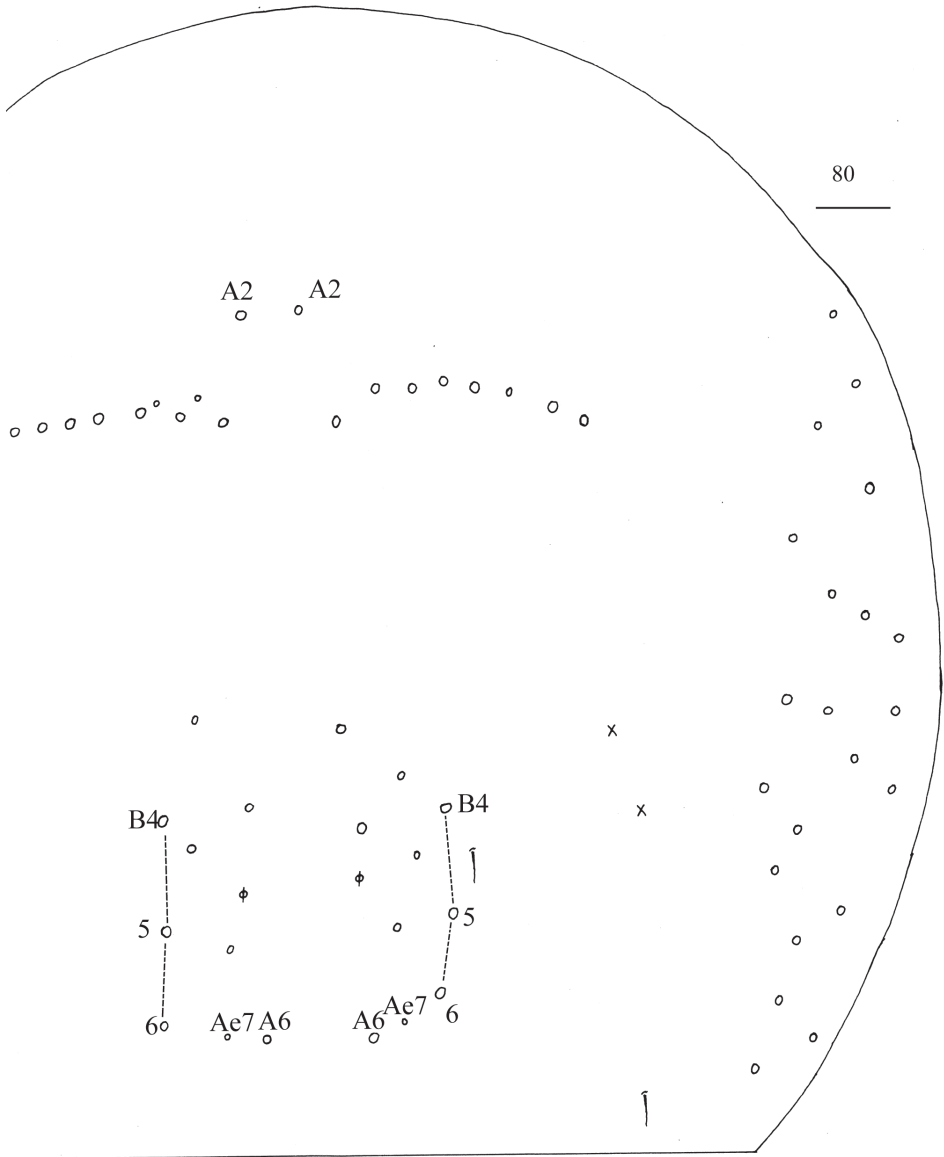
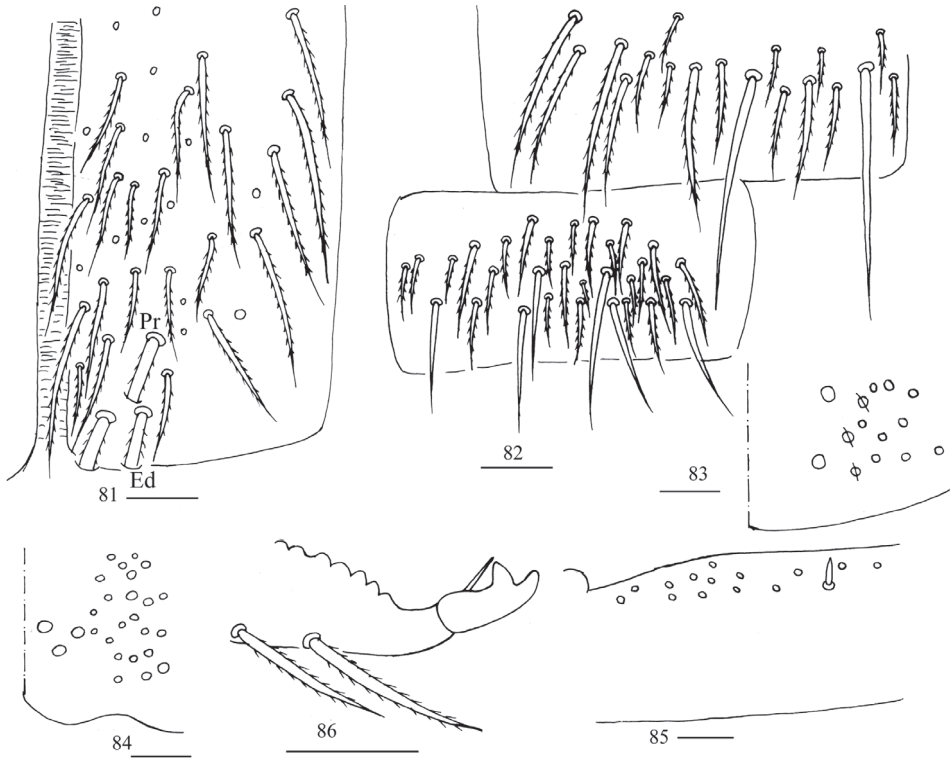


**Figure 80.** Chaetotaxy of Abd. IV of *Homidia socia*. Scale bar: 50 μm.

anteriorly with eight or nine mac arranged in irregular transverse row, A2 always present and anterior to transverse row; posteriorly with 6–10 central mac; laterally with 18–22 mac (Fig. 80). Anterior face of ventral tube with 39 ciliate chaetae, 3+3 of them as mac, line connecting proximal (Pr) and external-distal (Ed) mac oblique to median furrow (Fig. 81); posterior face with two distal smooth and numerous ciliate chaetae; lateral flap with six smooth and 24 ciliate chaetae (Fig. 82). Manubrial plaque dorsally



**Figures 81–86.** *Homidia socia* **81** anterior face of ventral tube **82** posterior face and lateral flap of ventral tube **83** manubrial plaque **84** ventro-apical part of manubrium **85** proximal section of dens (circles also representing spines) **86** mucro. Scale bars: 20  $\mu$ m.

with 11–14 ciliate chaetae and three pseudopores (Fig. 83); ventrally with 26 ciliate chaetae on each side (Fig. 84). Dens with 15 smooth inner spines (Fig. 85). Mucro bi-dentate with subapical tooth larger than apical one; tip of basal spine reaching apex of subapical tooth; distal smooth section of dens shorter than mucro in length (Fig. 86).

**Ecology.** In the litter of leaves of *Phyllostachys edulis*.

**Remarks.** This species was first described from Fujian Province, China by Denis (1929), mainly based on its colour pattern with three longitudinal stripes on dorsal side. Yosii (1942), Stach (1965), Lee and Park (1989), and Christiansen and Bellinger (1980, 1992) reported it from Japan, Vietnam, Taiwan (China), and USA, respectively, and their descriptions were relatively simple. Jordana (2012) also reported it based on Vietnamese and Japanese specimens that corresponded in colour pattern to *H. socia* forma *flava* Yosii, 1953 from Japan. In this work, several characters not previously mentioned are added, such as the chaetotaxy of the head, ventral tube, and manubrial plaque. Differences exist between the specimens collected from Jiangxi Province and other authors' previous descriptions that are listed in Table 4. Our specimens, with 15 spines on dens, are similar to those examined by Jordana (2012) which had 14 spines.

**Table 4.** Comparison of *H. socia* between different descriptions.

Characters	This work	Denis (1929)	Christiansen and Bellinger (1980, 1992)	Stach (1965)	Jordana (2012)
Chaetal formula of labial base	MREL <sub>1</sub> L <sub>2</sub>	unknown	MREL <sub>1</sub> L <sub>2</sub>	unknown	unknown
Mac on Abd. I	10	unknown	11 or 15	9	unknown
Central mac on Abd. II	6	unknown	5–6	6	6
Central mac on Abd. III	2–3	unknown	3	3	3
Mac A2 on Abd. IV	present	unknown	present	unknown	present
Mac of transverse row on Abd. IV	8–9	unknown	8	8	7
Centro-posterior mac on Abd. IV	6–10	unknown	5	8	5
Dental spines	15	up to 30	<20	7 or 11	14*

\* Jordana (2012) gave 14 spines on dens on the specimens of Vietnam and Japan he examined, and 14–30 spines in the species redescription that included the values given by Denis (1929) in the original description.

Up to 30 spines were given by Denis (1929) for the type specimens of large size from Fujian. These specimens or specimens from the type locality will therefore need to be redescribed to confirm the assignment of our specimens as well as those described by Jordana (2012) to *H. socia*.

**Distribution.** Japan, USA, Vietnam, and China (Anhui, Fujian, Guangxi, Jiangsu, Jiangxi, Taiwan, Zhejiang).

## Discussion

The genus contains 75 known species that are distributed in the U.S.A. and the eastern part of Asia, especially China, Korea, and Japan (Table 5). They usually live in coastal areas from tropical to temperate zones, maybe because humidity is high in these regions. Most species of the genus are endemic (Table 5). However, some of them, such as *H. sauteri* and *H. socia*, are widespread, and were reported from China, Japan, Korea, and the U.S.A. Jia et al. (2005) pointed out that these two species are so widely distributed that they may have been transported by human activity. This hypothesis would, however, need more evidence.

**Table 5.** Distribution records of *Homidia* species around the world.

Species	China	Japan	Korea	India	Indonesia & Singapore	Vietnam	USA
<i>H. acutus</i> sp. nov.	√						
<i>H. allopsila</i> (Börner, 1909)		√					
<i>H. amethystinoides</i> Jordana & Baquero, 2010		√					
<i>H. anhuiensis</i> Li & Chen, 1997	√						
<i>H. apigmenta</i> Shi, Pan & Zhang, 2010	√						
<i>H. breviseta</i> Pan, 2022	√						
<i>H. changensis</i> sp. nov.	√						

Species	China	Japan	Korea	India	Indonesia & Singapore	Vietnam	USA
<i>H. chosonica</i> Szeptycki, 1973			√				
<i>H. chroma</i> Pan & Yang, 2019	√						
<i>H. chrysothrix</i> Yosii, 1942		√					
<i>H. cingula</i> (Börner, 1906)					√		
<i>H. dianbaiensis</i> (Lin, 1985)	√						
<i>H. emeiensis</i> Jia, Chen & Christiansen, 2004	√						
<i>H. fascia</i> Wang & Chen, 2001	√						
<i>H. flava</i> Yosii, 1953		√					
<i>H. flavonigra</i> Szeptycki, 1973			√				
<i>H. formosana</i> Uchida, 1943	√						
<i>H. fujiyamai</i> Uchida, 1954		√					
<i>H. glassa</i> Nguyen, 2001						√	
<i>H. grisea</i> Lee & Lee, 1981			√				
<i>H. haikea</i> Christiansen & Bellinger, 1992							√
<i>H. hangzhouensis</i> Pan & Ma, 2021	√						
<i>H. heugsanica</i> Lee & Park, 1984			√				
<i>H. hexaseta</i> Pan, Shi & Zhang, 2011	√						
<i>H. hibiū</i> Christiansen & Bellinger, 1992							√
<i>H. hjesanica</i> Szeptycki, 1973			√				
<i>H. huashanensis</i> Jia, Chen & Christiansen, 2005	√						
<i>H. insularis</i> (Carpenter, 1904)							√
<i>H. jordanai</i> Pan, Shi & Zhang, 2011	√						
<i>H. kali</i> (Imms, 1912)				√			
<i>H. koreana</i> Lee & Lee, 1981			√				
<i>H. laba</i> Christiansen & Bellinger, 1992	√						√
<i>H. lakhanpurii</i> Baquero & Jordana, 2015				√		√	
<i>H. latifolia</i> Chen & Li, 1999	√						
<i>H. lei</i> Chen & Li, 1997	√						
<i>H. leniseta</i> Pan & Yang, 2019	√						
<i>H. linhaiensis</i> Shi, Pan & Qi, 2009	√						
<i>H. maijiensis</i> Zhou & Ma, 2022	√						
<i>H. mediaseta</i> Lee & Lee, 1981			√				
<i>H. mediofascia</i> Shi, Pan & Bai, 2009	√						
<i>H. minuta</i> Kim & Lee, 1995			√				
<i>H. multidentata</i> Nguyen, 2005						√	
<i>H. munda</i> Yosii, 1956		√	√				
<i>H. nigra</i> Lee & Lee, 1981			√				
<i>H. nigrifascia</i> Ma & Pan, 2017	√						
<i>H. nigrocephala</i> Uchida, 1943	√	√					
<i>H. obliquistria</i> Ma & Pan, 2017	√						
<i>H. pentachaeta</i> Li & Christiansen, 1997	√						
<i>H. phjongjangica</i> Szeptycki, 1973	√		√				
<i>H. polyseta</i> Chen, 1998	√						
<i>H. pseudofascia</i> Pan, Zhang & Li, 2015	√						
<i>H. pseudoformosana</i> Kang & Park, 2012			√				
<i>H. pseudosinensis</i> Shi & Pan, 2012	√						
<i>H. qimenensis</i> Yi & Chen, 1999	√						
<i>H. quadrimaculata</i> Pan, 2015	√						
<i>H. quadriseta</i> Pan, 2018	√						

Species	China	Japan	Korea	India	Indonesia & Singapore	Vietnam	USA
<i>H. rosannae</i> Jordana & Baquero, 2010		√					
<i>H. sauteri</i> (Börner, 1909)	√	√	√				√
<i>H. sichuanensis</i> Jia, Zhang & Jordana, 2010	√						
<i>H. similis</i> Szeptycki, 1973	√		√				
<i>H. sinensis</i> Denis, 1929	√	√				√	
<i>H. socia</i> Denis, 1929	√	√				√	√
<i>H. sotoi</i> Jordana & Baquero, 2010		√					
<i>H. speciosa</i> Szeptycki, 1973			√				
<i>H. subcingula</i> Denis, 1948						√	
<i>H. taibaiensis</i> Yuan & Pan, 2013	√						
<i>H. tiantaiensis</i> Chen & Lin, 1998	√						
<i>H. tibetensis</i> Chen & Zhong, 1998	√						
<i>H. transitoria</i> Denis, 1929	√						
<i>H. triangulimacula</i> Pan & Shi, 2015	√						
<i>H. unichaeta</i> Pan, Shi & Zhang, 2010	√					√	
<i>H. wanensis</i> Pan & Ma, 2021	√						
<i>H. xianjuensis</i> Wu & Pan, 2016	√						
<i>H. yandangensis</i> Pan, 2015	√						
<i>H. yosiii</i> Jordana & Baquero, 2010		√					
<i>H. zhangii</i> Pan & Shi, 2012	√						
<i>H. ziguiensis</i> Jia, Chen & Christiansen, 2003	√						

Most species of *Homidia* are heavily pigmented and their colour patterns vary only slightly among specimens of the same species, so colour pattern appears to be a significant character for the morphological taxonomy of the genus. However, colour pattern may exhibit some variability between some species, such as *H. fascia* Wang & Chen, 2001 and *H. pseudofascia* Pan, Zhang & Li, 2015. The new species, *H. acutus* sp. nov. described here shares almost the same colour pattern as *H. zhangii*, but the differences in other characters are significant.

**Key to the Chinese species of *Homidia***

- 1 Mental chaetae expanded or leaf-like..... 2
- Mental chaetae normal ciliate ..... 9
- 2 Body without obvious colour pattern except eye patches..... ***H. apigmenta***
- Body with obvious colour pattern except eye patches..... 3
- 3 Abd. I–III laterally with oblique stripes..... ***H. obliquistria***
- Abd. I–III laterally without oblique stripes..... 4
- 4 Abd. IV with mac A2..... ***H. ziguiensis***
- Abd. IV without mac A2 ..... 5
- 5 Central Abd. IV with roughly Y-shaped patch..... ***H. qimenensis***
- Abd. IV without Y-shaped patch ..... 6

6	Abd. IV anteriorly with an interrupted dark transverse stripe.....	7
–	Abd. IV anteriorly without dark transverse stripe.....	8
7	Abd. IV anteriorly with 4–7 mac on each side .....	<i>H. latifolia</i>
–	Abd. IV anteriorly with 22–24 mac on each side .....	<i>H. polyseta</i>
8	Labial basal chaetae $L_1$ and $L_2$ expanded.....	<i>H. triangulimacula</i>
–	Labial basal chaetae $L_1$ and $L_2$ unexpanded .....	<i>H. wanensis</i>
9	Body without obvious colour pattern except eye patches.....	10
–	Body with obvious colour pattern except eye patches.....	12
10	Labial basal chaeta $L_1$ ciliate, Abd. III without mac a2 .....	<i>H. jordanai</i>
–	Labial basal chaeta $L_1$ smooth, Abd. III with mac a2.....	11
11	Abd. IV anteriorly with 3–8 mac and posteriorly 1 mac on each side.....	.....
–	Abd. IV anteriorly with 10–12 mac and posteriorly 2 mac on each side.....	<i>H. unichaeta</i>
–	.....	<i>H. tibetensis</i>
12	Head entirely dark .....	13
–	Head not entirely dark.....	15
13	Abd. IV anteriorly with a transverse stripe .....	<i>H. nigrocephala</i>
–	Abd. IV anteriorly without transverse stripe.....	14
14	Th. II–III entirely dark.....	<i>H. anhuiensis</i>
–	Th. II–III with slightly brown pigment .....	<i>H. taibaiensis</i>
15	Abd. IV with mac A2.....	16
–	Abd. IV without mac A2 .....	18
16	Labial basal chaetae E & $L_1$ ciliate.....	<i>H. socia</i>
–	Labial basal chaetae e & $L_1$ smooth .....	17
17	Abd. III laterally with 5 mac .....	<i>H. linhaiensis</i>
–	Abd. III laterally with 4 mac .....	<i>H. tiantaiensis</i>
18	Abd. IV almost entirely dark or with uniform colour .....	19
–	Abd. IV with some colour patterns .....	25
19	Abd. IV almost entirely dark.....	<i>H. emeiensis</i>
–	Abd. IV not entirely dark.....	20
20	Abd. III laterally with 5 chaetae .....	<i>H. pentachaeta</i>
–	Abd. III laterally with 4 chaetae .....	21
21	Tenent hairs pointed.....	<i>H. acutus</i> sp. nov.
–	Tenent hairs clavate.....	22
22	Th. II–III medially with a longitudinal stripe.....	<i>H. yandangensis</i>
–	Th. II–III medially without a longitudinal stripe.....	23
23	Th. III without mac p4, labial chaeta $L_1$ smooth .....	<i>H. zhangii</i>
–	Th. III with mac p4, labial chaeta $L_1$ ciliate .....	24
24	Ground colour hazel, dens with 80–114 spines.....	<i>H. huashanensis</i>
–	Ground colour yellow, dens with 16–28 spines.....	<i>H. changensis</i> sp. nov.
25	Abd. III without obvious colour pattern .....	26
–	Abd. III with obvious colour pattern.....	34

26	Th. II medially with colour pattern .....	27
–	Th. II medially without colour pattern.....	29
27	Th. II medially with a longitudinal stripe.....	<i>H. mediofascia</i>
–	Th. II medially with a pair of stripes .....	28
28	Th. III with a pair of patches.....	<i>H. fascia</i>
–	Th. III without a pair of patches .....	<i>H. pseudofascia</i>
29	Abd. IV anteriorly with obvious colour pattern.....	30
–	Abd. IV anteriorly without obvious colour pattern .....	32
30	Mac a2 on Abd. III absent .....	<i>H. formosana</i>
–	Mac a2 on Abd. III present .....	31
31	Head with 8 sutural mac.....	<i>H. hangzhouensis</i>
–	Head with 9 sutural mac.....	<i>H. hexaseta</i>
32	Ground colour pale yellow.....	<i>H. dianbaiensis</i>
–	Ground colour not pale yellow.....	33
33	Labial basal chaeta E ciliate .....	<i>H. maijiensis</i>
–	Labial basal chaeta e smooth .....	<i>H. phjongjangica</i>
34	Abd. IV anteriorly with 2 mac on each side .....	35
–	Abd. IV anteriorly with more than 2 mac on each side .....	36
35	Labial chaetae $l_1$ and $l_2$ smooth.....	<i>H. leniseta</i>
–	Labial chaetae $l_1$ and $l_2$ ciliate .....	<i>H. quadriseta</i>
36	Abd. IV posteriorly with 9–11 mac on each side.....	<i>H. xianjuensis</i>
–	Abd. IV posteriorly with less than 9 mac on each side.....	37
37	Th. III dorsally without obvious colour pattern.....	38
–	Th. III dorsally with obvious colour pattern.....	40
38	Th. II medially with colour pattern, Abd. II entirely dark .....	<i>H. nigrifascia</i>
–	Th. II medially without colour pattern, Abd. II not entirely dark.....	39
39	Unguis with 3 inner teeth .....	<i>H. chroma</i>
–	Unguis with 4 inner teeth .....	<i>H. laba</i>
40	Th. II medially without colour pattern.....	41
–	Th. II medially with colour pattern .....	45
41	Transverse band of Th. III not reaching lateral edge of body .....	42
–	Transverse band of Th. III reaching lateral edge of body.....	43
42	Abd. I with 14 mac.....	<i>H. breviseta</i>
–	Abd. I with 9 mac.....	<i>H. similis</i>
43	Dens with 10 spines.....	<i>H. transitoria</i>
–	Dens with more than 20 spines.....	44
44	Abd. IV centrally with a transverse band.....	<i>H. sauteri</i>
–	Abd. IV centrally without a transverse band.....	<i>H. sinensis</i>
45	Labial basal chaeta E ciliate.....	<i>H. leei</i>
–	Labial basal chaeta e smooth .....	46
46	Th. II posteriorly with a M-shaped transverse stripe.....	<i>H. pseudosinensis</i>
–	Th. II posteriorly without a M-shaped transverse stripe.....	47
47	Labial basal chaeta $l_1$ smooth.....	<i>H. quadrimaculata</i>
–	Labial basal chaeta $l_1$ ciliate.....	<i>H. sichuanensis</i>

## Acknowledgements

This research was funded by the National Natural Science Foundation of China, grant number 36101880 and Large Instruments Open Foundation of Nantong University.

## References

- Bellinger PF, Christiansen K, Janssens F (1996–2022) Checklist of the Collembola of the World. <http://www.collembola.org> [accessed 24 May 2022]
- Börner C (1906) Das system der Collembolen nebst Beschreibung neuer Collembolen des Hamburger Naturhistorischen Museums. Mitteilungen aus dem Naturhistorische Museum in Hamburg 23: 147–188.
- Börner C (1909) Japan's Collembolenfauna (Vorläufige Mitteilung). Sitzungsberichte der Gesellschaft Naturforschender Freunde zu Berlin 2: 99–135.
- Christiansen K, Bellinger P (1980) The Collembola of North America North of the Rio Grande. Part 3 Family Entomobryidae. Grinnell College, Iowa 785–1041.
- Christiansen K, Bellinger P (1992) Insects of Hawaii: volume 15: Collembola, University of Hawaii Press, Honolulu, 445 pp.
- Denis JR (1929) Notes sur les collemboles récoltés dans ses voyages par le Prof. F. Silvestri. I. Seconde note sur les collemboles d'Extrême-Orient. Bolletino di Zoologia Generale e Agricola Portici 22: 305–320.
- Gisin H (1964) European Collembola. VII. Revue Suisse de Zoologie 71(4): 649–678. <https://doi.org/10.5962/bhl.part.75615>
- Jia SB, Chen JX, Christiansen K (2005) A New Entomobryid Species of *Homidia* from Shaanxi, China (Collembola: Entomobryidae). Journal of the Kansas Entomological Society 78(4): 315–321. <https://doi.org/10.2317/040413.1>
- Jordana R (2012) Capbryinae and Entomobryini. In: Synopses on palearctic Collembola. Soil Organisms 84(1): 1–391.
- Lee BH, Lee WK (1981) A taxonomic study of soil microarthropods with reference to *Homidia* (Collembola) and *Oribatei* (Acari). Annual Report of Biological Research 2: 129–148.
- Lee BH, Park KH (1989) Systematic studies on Chinese Collembola (Insecta), 1. Four new species and three new records of Entomobryidae from Taiwan. Chinese Journal of Entomology 9(2): 263–282.
- Mari-Mutt JA (1986) Puerto Rican species of *Lepidocyrtus* and *Pseudosinella* (Collembola: Entomobryidae). Caribbean Journal of Science 22(1–2): 1–48. <https://doi.org/10.11646/zootaxa.4995.1.11>
- Pan ZX, Shi SD (2012) Description of a new species in the genus *Homidia* (Collembola: Entomobryidae) from Dalei Mountain, Zhejiang Province. Entomotaxonomia 34(2): 96–102.
- Pan ZX, Shi SD, Zhang F (2010) A new species of the genus *Homidia* (Collembola: Entomobryidae) from Zhejiang Province, China. Entomotaxonomia 32(4): 241–247.
- Pan ZX, Shi SD, Zhang F (2011) A new species of *Homidia* (Collembola: Entomobryidae) from east China with description of the first instar larvae. ZooKeys 152: 21–42. <https://doi.org/10.3897/zookeys.152.1455>

- Pan ZX, Zhang F, Li YB (2015) Two closely related *Homidia* species (Entomobryidae, Collembola) revealed by morphological and molecular evidence. *Zootaxa* 3918(2): 285–294. <https://doi.org/10.11646/zootaxa.3918.2.9>
- Shi SD, Pan ZX, Qi X (2009) A new species of of the genus *Homidia* Börner, 1906 (Collembola: Entomobryidae) from East China. *Zootaxa* 2020(1): 63–68. <https://doi.org/10.11646/zootaxa.2020.1.4>
- Stach J (1965) On some Collembola of North Vietnam. *Acta Zoologica Cracoviensia* 30(4): 345–372.
- Szeptycki A (1973) North Korean Collembola. I. The genus *Homidia* Börner, 1906 (Entomobryidae). *Acta Zoologica Cracoviensia* 31: 23–40.
- Szeptycki A (1979) Morpho–systematic studies on Collembola. IV. Chaetotaxy of the Entomobryidae and its phylogenetical significance. *Polska Akademia Nauk, Kraków*, 219 pp.
- Wang SJ, Chen JX (2001) A new species of the genus *Homidia* (Collembola: Entomobryidae) from Jiangsu, China. *Entomotaxonomia* 23(4): 235–239.
- Yosii R (1942) Japanische Entomobryinen (Ins., Collemb.). *Archiv für Naturgeschichte* 10(4): 476–495.